UNIVERSITAT DE BARCELONA

Structure and Kinematics of the SW Taiwan Fold and Thrust belt

Cristina Biete Castells

The south central Taiwan fold-and-thrust belt (FTB) comprises a roughly N-S striking, west verging imbricate thrust system that has been developing since the Late Miocene. In this thesis, we adopt a multidisciplinary approach in order to test whether or not the inherited structural and morphological architecture of the Eurasian margin, which is being incorporated in the deformation from the outer shelf to the base of the slope, may be influencing the development of FTB. Our results show that the most important along-strike change takes place at the eastward prolongation of the upper part of the margin necking zone, where there is an interpreted link between fault reactivation, basement involvement, seismicity concentration, and high topography formation. The contemporaneous stress, strain and displacement fields also show an orientation marked change across the upper part of the margin necking zone. In the necking zone, the detailed 3D structural analysis shows a less marked along-strike change in the structure. This change takes place across a transverse zone composed of a suite of structures at the surface that we call the Hsinhua transverse zone. We suggest that this transverse zone coincides with variations in the geometry of the basal thrust which, in turn, has a causal relationship to (possibly fault bounded) basement highs and lows that are inherited from the continental margin. We interpret all these along-strike changes in the fold-and-thrust belt to be related to the reactivation of east-northeast striking faults inherited from the rifted Eurasian margin.

Cristina Biete Castells - 2019

STRUCTURE AND KINEMATICS OF SW TAIWAN FOLD AND THRUST BELT

STRUCTURE AND KINEMATICS OF THE SW TAIWAN FOLD AND THRUST BELT

Cristina Biete Castells

Doctoral Thesis

July 2019

Institute of Earth Sciences 'Jaume Almera'

Spanish National Research Council (CSIC)

Structure and Kinematics of the SW Taiwan Fold and Thrust belt

Ph.D. thesis presented in the Earth Sciences doctoral program of the University of Barcelona

to obtain the degree of Doctor in Geology

Ph.D. candidate:

Cristina Biete Castells[1,2]

Supervisors:

Dr. Joaquina Alvarez-Marron[1] & Dr. Dennis Brown[1]

Tutor:

Prof. Eduard Roca Abella[2]

[1]Institute of Earth Sciences 'Jaume Almera', ICTJA-CSIC

[2]Institut de Recerca Geomodels, Departament de Dinàmica de la Terra i de l'Oceà, University of Barcelona

July 2019

Cover: watercolor paint representing a seismic tomography section of SW Taiwan, with earthquake hypocenters. The picture also shows interpreted faults. By Cristina Biete Castells

CSIC ICTJA UNIVERSITAT DE BARCELONA

Als meus pares

…i al Roger

It is the path to the top which give meaning to the summit.
Without the experience of the voyage,
the top is meaningless, it is only a viewpoint.
The path up the mountains fuses the sensations and experiences
of our inner voyage with the grandeur of the exterior.

"La cumbre mística" Revista voluntad
in "la Senda", Steph Cracknell

Table of Content

Abbreviations

Places:

AR = Alishan Range
CoR = Coastal Range
CP = Coastal Plain
CR = Central Range
ECM = Eurasian continental margin
FR = Failed Rift
HM = Hsuehshan Mountain
HR = Hsuehshan Range
PB = Puli BasinP = Pingtung Plain
PPS = Philippine sea plate
RS = Ryukyu Subduction Zone
S/S = Shelf/Slope break
TN = Tainan Basin
TsB = Taishi Basin
WF = Western Foothills
YM = Yushan Mountain

Faults & Thrusts:

BF = B fault
CF= Chiali fault
ChF = Chauchou fault
ChT = Changhua thrust
CiT = Chishan thrust
CT = Chelungpu thrust
CuT = Chutochi thrust
HF = Hsinshua fault
LF = Lishan fault
LT = Lungchuan thrust
PT = Pingshi thrust
SkF = Shuilikeng fault
ST = Shuangtung Thrust
TT = Tili Thrust
YF = Yichu fault
ZF = Zuojhen fault

Folds:

HS = Hsiaolin syncline
KS = Kuanglin synform
NA = Niushan anticline
NeA = Neiyingshan anticlinorium
SS = Shihchangli syncline
TA = Tainan anticline
TS = Tingpinglin syncline
YS = Yuching syncline

Institutions and Projects:

CSIC = Spanish National Research Council
CWB = Central Weather Bureau
ICTJA = Institute of Earth Sciences Jaume Almera
TAIGER = Taiwan Integration Geodynamic Research

Others:

DEM = Digital Elevation Model
FTB = Fold-and-thrust belt
Ml = Local magnitude

List of Figures

Preface

This thesis has been carried out in the Institute of Earth Science Jaume Almera (ICTJA) of the Spanish National Research Council (CSIC) from April 2015 through July 2019. The funding to develop the thesis comes from the FPI pre-doctoral grant with reference BES-2014-070122 of the Ministerio de Economia y Competititvidad of Spain. It is part of the project "Controls of inherited continental margin architecture on the deformation and kinematics of orogenic wedges in arc-continent collisions" (CGL2013-4377-P).

This thesis is presented as a compilation of three scientific articles published in Science Citation Index (SCI) journals, from which the Ph.D. candidate is first author of two and co-author of one. These articles are presented in Appendix 1. They are:

Within the context of the research project, the Ph.D. candidate undertook two field campaigns in Taiwan to collect structural data, and two short three month stays in other research institutions to work with earthquake hypocenter relocations and perform stress inversions from earthquake focal mechanisms. She attended workshops and participated in a total of five international and national conferences presenting either as poster or oral presentations. In detail the activities related with this thesis are:

- Two field campaigns of approximately one month each in southwest Taiwan, in the years 2016 and 2017, with the Ph.D. supervisors;
- Two short stays of approximately three months each:
    - ◊ Stay at the Department of Earth Sciences, National Central University, Taiwan, from the 4th of April 2016 to the 4th of July 2016. The Ph.D. candidate visited Dr. Hao Kuo-Chen to learn about earthquake relocation techniques.

◊ Stay at the Department of Earth Sciences, Uppsala University, Sweden, from the 6th of October 2017 to 22nd of December 2017. The Ph.D. candidate visited Dr. Björn Lund and worked on determining the stress field in south central Taiwan from the inversion of earthquake focal mechanisms;

- Attended a ten day workshop in Galway, Ireland called: "Comparative Studies of the Tectonophysics of Taiwan and West-Ireland Orogenies". The workshop was lead by Dr. Paul Ryan and took place from the 3rd to the 9th of September 2016;
- Attended a two day workshop organized by the IX Spanish Geological Congress called: "De Avalonia al suroeste de Iberia: anatomía de una cuña orogénica varisca, el "rifting" proto-Atlántico y tectónica reciente", lead by Drs F.M Alonso-Chavez, E. Garcia-Navarro, C. Fernandez-Rodriguez and M.A. Camacho-Cerro. The workshop took place from the 16th to the 17th of September 2016;
- Attended international conferences, including the General Assembly of the European Geophysical Union (EGU) with poster presentations in 2015, 2016 and 2017, and the American Geophysical Union (AGU) Fall Meeting in 2016 with an oral presentation. The abstracts of the presentations are given in Appendix 2.
- Attended the national IX Geological Congress of Spain in 2016 with an oral presentation. The extended abstract is given in Appendix 2.

This thesis is organized in four chapters and four appendices, following the recommendations of the Earth Sciences doctoral program of the University of Barcelona. **Chapter 1** presents the general introduction to the thesis, with an introduction to the topic, the objectives of the research, and the publications that make up the thesis. The coherence between the papers is explained, as is the Ph.D. candidate's contribution. This chapter also includes the geological background, and the methodological approach. In **Chapter 2** the results of each paper are summarized. **Chapter 3** presents a discussion that integrates all three papers, and **Chapter 4,** presents the conclusions. These chapters are followed by the **Acknowledgements**, and finally the **References** cited in the text.

The thesis also includes four Appendices: **Appendix 1** presents the published papers; **Appendix 2** gives the abstracts of the poster and oral presentations of the Ph.D. candidate conference presentations. The following three appendices present the supplementary data. **Appendix 3** presents an A3 size geological map of southwest Taiwan fold-and-thrust belt, the area mapped by the Ph.D. candidate. **Appendix 4** presents the complete inputs and outputs of the stress inversion results, and a table with focal mechanism clusters statistics values.

Abstract

Studies of mountain belts worldwide show that along-strike changes are common in their foreland fold-and-thrust belts. These are typically caused by processes related to fault reactivation and/or fault focusing along changes in sedimentary sequences. The study of active orogens, such as Taiwan, can provide insights into how these processes influence transient features such as seismicity, contemporaneous stress and strain fields and topography. In Taiwan, the fold-and-thrust belt comprises a roughly N-S striking, west verging imbricate thrust system that has been developing since the Late Miocene. This fold-and-thrust belt is deforming the sediments from the outer shelf to the base of the slope of the Eurasian continental margin, incorporating structural (e.g., necking zone, extensional fault system, failed rift) and morphological (e.g., the shelf, shelf/slope break, the slope) features of the margin.

In this thesis, we adopt a multidisciplinary approach in order to test the hypothesis of whether or not the inherited structural and morphological architecture of the Eurasian continental margin may be influencing the development of the south central Taiwan fold-and-thrust belt. We first trace regional-scale features from the outer shelf to the slope base of the Eurasian continental margin in the Taiwan Strait into the south central Taiwan fold-and-thrust belt. We then present a regional-scale new surface geological mapping that we combine with P-wave velocity maps and sections, seismicity, and topography data to test the hypothesis in a regional-scale to investigate causal links between these features of the fold-and-thrust belt and those from the margin.

We further test the hypothesis in regional-scale to see whether or not structural and morphological features inherited from the margin are affecting the contemporaneous stress and strain fields in south central Taiwan. The principal stress directions (σ_1, σ_2, and σ_3) are estimated from the inversion of clustered earthquake focal mechanisms and the direction of maximum compressive horizontal stress (S_H) is calculated throughout the study area. From these data the most likely fault plane orientations and their kinematics are inferred. The directions of displacement, compressional strain rate, and maximum shear strain rate derived from GPS data are also calculated and plotted. These are discussed together with the stress inversion results.

Finally, the structure of the area in southwest Taiwan fold-and-thrust belt corresponding to the necking zone is investigated in more detail. We define its structure, presenting new surface geological mapping from which we construct balanced and restored cross-sections and along-strike sections. From these we compile maps of the basal thrust, thrust branch lines and, where possible, stratigraphic cut-offs.

These data show that the most important along-strike change takes place at the eastward prolongation of the upper part of the margin necking zone, where there is an interpreted link between fault reactivation, involvement of basement in the thrusting, concentration of seismicity, and the formation of high topography. The contemporaneous stress and strain fields also show a marked change across

the upper part of the margin necking zone. The direction of S_H changes from north to south across the study area (≈ 8.2 cm/yr toward 306°), with the direction of S_H remaining roughly sub-parallel to the relative plate motion vector in the north, whereas in the south it rotates nearly 45° counter-clockwise. The direction of horizontal maximum compression strain rate (ε_H) and associated maximum shear planes, together with the displacement field display an overall similar pattern between them, although undergoing a less marked rotation.

In the southwest Taiwan fold-and-thrust belt, in the area corresponding to the margin necking zone, the detailed 3D structural analysis shows a less marked but still important along-strike change in the structure than that described for the upper part of the necking zone. This change takes place across a transverse zone that is composed of a suite of structures at the surface that we call the Hsinhua transverse zone. We suggest that this transverse zone coincides with variations in the geometry of the basal thrust which, in turn, has a causal relationship to (possibly fault bounded) basement highs and lows that are inherited from the continental margin.

We interpret all these along-strike changes in the fold-and-thrust belt to be related to the reactivation of east-northeast striking faults inherited from the rifted Eurasian margin. In the upper part of the margin necking zone, the strike-slip reactivation of east-northeast striking extensional faults is causing sigmoidal offset of structures and topographic ridges, and the rotation of the S_H and ε_H directions, together with that of the horizontal displacement field. In the necking zone, the reactivation of east-northeast striking faults is also influencing the development of the fold-and-thrust belt, although with a less marked effect.

CHAPTER 1 Introduction

1.1 Introduction

Along-strike changes occur in the foreland fold-and-thrust belts of many orogens worldwide [e.g., *Thomas, 1985; Perez-Estaun et al., 1997; Duncan et al., 2003; Mouthereau et al., 2006; Yin, 2006; Turner et al., 2010; Arora et al., 2012*]. In particular, the along-strike changes related to lateral structures of thrust systems, such as lateral ramps and tear faults, have been very well documented in fossil and active orogens [e.g., *Albers, 1967; Apotria, 1995; Alvarez-Marron et al., 1995; Mugnier et al., 1999; Hessami et al., 2001; Scott Wilkerson et al., 2002; Koyi et al., 2016*]. In most cases, the along-strike changes in the structural architecture of a fold-and-thrust belt are interpreted to be caused by the reactivation of preexisting faults or changes in sedimentary thicknesses and facies that were inherited from the original continental margin architecture involved in the orogenic system, although generally without specifics of where on the margin these came from or what their original architecture was [e.g., *Thomas, 1985; Pérez-Estaún et al., 1997; Duncan et al., 2003; Mouthereau et al., 2006; Yin, 2006; Turner et al., 2010; Arora et al., 2012*]. While along-strike changes in structural architecture and in sedimentary depositional systems of fold-and-thrust belts are well documented in fossil orogens, investigating those in active orogens can yield important information about how a margins morphology and structure affect not only the structural architecture of a fold-and-thrust belt but also transient features such as seismicity, contemporaneous stress and strain fields, and topography. For example, *Yin [2006], Arora et al., [2012]*, and *Godin and Harris [2014]* have shown how preexisting faults on the Indian Plate that are oriented at a high angle to the structural grain of the foreland of the Himalaya are causing along-strike changes in the structure, seismicity, and topography of its foreland fold-and-thrust belt.

In an active mountain belt, the contemporaneous stress field derived from the stress inversion of earthquake data can provide important information for understanding the role that is played by the reactivation of preexisting faults in along-strike changes in the structure of a fold-and-thrust belt. Furthermore, when combined with GPS data, information about the mechanics and kinematics of the thrust system and its reactivating basement faults can be investigated. For example, based on studies in both active and fossil fold-and-thrust belts, *Tavani et al., [2015*] concluded that, although the stress and strain fields can be locally complex, even during syn-thrusting, a strike-slip stress field is the most common. While they suggest that this conclusion is perhaps somewhat counterintuitive, they interpret it to result from the reactivation of inherited structures. *Célérier [2008]* proposed that the reactivation of faults with near optimal orientations [e.g., *Sibson 1990, 1994; Kelly et al., 1999; Leclère & Fabbri 2013*] controls the state of stress in the crust. Investigating the role played by margin features in the development of along-strike changes is therefore not only of importance for determining structural processes, sediment pathways, and facies distribution in a fold-and-thrust belt, it is also important for understanding, and possibly mitigating, the focusing of geological hazards that are related to seismicity and topographic relief in areas such as Taiwan.

In Taiwan, the main morphological and structural parts of the continental margin, including the shelf, the shelf/slope break (defined as the 200 m bathymetry contour), and the hyperextended part of the margin (starting at about the 3,000 m bathymetry contour [e.g., *McIntosh et al., 2014*]), as well as the extensional fault systems [*Yang et al., 1991; Lin et al., 2003*] that make up the structural necking

zone, are well known [e.g., *Teng et al., 1991; Yang et al., 1991; Lin et al., 2003; Teng and Lin, 2004*] (**Figs. 1.1 and 1.2**). These margin features are all at a high angle to the developing structural grain of the fold-and-thrust belt, which makes it possible to trace them into the fold-and-thrust belt and to readily determine how (or if) they are affecting its structural evolution [e.g., *Suppe, 1986; Mouthereau et al., 1999, 2002; Yang et al., 2007, 2016; Alvarez-Marron et al., 2014; Brown et al., 2017*]. Moreover, Taiwan has a wealth of on-land geological, geophysical, and geodetic data that can be used to trace these margin features into the fold-and-thrust belt [e.g., *Suppe, 1986; Deffontaines et al., 1997, Lacombe et al., 1999; Mouthereau et al., 2002; Yang et al., 2006, 2016; Byrne et al., 2011; Alvarez-Marron et al., 2014; Camanni et al., 2016*]. Therefore, Taiwan is a particularly propitious place to investigate how the structural and the morphological features of a continental margin could possibly contribute to along-strike changes in the structure, seismicity, contemporaneous stress and strain fields, and topography of a fold-and-thrust belt.

The aim of this thesis is to test the hypothesis of whether or not along-strike changes in the south central Taiwan fold-and-thrust belt are being caused by preexisting structures on the Eurasian continental margin that are being incorporated into it, and being reactivated by the deformation that is currently taking place there. The thesis is organized around three publications. The first of these papers sets up the hypothesis and presents evidence for a causal link between the reactivation of the margins structures and along-strike changes in the fold-and-thrust belts of south central Taiwan. The second paper builds on the first by examining whether or not the reactivation of the major structures of the margin are having an effect on the contemporaneous stress and strain fields of this part of the fold-and-thrust belt. Finally, in the third paper we present a detailed structural analysis of the fold-and-thrust belt in southwest Taiwan to further test our hypothesis by examining how the structurally complex necking zone of the margin is affecting the development of the fold-and-thrust belt there. Throughout this thesis, we refer to south central Taiwan when talking about the area from around 24.3° N to 22.2° N (black box in **Figure 1.1** inset), which is the study area of Paper I and Paper II, and southwest Taiwan when referring only to that part of the fold-and-thrust belt from around 23.3° N to 22.2° N (green box in **Figure 1.1** inset), which is the study area of Paper III.

1.2 Objectives

The Taiwan ICTJA research group led by Drs. Joaquina Alvarez-Marrón and Dennis Brown has been studying the Taiwan fold-and-thrust belt for several years. Recently, their work has focused on the investigation of how the inherited structural and morphological architecture of the Eurasian continental margin may be influencing the development of the fold-and-thrust belt in Taiwan [*Brown et al., 2012; Camanni et al., 2014a, 2014b, 2016; Alvarez-Marron et al., 2014; Camanni, 2014*]. These previous studies, located in the central part of Taiwan, focused on the influence of the inherited structures from the shelf to the upper slope of the continental margin. The research presented in this thesis expands on this theme by examining how these inherited structures may be affecting, in a regional-scale, the structure of the Taiwan active fold-and-thrust belt, as well as transitory features such as the seismicity, the contemporaneous stress and strain fields, and the topography. It then focuses on the detailed structure of the fold-and-thrust belt in southwest Taiwan to investigate how these inherited faults are affecting the structure there.

The specific objectives of the thesis are:

- Determine the 3D geological structure and kinematics of southwest Taiwan fold-and-thrust belt with special emphasis on defining its along-strike changes.
- Investigate the relationship between transient features such as seismicity and topography with the geological structure and its along-strike changes.
- Investigate whether or not a causal relationship can be established between the along-strike structural changes and related transient features with the reactivation of inherited structures.
- Determine how (or if) the preexisting structures of the margin affects the contemporaneous stress and strain fields derived from the seismicity and GPS data.
- Determine the orientation and kinematics of the faults that are likely to have been active at depth.
- Test the objective indicated above by determining the influence of inherited structures from the Eurasian continental margin in the structural evolution of the fold-and-thrust belt in Taiwan.

1.3 Published articles

The research involved in this thesis has resulted in three new publications in science citation index journals. These are the result of collaboration with several international co-authors. They can be found in Appendix 1. The three papers investigate several aspects of the structure and kinematics of the fold-and-thrust belt and focus on testing the hypothesis stated in the introduction.

In **Paper I**, the ideas behind the hypothesis are developed. The regional-scale features of the Eurasian continental margin in the Taiwan Strait are traced into south central Taiwan. Then, the newly mapped surface geology of the south central Taiwan fold-and-thrust belt is integrated with P-wave velocity maps and sections, seismicity, and topography. This paper concludes that, on a regional-scale, the most important along-strike change of the fold-and-thrust belt takes place at the eastward prolongation of the upper part of the margins necking zone. Less pronounced but also important along-strike changes in the fold-and-thrust belt structure are taking place in relation with the reactivation of faults from the faulted necking zone. This paper further suggests that there is a causal link between fault reactivation, involvement of basement in the thrusting, concentration of seismicity, and the formation of high topography.

In **Paper II**, we test further the hypothesis stated in Paper I by examining whether or not structural and morphological features inherited from the Eurasian continental margin are affecting the contemporaneous stress and strain fields in south central Taiwan. We estimate the principal stress directions (σ_1, σ_2, and σ_3) from the inversion of clustered earthquake focal mechanisms and calculate the direction of maximum compressive horizontal stress (S_H) throughout the study area. From these data we infer the most likely fault plane orientations and their kinematics. We then discuss the results of the stress inversion together with the directions of displacement, compressional strain rate, and maximum shear strain rate derived from GPS data. These data show that there is a marked contrast in the direction of S_H from north to south across the study area, with the direction of S_H remaining roughly sub-parallel to the relative plate motion vector (≈ 8.2 cm/yr toward 306°) in the north, whereas in the south it rotates nearly 45° counterclockwise. The direction of horizontal maximum compression strain rate (ε_H), together with the displacement field display an overall similar pattern between them, although undergoing a less marked rotation. This paper concludes that the southward change in the S_H, ε_H, together with that of the horizontal displacement field is related to the reactivation of east-northeast striking faults inherited from the rifted Eurasian margin and to the shelf/slope break.

In **Paper III**, we describe the detailed structure of the southwest Taiwan fold-and-thrust belt, where the margin faulted necking zone, the shelf/slope break, and the slope are involved in the deformation. For this purpose, several field campaigns were carried out to map the surface structure in the southwestern part of the island. The paper presents the new geological map, from which we constructed balanced and restored cross-sections, and along-strike sections. From these we compile maps of the basal thrust, thrust branch lines, and where possible stratigraphic cut-offs. The structure in the subsurface and beneath the basal thrust is interpreted by the integration of a P-wave velocity model with the structural data. From these, we obtain the 3D structure of the fold-and-thrust belt, and show that there is a significant along-strike change in the structure. This takes place across a transverse zone

composed of a suite of structures at the surface. We suggest that this transverse zone coincides with variations in the geometry of the basal thrust which, in turn, has a causal relationship with (possibly fault bounded) basement highs and lows that are inherited from the continental margin.

1.3.1 Ph.D. candidate's contribution

Paper I: Brown et al [2017]

Ph.D. candidate contribution:

- Carried out structural mapping fieldwork;
- Constructed one of the geological cross-sections in collaboration with Ph.D. supervisors;
- Produced figures of the seismicity, the P-wave velocity slices and vertical sections from the available tomography and the shadow relief map from the topography;
- Reviewed the text.

Paper II: Biete et al., [in press]

Ph.D. candidate contribution:

- Analyzed the earthquake focal mechanism data, set up the binning system and performed the stress inversion during a three month stay under the supervision of Dr. Björn Lund at the Earth Sciences Department of the University of Uppsala, Sweden;
- Analyzed the GPS data, plot the displacement vectors and determined the strain field and rates;
- Did the illustrations;
- Wrote the manuscript with the supervision of the Ph.D. supervisors.

Paper III: Biete et al., [2018]

Ph.D. candidate contribution:

- Carried out structural mapping fieldwork;
- Constructed the balanced and restored cross-sections, the along-strike sections, the 3D basal thrust and cut-off maps in collaboration with Ph.D. supervisors;
- Did the illustrations;
- Wrote the manuscript with the supervision of the Ph.D. supervisors.

1.4 Geological Background

The Taiwan orogen is evolving as a result of the latest Miocene to present collision between the Philippine Sea Plate and the Eurasian Plate [*Suppe, 1981; Ho, 1986*]. The Philippine Sea Plate is moving c. 8.3 cm/yr towards 306° with respect to Eurasia [*Yu et al., 1997*] (**Figs. 1.1 and 1.2A**). Within this framework, the Eurasian Plate is subducting beneath the Philippine Sea Plate, causing the oblique collision between the roughly north-south trending Luzon Arc on the Philippine Sea plate with the Eurasian continental margin (**Figs. 1.1 and 1.2A**).

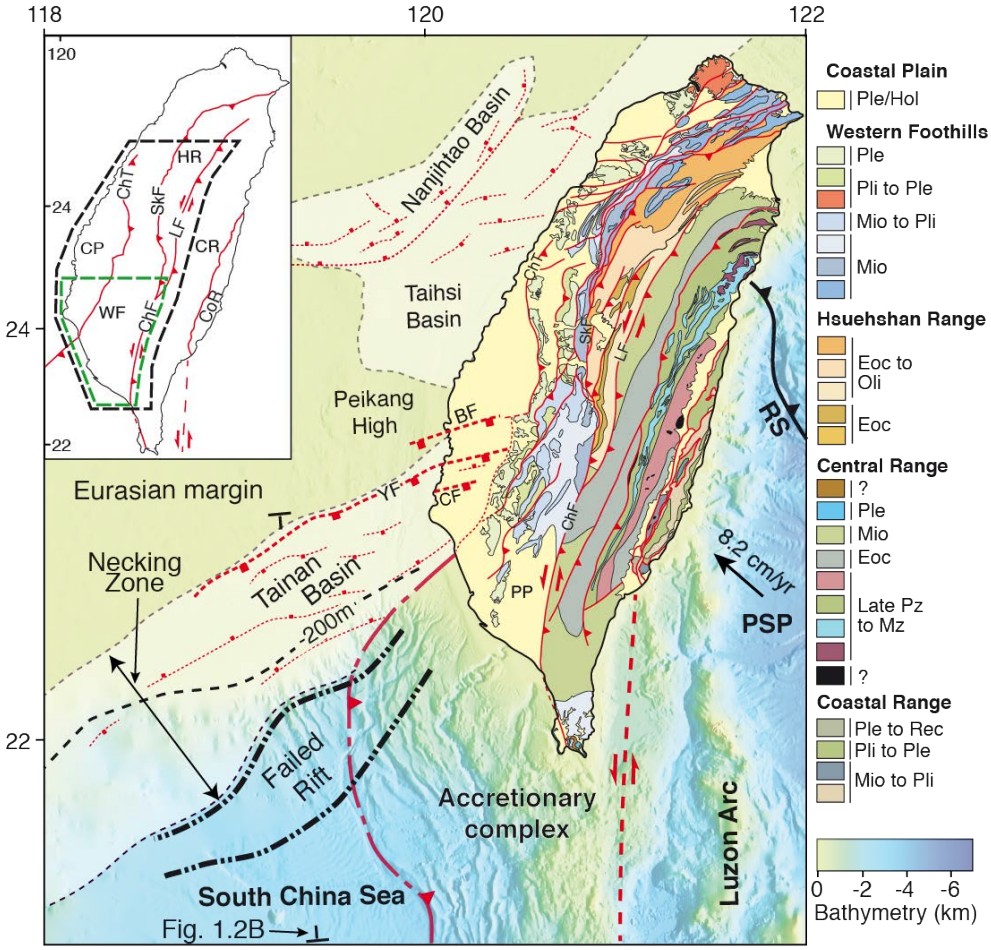

FIGURE 1.1: Tectonic setting of the Taiwan arc-continent collision orogen with the location of the Taiwan island in relation with the Luzon arc and its accretionary complex, the Ryukyu subduction zone (RS) and major basins of the Eurasian margin. A simplified geological map is shown in the Taiwan island [after *Chen et al., 2000*]. The Tainan, Taihsi and Nanjihtao basins offshore Taiwan include significant extensional structures. The structural (necking zone, failed rift, extensional basins, major faults) and morphological features (shelf/slope break at 200 m water depth) of the Eurasian continental margin are shown. The location of the schematic cross-section of the margin shown in **Figure 1.2B** is also given. The convergence vector of c. 8.2 cm/yr of the Philippine sea plate is given. RS = Ryukyu subduction zone, PPS = Philippine sea plate, PP = Pingtung Plain, ChT = Changhua thrust, LF = Lishan fault, SkF = Shuilikeng fault, ChF = Chauchou fault, BF = B fault, YF = Yichu fault, CF= Chiali fault. The inset shows the tectono-stratigraphic units of the Taiwan orogen, and the study area of Paper I and II in black box called south central Taiwan fold-and-thrust belt, and the study area of Paper III in green box called southwest Taiwan fold-and-thrust belt. The green box corresponds to the area mapped by the Ph.D. candidate with her supervisors. CP = Coastal Plain, WF = Western Foothills, HR = Hsuehshan Range, CR = Central Range, CoR = Coastal Range.

The Taiwan mountain belt is divided into several roughly N-S striking tectono-stratigraphic units (**Fig. 1.1**) [e.g., *Ho, 1988*] that, from west to east are: the Coastal Plain (CP), the Western Foothills (WF), the Hsuehshan Range (HR), the Central Range (CR) and the Coastal Range (CoR). The eastern Central Range and the Coastal Range (CoR) are outside the objectives of this thesis and a detailed geological description of them is out of its scope. For the sake of simplicity, in this thesis the Coastal Plain, Western Foothills, and Hsuehshan Range are grouped together under the term fold-and-thrust belt. In the north, the Western Foothills and the Hsuehshan Range are juxtaposed along the Shuilikeng fault (SkF), (**Fig. 1.1**), while southward the Chouchou fault (ChF) juxtaposes the Western Foothills against the Central Range. The Hsuehshan Range is juxtaposed against the Central Range by the Lishan fault (LF). The Chaochou and Lishan faults comprise the eastern boundary of the fold-and-thrust belt, and here after are called the Chouchou-Lishan fault system (**Fig. 1.1**). The western boundary of the fold-and-thrust belt is generally interpreted to be the partially buried trace of the Changhua thrust (ChT) (CT; **Fig. 1.5**; see also, *Yu et al., 1997; Shyu et al., 2005; Yang et al., 2007; Rodriguez-Roa & Wiltschko, 2010; Ching et al., 2011*). Below we give a brief description of the geological background of the Eurasian continental margin (section 1.4.1) followed by an overview of the geology of south central Taiwan fold-and-thrust belt (section 1.4.2).

1.4.1 Eurasian continental margin

The part of the Eurasian continental margin that is currently involved in the deformation in south central Taiwan has gone through several tectonic events that led to the pre-collisional configuration of the margin. The margin evolved from a sub-continental subduction system in the Late Cretaceous [e.g., *Li et al., 2007, Lan et al., 2008*] to a rifting margin by the Early Eocene, with sea-floor spreading starting in the South China Sea by the late Early Oligocene [e.g., *Briais et al., 1993; Sibuet and Hsu, 1997; Hsu et al., 2004*]. Throughout this thesis, the pre-Eocene rocks are defined as the basement of the continental margin, following the scheme of *Brown et al., [2012], Alvarez-Marron et al., [2014]* and *Camanni et al., [2016]*. Today's shelf/slope break is defined as the 200 m bathymetry contour (**Figs. 1.1** and **1.2**). Moreover, throughout the thesis, we use the structural term necking zone [e.g., *Mohn et al., 2012*] that refers to the region where the crust thins from the shelf to the South China Sea ocean basin (**Figs. 1.1** and **1.2B**). The upper part of the necking zone roughly coincides with the northern bounding-fault system of the Tainan Basin (a Middle Miocene-aged extensional basin that developed on the outer part of the margin) [e.g., *Lee et al., 1993; Lin et al., 2003; Ding et al., 2008*]. A variety of geophysical data show that the crustal thickness of the Eurasian shelf entering into the Taiwan orogen is about 30 ± 5 km [*Yeh et al., 1998; Kim et al., 2004; Kuo-Chen et al., 2012; Huang et al., 2014; Wu et al., 2014; Chen et al., 2016*]. Reflection and wide-angle seismic data show a thinning of the continental crust across the necking zone, from approximately 30 km on the shelf to approximately 18 km along the more than 300 km wide hyperextended distal part of the margin (**Figs. 1.1** and **1.2B**) [*Chen and Yang, 1996; Li et al., 2007; Lin et al., 2008; Huang et al., 2012; Yeh et al., 2012; Deng et al., 2012; McIntosh et al., 2013, 2014; Lester et al., 2014*]. *Yeh et al., [2012], McIntosh et al., [2014],* and *Lester et al., [2014]* interpret a failed rift to occur at the base of the slope (**Fig. 1.1** and FR in **Fig. 1.2B**). The continent to ocean transition occurs south of the area shown in **Figures 1.1** and **1.2A** [e.g., *Nissen et al., 1995; Tsai et al., 2004; Zhao et al., 2010; Deng et al., 2012; Yeh et al., 2012; McIntosh et al., 2013; Lester et al., 2014*].

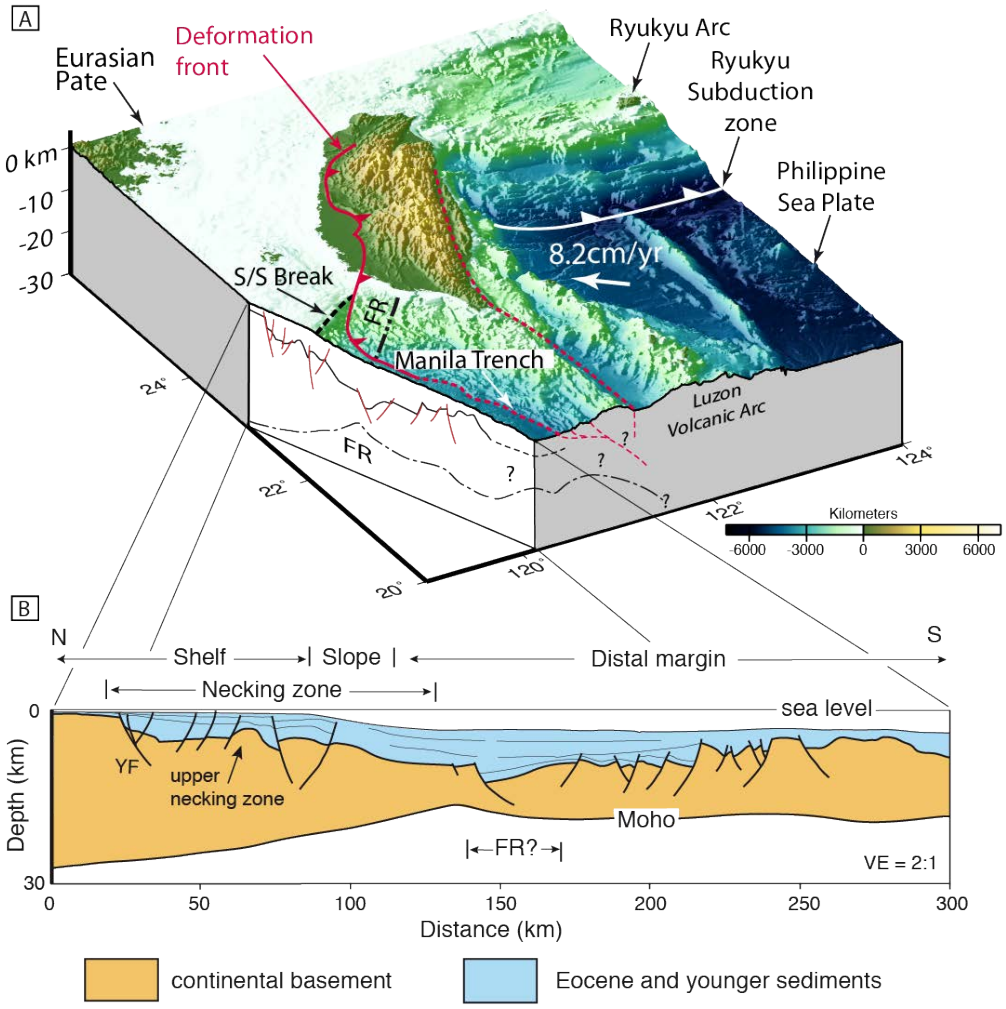

FIGURE 1.2: A) 3D topographic view of the tectonic setting of the Taiwan arc-continent collision orogen with the location of the Taiwan island in relation with the Luzon arc, the Manila trench and the Ryukyu subduction zone. Also shown is the location of **Figure B** with a schematic drawing of it. The structure depicted in the E-W oriented vertical section of the 3D view is simplified from *McIntosh et al., [2005; 2013]* and *Eakin et al., [2014]*. S/S Break = Shelf/slope break. The vertical exaggeration is 3:1. B) A schematic cross-section of the continental margin to the southwest of Taiwan. It gives the terminology for the margin used in the text. The location of the section is also shown in **Figure 1.1**. The structure depicted in the upper crust of the shelf area is from *Lin et al., [2003]*, whereas that in the slope and distal margin is simplified from *Yeh et al., [2012]* and *Lester et al., [2014]*. The moho depth in the distal margin is from *Lester et al., [2014]*, whereas that beneath the shelf and slope area is from *Tsai et al., [2004]*. The continent to ocean transition lies to the south of this diagram. YF = Yichu fault. FR = failed rift of *Yeh et al., [2012]*, *Lester et al., [2014]*, and *McIntosh et al., [2014]*. The vertical exaggeration is 2:1.

The Eurasian margin registered several extensional periods from the Early Eocene [e.g., *Lin & Watts, 2002; Lin et al., 2003; Teng & Lin, 2004; Huang et al., 2012*]. During the Eocene several roughly northeast trending basins (e.g., Taishi and the Nanjihtao basins) developed and were filled with up to 5 km of sediments [*Hsu et al., 2001; Lin & Watts 2002; Lin et al., 2008; Huang et al., 2012; Yeh et al., 2012*]. Of these, the Taihsi Basin is now involved in the Taiwan orogen (**Fig. 1.1**), with its eastern flank, the Hsuehshan Trough of *Teng et al., [1991]* and *Teng and Lin [2004]*, now forming the Hsuehshan Range (**Fig. 1.1**). During the Miocene, several extensional events occurred in the outer part of the margin shelf that resulted in an array of east-northeast striking extensional faults (e.g., B, Yichu, etc. **Fig. 1.1**) and the formation of the Tainan Basin (**Fig. 1.1**) [e.g., *Yang et al., 1991; Lin &*

Watts 2002; Lin et al., 2003; Ding et al., 2008]. The sediments and faults associated with the Tainan Basin have been traced from the offshore western Taiwan onshore through the undeformed foreland [*Lin et al., 2008; Yang et al., 2006; 2016*] and into the fold-and-thrust belt of south central Taiwan (**Fig. 1.1**) [e.g., *Lin et al., 2003; Rodriguez-Roa & Wiltschko 2010; Alvarez-Marron et al., 2014; Yang et al., 2016; Brown et al., 2017*].

1.4.2 Geology of the south central Taiwan fold-and-thrust belt

1.4.2.1 Stratigraphy

In this thesis, we use the chrono-stratigraphic nomenclature of *Brown et al., [2012]* and *Alvarez-Marron et al., [2014]* (**Fig. 1.3**). For the Miocene through to Holocene sedimentary rocks, this scheme follows the stratigraphic correlation of *Shea et al., [2003]*. We have subdivided a thick, latest Miocene through to Late Pleistocene-age, unit of mudstone with ribbons of sandstone that crops out in the southwestern part of the study area (the Gutingkeng Fm: **Fig. 1.3**) using the chronological divisions for it that are provided by *Horng and Shea [1994]* and *Horng [2014]*. The stratigraphic thickness for each formation is, where possible, taken from published borehole data [**Fig. 1.4**; *Chang, 1963; Chiang, 1971; Chou, 1971; Shaw, 1996; C.-H. Tang, 1977; Yuan & Huang, 1985; Huang et al., 2004; Tensi et al., 2006*] and isopach maps [*Chou, 1980; Shaw, 1996; Lin et al., 2003; Tang, 1977*] within the study area, and from the geological map (**Fig. 1.5**).

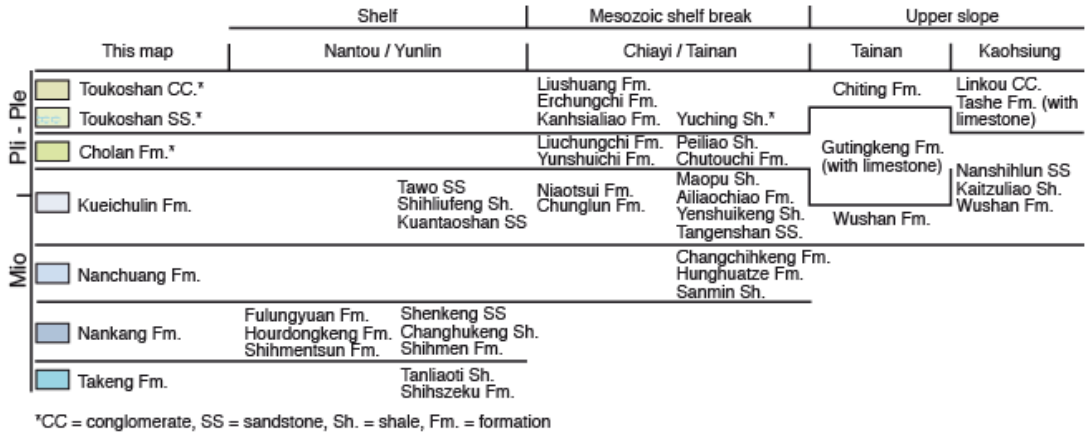

FIGURE 1.3: Chrono-stratigraphic correlation chart used in the mapping. It is based on *Shea et al., (2003)*. The Gutingkeng Fm chronological divisions are based on *Horng and Shea (1994)* and *Horng (2014)*.

In this thesis, we have defined the basement as all pre-Eocene rocks upon which the Cenozoic Eurasian continental margin was built. Mesozoic rocks do not crop out in the fold-and-thrust belt. However, they crop out extensively in the Central Range where they comprise predominantly marbles and schists [*Ernst, 1983; Stanley et al., 1981; Ho, 1988; Lan et al., 2008*], and these rocks may make up part of the basement in western Taiwan and in the Taiwan Strait [*Jahn et al., 1992*]. In south central Taiwan, weakly metamorphosed siliciclastic rocks and marble that have been interpreted to be Mesozoic in age have been intersected in two boreholes (CLI-1 and MLN-1) on-land (**Fig. 1.4**) and several boreholes offshore western Taiwan [*Chiu, 1975; Ho, 1988; Jahn et al., 1992; Shaw, 1996*]. We therefore interpret these types of lithologies, capped locally by weakly metamorphosed clastic

rocks, to comprise the basement beneath the study area. Within south central Taiwan, this basement can be unconformably overlain by Eocene through to Early Miocene rocks, since boreholes indicate that neither the Eocene nor the Oligocene rocks are present everywhere [*Chiu, 1975; Ho, 1988; Shaw, 1996*; **Fig. 1.4**].

The outcropping stratigraphy of the fold-and-thrust belt (Coastal Plain, Western Foothills and Hsuehshan Range) consists of Eocene- through Holocene-age siliciclastic rocks and unconsolidated sediments [*Chiu, 1975; Covey, 1986; Ho, 1988; Teng, 1992; Shaw, 1996; Chen et al., 2001; Lin et al., 2003; Huang et al., 2012].* Eocene-age synrift siliciclastic rocks crop out extensively in the Hsuehshan Range. They are composed of conglomerates, sandstones and shales, are variably metamorphosed and were deposited in what is commonly interpreted to have been the rift-related Hsuehshan Trough (or Basin) [*Ho, 1988; Teng et al., 1991; Lin et al., 2003; Teng and Lin, 2004; Huang et al., 2012*]. In the Hsuehshan Range they are unconformably overlain by late Early Oligocene postrift siliciclastic rocks comprised of predominantly interbedded sandstones and shale [*Lee, 1979; Lin et al., 2003; Huang et al., 2012]*. These Oligocene rocks are interpreted to be the rift-drift unconformity and to reflect thermal subsidence of the rifted margin following the opening of the South China Sea [*Lin et al., 2003; Teng and Lin, 2004; Huang et al., 2012*].

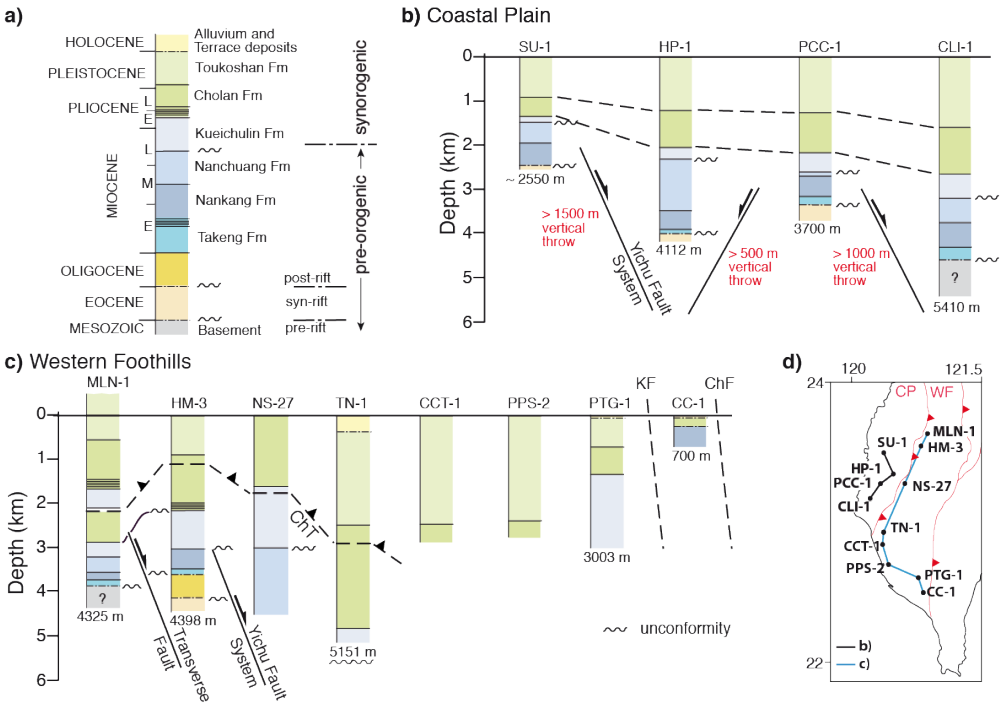

FIGURE 1.4: General stratigraphy and tectonostratigraphic units showing the names of formations used in this thesis. (b) Stratigraphic correlation of boreholes SU-1, HP-1, PCC-1, and CLI-1 along the Coastal Plain (borehole data from *Shaw, 1996; Tang, 1977; Tensi et al., 2006*). The interpreted approximate vertical throw accumulated by structures between boreholes is shown. (c) Stratigraphic correlation of boreholes MLN-1, HM-3, NS-27, TN-1, CCT-1, PPS-2, PTG-1, and CC-1 from the frontal part of the fold-and-thrust belt (borehole data from *Chiang, 1971; Chou, 1972; Huang, 1984; Huang et al., 2004; Tang, 1977, Yang et al., 2007*). The location of the basal thrust in MLN-1, HM-3, NS-27, and TN-1 is marked as ChT (Changua thrust). (d) Inset indicates location of the boreholes also shown in map of **Figure 1.5**. CP = Coastal Plain; WF = Western Foothills.

In the Western Foothills, Eocene-age volcanoclastic rocks crop out locally in the north, where they are unconformably overlain by Miocene-age siliciclastic rocks (**Fig. 1.5**) [e.g., *Ho, 1988; Castell-*

tort et al., 2010; Brown et al., 2012]. Southward of this, Eocene-age rocks do not crop out, although, they have been intersected in several boreholes on-land and offshore [**Fig. 1.4 and 1.5**; *Chang, 1963; Chiang, 1971; Chou, 1971; Tang, 1977; Shaw, 1996; Yuan & Huang, 1985; Huang et al., 2004; Tensi et al., 2006*]. In these boreholes, the Eocene and Oligocene rocks each comprise up to several hundred meters of predominantly sandstone and shale, although they may be thicker in certain areas (**Fig. 1.4**).

The Miocene is divided in four crono-stratigraphic units, the Early to Middle Miocene Takeng and Nankang formations, the Middle to Late Miocene Nanchuang Fm and the Late Miocene to Early Pliocene Kueichulin Fm (**Fig. 1.3 and 1.4a**). From north to south, there is a growing importance of these formations in the outcropping stratigraphy. The Early to Middle Miocene Takeng and Nankang formations predominantly comprise sandstones and shale. They crop out in the northeast of the Western Foothills and several boreholes intersect them in the southwest, showing thicknesses from several hundred meters to nearly 1000 m [*Shaw, 1996; Yang et al., 2014*; **Fig. 1.4 and 1.5**]. The Middle to Late Miocene Nanchuang Fm is made up of thin- to thick-bedded sandstone intercalated with shale. From the on-land prolongation of the upper necking zone southward its thickness increases drastically from being absent in the north of the Western Foothills to more than 2000m in the south (**Fig. 1.4 and 1.5**). These changes in thickness are interpreted to be related to deposition of the Nanchuang Fm in marine extensional basins during the Middle Miocene development of the Tainan Basin [*Lin et al., 2003; Yang et al., 2006*]. The Late Miocene to Early Pliocene synorogenic Kueichulin Fm unconformably overlies the Nankang formation in the north of the Western Foothills and southward unconformably overlies the Nanchuang formation [*Lin et al., 2003*].

The Kueichulin Fm comprises thin- to very thick-bedded muddy sandstone and sandy mudstone. Based on refleccion seismic data in the Taiwan Strait, the Kueichulin Fm has been shown to be unconformable on the older Miocene formations. This unconformity is interpreted to be related to plate flexure caused by orogenic loading [*Lin and Watts, 2002; Tensi et al., 2006*]. The appearance of the Kueichilin Fm is taken to mark the onset of synorogenic sedimentation in the foreland basin [*Lin et al., 2003]*. This is in contrast to *Covey [1986], Teng [1987]* and *Hong [1997]*, who interpreted the onset of the synorogenic sediments during the Early Pliocene-age due to the occurrence of slate clasts at the base of the Cholan formation. The Kueichulin Fm predominantly crops out in the central and south-east of the Western Foothills with its thickness increasing significantly from east to west and from north to south, with thickness varying from ~150 m to more than 3000 m (**Figs. 1.4** and **1.5**) [*Chiang, 1971*].

The Early Pliocene to Early Pleistocene synorogenic Cholan Fm conformably overlies the Kueichilin Fm. It is made up of interbedded mudstone, shale, and muddy sandstone, and crops out extensively in the west of the Western Foothills reaching more than 4000 m in thickness (**Figs. 1.4** and **1.5**).

The Early Pleistocene synorogenic Toukoshan Fm conformably overlies the Cholan Fm. It comprises a coarsening upwards sequence of thick-bedded muddy sandstones and shales that, in its upper part, is interfingered with fluvial conglomerates. The Toukoshan Fm crops out predominately in the west of the Western Foothills, it contains a number of regional-scale uncorformities and can reach

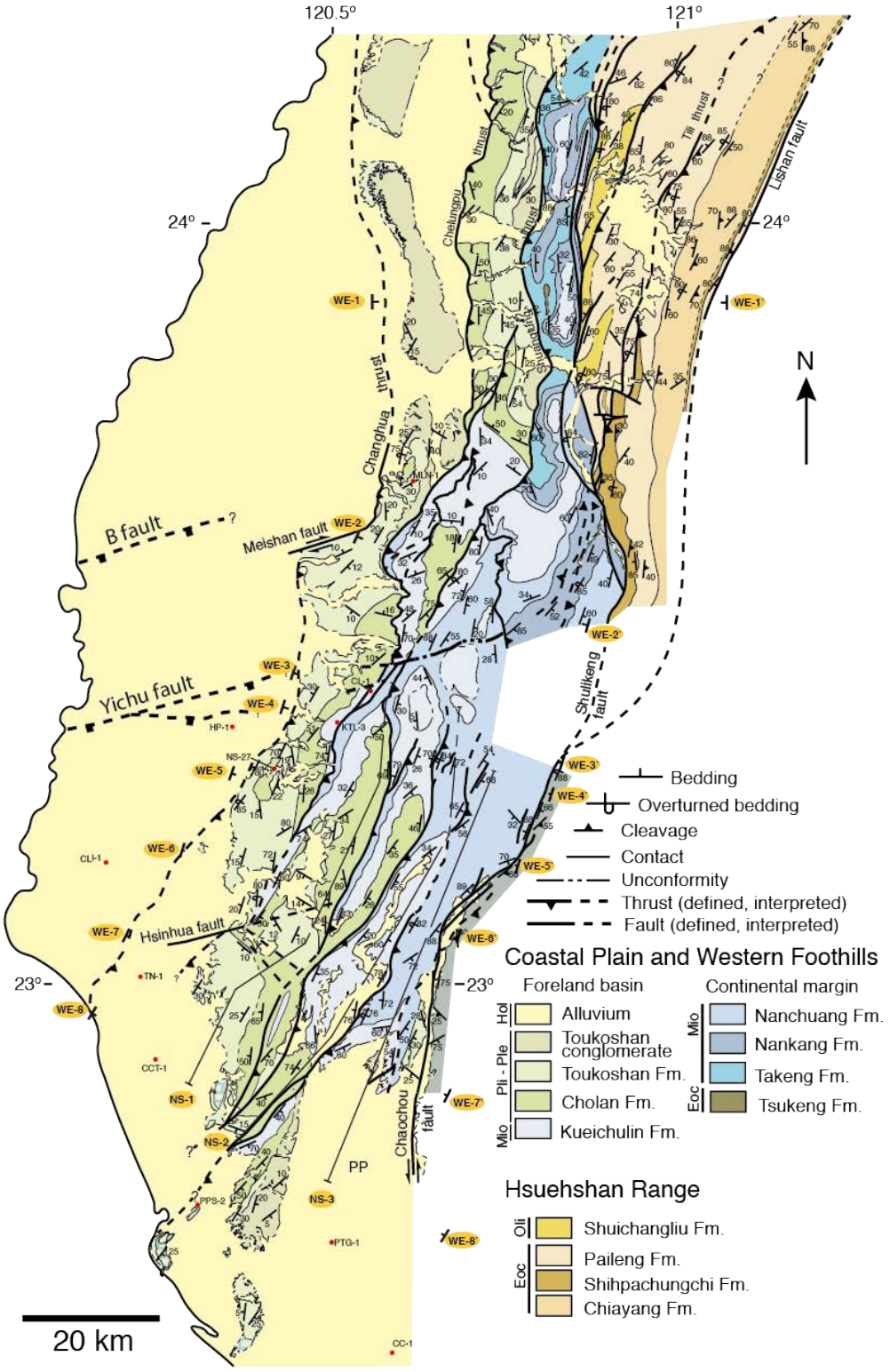

FIGURE 1.5: Geological map of the south central Taiwan fold-and-thrust belt with representative structural data. The locations of the west-east (WE-1 through -8) geological cross-sections and north-south (NS-1 through -3) along-strike sections used in the Papers are shown. The nomenclature used for the geological cross-sections is different from that of chapter 2. In section 2.1 cross-sections WE-1, -2 and -6 are labeled by letters A to C as in published paper I. In section 2.3, cross-sections WE-3 to WE-8 are labeled by letters A to F as in published paper III. The stratigraphic scheme used in the map is given in **Figure 1.3**. Boreholes used in **Figure 1.4** are shown. PP = Pingtung Plain.

more than 3000 m in thickness (**Figs. 1.4** and **1.5**). The Toukoshan Fm is overlain by Holocene-age fluvial gravels that, in some places, can reach several hundred meters in thickness.

1.4.2.2 Structure

The south central Taiwan fold-and-thrust belt is currently forming as the result of deformation and uplift of Eurasian margin basement rocks and Eocene to Holocene margin, and foreland basin sediments [e.g., *Suppe, 1980; Yue et al., 2005*]. The tip line of the fold-and-thrust belt is interpreted to be the Changhua thrust. To the west of the Changhua thrust, however, there is widespread seismicity in southwest Taiwan, indicating that deformation is also taking place beneath much of the Coastal Plain [e.g., *Shyu et al., 2005; Camanni et al., 2016*]. Along its eastern flank, the fold-and-thrust belt is juxtaposed against the Central Range along the oblique thrust to sinistral strike-slip Chaochou-Lishan fault system. This fault system has been interpreted to penetrate into the middle and even the lower crust [*Wiltschko et al., 2010, Tang et al., 2011, C. Huang & Byrne 2014, Kuo-Chen et al., 2015*] (**Figs. 1.5**).

The fold-and-thrust belt has a roughly north-south structural grain that becomes more northeast-southwest oriented in the south (**Fig. 1.5**). At the surface, it comprises Eocene rocks through to recent Holocene sediments, and is interpreted as a roughly west-verging imbricate thrust system [e.g., *Suppe, 1976, 1981; Yue et al., 2005; Brown et al., 2012; Alvarez-Marron et al., 2014*]. In the west and south, the thrust system is mostly covered by Holocene sediment (**Fig. 1.5**). Major along-strike changes in the structure are described in the foreland fold-and-thrust belt [e.g., *Yang et al., 2006, 2007, 2016; Mouthereau & Lacombe, 2006; Rodriguez-Roa & Wiltschko, 2010; Alvarez-Marron et al., 2014*]. These include changes in the strike of thrusts and fold traces, the elevation of thrusts and stratigraphic contacts, and the presence of east-northeast striking dextral strike-slip faults (e.g., Meishan and Hsinhua faults: **Fig. 1.5**). The thrust system is interpreted to be developing above a basal thrust that dips overall gently eastward at about 4° to 6° [e.g., *Brown et al., 2012; Alvarez-Marron et al., 2014*]. The basal thrust is commonly interpreted to ramp steeply down into the basement along the Shuilikeng fault in the north and in the Chaochou fault in the south [e.g., *Mouthereau et al., 2002; Brown et al., 2012; Alvarez-Marron et al., 2014*]. Some authors, on the contrary, suggest that it extends eastward beneath the Hsuehshan Range and the Central Range to ramp down into the middle crust beneath the Coastal Range [e.g., *Suppe 1976; 1980b; 1981; Ding et al., 2001; Carena et al., 2002; Yue et al., 2005; Malavielle & Trullenque, 2009*]. Beneath the Coastal Plain and Western Foothills there is widespread seismicity till more than 45 km depth, indicating that both, the thrust system and its footwall are active [e.g., *Wu et al., 1997, 2014; Lacombe and Mouthereau, 2002; Yue et al., 2005; Camanni et al., 2016*].

In the northeast, the fold-and-thrust belt includes the Hsuehshan Range that is comprised of variably metamorphosed Eocene rocks unconformably overlain by Oligocene rocks (**Fig. 1.5**) [*Lin et al., 2003; Brown et al., 2012*]. Its structure is that of a thrust system with roughly north-south structural grain, where its eastern and western boundaries, the Shuilikeng and Lishan faults respectively, are interpreted to be active steeply dipping faults rooted into the middle and, perhaps even the lower crust [e.g., *Wu et al., 1997; Brown et al., 2012; Alvarez-Marron et al., 2014; Camanni et al., 2014b;*

Kuo-Chen et al., 2015]. The structure of the Hsuehshan Range and its steeply dipping bounding faults suggests that this region can be interpreted as a pop-up structure [e.g., *Brown et al., 2012; Camanni et al., 2014a; 2014b*], related with the reactivation of preexisting Eurasian continental margin structures [e.g., *Mouthereau et al., 2002; Mouthereau & Lacombe, 2006; Byrne et al., 2011; Brown et al., 2012*]. Internally, the Hsuehshan Range is comprised of two distinct thrust sheets; an eastern one with a penetrative southwest dipping cleavage and a western one without a cleavage [*Brown et al., 2012*]. These are juxtaposed across the Tili thrust (**Fig. 1.5**).

1.5 Methodology & data sets

This thesis adopts a multidisciplinary approach that integrates several data sets and methods. For this thesis, we carried out geological mapping in the fold-and-thrust belt in southwest Taiwan. This mapping is the southward continuation of earlier mapping carried out by the ICTJA group. It provides the primary data set that is used to interpret the 3D structure in this part of the fold-and-thrust belt, and is incorporated with earlier mapping to the north to investigate along-strike changes in structure, seismicity, topography, contemporaneous stress and strain fields (**Fig. 1.1**). The 3D structure is obtained by constructing a set of transverse balanced and restored geological cross-sections and strike-parallel sections. These sections are constructed iteratively along with stratigraphic cut-off maps, thrust branch line maps, and a contour map of the basal thrust. The interpretation of the structure at depth is aided by the use of several geophysical datasets. These include the local tomography 3D P-wave velocity model of *Kuo-Chen et al [2012]*, a seismicity data set of 96,907 earthquakes, and 2,465 earthquake focal mechanisms. The contemporaneous stress field is determined from earthquake focal mechanisms. GPS data is used to gain insight into fault kinematics and current strain field.

Two Digital elevation models (DEM), one with 40 m and another of 20 m resolution, are available from the Taiwan Ministry of the Interior. These are used to build shaded relief topography maps in ArcGIS.

A brief description of the different data sets and the methodologies that we use in this thesis is given in the sections that follow. Finally, an overview of the uncertainties assumed as a result of using data sets and methodologies with inherent accuracy errors is presented.

1.5.1 Geological mapping

The geological map in **Figure 1.5** shows the simplified version of the one used in this thesis. It covers the study area that we call south central Taiwan fold-and-thrust belt (**Fig. 1.1**) and comprises an area of approximately 14,000 km^2 [*Brown et al., 2012; Camanni et al., 2014a; Alvarez-Marron et al., 2014; Camanni, 2014*]. Mapping carried out by the Ph.D. candidate covers the southwestern part of the fold-and-thrust belt (green box in inset of **Fig. 1.1**). A simplified version of this map is presented in section 2.3, and an A3 size version with the complete set of structural data is included in Appendix 3.

The 1:50,000 geological maps of the Central Geological Survey of Taiwan were used as base maps. The field mapping involved the collection of structural data such as bedding, fault planes, local cleavage and fold axes. Where possible kinematic indicators such as slicken-lines and grooves are also measured. Basic lithological observations are also made.

1.5.2 Borehole data set & stratigraphic correlations

In order to have better control on the subsurface location and thickness of the stratigraphic units, we have compiled information from published borehole data and stratigraphic thickness maps. The nomenclature assigned to the chrono-stratigraphic units of the boreholes is that of **Figure 1.3**. The

boreholes are assumed to be vertical, therefore, we might be assuming some errors in the depth of the horizons. The locations of the boreholes might have errors as well due to the poor resolution of some of the location maps from which these data were extracted. From these boreholes, the most representative ones for the study area are selected and two north to south stratigraphic correlations were made (**Fig. 1.4b and c**). One stratigraphic correlation is located in the foreland basin (Coastal Plain) (**Fig. 1.4b**), and the second one is in the frontal part of the foreland fold-and-thrust belt (west of Western Foothills) (**Fig. 1.4c**). Where possible, we have indicated interpreted extensional structures responsible for stratigraphic changes between the boreholes. The Changhua thrust is also correlated across boreholes in the north of the Western Foothills (**Fig. 1.4b**).

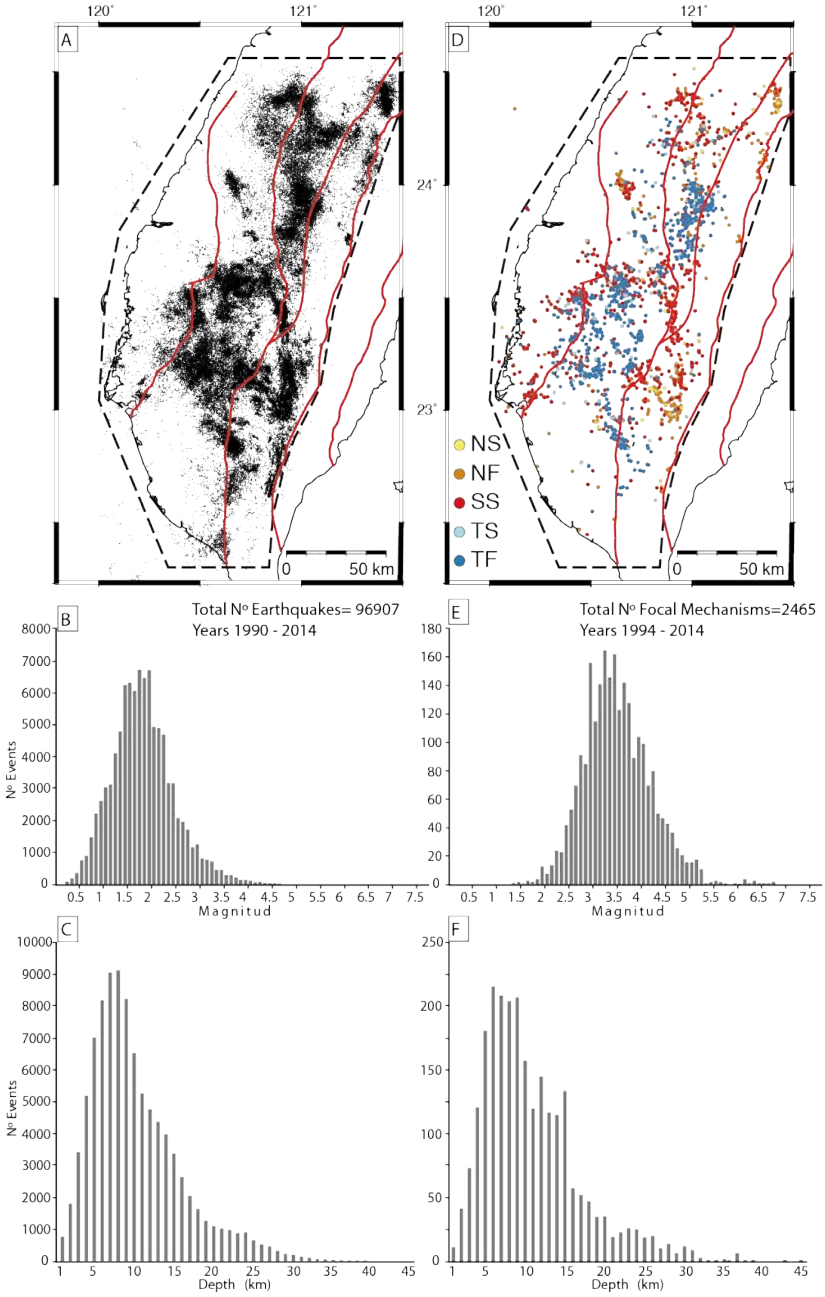

FIGURE 1.6. A) Seismicity data set distribution. B) Seismicity magnitude distribution histograms. C) Seismicity depth distribution histograms. D) Focal mechanisms data set distribution and faulting types. The faulting types follow the classification scheme of *Zoback [1992]*. E) Focal mechanisms magnitude distribution histograms. F) Focal mechanisms depth distribution. The location of the study area is shown with a black dashed line.

1.5.3 3D structural interpretations

To interpret the structure, balanced geological cross-sections were constructed following the standard construction techniques [*Dahlstrom, 1969; Hossack, 1979; De Paor, 1988*]. The orientation of the cross-sections was chosen to be roughly perpendicular to the regional strike of structures (bedding, thrusts, and fold axes), and plane strain was assumed along these sections. Where possible, additional constraints relative to the structure and the stratigraphic thicknesses were added by using published borehole data and maps. Boreholes were projected along the bedding strike onto the plane of the cross-sections. In order to validate the cross-sections and calculate the accumulated shortening of each cross-section, they were line balanced (while conserving area) and restored. There is one exception to this, section C-C' crosses an oblique structure, where it is not possible to assure plane strain, so it was not restored. The cross-section locations are shown in **Figure 1.5** (from WE-1 through WE-8). The western pin line for the cross-sections restorations was placed in the undeformed rocks to the west of the Changhua thrust tip line. The sections were restored assuming horizontal deposition of the top of the Kueichulin Fm. This contact is a regional-scale marker that can be mapped throughout much of the study area. Minimum shortening estimations for each cross-section was also calculated.

In the southwestern part of the fold-and-thrust belt, an iterative process was used to construct the cross-sections, and the three roughly north-south strike-parallel sections (NS-1, NS-2, and NS-3 in **Fig. 1.5**) were readjusted until they fit in a coherent way with the map of the basal thrust, thrust branch line maps, and stratigraphic cut-off maps that were drawn at the same time. This iterative approach insured 3D geometrical consistency of the structural interpretation and assured the geological viability of the cross-sections.

1.5.4 P-wave velocity model

The 3D P-wave velocity model was taken from the local tomography of *Kuo-Chen et al., [2012]*. We refer to *Kuo-Chen et al., [2012]* for the acquisition and processing parameters. In the Vp velocity maps and sections presented in this thesis, we can expect a resolution of at least 20 x 20 x 10 km (see the check-board test of *Kuo-Chen et al., [2012]*). The P-wave perturbation model presented in **Paper I** is derived using the 1D velocity depth function provided in *Kuo-Chen et al., [2012 supplementary data set]*.

An important feature of the sub-surface geology for the interpretations that follow is the contact between the Mesozoic basement rocks and the overlying sediments. Understanding where this contact is allows us to interpret the role played by the margin's basement in the structure of the fold-and-thrust belt. In the absence of any surface data about this contact in south central Taiwan, and with a limited number of borehole data, we made a velocity description of it in which a Vp of 5.2 km/s is taken as a proxy for the velocity of the rocks near the top of the basement. We chose this velocity for two reasons: (1) because it is in keeping with laboratory measurements of Vp carried out on clastic rocks [*Christensen, 1989; Mavko et al., 1998; Johnston and Christensen, 1992, 1993; Christensen and Stanley, 2003*] that are similar in lithology to those described as Mesozoic in boreholes from south central Taiwan [*Chiu, 1975; Shaw, 1996*] and (2) because it is in keeping with the measured Vp (<5

km/s) of the Late Miocene and younger sediments intersected by the Taiwan Chelungpu Fault Drilling Project borehole A [*Hung et al., 2009*]. We stress, however, that a Vp of 5.2 km/s serves only as a proxy. It is meant to help with the interpretation of the location of these rocks at depth, but because of the uncertainties in the velocity model and in the petrophysical assumptions it may not coincide exactly with the basement-cover interface.

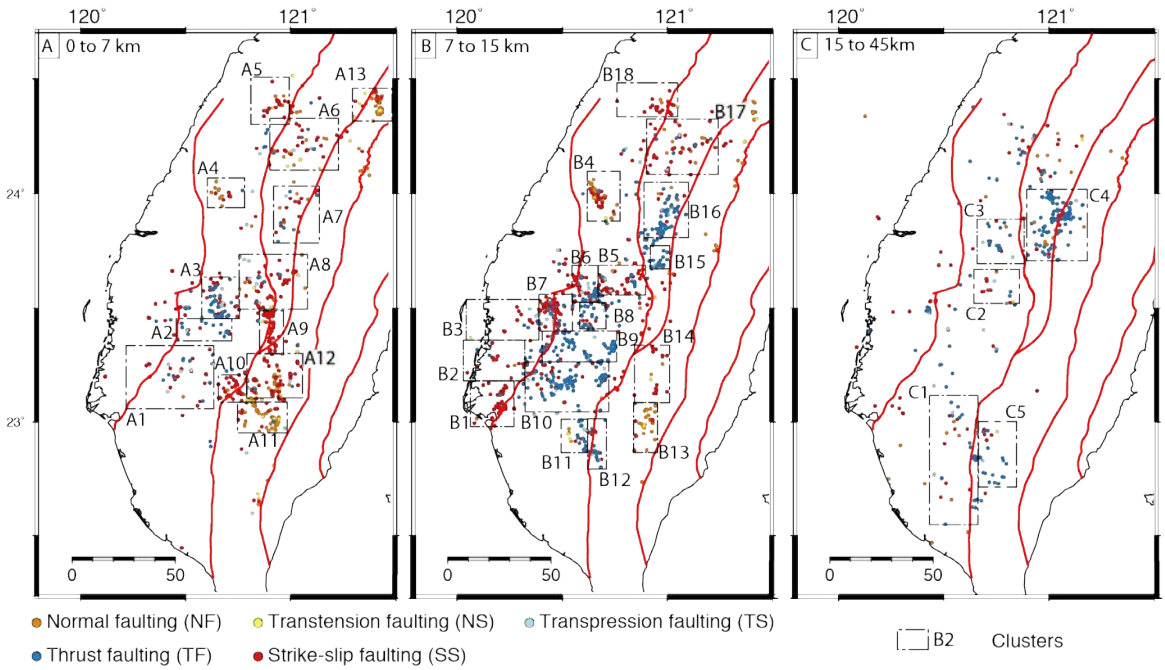

FIGURE 1.7. Clustered focal mechanism distribution and fault type for each depth level. The fault types follow the classification scheme of *Zoback [1992]*. A) The 0 to 7 km depth level with 13 clusters labeled A1 to A13. B) The 7 to 15 km depth level with 18 clusters labeled B1 to B18. C) The 15 to 45 km depth level with 5 clusters labeled C1 to A5. The whole focal mechanisms data set is shown in **Figure 1.6D**. Clusters correspond to the results shown in **Figure 1.8** and supplementary **Figure SD2_A4**.

1.5.5 Earthquake hypocenter & focal mechanism data sets

In this thesis we used the catalogue of earthquakes recorded from 1994 through 2015 by the Central Weather Bureau of Taiwan. The earthquake hypocenters were relocated by our Taiwanese colleagues using the double-difference technique [*Waldhauser and Ellsworth, 2000*] within the local 3D Vp model of *Kuo-Chen et al., [2012]* and the HypoDD3D software [*Waldhauser, 2001*]. The relocation was carried out on all events shallower than 60 km depth. In the study area, the catalogue contains 96,907 earthquakes (**Fig. 1.6A**) with local magnitudes (M_L) ranging from 0.1 to 7.8, with a mean M_L of 1.89 (**Fig. 1.6B**). We integrated this dataset with the geological interpretations by plotting horizontal and vertical sections and projecting the earthquake hypocenters onto the horizontal sections 3 km either side, and on to the horizontal sections 4.99 km either side.

Focal mechanisms were calculated for 2,465 events (**Fig. 1.6D**) by our Taiwanese colleagues using first motion polarities of P-waves [*Wu et al., 2008*]. The data set contains events ranging from local magnitudes (M_L) 1.4 to 6.8, with a mean M_L of 3.6 (**Fig. 1.6E**) and depths ranging from 0 to 45 km (**Fig. 1.6F**). 90% of the event magnitudes are ranging between 2.5 and 4.8 (**Fig. 1.6E**). The

focal mechanisms were used to determine possible fault types and their kinematics. Fault types were determined from focal mechanisms data set using the method of *Zoback [1992]* and are classified as normal (NF), transtensional (NS), strike-slip (SS), transpressional (TS) and thrust (TF) faults depending on their P-, T- and B-axes plunge (**Fig. 1.6D**). The focal mechanism data set was used to determine the contemporaneous stress field in south central Taiwan (**Fig. 1.6A**).

1.5.6 Stress inversion methodology & most likely active fault planes

The stress inversion from focal mechanisms was used to estimate the contemporaneous stress field, inferring the principal stress directions (s_1, s_2, and s_3), the maximum horizontal compressive stress (S_H) and the most likely active fault plane orientations and their kinematics in south central Taiwan.

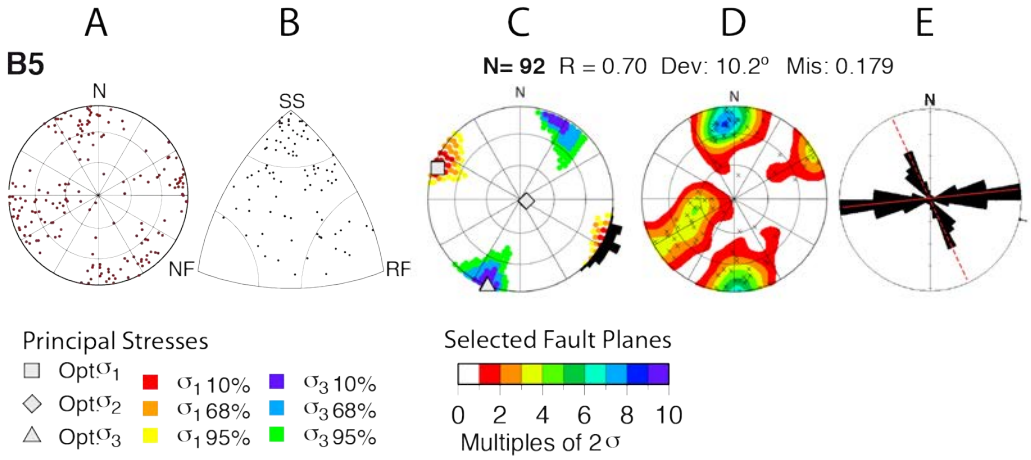

FIGURE 1.8. Example of cluster B5 input and output results from the inversion of earthquake focal mechanisms. The location of the cluster is shown in **Figure 1.7**. For each cluster there are five plots, from left to right these are: A) stereonet with poles to the nodal planes. B) Triangular distribution plot depending on the faulting type after *Kagan [2005]*. C) Best fitting stress tensor, with σ_1, σ_2, and σ_3 directions (symbols: square, diamond, triangle, respectively) and the 10%, 68% and 95% confidence limits of σ_1 and σ_3 colored, in warm and cold colors respectively. At the edge of the plot is the S_H azimuth with its confidence limit as a histogram. D) Stereonets showing the Kamb contours of the poles to the selected fault planes that best fit the stress tensor. E) Rose diagram with the strikes of the selected fault planes from E), highlighting the mean strike of the primary and secondary fault families in red solid and dashed lines, respectively. Parameters of the inversion results: N = number of events, R = relative size of the intermediate principal stress, Dev = Deviation and Mis = Misfit. The locations of the clusters are shown in **Figure 1.7**. The complete set of cluster results inputs and outputs is given in Supplementary data set **Figure SD2_A4** in Appendix 4.

In this thesis we used a hypothesis driven approach [e.g., *Hardebeck & Michael, 2004*] to do the binning of the focal mechanisms data for the stress inversion. Since much of the seismicity of the study area occurs within the basement we have divided the crust into three depth levels (**Fig. 1.7**). From 0 to 6.9 km depth comprises the sedimentary carapace overlying the basement. Some 37% of earthquakes occur within this depth level. From 7 to 45 km comprises the basement. The basement was divided into two depth levels: From 7 to 14.9 km contains 47% of earthquakes and its base was chosen to coincide with the depth of the expected thermal cut-off for seismicity (about 350 + 100 °C; *Sibson [1983], W. Chen & Molnar [1983]*) given a geothermal gradient of around 30° C/km in western Taiwan [*Wu et al., 2013*] and, from 15 to 45 km depth a layer that included the deepest earthquakes,

(16% of the total seismicity) until the base of the crust. Within each depth level, the focal mechanisms have been divided into clusters (**Fig. 1.7**) with each cluster having a minimum of 20 events (except A4 with 17 events), and the proximity of events and their distribution in swarms (i.e., main shock and aftershocks) were taken into account.

To estimate the principal stress directions (σ_1, σ_2, and σ_3) we used the stress tensor inversion scheme of *Lund & Slunga [1999]*. The methodology accounts for uncertainties in the focal mechanisms by perturbations to the P-, T- and B-axes up to some angle during the inversion [*Lund & Slunga 1999, Hensch et al., 2016*]. Here we allowed 10° – 15° maximum perturbation in keeping with the 18° average focal mechanism uncertainty estimated by *Wu et al. [2008]*. In order to select which of the two nodal planes is the most likely fault plane, the *Lund & Slunga [1999]* methodology applies a Mohr-Coulomb stability criterion to assess which nodal plane is more unstable over a range of coefficient of friction (μ) values. Here we used a μ-range of 0.4 – 1.2 and if one nodal plane is consistently more unstable over this range, that nodal plane was chosen as the fault plane and used in the inversion. If, on the other hand, the most unstable nodal plane changes over this range then the nodal planes are similarly stable and choosing one over the other would mean an implicit choice of μ. The fault plane was then instead chosen based on the goodness of fit. Using the focal mechanisms of the considered cluster, the inversion performs a grid search of the principal stress directions and the stress ratio R=(σ1 – σ2)/(σ1 - σ3). For each point on the grid it searches through all perturbations of the focal mechanisms and for each calculates the angular misfit between the shear stress direction on the chosen fault plane and the observed slip direction. This process determines the directions of the three principal stress axes (σ_1, σ_2, and σ_3) and an estimate of the relative size of the intermediate principal stress, the stress ratio R [*Lund & Slunga 1999*]. When the entire set of focal mechanisms of the cluster has been searched at all stress directions, the optimal stress tensors and its confidence limit are calculated using statistics for one-norm misfit (**Figs. 1.8C**). The direction of the maximum compressive horizontal stress (S_H) and its confidence limits are then determined using the methodology of *Lund & Townend [2007]*. The S_H results are plotted as a histogram around the stereonet (**Figs. 1.8C**). In map view, S_H is plotted as wedges that represent the 95% confidence limit and the stress regime of each (i.e., reverse, normal, strike-slip) is determined from the stress tensor. Then, the poles to the estimated fault planes, determined from the two nodal planes of each focal mechanism [*e.g., Lund & Slunga 1999*] are plotted and contoured using the Kamb method (**Figs. 1.8D**). We also plotted the strikes of the estimated fault planes in a rose diagram (**Figs. 1.8E**) using the Stereonet3D software of *Allmendinger et al., [2012]*. The length of the petals corresponds to the percentage of the total number of strikes that falls within a 10° bin, and the two most frequent strikes were chosen as the primary (most frequent) and secondary fault planes. The kinematics of each fault plane was estimated using the inversion resultant stress tensor. Finally, to assess how the instability fault selection criterion performed, we illustrate the chosen fault planes in Mohr-Coulomb diagrams, with the relative stress magnitudes calculated in the inversion using an average coefficient of friction (μ) of 0.6. A complete set of results inputs and outputs for each cluster is given in Supplementary data set **Figure SD2_A4**.

1.5.7 Displacement vectors & strain field from GPS data

We use data from the Taiwan GPS network consisting of continuous measurements ranging

between 2005 and 2009 to determine the displacement vectors and derive the current strain field and strain rates. The station coverage of the GPS network in the study area and the horizontal displacement vectors are shown in **Figure 1.9A and B**, respectively. The data was processed by our Taiwanese colleagues using the method of *Yu et al., [1997]*, and the reader is referred there for details. Horizontal velocities are calculated relative to station S01R located on the island of Penghu on the stable Eurasia margin in the Taiwan Strait (**Fig. 1.9A**).

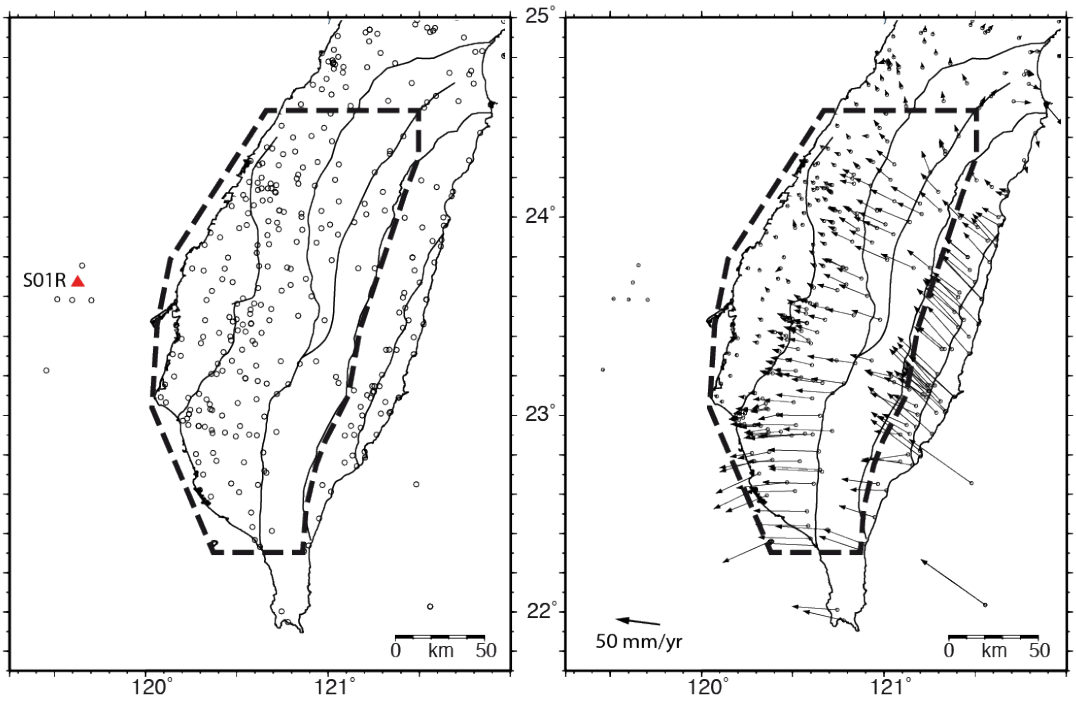

FIGURE 1.9. A) GPS stations in the study area and surrounding areas. The velocities are calculated relative to the station S01R on the stable Eurasia margin in the Taiwan Strait and shown as a red triangle. B) Horizontal velocity vectors. Black dashed line box show the study area.

Strain rates are calculated from the displacement vectors using the SSPX software of *Cardozo & Allmendinger [2009]*, and the reader is referred there for the background theory. We used a 5 x 5 km grid and a grid-nearest neighbour interpolation method using the 10 nearest stations within a maximum radius of 35 km. SSPX determines the best fitting strain tensors for each 2D surface of the grid and its corresponding strain ellipse. With this methodology we determine the rotation rate about a vertical axis, the dilatation strain rate, and the maximum shear strain rate, as well as the horizontal maximum compressive and extension strain axes (ε_H and ε_h, respectively) and the maximum shear strain planes.

1.5.8 Errors & uncertainties

Before presenting the results of the different studies that make up this thesis some remarks are appropriate on the uncertainties imposed by some errors and assumptions related with the data sets and methodologies we use.

The geological map is the primary dataset for all the structural interpretations. During our mapping we have made a number of assumptions that could have led to errors in the map. These include;

(1) making a chronostratigraphic correlation that link different rock units and facies together on the basis of age and, (2) correlating thrusts and stratigraphic contacts along-strike through difficult terrain with, locally, sparse outcrop information. Any uncertainties generated in this way were then introduced into the cross-sections and these, together with the general assumptions involved in the cross-section construction, such as plane strain, no layer parallel slip, a horizontal disposition of the top of the Kueichulin at the time of deposition, or the depth to the basal thrust calculations, also may have lead to errors. A weakly constrained stratigraphic template precluded doing rigorous area balancing. Furthermore, we did not have access to either the original borehole descriptions or their locations. The borehole information presented in this thesis has been taken from various publications and may therefore contain significant errors.

To estimate the basement-cover interface in the subsurface, we have used a 3D velocity model from the seismic tomography of *Kuo-Chen et al., [2012]*, and used a Vp of 5.2 km/s as a proxy for the top of the basement. The uncertainties inherent in the velocity model, its low resolution (20 km by 20 km by 10 thick) compared to that of the surface geology, and the petrophysical assumptions made for conversion of Vp to rock type all mean that this assumption for the basement-cover interface may not be valid everywhere. While we have taken care to keep all of these uncertainties to a minimum in the geological interpretations, we nevertheless present the maps and the cross-sections as interpretations, the restorations as approximations, and the displacement and shortening calculations as minimums.

In the case of the seismicity, the main uncertainty in hypocenter location is related with the accuracy of the velocity model that is used for its location. Earthquake hypocenter location is usually determined by the misfit between observed arrival times at seismic stations, and prediction of these arrival times for different source locations, hence an accurate velocity model is important [*Husen & Herdebeck, 2010*]. To minimize the uncertainties in the location of the hypocenters, the 3D Vp model of *Kuo-Chen et al., [2012]* is used. The HypoDD technique for the relocation of events is carried out on all events with a minimum of six readings with a reading weight >3 (assigned as good quality). With this process, the average travel time residual is reduced, indicating that the spatial resolution is improved. However, the Vp model resolution in the upper km (c. 6-7km) is very poor, so hypocenter locations within this depth range are less well constrained.

The earthquake focal mechanisms were calculated from P-wave first arrivals using the generic algorithm [*Wu et al., 2008*]. Each focal mechanism was assigned a quality index factor (Qfp) to assess the solution quality depending on the number of polarity readings (Npor), the azimuthal gap (Gap), a relative number of up versus down polarity readings (Rup), and the data fit from the genetic focal mechanisms estimation algorithm (for details on Qfp calculations see *Wu et al., [2008]*). The data set is composed of focal mechanisms solutions with Npor > 10 and Gap < 180°. The focal mechanisms were calculated in all events of the seismicity database that had 10 or more polarity readings, and Qfp > 0.1 and, generally, a solution is considered to be unconstrained if Qfp = 0, and good with Qfp > 1 [*Wu et al., 2008*]. All of these values are given for each event in the online supplementary table SD1 of Paper II.

The stress inversion is calculated with clustered focal mechanisms. The uncertainties in the inversion results can increase due to instability of the inversion methodology, poor quality of the focal

mechanisms within each cluster, and mistaking which is the activated fault plane during the Mohr-Coulomb instability selection criterion. Then, in order to assess the uncertainties generated by instability during the inversion, each cluster has a minimum of 20 events (except cluster A4 with 17). This has been shown to be a sufficient number to give a stable inversion result [e.g., *Hardebeck & Hauksson, 2001; Townend & Zoback, 2006; Arnold & Townend, 2007; Vavrycuk, 2014*]. In order to evaluate the quality of the focal mechanisms in each cluster, we have statistically studied their Qfp. Overall, the clusters have an average of Qfp 1.15 ± 0.46 (average of the median cluster Qfp), with only an 11% ± 6 in average of percentage of events with Qfp < 0.2 in each cluster (supplementary **Table ST1_A4**). Nineteen clusters have a median Qfp > 1, which we consider being high quality clusters. Eleven clusters have a median Qfp between 0.7 and 1, which is fair, and 6 have median Qfp below 0.7, which is acceptable [*Wu et al., 2008*] (supplementary **Table ST1_A4** contains more information on cluster Qfp statistics). Finally, to assess how the instability fault selection criterion performed we note that on average 70% ± 12% of the fault planes were chosen based on stability and that in only three clusters (A4, B14 and B16) were less than 50% of the planes chosen by stability (supplementary **Table ST1_A4**). In supplementary **Figure SD3_A4** we illustrate the chosen fault planes in Mohr-Coulomb diagrams, with the relative stress magnitudes calculated in the inversion using an average coefficient of friction (μ) of 0.6 (supplementary **Figure SD2_A4** column G). The quality of the fault plane determinations can be observed from the deviation angles (Dev. in **Fig. SD2_A4**) (defined as the mean of the angular differences in the fault planes between the observed slip directions and the directions of calculated maximum shear stress) given for each cluster. As an estimate of quality, we divide the results into 3 classes based on the estimated average uncertainties in the focal mechanisms [*Wu et al., 2008*]: < 10° is good (26 clusters), 10° to 15° is fair (8 clusters), and > 15° is poor (2 clusters) [*Lund and Slunga, 1999*]. In conclusion, the stress inversion results for the 94% of the clusters are good or fair, while the 6% are poor.

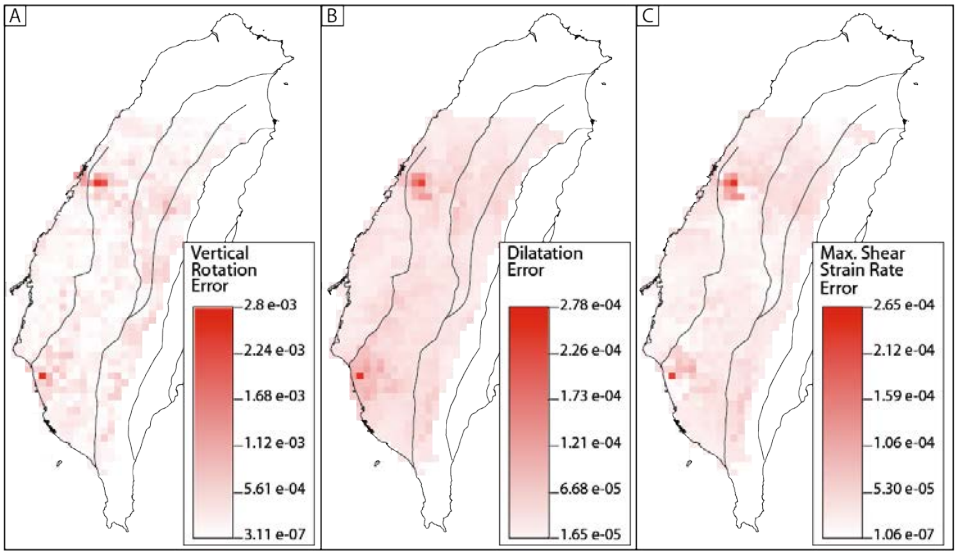

FIGURE 1.10. A) Error grid for vertical rotation strain rate. B) Error grid for dilatation strain rate. C) Error grid for maximum shear strain rate.

GPS data was acquired and processed by our Taiwanese colleagues. Information about uncertainties in the acquisition and processing can be found in *Yu et al., [1997]*. The SSPX software [*Cardozo & Allmendinger, 2009*] used to calculate the strain rates, estimates the error as the absolute difference between the computed strain value using the displacement gradient tensor, and the computed strain value using the displacement gradient tensor plus its error [*Cardozo & Allmendinger, 2009*]. Thus, the error reported is a maximum estimate. We plot errors grids (5 x 5 x 5 km) for each strain rate calculated (vertical rotation, dilatation and maximum shear strain) (**Fig. 1.10**). There are two small areas where relatively high uncertainties are expected in the strain rate results located in the northwest and southwest of the Western Foothills (**Fig. 1.10**). Uncertainties in the strain rate results are also expected in those areas where the coverage of GPS stations is scarce, such as those areas with high topography and/or limited access as the Hsuehshan Range and the Central Range (**Fig. 1.9A**).

CHAPTER 2 Results

2.1 Paper I: How the structural architecture of the Eurasian continental margin affects the structure, seismicity, and topography of the south central Taiwan fold-and-thrust belt [*Brown et al., 2017*]

The well known preexisting structural and basin architecture of the margin shelf, shelf-to-slope transition, and slope [e.g., *Teng et al., 1991; Yang et al., 1991; Lin et al., 2003; Teng and Lin, 2004*] and the wealth of on-land geological, geophysical, and geodetic data [e.g., *Suppe, 1986; Deffontaines et al., 1997, Lacombe et al., 1999; Mouthereau et al., 2002; Yang et al., 2006, 2016; Byrne et al., 2011; Alvarez-Marron et al., 2014; Camanni et al., 2016*] makes Taiwan an excellent location for the study of how inherited features of the continental margin can affect the evolution of a fold-and-thrust belt. The study area comprises the south central Taiwan fold-and-thrust belt, from latitudes around 24.3° N to 22.2° N (**Figs. 1.1 and 2.1**). The aim of this paper is to test the hypothesis of whether or not the regional-scale features of the margin are contributing to along-strike changes in structural style, seismicity, and topography of the south central Taiwan fold-and-thrust belt. It presents the basic ideas and concepts upon which the following two papers and this thesis are built. For these reason, an extensive overview of this paper is given below.

In this section, we first explain how we trace the regional-scale structural and morphological features of the continental margin into the south central Taiwan fold-and-thrust belt by combining the top of a Mesozoic basement map from the Taiwan Strait [*Lin et al., 2003*] with seismic tomography on-land (**Fig. 2.1**). Then, we proceed with the explanation of the results of the integration of the new geological mapping, the P-wave velocity maps and sections, the earthquake hypocenter data set, and the high-resolution topography.

In order to correlate the subsurface structure on-land with the structure and morphology of the continental margin we use three depth slices from the 3D P-wave perturbation (dVp) model derived from the local tomography of *Kuo-Chen et al., [2012]* (**Fig. 2.1**). At 8 km depth, in the northwest of the study area, the dominant negative dVp values to the west of the Shuilikeng fault (SkF in **Fig. 2.1A**) provide good correlation with the sediments of the Taihsi and foreland basins. At this depth, the significant increase in the relative dVp below the Hsuehshan and Alishan Ranges (HR and AR, respectively, in **Fig. 2.1**) are interpreted to be caused by the presence of high-velocity basement rocks at a shallow crustal level [see *Camanni et al., 2014a, 2016; Alvarez-Marron et al., 2014*]. Beginning at 8 km depth, but becoming especially prominent at 12 km and 16 km depth, there is an embayment of relatively high dVp that is associated with the high-velocity basement rocks that comprise the Peikang Basement High (PH in **Fig. 2.1**) [e.g., *Wu et al., 2007; Byrne et al., 2011; Kuo-Chen et al., 2012; Huang et al., 2014*]. The southern flank of this area (the Peikang Basement High) of relatively high dVp coincides with the on-land projection of the upper part of the necking zone (**Fig. 2.1**), indicating that it can be traced from the margin into the fold-and-thrust belt. South of this, in the Western Foothills and on the Coastal Plain, the negative dVp values reach to about 12 km depth and are interpreted to be due to thicker Miocene and foreland basin sediments that were deposited on the slope of the margin and which are

now involved in the fold-and-thrust belt deformation [e.g., *Wu et al., 2007; Kuo-Chen et al., 2012; Huang et al., 2014*]. Below the southwestern part of the fold-and-thrust belt, there is a weak dVp high extending northeastward from a basement high on the margin (**Fig. 2.1**).

Three zones (A, B and C in **Fig. 2.2**) mark important along-strike changes in the structure, seismicity and topography in south central Taiwan fold-and-thrust belt. In the northern part of the study area (north of zone A), corresponding to the shelf area of the margin, the outcropping geology of the Coastal Plain and the Western Foothills comprise Pliocene to Holocene synorogenic sediments of the foreland basin with, eastward, synrift Eocene-age sedimentary and minor volcanic rocks that are unconformably overlain by Miocene sedimentary rocks. The structure is that of a west verging imbricate thrust system with a roughly N-S striking structural grain (**Fig. 2.2** and section A-A' in **Fig. 2.3**). Its basal thrust is interpreted to be located near the base of the low velocity (<5 km/s [*Hung et al., 2009*]) synorogenic sediments in the Western Foothills (**Figs. 2.4 and 2.5A**). Along the eastern flank of the Western Foothills, Eocene through Miocene rocks overthrust the Pliocene to Holocene synorogenic sediments along the Shuangtung thrust (ST in section A-A' in **Figs. 2.3 and 2.5**). Seismicity in this imbricate thrust system is scattered (**Fig. 2.6**), with no clear correlation with any individual fault (section A-A' in **Fig. 2.5**). Beneath the imbricate thrust system, seismicity reaches to approximately 30 km depth, but there is no well-defined clustering that would suggest the location of any particular fault in the basement (section A-A' in **Fig. 2.5** and **Fig. 2.6**). The topography of the imbricate thrust system area is dominantly subdued, with elongated hills developed in the immediate hanging walls of the frontal thrusts (**Fig. 2.7A**). Only at the rear of the thrust system, where Miocene sediments crop out, do elevations reach more than 500 m.

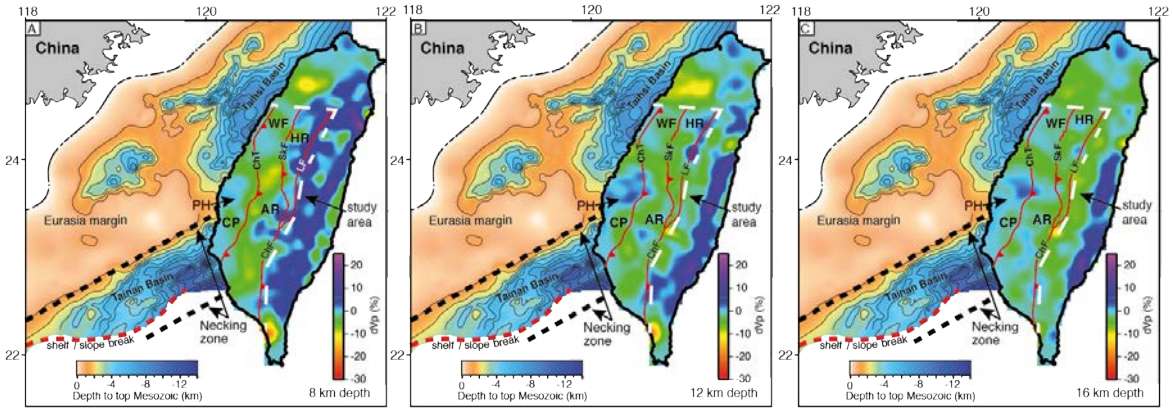

FIGURE 2.1: P-wave velocity perturbation models (dVp (%)) for the island of Taiwan at various depths. In the Taiwan Strait, the depth to the top of the Mesozoic basement [from *Lin et al., 2003*]. The location of the necking zone offshore is indicated by the thick dashed black lines and the shelf/slope break by the thick dashed red line. The study area on-land in Taiwan is outlined by the dashed box. AR = Alishan Range, CP = Coastal Plain, WF = Western Foothills, HR = Hsuehshan Range, CR = Central Range, PH = Peikang basement high. Faults = ChT = Changhua thrust, LF = Lishan fault, SkF = Shuilikeng fault, ChF = Chauchou fault.

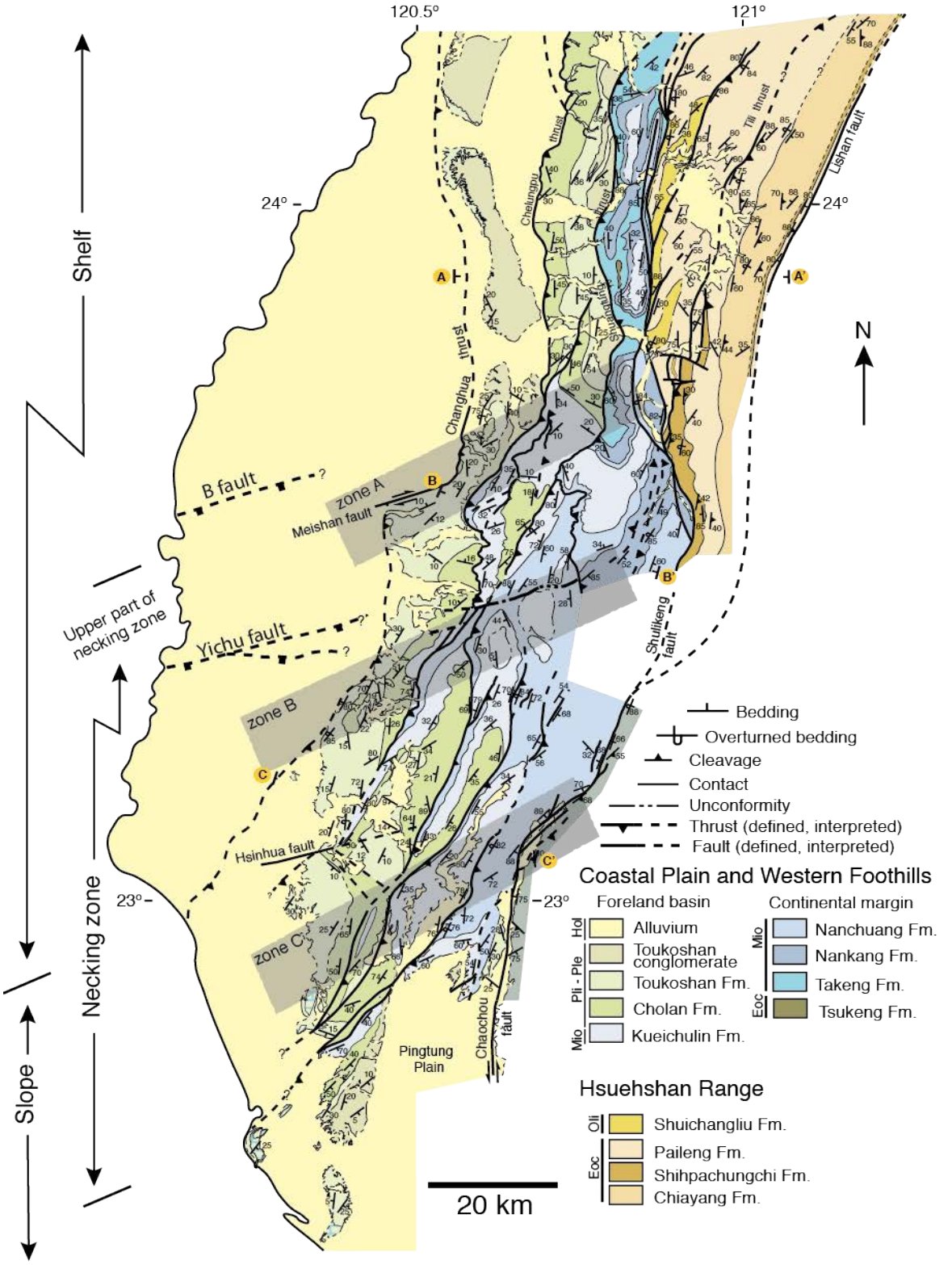

FIGURE 2.2. Geological map of the study area, with representative structural data. The locations of the cross-sections in **Figure 2.3** are shown. The transparent gray boxes are zones A, B, and C that highlight areas where there are marked changes in the structural grain of the fold-and-thrust belt. The northernmost of these corresponds to the on-land projection of the upper part of the necking zone. The stratigraphic scheme used in the map is given in **Figure 1.3**.

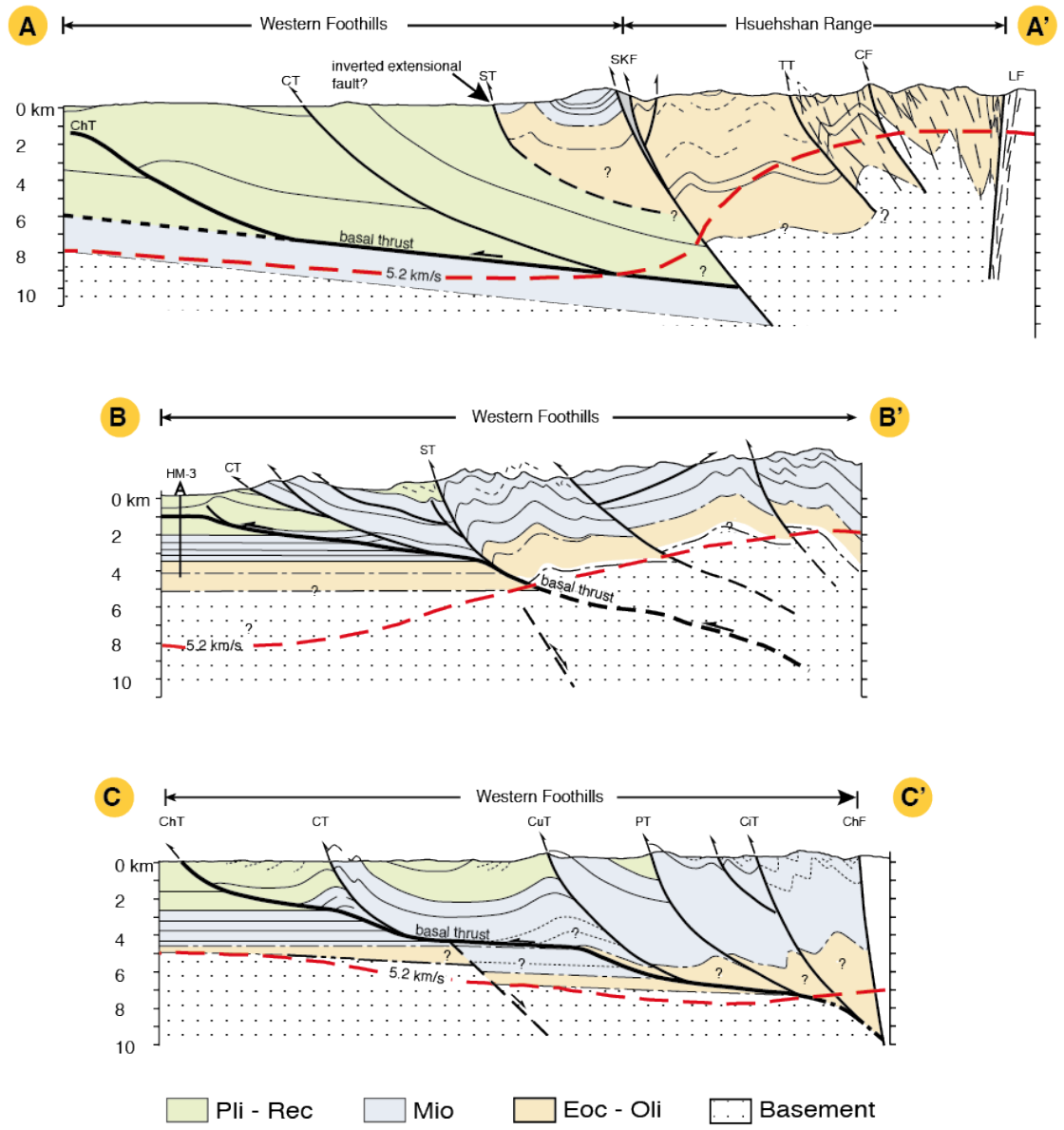

FIGURE 2.3. Geological cross-sections through south central Taiwan. The locations are given in **Figure 2.2**. ChT = Changhua Thrust, CT = Chelungpu Thrust, TT = Tili thrust, SkF = Shuilikeng Fault, ST = Shuangtung Thrust, CuT = Chutochi Thrust, PT = Pingshi Thrust, CiT = Chishan Thrust, LF = Lishan Fault, ChF = Chaochou Fault. The dashed red line is the 5.2 km/s isovelocity contour line.

In the area to the north of zone A, the imbricate thrust system is bound to the east by the Shuilikeng fault, a major structural boundary across which there is an important change in the outcropping rocks and in the structure of the fold-and-thrust belt [see also, *Brown et al., 2012; Camanni et al., 2014b*] (**Fig. 2.2** and section A-A' in **Fig. 2.3**). East of the Shuilikeng fault, the Hsuehshan Range comprises Eocene-age synrift sediments from the Hsuehshan Trough, which are unconformably overlain by Late Oligocene postrift sediments. The structure of the Hsuehshan Range can be divided into two thrust sheets, the westernmost of which comprises open to tight, west verging anticlines and synclines and, from the Tili thrust (TT in section A-A' in **Fig. 2.3**) to the east, a set of west verging folds with a penetrative axial planar cleavage and associated thrusts that overall form an anticlinorium with a steep to overturned forelimb. The involvement of older

and, at depth, higher Vp (Fig. 2.4 and section A-A' in Fig. 2.5) rocks in this part of the fold-and-thrust belt provides unequivocal evidence that the basal thrust ramps down to a deeper crustal level beneath the Hsuehshan Range [see *Yue et al., 2005; Brown et al., 2012; Chuang et al., 2013*]. In the subsurface, the location of the ramp can be inferred from an east dipping cluster of seismicity that reaches to about 20 km depth (section A-A' in Fig. 2.5) [see *Chuang et al., 2013; Camanni et al., 2014a, 2014b*]. We interpret both the Shuangtung and Shuilikeng faults to be linked to this ramp, with the Shuangtung thrust having been cut by the Shuilikeng fault [*Brown et al., 2012; Chuang et al., 2013*].

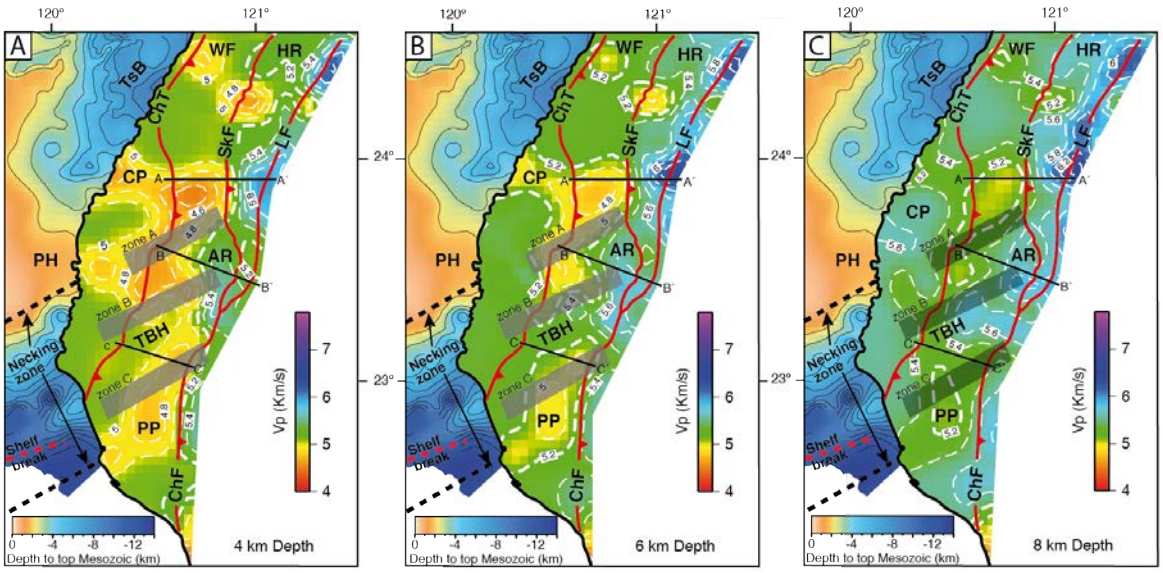

FIGURE 2.4. Horizontal Vp maps at (A) 4 km depth, (B) 6 km depth, and (C) 8 km depth. The depth to the top of the Mesozoic basement in the Taiwan Strait is as in Figure 2.1. The Peikang Basement High (PH) is interpreted to represent a fault-bounded basement high whose southern flank corresponds to the upper part of the necking zone. Zones A, B, and C are shown as transparent gray boxes marking the areas where there is a change in the structural grain of the fold-and-thrust belt. The location of the necking zone offshore is indicated by the thick dashed lines and the shelf/slope break by the thick dashed red line. The locations of the velocity sections in Figure 2.5 are shown. TsB = Taihsi Basin, PH = Peikang Basement High, PP = Pingtung Plain. Other labels are as in Figure 2.1.

The uplift of higher Vp rocks (>5.2 km/s) beneath the Hsuehshan Range (Figs. 2.4 and section A-A' in Fig. 2.5) is interpreted to indicate basin inversion and the involvement of Mesozoic basement in the deformation. In this northern part of the study area, the Hsuehshan Range is the most seismically active part of the fold-and-thrust belt, with significant seismicity extending to over 30 km depth (Fig. 2.6). The deepest seismicity in the Hsuehshan Range is seen in the cross-section to form a steeply west dipping cluster that is interpreted to be associated with the Lishan fault (LF in Fig. 2.5 section A-A' and Fig. 2.6) [see *Wu et al., 2004; Brown et al., 2012; Camanni et al., 2014a, 2014b; Kuo-Chen et al., 2015*]. In the study area, the Hsuehshan Range has the highest elevations in the fold-and-thrust belt. The two highest mountains in Taiwan are found there: Yushan and Hsuehshan mountains, respectively (YM and HM, in Fig. 2.7). The Puli Basin (PB in Fig. 2.7) forms a pronounced topographic low within the Hsuehshan Range, and it is roughly centered on a marked Vp high (Figs. 2.1 and 2.4).

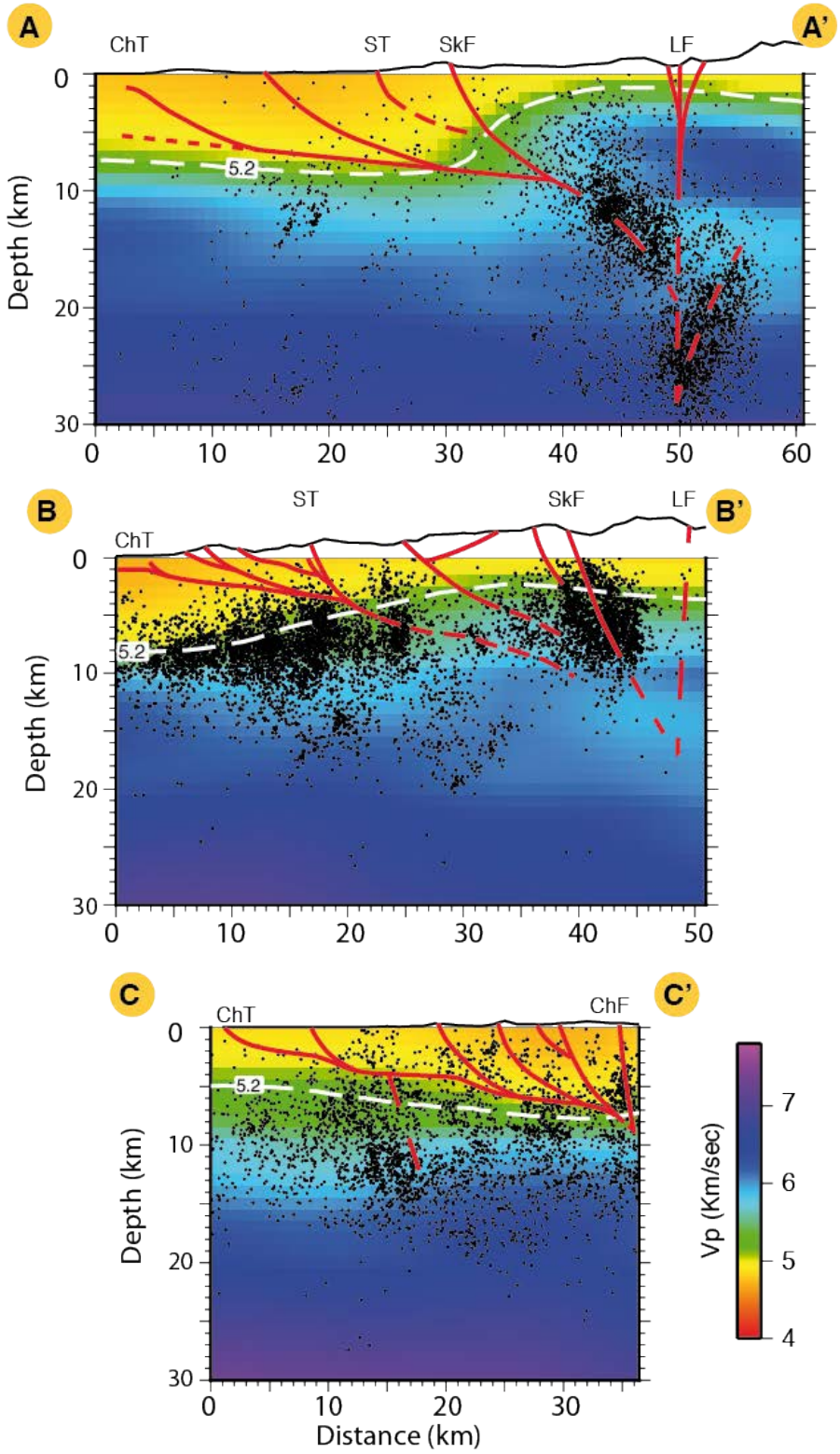

FIGURE 2.5. Vp sections with the fault traces taken from the geological cross-sections in **Figure 2.2** shown in red. Locations are shown in **Figure 2.4**. Earthquake hypocenters are projected onto the sections from 3 km either side. Fault labels are as in **Figure 2.3**.

The upper part of the necking zone (**Fig. 1.1**) marks a major change in the structure of the margin offshore western Taiwan. From north to south, across its on-land prolongation (zone A, **Fig. 2.2**), there are significant along-strike changes in structure, stratigraphy, seismicity, and

topography of the fold-and-thrust belt. With regard to the structure, zone A marks a roughly north-south to northeast-southwest, en echelon change in the strike of thrusts that culminates with approximately 10 km westward shift of the tip line of the Changhua thrust along the dextral strike-slip Meishan fault (**Fig. 2.2**). The Meishan fault is thought to link westward under the Coastal Plain with an extensional fault system that is also found offshore, along the upper part of the necking zone [e.g., *Lin et al., 2003; Yang et al., 2016*]. Immediately south of zone A, the Changhua (ChT) and Chelungpu (CT) thrusts in the western part of the fold-and-thrust belt merge into a gently east dipping basal thrust that is much shallower than to the north (compare ChT and CT in sections A-A' and B-B' in **Figs. 2.3**). Concomitant with the shallowing of the basal thrust, there is a decrease in the thickness of the Pliocene to Recent synorogenic sediments of about 5 km, and its base is uplifted by approximately 7 km in the Chelungpu thrust sheet. East of the Shuangtung thrust (ST in section B-B' in **Fig. 2.3**), the basal thrust is interpreted to ramp down section, and the hanging wall structure is that of an approximately 20 km wide anticlinorium. This anticlinorium includes a thicker Miocene sequence than that present to the north of zone A. The southward appearance of the Middle to Late Miocene Nanchuang Fm at zone A (**Fig. 2.2**) corresponds to the occurrence of this formation along the northern margin of the Tainan Basin. In structural cross-sections [e.g., *Suppe, 1986; Rodriguez-Roa & Wiltschko, 2010; Yang et al., 2007, 2016; Alvarez-Marron et al., 2014*], its appearance in the fold-and-thrust belt is interpreted to take place along a reactivated Middle Miocene-age extensional fault that coincides with the Chelungpu thrust. Through zone A, the upper crustal Vp contours have a northeast strike (note in particular the trace of 5.2 km/s contour in **Fig. 2.4**) that parallels the surface structural grain (**Fig. 2.2**) and which continues with higher Vp values through the Alishan Ranges (AR in **Fig. 2.4**), at the rear of the fold-and-thrust belt. We interpret the shallowing of the 5.2 km/s isovelocity contour across the Shuangtung thrust in the Alishan Ranges to indicate the presence of basement rocks that are involved in this part of the fold-and-thrust belt (section B-B' in **Figs. 2.3** and **2.5**) [see *Alvarez-Marron et al., 2014*].

Zone A also marks an abrupt north to south increase in the amount of upper crustal seismicity (**Figs. 2.6A** and **B**). South of zone A, seismicity is widespread in the upper 10 km across the Western Foothills and extends up to the coastline in the Coastal Plain. Events at 20 km depth are scattered, both to the north and south of zone A, while at 30 km depth seismicity occurs dominantly to the north. Beneath the Alishan Ranges, there is a good correlation between seismicity and the Shuilikeng fault (section B-B' in **Fig. 2.5**), although to the west, seismicity clusters near the basement-cover interface, well below the interpreted location of the basal thrust. Finally, zone A marks a significant north-south increase in the topography of the fold-and-thrust belt, especially in the Western Foothills but also in the Hsuehshan Range, to the south of the Puli Basin (**Fig. 2.7A**). Across zone A, the topography of the Western Foothills rises from just above sea level to form the northwest facing slope of the Alishan Ranges, which, at over 2,400 m high, has the highest elevation in the Western Foothills of south central Taiwan (**Fig. 2.7**).

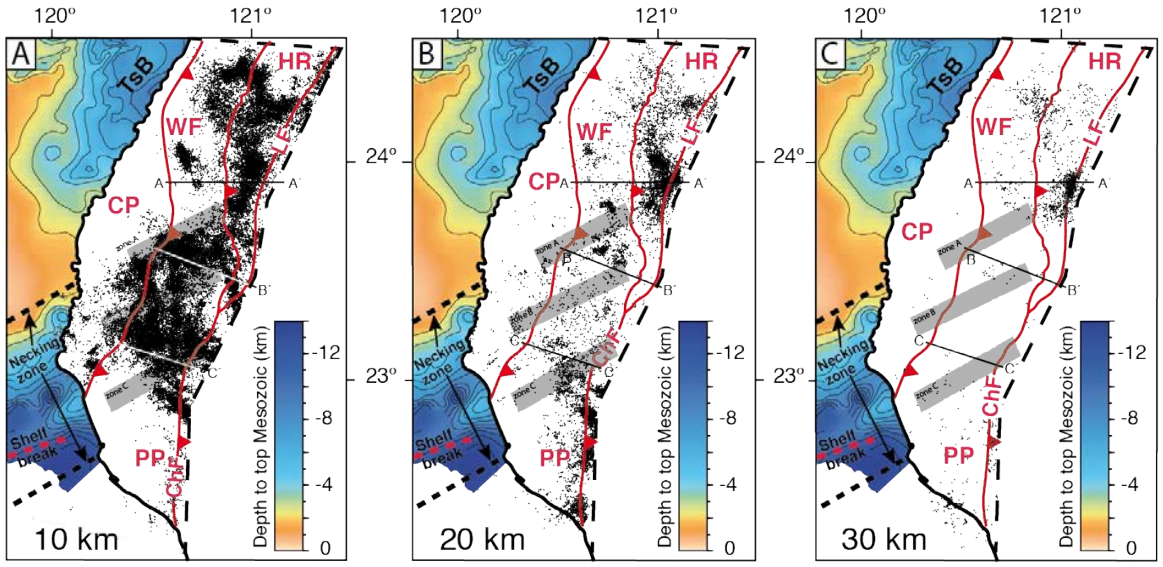

FIGURE 2.6. Earthquake epicenter depth slices for the study area. Events are projected 4.99 km each side of the depth slice. The depth to the top of the Mesozoic basement in the Taiwan Strait is as in **Figure 2.1**. The locations of the seismicity sections in **Figure 2.5** are shown. The location of the necking zone offshore is indicated by the thick dashed lines and the shelf/slope break by the thick dashed red line. Other labels are as in **Figures 1.1** and **2.1**.

Farther south, on the area that correlates with the necking zone (**Fig. 2.2**), zones B and C both mark northeast striking, en echelon changes in the orientations of thrusts and curvature of fold axial traces as they take on a northeast-southwest strike. The thrust front is also interpreted to turn northeast-southwest and then continue southwestward into the offshore where it becomes the deformation front of the marine accretionary prism that is climbing up the slope [e.g., *Shyu et al., 2005; Lin et al., 2008*]. From zone B southward, the fold-and-thrust belt widens into an imbricate thrust system that comprises mostly thrust sheets with anticline-syncline pairs. The synclines are wide and the narrow ramp anticlines are in their western part (**Fig. 2.2** and section C-C' in **Fig. 2.3**). The synclines in the Chelungpu and Chutochi thrust sheets terminate northward at zone B, from where they plunge gently southward, and Miocene and younger sediments thicken. Eastward, across the Chishan thrust (CiT in section C-C' in **Fig. 2.3**), the broad anticlinorium of the Alishan Ranges narrows to less than half its width before terminating southward in a syncline that plunges beneath the alluvial sediments of the Pingtung Plain (PP in **Fig. 2.2**). South of zone C, which coincides with the on-land prolongation of the present shelf/slope break, thrusts are almost entirely buried by the synorogenic sediments, and an active thrust top basin (the Pingtung Basin of *Chiang et al., [2004]*) is forming in the hanging wall of the Chishan thrust. The basal thrust is interpreted to comprise a series of narrow ramps and wide flats as it cuts gently down through the sedimentary section toward the east, where it ramps steeply into the basement. Zones B and C are located on the northern and southern flanks, respectively, of a roughly northeast striking P-wave velocity high (>5.2 km/s) that extends northeastward from beneath the Coastal Plain through to the velocity high beneath the Alishan Ranges (**Fig. 2.4**). We interpret this velocity high to be caused by basement rocks, and herein call it the Tainan Basement High (TBH in **Fig. 2.4**). South of zone C, a pronounced velocity low suggests a deepening of the basement rocks and

a concomitant increase in the thickness of the slope and foreland basin sediments. Along section C-C', the basement-cover interface (Vp ≥ 5.2 km/s) dips gently eastward below the basal thrust (section C-C' in **Figs. 2.3 and 2.5**).

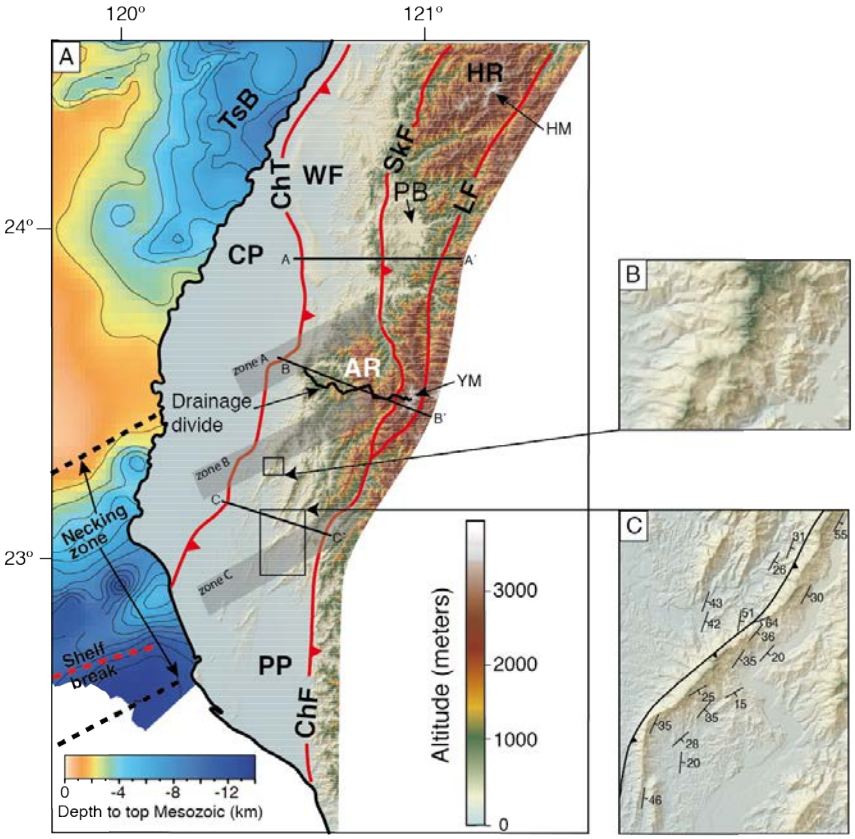

FIGURE 2.7. A) Digital elevation model of the study area and (B and C) details of sigmoidal topographic features in south central Taiwan. The location of the necking zone offshore is indicated by the thick dashed lines and the shelf/slope break by the thick dashed red line. The locations are shown by black boxes. The depth to the top of the Mesozoic basement in the Taiwan Strait is as in **Figure 2.1**. The locations of the topography sections in **Figure 2.5** are shown. YM = Yushan Mountain, HM = Hsuehshan Mountain. Other labels are as in **Figures 2.1** and **2.4**.

There is widespread but scattered seismicity between zones B and C that roughly coincides with the Tainan Basement High (**Fig. 2.6**). In the upper 10 km there is a southward decrease in seismicity across zone C in the western part of the fold-and-thrust belt, although at 20 km and 30 km depth there are events scattered throughout the southwest. The absence of any clear clustering of events makes it difficult to interpret the seismicity in terms of the structure of the fold-and-thrust belt in this area (section C-C' in **Fig. 2.5**). There is a very marked change in topography across zone B, from the widespread, high elevations of the Alishan Ranges, to several roughly southwest-northeast oriented ridges that end south-westward (**Fig. 2.7A**). At both zones B and C, these ridges undergo sharp, sigmoidal changes in strike with offsets of several kilometers toward the west (e.g., **Figs. 2.7B** and **C**). The ridges follow the trace of related thrusts and confine a set of south and southwest draining river basins. South of zone C, the topography is very subdued and only a few hills reach elevations of up to several tens of meters. In a large part of this area, the fold-and-thrust belt is buried by around 5,000 m of Pliocene to Holocene sediments [see *Mouthereau et al., 2002; Chiang et al., 2004*].

2.2 Paper II: The influence of inherited continental margin structures on the stress and strain fields of the south central Taiwan fold-and-thrust belt. [*Biete et al., in press*]

In **Paper II** we continue to explore the possible effects that the reactivation of inherited structures of the Eurasian continental margin are having on the fold-and-thrust belt in south central Taiwan, from latitudes around 24.3° N to 22.2° N (**Fig. 1.1**). Here, we estimate the principal stress directions (σ_1, σ_2, and σ_3) using inversion of clustered earthquake focal mechanisms and calculate the direction of maximum compressive horizontal stress (S_H). These are used to determine the orientations and kinematics of the fault planes that are likely to have been activated at depth during earthquake rupture. We discuss the combined results of the stress inversions with the directions of displacement, and the compressional, rotational, and maximum shear strain rates derived from GPS data. The hypothesis to be tested is whether or not the previously proposed causal link between the inherited features of the margin and the structure of the fold-and-thrust belt is supported by the contemporary stress and strain fields in south central Taiwan. Below only selected input and output results of the stress inversion are shown. A complete set of the stress inversion input and output results for each cluster is given in supplementary **Figure SD2_A4** in Appendix 4.

2.2.1 Stress tensor and maximum horizontal compressive stress (S_H)

The results obtained from the stress inversion indicate that, throughout the fold-and-thrust belt, the principal compressive stress (σ_1) at all depth levels generally plunges gently toward the west-northwest to west with some local exceptions (Column C, **Figs. 2.8**). For example, from 0 to 7 km depth, the state of stress in the Coastal Plain, Western Foothills, and the Hsuehshan Range is predominantly in the strike-slip regime. In the southern part of the Western Foothills, from 7 to 15 km depth, there is a dominantly compressional stress regime. Although there are few data in the 15 to 45 km depth level (**Fig. 1.7C**), these show a compressional stress regime in the north and a strike-slip regime in the central and southern parts of the study area. An extensional stress regime is rare in the fold-and-thrust belt, being found only in clusters A4 and B4. An extensional stress regime is common, however, in the upper 15 km of the Central Range (clusters A11, A12, A13, B13, and B14). At the deepest level, in the southern part of the Central Range, a compressional stress regime dominates (cluster C5).

Throughout the fold-and-thrust belt, the direction of the maximum compressive horizontal stress (S_H) varies appreciably from north to south, although it shows only minor, local variation with depth (**Fig. 2.9**). In general, the direction of S_H fans from roughly northwest in the north (clusters A4 and B4 are exceptions), through to west-southwest in the southwest part of the study area. The direction of S_H in the Central Range is constantly northwest oriented, except at the deepest depth level in the south, where it is west-southwest oriented.

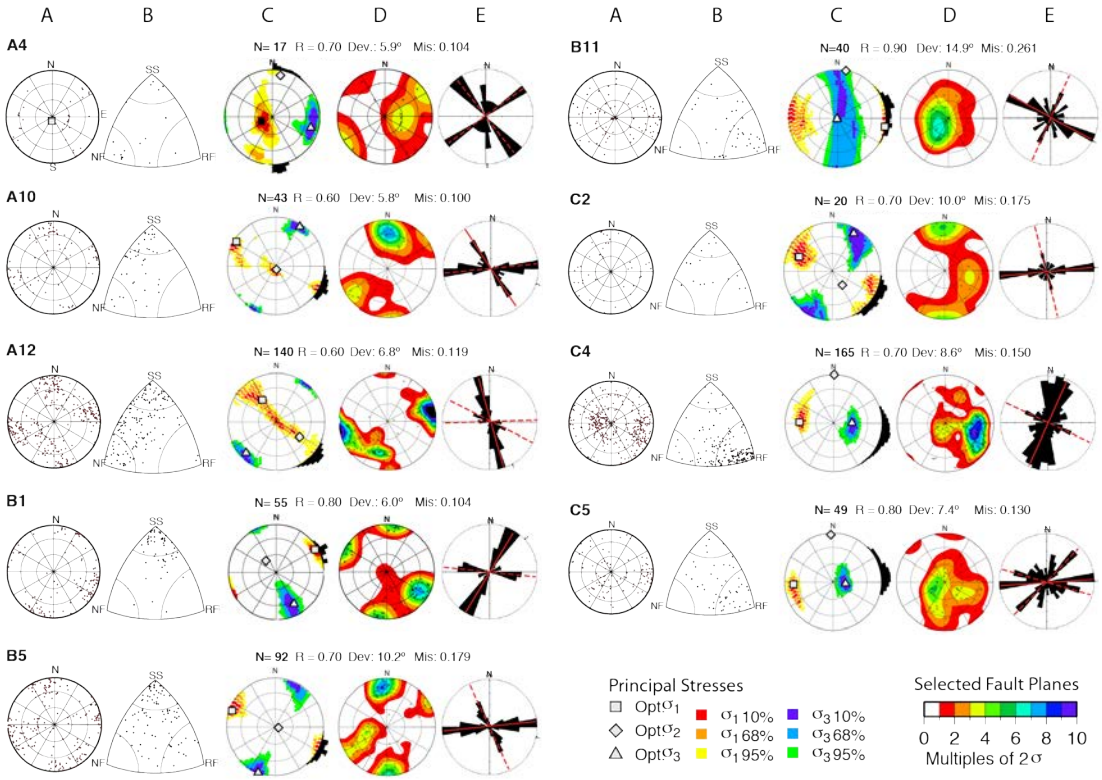

FIGURE 2.8. Selected input and output results from the stress inversion of three cluster for each depth level. A4, A10 and A12 corresponds to 0 to 7 km depth level; B1, B5 and B11 corresponds to the 7 to 15 km depth level; and C2, C4 and C5 corresponds to the 15 to 45 km depth level. The complete set of input and output results for each cluster is given in supplementary **Figure SD2_A4** in Appendix 4. The cluster locations are shown in **Figure 1.7**. For each cluster there are five plots, from left to right these are: Column A) stereonet with poles to the nodal planes. Column B) Triangular distribution plot depending on the faulting type after *Kagan [2005]*. Column C) Best fitting stress tensor, with σ_1, σ_2, and σ_3 directions (symbols: square, diamond, triangle, respectively) and the 10%, 68% and 95% confidence limits of σ_1 and σ_3 colored, in warm and cold colors respectively. At the edge of the plot is the S_H azimuth with its confidence limit as a histogram. Column D) Stereonets showing the Kamb contours of the poles to the selected fault planes that best fit the stress tensor. Column E) Rose diagram with the strikes of the selected fault planes from Column D), highlighting the mean strike of the primary and secondary fault families in red solid and dashed lines, respectively. Parameters of the inversion results: N = number of events, R = relative size of the intermediate principal stress, Dev = Deviation and Mis = Misfit.

2.2.2 Most likely active fault planes

A derivative of the process of determining the stress tensor is the possibility to estimate the most likely fault plane orientations and kinematics for the region of each earthquake cluster (Columns E and D in **Fig. 2.8 and Fig. 2.10**). Orientations are given following the right hand rule.

From 0 to 7 km depth (**Fig. 2.10A**), northwest to north-northeast striking sinistral transpressional faulting to thrust faulting dominate in the southern part of the Western Foothills, whereas nearly east striking dextral strike-slip faulting and northwest striking dextral transtensional faulting occurs in the north. Roughly northwest striking sinistral transpressional faulting dominates in the Hsuehshan Range, whereas northwest striking extensional to sinistral transtensional faulting are typical in the Central Range.

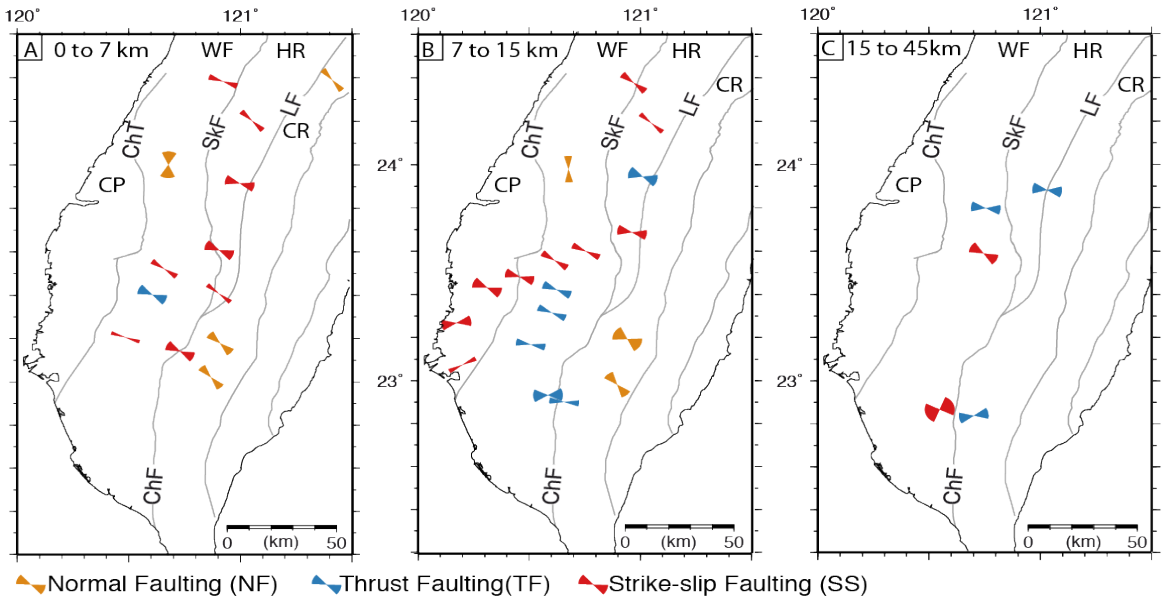

FIGURE 2.9. Direction of the maximum horizontal compressive stress (S_H) for each cluster at their respective depth level. Each wedge corresponds to the 95% confidence interval. The result from each cluster is colored depending on faulting type. A summary of all the relevant data of the resultant inversion for each cluster is in **Figure 2.8** and a complete set in **Figure SD2_A4**. The location of the clusters is in **Figure 1.7**. CP = Coastal Plain, WF = Western Foothills, HR = Hsuehshan Range, CR = Central Range. Faults ChT = Changhua thrust, LF = Lishan fault, SkF = Shuilikeng fault, ChF = Chauchou fault.

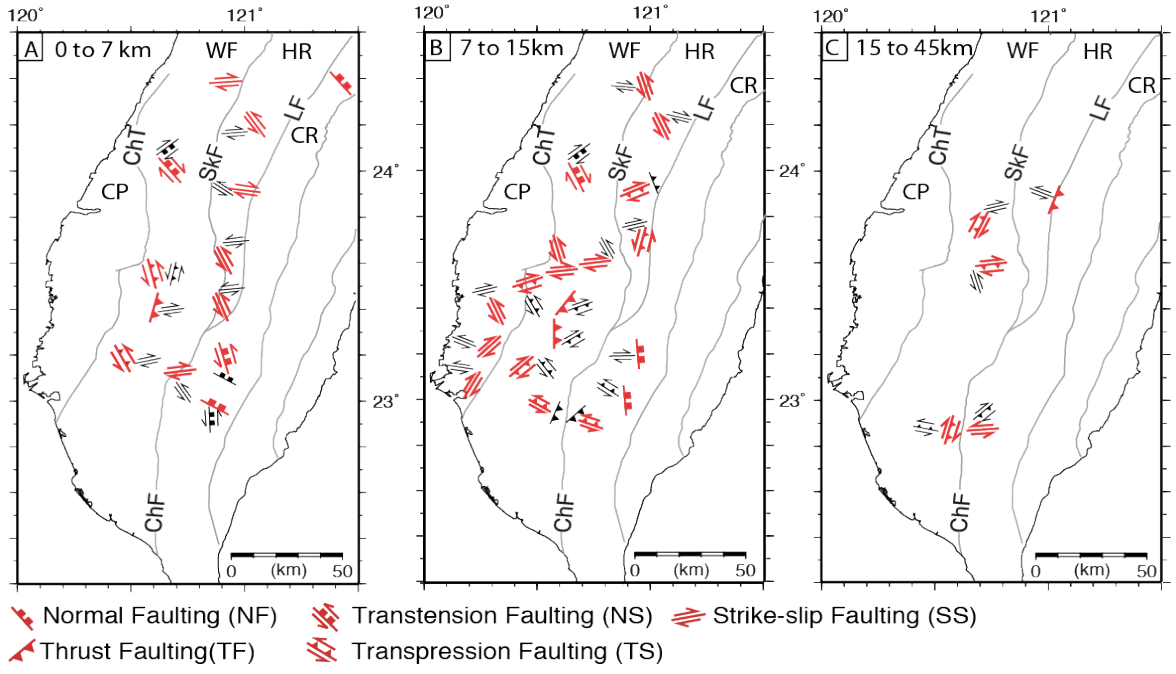

FIGURE 2.10. Selected fault planes orientations with their interpreted most probable kinematics determined from the inversion results shown in columns D and E of **Figures 2.8** (primary orientations/kinematics in red, secondary in black). A) The 0 to 7 km depth level, B) The 7 to 15 km depth level, and C) The 15 to 45 km depth level. All the relevant data of the resultant inversion for each cluster is in **Figure 2.8** and a complete set in **Figure SD2_A4** and the location of the clusters in **Figure 1.7**. Labels of main faults and tectono-stratigraphic units are as in **Figure 2.9**.

From 7 to 15 km depth (**Fig. 2.10B**), north-northwest and north-northeast striking dextral and sinistral stike-slip faulting are common in the south of the Coastal Plain. Faulting in the southern part of the Western Foothills is characterized by north-northwest and north-northeast striking dextral and sinistral transpressional faulting together with north-northeast and north striking thrust faulting, whereas in the north only northwest striking transtensional faulting takes place. The central part of the Western Foothills is dominated by a zone of east-northeast striking, dextral strike-slip faulting (**Fig. 2.10B**). At this depth level, the Hsuehshan Range is characterized by northwest through northeast striking sinistral and dextral transpressional and thrust faulting. The southern part of the Central Range has roughly north striking extensional faulting with predominantly roughly east-west sinistral transpressional faulting in the immediate hangingwall of the Chaochou fault.

From 15 to 45 km depth (**Fig. 2.10C**), southwest and nearly east striking dextral transpressional faulting is taking place in the Western Foothills, whereas in the far southeast north striking dextral faulting is taking place in the immediate footwall to the Chaochou fault. At this depth level, in the Central Range north-northeast striking thrust faulting is taking place along the hangingwall of the Lishan fault, and roughly east-west sinistral strike-slip faulting in the immediate hangingwall of the Chaochou fault.

2.3 Displacement vectors & strain rates of south central Taiwan

Data from the Taiwan GPS network is used to investigate the displacement field and strain rates in the south central Taiwan fold-and-thrust belt and the western flank of the Central Range. It is also used to gain insights into its surface kinematics.

The horizontal GPS velocity vectors display an overall northwest to west-northwest sense of displacement in the northern part of the study area, changing to dominantly west directed in the central and much of the southern areas (**Fig. 2.11A**). In the southwest, along the coast, the velocity vectors are more southwest directed. There is a marked decrease in the amount of displacement from the Western Foothills to the Coastal Plain.

The sense of vertical rotation strain rate undergoes several changes from north to south (**Fig. 2.11B**), with a clockwise rotation dominating in the Hsuehshan Range and the northern part of the Central Range, whereas counter clockwise rotation is more common in the northern part of the Western Foothills and the Coastal Plain. From about 23.5° N to 22.8° N there is a pronounced zone of clockwise rotation that ends abruptly southward, where a counter clockwise rotation dominates in the extreme southwest. The pattern of dilatation strain changes from west to east across the Chaochou-Lishan fault system, with negative values (compression) everywhere in the fold-and-thrust belt and positive values (extension) in the Central Range (**Fig. 2.11C**). There is a marked decrease in the dilation strain rate in the northwestern part of the Western Foothills and the northern part of the Coastal Plain. The direction of the horizontal maximum compressional strain axes (ε_H) is oriented roughly northwestward in the northern and northeastern part of the

fold-and-thrust belt, rotating to west-northwest in the central and southern part. In the Central Range, the orientation of the extension axes is roughly northeast in the northern part, becoming more westward to west-southwest in the south. The maximum shear strain rate is fairly uniform throughout much of the study area (**Fig. 2.11D**). The Western Foothills show slightly higher shear strain rate than the surrounding areas, and there is a slight southward increase. There is a local, east-northeast striking, zone of high maximum shear strain rate in the southwest of the study area. There is a marked, although moderate, roughly east-northeast striking southward increase in the maximum shear strain rate at about 23.5° N. The orientations of the dextral maximum shear planes (black in **Fig. 2.11D**) change from nearly east-west striking in the northern part of the study area to more southwest striking from c. 24° N southward. In the south, the orientations of the dextral maximum shear planes change eastward from southwest striking to more west striking.

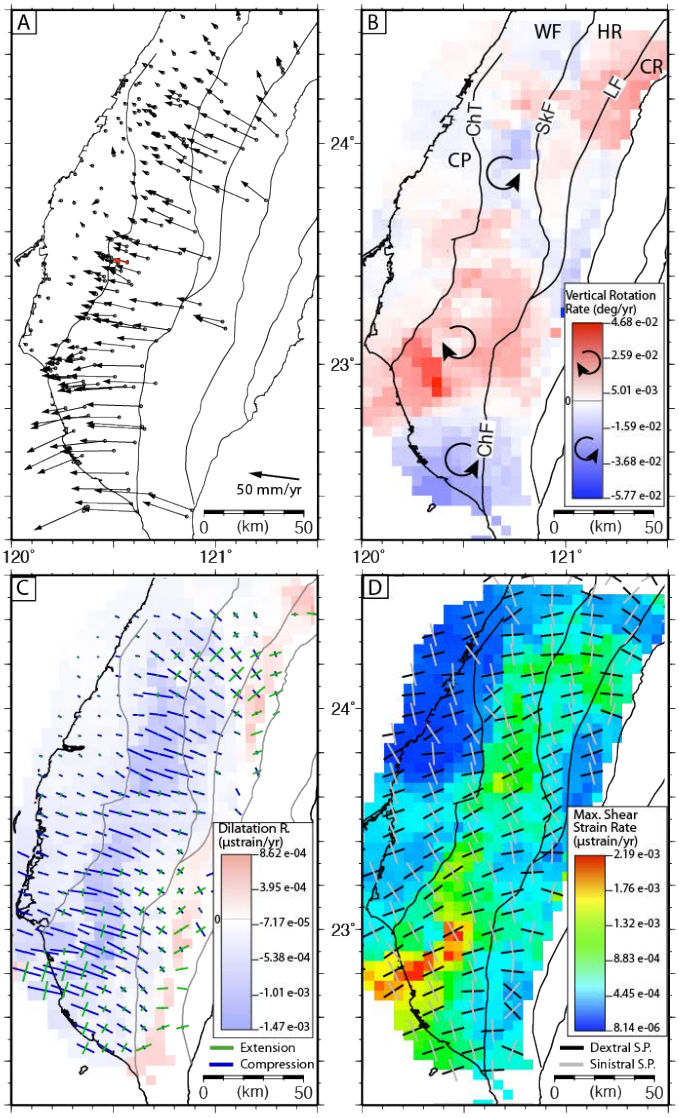

FIGURE 2.11. Geodetic velocities and strain rates. A) GPS horizontal velocity vectors. B) Vertical rotation strain rate. Blue colors represent counterclockwise and red colors clockwise rotation. C) Dilatation strain rates. Blue colors representing compression and red extension. The horizontal maximum compression strain (ε_H) and extension strain rate axes are shown by the blue and green lines, respectively. D) Maximum shear strain rates. Dextral and sinistral shear planes (black and gray lines, respectively) are given. Labels of main faults and tectono-stratigraphic units shown in B are as in **Figure 2.9**.

2.4 Paper III: The Structure of Southwest Taiwan: The Development of a Fold-and-Thrust Belt on a Margins Outer Shelf and Slope [*Biete et al., 2018*]

In **Paper I** [*Brown et al., 2017*], **Paper II** [*Biete et al., in press*] and in a number of recent publications of the ICTJA Taiwan group [e.g., *Alvarez-Marron et al., 2014; Brown et al., 2012; Camanni et al., 2016*], we proposed that effects of both the morphological (the shelf, the shelf/slope break, the slope) and the structural (the necking zone) parts of the margin can be seen in the Taiwan fold-and-thrust belt as along-strike changes in structure, seismicity, contemporaneous stress and strain fields, and topography [*Brown et al., 2017; Biete et al., in press*]. In **Paper III** we investigate this theme further, presenting the results of new geological mapping of the fold-and-thrust belt in southwest Taiwan (from latitudes around 23.3° N to 22.2° N; **Figs. 1.1 and 2.12**), providing a detailed analysis of its structural architecture and how the structure changes from north to south. We go on to propose how these along-strike structural changes can be related to the preexisting structure of the Eurasian continental margin. Below we give a description of the results obtained from the structural analysis that was based on geological mapping, construction of balanced cross-sections and their restoration, along-strike sections, stratigraphic cut-offs and thrusts branch line maps, and a contour map of the basal thrust. The new geological mapping of southwest Taiwan fold-and-thrust belt is shown in **Figure 2.12** with only representative structural data, an A3 size map with all the bedding dip data can be found in the supplementary **Figure SD1_A3** of the Appendix 3.

2.4.1 Surface geology

The study area covers the Coastal Plain and the Western Foothills (including the area covered by Holocene sediments in the south and on the Pingtung Plain) of southwest Taiwan (**Figs. 1.1 and 2.12**). In this area, the Chaochou Fault (ChF) bounds the fold-and-thrust belt to the east and in the west it is bounded by the buried tip line of the Changhua thrust (CT; **Fig. 2.12**; see also, *Yu et al., 1997; Shyu et al., 2005; Yang et al., 2007; Rodriguez-Roa & Wiltschko, 2010; Ching et al., 2011*). However, seismicity to the west of the Changhua thrust indicates that deformation is also taking place beneath most of the Coastal Plain (**Figs. 1.6A and 2.6**)[e.g., *Shyu et al., 2005; Camanni et al., 2016; Brown et al., 2017*].

The structural grain of the fold-and-thrust belt is roughly north-northeast striking, with pronounced, sigmoidal, en echelon changes toward a more northeast strike (**Fig. 2.12**). In the central part of the study area, there is a pronounced north-south change in structural architecture. This change takes place across a complex, roughly east-west striking zone that we call the Hsinhua transverse zone (**Fig. 2.13**). We use the term transverse zone, as defined by *Thomas [1990]*, to be a systematic alignment of lateral connectors between two sets of differing structures. According to this definition, a transverse zone can be manifested as a suite of possible structures (these are described for the Hsinhua zone below) with a range of probable causes (which are specifically

discussed in Paper III discussion section). To the north of the Hsinhua transverse zone, the fold-and-thrust belt area comprises five thrust sheets: the Changhua, Chelungpu, Chutochi, Pingshi, and Chishan thrust sheets, whereas to the south of the transverse zone consists of the Changhua thrust sheet, the Xuxian antiform, and the Kuanglin synform (**Figs. 2.12 and 2.13**).

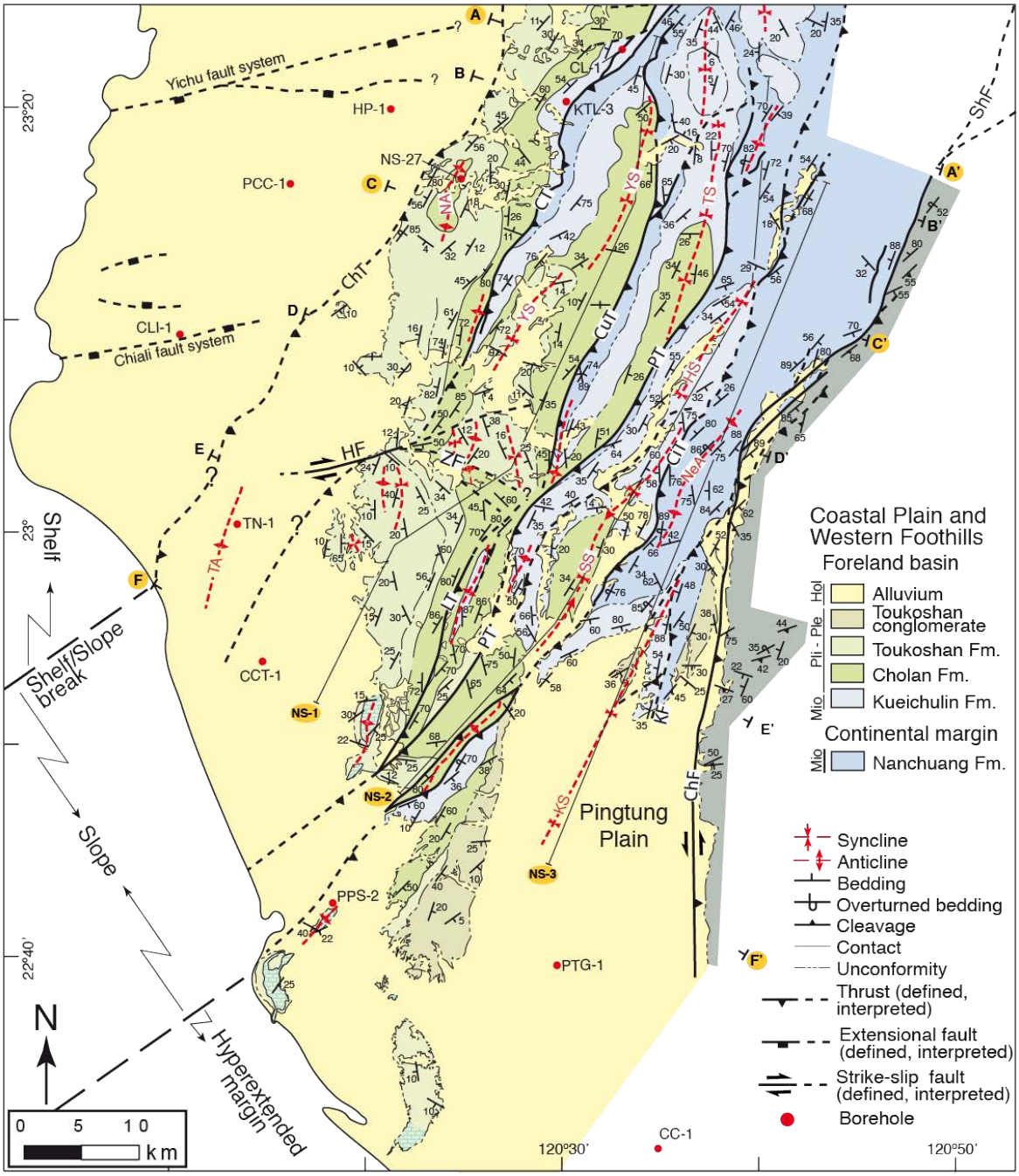

FIGURE 2.12. Geological map of southwest Taiwan with only representative structural data shown. It includes the location of the geological cross-sections from A to F included in Figure 6 of Paper III [*Biete et al., 2018*] in Appendix 1, from which A, C and F are shown in **Figure 2.14**. It also includes the longitudinal cross-sections NS-1 to NS-3 shown in **Figure 2.16**, and the boreholes locations shown in **Figure 2.14**. Structures discussed in the text are labeled. Thrusts: ChT = Changhua thrust; CiT = Chishan thrust; CT = Chelungpu thrust; CuT = Chutochi thrust; LT = Lungchuan thrust; PT = Pingshi thrust. Faults: ChF = Chauchou fault; HF = Hsinshua fault; ZF = Zuojhen fault. Folds: NA = Niushan anticline; NeA = Neiyingshan anticlinorium; SS = Shihchangli syncline; TA = Tainan anticline; TS = Tingpinglin syncline; YS = Yuching syncline; HS = Hsiaolin syncline; KS = Kuanglin synform.

North of the Hsinhua transfer zone, the surface geology shows that the Changhua thrust sheet comprises predominately Cholan and Toukoshan formations, with a minor amount of Kueichulin Fm in the northeast (Fig. 2.12). The Chelungpu, Chutochi and Pingshi thrust sheets, contain predominantly sediments of Middle Miocene-age in its western part through Early Pleistocene in the east, reaching to Holocene in the Chelungpu thrust sheet, whereas the Chishan thrust sheet is composed entirely by Middle to Late Miocene-age Nanchuang Fm (Fig. 2.12).

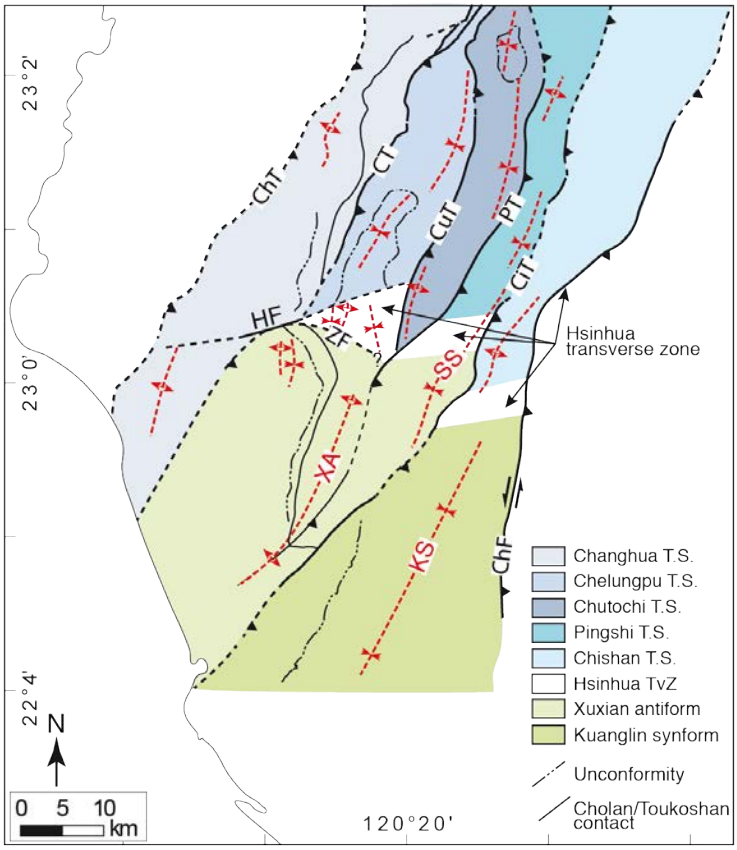

FIGURE 2.13. Structural units of the southwest Taiwan fold-and-thrust belt described in the text. The Hsinhua transverse zone marks the transition from a mostly emergent thrust system in the north to a southern area dominated by the Xuxian antiform and the Kuanglin synform where large areas of the thrust sheets are buried. Labels are as in Figure 2.12.

In the northern part of the Changhua thrust sheet, the structure is that of a steep to gently west dipping, doubly plunging Niushan anticline (NA in Fig. 2.12), whose western limb is locally steep to overturned. In the south, the thrust sheet is covered by Holocene sediments. The roughly east-northeast striking Hsinhua fault (Fig. 2.12) marks the dextral oblique-slip surface rupture of the 1946 Hsinhua earthquake [*Bonilla, 1975; Shyu et al., 2016*]. In the very southwest, the Tainan anticline does not crop out but is marked at the surface by a small area of low topography. The anticline structure is imaged in reflection seismic data [*Huang et al., 2004*].

The Chelungpu and Chutochi thrust sheets show a similar structure, comprised predominately of the gently to moderately south-southwest plunging Yuching and Tingpinglin synclines, respectively. In the immediate hanging wall of the Chelungpu and Chutochi thrusts, the Nanchuang

and Kueichulin formations dip steeply to moderate to the east-southeast before the dips shallow in the Cholan Fm that cores the synclines. In the Yuching syncline the Cholan Fm has numerous local southeast dipping unconformities, and is itself unconformably overlain by the gently south dipping Toukoshan Fm. A connecting splay between the Chutochi and Pingshi thrusts cuts the northern part of the Chutochi thrust sheet. Southward, the Chelungpu thrust sheet, ends against the Hsinhua fault (HF in **Fig. 2.12**). The Chutochi thrust ends against the Pingshi thrust, which cuts across both limbs of the Tingpinglin syncline.

In the north, the internal structure of the Pingshi thrust sheet and the traces of both the Pingshi and Chishan thrusts, are not well resolved because of difficult access and dense forest cover. Despite this, a number of small splays and their related folds have been mapped along the margins of the thrust sheets. The moderately southwest plunging Hsiaolin syncline and the doubly plunging Shihchangli syncline (HS and SS, respectively in **Fig. 2.12**) dominate the structure of the Pingshi thrust sheet. On the basis of an increased thickness of the Kueichulin Fm along the western limb of the Hsiaolin syncline, we interpret the presence of a minor thrust that thickens the Kueichulin Fm and causes minor folding in its hanging wall. The Pingshi thrust is interpreted to continue southward into the eastern limb of the Xuxian antiform (PT in **Fig. 2.12**).

Because of difficult access, only the margins of the northernmost part of the Chishan thrust sheet have been mapped in this study. In this area, the Nanchuang Fm rocks are intensely folded and faulted. The southern part of the Chishan thrust sheet comprises tightly folded and faulted rocks of the Nanchuang Fm, forming the west verging, south-southwest plunging Neiyingshan anticlinorium (NeA in **Fig. 2.12**). We interpret the Chishan thrust sheet to continue southward beneath the Pingtung Plain, although with a prominent along-strike change from the Neiyingshan anticlinorium to the Kuanglin synform (**Figs. 2.12 and 2.13**).

South of the Hsinhua transfer zone, the Changhua and Chishan thrust sheets are mostly covered by Holocene sediments. The Xuxian antiform is composed of Late Miocene through Pleistocene rocks and is bounded to the west by the buried Chelungpu thrust and to the east by the Chishan thrust. Along the western limb of the antiform, there is a pronounced west to southwest dipping Late Pleistocene-age unconformity within the Toukoshan Fm that marks a change from shallow marine to predominately fluvial facies sediments (**Figs. 2.12 and 2.13**). Smaller, local unconformities are widespread within the shallow marine facies rocks of the Lower Toukoshan and Cholan formations.

The Kuanglin synform is bounded by the Chishan thrust in the west and the Chaochou fault in the east (**Figs. 2.12 and 2.13**). It crops out only along its western side and its hinge area in the north. In the west, the Chishan thrust juxtaposes moderately to steeply southeast dipping Late Miocene through Pleistocene rocks against the eastern flank of the Xuxian antiform. Along the western limb of the synform, there is a marked Late Pleistocene erosional unconformity along which fluvial facies of the Toukoshan Fm conglomerate overlies shallow marine sandstone of the same formation (**Figs. 2.12 and 2.13**). In the north, the hinge zone of the Kuanglin synform is

composed of steeply southeast dipping and west dipping Kueichulin Fm thick-bedded sandstone, with and isolated outcrop of Late Pleistocene-age, slate-bearing conglomerate.

The Hsinhua transfer zone (**Fig. 2.13**) marks by an important change along-strike in structure. The zone across which this change takes place is not a single, discrete structure, but is composed of a suite of structures whose northern and southern boundaries are sometimes transitional into the regional-scale structures on either side. In the west, it comprises the roughly east-northeast striking, dextral strike-slip Hsinhua fault (HF in **Figs. 2.12 and 2.13**). The Zuojhen fault (ZF in **Figs. 2.12 and 2.13**) is a zone that consists of several roughly east-southeast striking faults that splay from the Hsinhua fault in the west to form a strike-slip fault system. Eastward, the Pingshi and the Chishan thrusts, as well as the bedding in their hanging walls display marked sigmoidal surface traces. The Pingshi thrust cuts across both limbs of the Tingpinglin syncline, and the Chutochi thrust is cut by it. Between the area of sigmoidal trace of the Pingshi and Chishan thrusts, the Shihchangli syncline (SS in **Fig. 2.12**) plunges moderately southward (approximately 50°) and gently northward (<5°) in its northern and southern parts, respectively. Eastward, in the hanging wall of the Chishan thrust, where it goes through a change in strike, the Neiyingshan antiform terminates abruptly in a southward-dipping monocline and the Kuanglin synform appears (NeA and KS, respectively, in **Fig. 2.12**).

2.4.2 Subsurface structure

The subsurface structure of the fold-and-thrust belt is analyzed using six balanced and restored cross-sections (A-A' through F-F' in **Fig. 2.12**) from which we show three of them in **Figure 2.14,** with the restoration of C-C' and F-F', in **Figure 2.15** (the reader is referred to Paper III in Appendix 1 for the complete set of cross-sections and their restorations), three along-strike sections (NS-1, NS-2 and NS-3 in **Fig. 2.16**), and the contour line map of the basal thrust, thrust branch lines and where possible stratigraphic cut-off maps (**Fig. 2.17**). In the cross-sections we also show the 5.2 km/s isovelocity contour line that provides insights on the location of the top of the basement. Because of the north-south differences in structure across the study area, we divide the description that follows into that to the north of the Hsinhua transverse zone and that to the south of it. We interpret the tip line of the Changhua thrust (ChT) to be that of the basal thrust (**Fig. 2.14**). North of the Hsinhua transverse zone (e.g., sections A-A' and C-C', **Fig. 2.14**), the basal thrust in the west forms a shallow (~1 km depth) flat within the Pliocene or Pleistocene rocks before it ramps down eastward into the Middle Miocene. In this part of the study area, we interpret that the juxtaposition of the Chelungpu, Chutochi, and Pingshi thrust sheets, with their leading thrusts located predominately in the Nanchuang Fm, together with the similar (although slightly increasing toward the east) erosion level in the cores of their respective synclines, to indicate that the basal thrust has a very gentle dip of about 4° toward the east within the Middle Miocene rocks. East of the Pingshi thrust sheet, on the basis of the increased thickness of folded Miocene rocks, and on the uplift of higher velocity rocks (>5.2 km/s), we interpret the basal thrust to ramp down into the basement east of the Chishan thrust branch point (e.g., sections A-A' and

C-C' Fig. 2.14). Displacement along individual thrusts in section A through F, measured as the distance that the top of Kueichulin moved along a thrust surface, generally decreases southward and increases eastward. Note, however, that we have poor control on section A and limited information for the Chishan thrust where this cut-off is not found (Fig. 2.14). From restored cross-sections, we estimate the minimum shortening in the north of the Hsinhua transvers zone to be between 17 and 25 km (restored section C; Fig. 2.15 and Fig. 7 in *Biete et al., [2018]*).

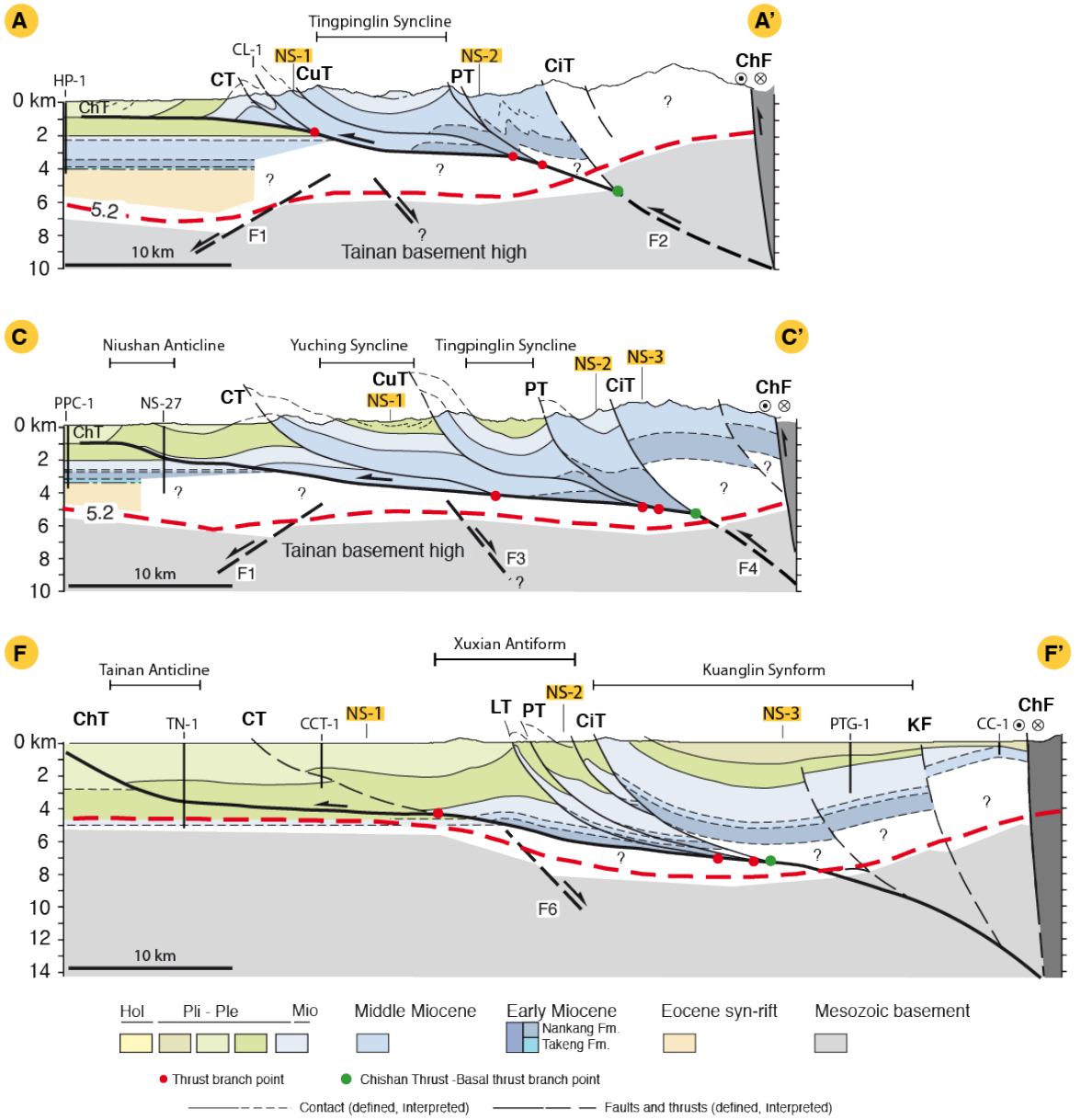

FIGURE 2.14. Three geological cross-sections through the southwest Taiwan fold-and-thrust belt. Their locations are shown in Figure 2.12. They include the projected location of the boreholes used for their construction located in Figure 2.12, and the branch points (red dots) of individual thrusts. The branch point of the CiT (green dots) is interpreted to mark the ramp down into the basement of the basal thrust. Branch points were used to construct the branch line map in Figure 2.17. The restoration of sections C and F are shown in Figure 2.15. Red dashed line is the 5.2 km/s isovelocity contour from the local tomography. Faults interpreted in the basement are labeled F1 to F6 for correlation with Figures 2.15 and 2.16. Labels are as in Figure 2.12. See Figure 6 in *Biete et al., [2018]* in Appendix 1 for the complete set of cross-sections.

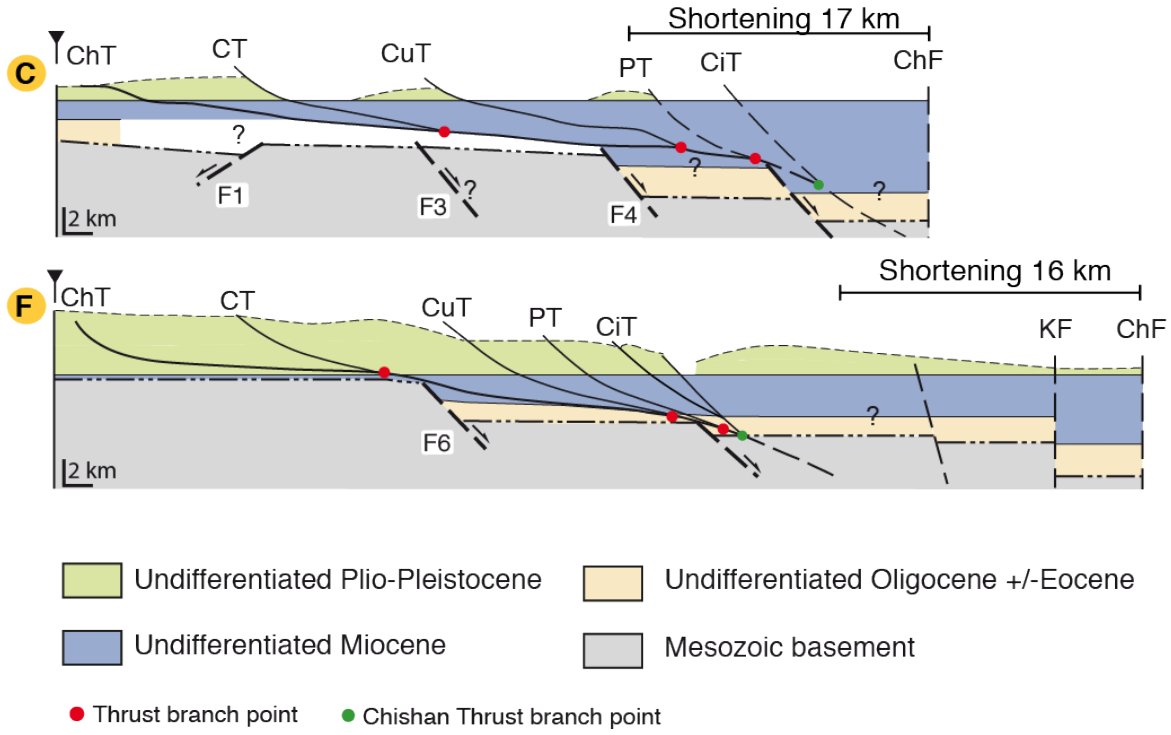

FIGURE 2.15. Restored sections C and F. The sections have been restored using bed-length balancing of top and base of Kueichulin Fm and are area balanced for the rest of the Miocene units above the basal thrust. Faults interpreted in the basement are labeled F1 to F6 and correspond to those in Figures 2.14 and 2.16. Abbreviations are as in Figure 2.12. See Figure 7 of *Biete et al., [2018]* in Appendix 1 for the complete set of restored sections.

South of the Hsinhua transverse zone (section F-F', Figs. 2.14), the fold-and-thrust belt is poorly exposed, being buried by Holocene sediments in thrust-top basins. Data from published boreholes was used in order to place constraints on stratigraphic thickness. Borehole TN-1 (section F-F' in Fig. 2.14) shows that the Cholan and Toukoshan formations thicken significantly compared to north of the Hsinhua transverse zone, whereas along the western limb of the Xuxian anticline the Miocene thins or even disappears. In agreement with the interpretation of *Huang et al., [2009]* and *Mouthereau et al., [2001],* we interpret the basal thrust to be listric along its westernmost part before forming a flat within the Cholan Fm at ~4 km depth (e.g., section F-F' in Fig. 2.14). Eastward, we interpret it to ramp down into the Middle Miocene rocks beneath the Xuxian antiform, since these rocks are exposed in its core and in thrust sheets along its eastern flank. Based on the shallowing of the 5.2 km/s isovelocity line, we interpret the basal thrust to ramp down into the basement east of the Chishan thrust (e.g., section F-F' in Fig. 2.14).

The Kuanglin synform is only exposed north of the Pingtung Plain (Fig. 2.12). On the basis of our surface structural data, boreholes PTG-1 and CC-1 (section F-F' in Fig. 2.14), and following *Mouthereau et al., [2001]* and *Chiang et al., [2004]*, we interpret the Kuanglin synform to widen southward into a broad, open syncline. Despite limited control on stratigraphic cut-offs we nevertheless interpret displacement to increase eastward, and in section E calculate a minimum shortening of around 16 km, although this calculation is highly speculative.

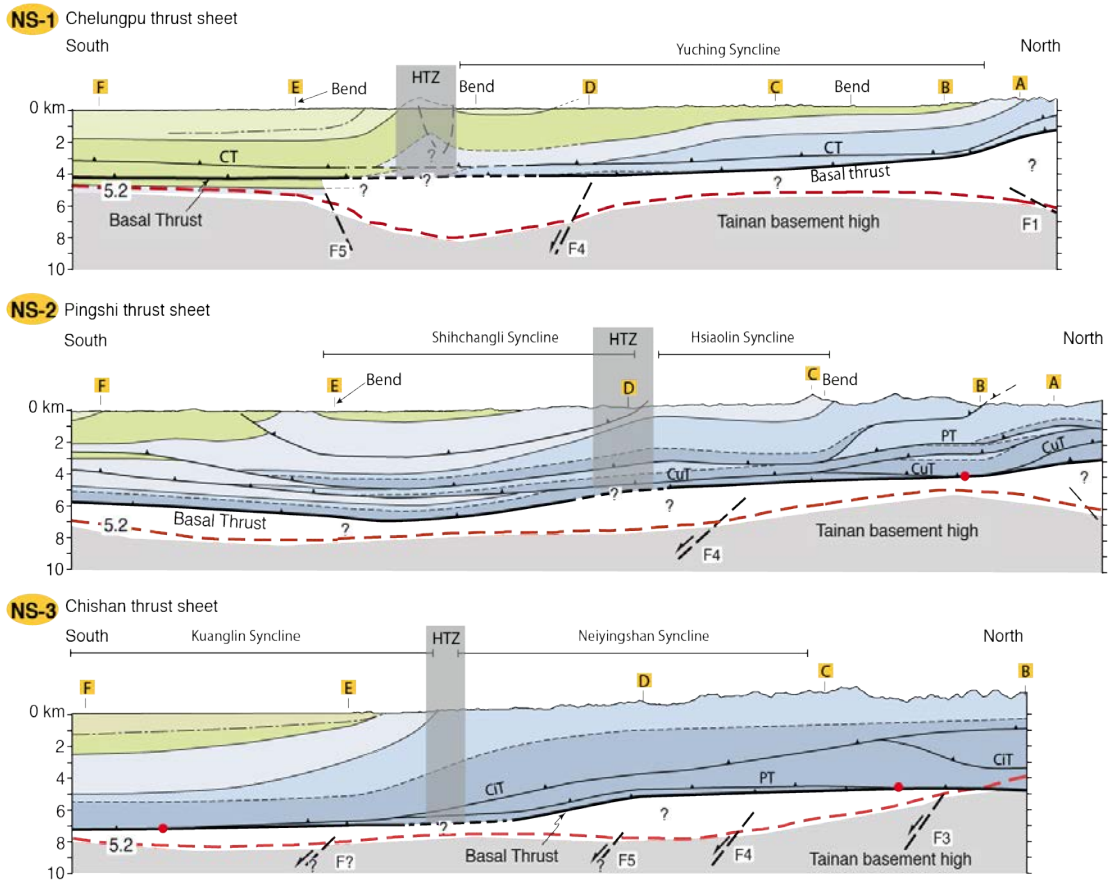

FIGURE 2.16. North-south geological cross sections. NS-1 along the Chelungpu thrust sheet, NS-2 along the Pingshi thrust sheet, and NS-3 along the Chishan thrust sheet. The area corresponding to the Hsinhua transverse zone (HTZ) of Figure 2.13 is shown by the gray shaded box. The dashed part of the basal thrust below the HTZ that is marked by a question mark indicates uncertainty about what the interaction between the two is. Faults labeled F1 to F6 correspond to those in Figures 2.14 and 2.15. Legend is as in Figure 2.14. Red dashed line is the 5.2 km/s isovelocity contour from the local tomography. Abbreviations are as in Figure 2.12.

A pronounced, asymmetrical, and faulted anticline appears in the along-strike section NS-1 associated with the Hsinhua transverse zone (Fig. 2.16). We interpret this anticline to form a dextral, positive flower structure that possibly affects the basal thrust (NS-1 in Fig. 2.16). We interpret the transition in structure across the Hsinhua transverse zone, in along-strike sections NS-2 and 3 (Fig. 2.16), to be marked by the smooth, continuous, and general southward dip of all contacts. Although, the details of this area of transition may be more complex, and it cannot be fully resolved with the current data set.

A contour map of the basal thrust surface is obtained from the six cross-sections and three along-strike sections (Fig. 2.17). This map shows that the basal thrust dips overall gently toward the southeast. Two areas were there are changes in strike of the depth contours are interpreted to be oblique ramps in the basal thrust. We call these the Yichu and Hsinhua oblique ramps (Fig. 2.17a). Both ramps end at the Chishan thrust branch line. On the basis of the shallowing of the 5.2 km/s isovelocity surface, the basal thrust is interpreted to ramp down into the basement east of the Chishan thrust branch line (gray area in Fig. 2.17b). From north to south, the branch line of the Chelungpu thrust undergoes a marked change in strike, from nearly downdip along the Yichu

ramp to roughly parallel to the basal thrust contours across the Hsinhua ramp (Fig. 2.17b). The branch lines of the Chutochi and Pingshi thrusts are oblique to the basal thrust contours across both the Hsinhua and Yichu ramps.

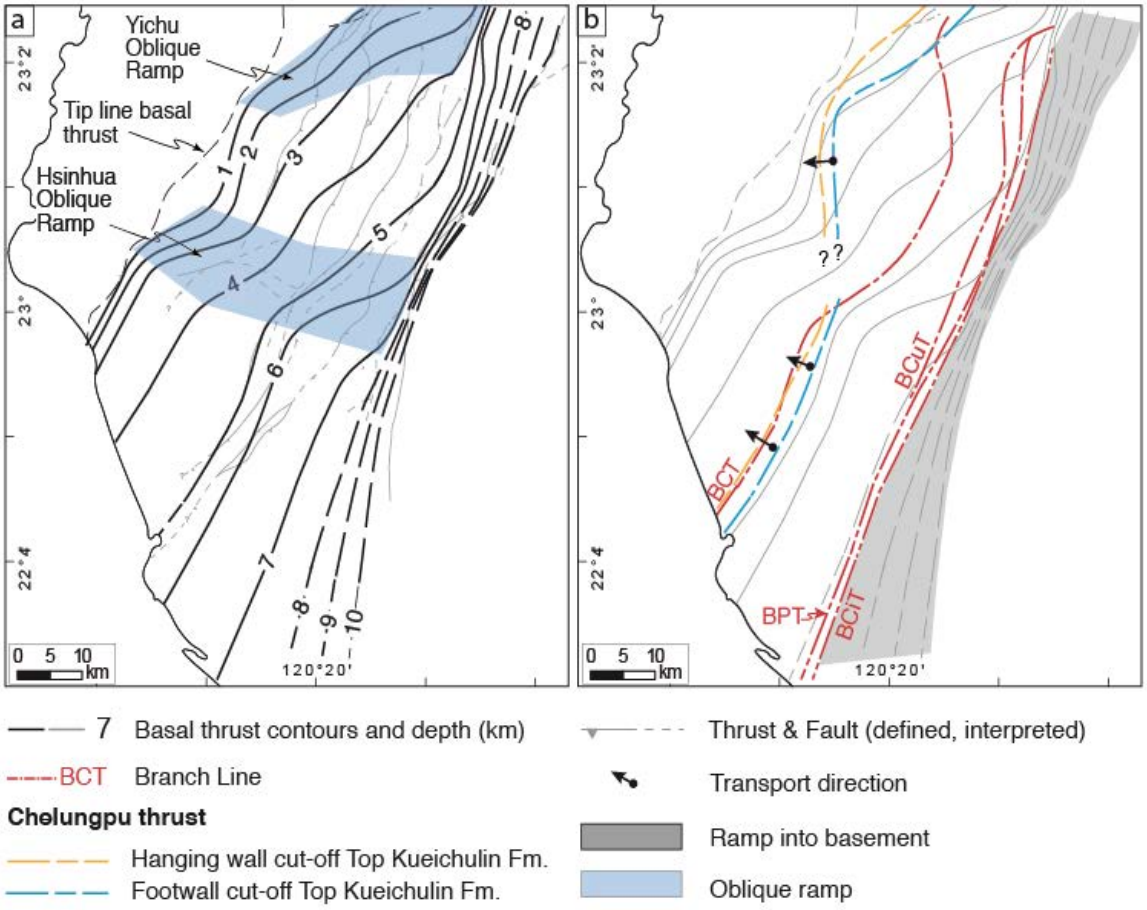

FIGURE 2.17. (a) Structural contour line (in km) map of the basal thrust, blue areas are the interpreted oblique ramps. Thrusts and faults are shown in light gray. (b) Hanging wall and footwall cut-off lines of the top of Kueichulin Fm in the northern and southern areas, and branch lines (red) of the Chelungpu (BCT), Pingshi (BPT), Chutochi (BCuT), and Chishan thrusts (BCiT) are shown superposed on the basal thrust contour lines. The arrows show the assumed displacement direction, which is interpreted to be perpendicular to the frontal stratigraphic cut-offs. The interpreted ramp into the basement is labeled in gray. This ramp starts from the BCiT that is at about 5 km in the north and deepens southward till more than 7 km.

From our data we can only determine the hanging wall and footwall cut-offs with respect to the basal thrust for the Kueichulin Fm (Fig. 2.17b). In the north, these cut-offs undergo significant changes in strike and location with respect to the basal thrust contour and the Chelungpu branch line compared to farther south. In the north, the cut-offs parallel the basal thrust contours along the Yichu ramp, reaching up to nearly 15 km west of the branch line at a depth of 1 to 2 km. They then take on a nearly north-south strike, cutting obliquely across the basal thrust contours along the Hsinhua oblique ramp to become parallel to them where they are east of the Chelungpu branch line at a depth of 5 to 6 km. The transport direction, which is calculated to be perpendicular to the footwall and hanging wall cut-offs, is approximately westward in the north, becoming more west-northwest in the south (Fig. 2.17b). These changes in orientation and loca-

tion of the cut-offs relative to the thrust branch line provide further evidence that the Yichu and, in particular, the Hsinhua oblique ramp have an important effect on the structure of the thrust system. Although these determinations of transport direction provide important kinematic information for our structural model, the information is limited since we were not able to resolve the location of the cut-offs across the Hsinhua oblique ramp, nor the cut-offs for other thrusts. Nevertheless, the transport directions obtained in this way are in good agreement with long-term dis- placements fields determined by *Lacombe et al., [1999, 2001]* and modeled with GPS data by *Ching et al., [2011]*. There are also significant changes in fold style, plunge direction, and plunge amount associated with both the Yichu and the Hsinhua oblique ramps (**Figure 9c** in *Biete et al 2018,* Appendix 1).

The structure beneath the basal thrust is highly interpretative throughout the study area, and to show this, we have left parts of the sections blank (**Figs. 2.14 and 2.16**). Nevertheless, we feel that it is essential for understanding the potential role played by the basement in the deformation to attempt some constraints on the structure beneath the basal thrust. From the borehole data and the surface geology (**Figs. 1.4, 2.12 and 2.14**), it is clear that there are changes in thickness of the Miocene rocks from one thrust sheet to another. These changes in thickness have been interpreted here (**Fig. 2.15**), and in a number of other studies in southwest Taiwan [*Suppe, 1986; Yang et al., 2007, 2016; Rodriguez-Roa & Wiltschko, 2010; Alvarez-Marron et al., 2014*], to indicate the presence of roughly east-northeast striking, Miocene-age, extensional faults that had developed on the outer shelf, and slope areas of the continental margin [e.g., *Lin et al., 2003; Yang et al., 1991*]. In our sections (**Figs. 2.14 and 2.16**) we have also interpreted changes in depth of the 5.2 km/s isovelocity line to coincide with several of these extensional faults allowing us, in a number of cases, to trace them from one section to another (e.g., F1 and F3 in **Figs. 2.14 and 2.16**) where they affect the geometry of the basement-cover interface proxy. We stress, however, that the details of the basement structure remain speculative.

CHAPTER 3 Discussion

In Chapter 2 of this thesis we have shown that regional-scale east-northeast striking faults that have been mapped on the necking zone of the Eurasian continental margin in the Taiwan Strait can be traced into the fold-and-thrust belt in south central Taiwan. A number of these are being reactivated, causing important along-strike changes in structural architecture, seismicity, topography, stress field, displacement field and strain field of the fold-and-thrust belt in this area, supporting the hypothesis given in Chapter 1. Of these fault systems, the most important along-strike change is associated with the upper part of the necking zone, where the Yichu (or A), Meishan, and B faults (Figs. 2.2 and 3.1A) are of particular importance. In the offshore, the entire necking zone of the margin has regional-scale basement highs and lows (i.e., the Northern Depression, Central Uplift, and Southern Depression [*Lin et al., 2003*], or the failed rift of *Yeh et al., [2012]* and *McIntosh et al., [2014]*) (**Figs. 2.1** and **3.1A**) that can be traced into the Coastal Plain and, we suggest, into the fold-and-thrust belt where the Tainan Basement High may correlate with the Central Uplift of the Tainan Basin (**Figs. 2.1** and **3.1B**) [c.f., *Lin et al., 2003; Li et al., 2007; Deng et al., 2008; Camanni et al., 2016*]. These basement highs and lows result in important changes in thickness of the Miocene and Pleistocene sediments [e.g., *Hsiao, 1970; Shaw, 1996; Yang et al., 2014*]. Furthermore, several east-northeast striking faults have been historically active in the Coastal Plain area, with the 1906 Meishan and the 1946 Hsinhua earthquakes causing dextral oblique-slip surface ruptures [*Bonilla, 1977; Shyu et al., 2016*]. We suggest, therefore, that there is sufficient evidence that regional-scale east-northeast striking faults on the necking zone of the Eurasian continental margin can be traced into the fold-and-thrust belt in south central Taiwan where they are being reactivated, and are having an important effect on the development of the fold-and-thrust belt. In this chapter we present a summary discussion that brings together the key take-away points from the three papers that form the main body of work of the thesis.

The most important along-strike change in the south central Taiwan fold-and-thrust belt takes place around 23.5° N (Zone A: **Fig. 3.1**), which is the on-land prolongation of the upper part of the necking zone. Zone A is widely recognized as an area of significant change in the structure, fault kinematics, and seismicity of the thrust belt [e.g., *Deffontaines et al., 1997; Lu et al., 1998; Lacombe et al., 1999; Mouthereau et al., 2002; Cheng et al., 2003; Mouthereau and Lacombe, 2006; Wu et al., 2008, 2010; Byrne et al., 2011; Alvarez-Marron et al., 2014*], and it has been suggested by numerous authors [*e.g., Lu et al., 1998; Lacombe et al., 1999*] that the intense deformation across it (section 2.1) is largely due to buttressing [*Hayward and Graham, 1989*] of the thrust system by the basement high. We concur with the previous authors that buttressing across the upper part of the necking zone appears to be an important deformation process. Zone A (**Fig. 3.1**) marks a significant southward increase in seismicity (**Fig. 2.6**), in topography, as well as a change in the directions of the contemporaneous maximum horizontal compressive stress (S_H), strain (ε_H), and the horizontal displacement vectors (**Figs. 2.11 and 3.2**). Focal mechanism determinations by *Chang et al., [2007], Hsu et al., [2010], Wu et al., [2010], Chao et al., [2011]*, and *Yang et al., [2016]* have shown that the dominant fault type across Zone A is dextral strike-slip with lesser oblique thrusting (**Fig. 1.6D**). The fault type determinations of these authors are in agreement with the results determined from our stress inversions, both indicating that east-northeast striking dextral strike-slip faults are active at depth (**Figs. 2.9, 2.10 and 3.2**).

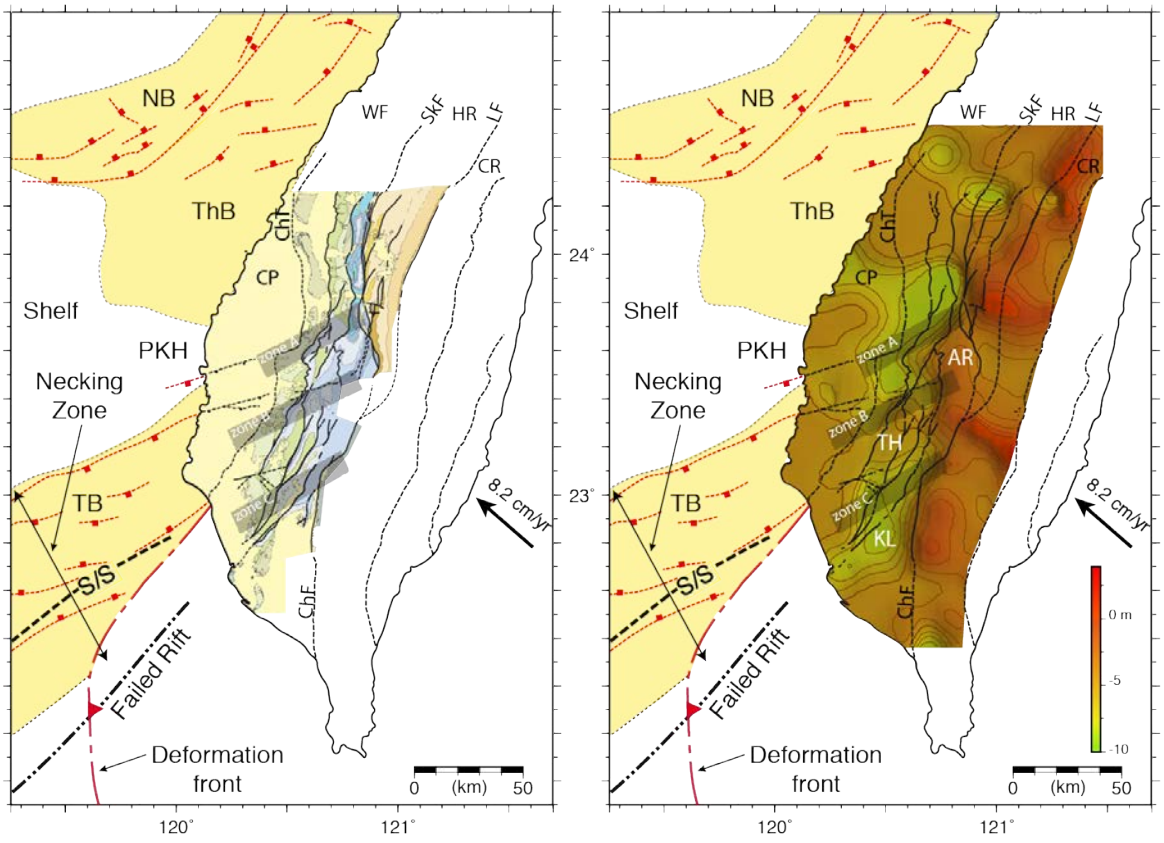

FIGURE 3.1. A) Simplified geological map of the south central Taiwan fold-and-thrust belt, set within the structural and morphological setting of the Eurasian continental margin. B) Map of the 5.2 km/s isovelocity surface for the depth to the top of the basement extracted from the 3D tomographic model of *Kuo-Chen et al., [2012]*. The main fault traces of the fold-and-thrust belts and faults juxtaposing tectono-stratigraphic units are shown in black solid and dashed (interpreted) lines and were extracted from **Figure A**. The transparent gray boxes, called zones A, B, and C, highlight areas where there are marked changes in the structural grain of the fold-and-thrust belt that we interpret to be due to reactivation of faults in the basement. CP = Coastal Plain, WF = Western Foothills, HR = Hsuehshan Range, CR = Central Range. Faults ChT = Changhua thrust, LF = Lishan fault, SkF = Shuilikeng fault, ChF = Chauchou fault. The axis of the failed rift of **Figure 1.1** is shown in thick black dashed line. S/S = shelf/slope break, TB = Tainan Basin, ThB = Tahishi Basin, NB = Nanjihtao Basin and PKH = Peikang Basement High, TH = Tainan basement high.

Many authors [e.g., *Hu et al., 1997; Bos et al., 2003; Chang et al., 2003; Mouthereau & Lacombe 2006; Ching et al., 2007, 2011; Wu et al., 2008, 2010; Hsu et al., 2009; Chen et al., 2017*] have interpreted the area of our Zone A to be a symmetrical structural high (the Peikang Basement High) on the margin shelf that acts as a symmetrical indenter around which rocks in the fold-and-thrust belt are moving. As was pointed out by *Mouthereau & Lacombe [2006]*, however, neither the paleostress nor the contemporaneous s1 trajectories fit with those estimated for a symmetrical basement high by analogue [*Lin & Huang 1998*] and numerical models [e.g., *Hu & Angelier 1996; Hu et al., 1997; Lin & Huang 1998*]. Nor do the contemporaneous stress trajectories, the horizontal displacement field, or the strain field (Figs. 2.11 and 3.2) fit with those predicted to occur around an indentor into a fold-and-thrust belt [e.g., *Macedo & Marshak 1999; Marshak 2004*]. We suggest, therefore, that the along-strike changes in structure, seismicity, topography, contemporaneous stress and strain fields, and displacement vectors that take place across Zone A have a causal relationship with the reactivation of

structures inherited from the upper part of the necking zone of the continental margin. We further suggest that these along-strike changes are indicative of an east-northeast striking, dextral strike-slip lateral structure (the Choshui lateral structure of *Alvarez-Marron et al., [2014]*) that is forming by the reactivation of preexisting Miocene basin-bounding faults along the upper part of the necking zone

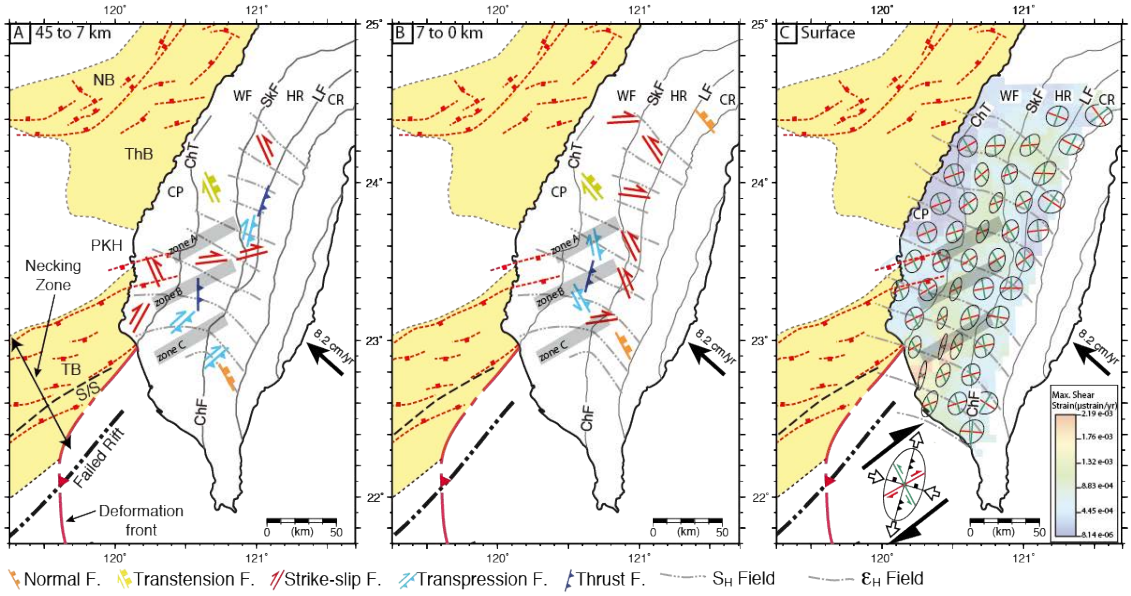

FIGURE 3.2. Summary of the stress and strain results for south central Taiwan set within the structural and morphological setting of the Eurasian continental margin. The relative plate motion vector between the Philippine Sea Plate and Eurasia is shown. A) The most probable fault planes and their kinematics calculated in the basement. An interpolated S_H trajectories are shown by dashed gray lines. B) The most probable fault planes and their kinematics calculated in the fold-and-thrust belt and sedimentary carapace. S_H as in A. C) Maximum shear strain with deformation ellipses determined for groups of four grid units. Dextral and sinistral maximum shear planes are shown in red and green. The interpolated horizontal maximum compression strain rate (ε_H) trajectories are shown by the dashed gray lines. The inset shows the expected fault orientations and kinematics in a dextral strike-slip fault system. The maximum compressive strain field (ε_H) directions from Figure C are shown by dashed gray contour lines. Labels of faults and tectono-stratigraphic units are shown in **Figure A** and as in **Figure 3.1**. The transparent gray boxes, called zones A, B, and C, highlight areas where there are marked changes in the stress and strain results in the fold-and-thrust belt that we interpret to be due to reactivation of faults in the basement. The axis of the failed rift of **Figure 1.1** is shown in thick black dashed line. S/S = shelf/slope break, TB = Tainan Basin, ThB = Tahishi Basin, NB = Nanjihtao Basin and PKH = Peikang Basement High.

Southward, zones B and C (**Fig. 3.1**) comprise two areas of along-strike change that are developing on the necking zone of the margin. These changes are not as pronounced as those at the upper part of the necking zone, but they are nevertheless significant features. There is an important change in the structural architecture across zone B, from the broad, basement-cored anticlinorium of the Alishan Ranges to the open synclines above a nearly horizontal basal thrust located in the Miocene and younger sediments (compare section B-B' and C-C' in **Fig. 2.3**). En echelon, sigmoidal changes in the strike of fold axial traces, the surface trace of thrusts (**Fig. 2.2**), and of topographic ridges (**Figs. 2.7B and C**) at zones B and C all combine to suggest that these are being offset dextrally by east-northeast oriented strike-slip faults. Sigmoidal offsets of structures and topography in fold-and-thrust belts are generally attributed either to reactivation of footwall basement faults or as transfer zones (tear faults) in the hanging wall that are caused by mechanical differences along the basal thrust

[e.g., *Albers, 1967; Mugnier et al., 1999; Ruh et al., 2014; Koyi et al., 2016*]. In southwest Taiwan, the homogeneity of the hanging wall structural architecture from zone B southward seems to argue against strong mechanical differences along the basal thrust. Finally, the numerous earthquakes in the area of the Tainan Basement High (**Figs. 2.6 and 3.1B**) that have dextral strike-slip focal mechanisms with one roughly east-northeast to northeast striking nodal plane [e.g., *Hsu et al., 2010; Wu et al., 2010*], together with the dextral east-northeast striking surface rupture of the 1946 Hsinhua earthquake (**Figs. 1.5 and 2.12**) [*Bonilla, 1977*], provide further support for the interpretation that the en echelon sigmoidal features observed at zones A and B are related to the dextral strike-slip reactivation of east-northeast striking basement faults along the flanks of the Tainan Basement High (**Fig. 3.1B**). From Zone B southward, the highly structured area of the necking zone as well as the shelf/slope break and the slope area (**Fig. 3.2**), display major changes in the S_H direction, in the strain rate derived directions of eH and dextral maximum shear planes, and in the horizontal displacement field vectors (**Figs. 2.9, 2.11 and 3.2**). The southward changes in all of the above data suggest that they are not due to a symmetrical indentor, but rather to the reactivation of faults related to the complex rifted margin geometry in this area.

A major objective of this thesis was to further test the hypothesis presented in Chapter 1 by carrying out detailed structural mapping across the area of the margins necking zone, the shelf to slope transition, and the slope (from Zone B to the south) (**Figs. 1.1 and 3.1**). In what follows, we briefly look at possible linkages between the morphological parts of the margin and the structure of the fold-and-thrust belt. In southwest Taiwan, both the mapped surface trace of thrusts and the subsurface contours of the basal thrust undergo a series of sigmoidal bends to take on an orientation that approximates that of the shelf/slope break and the onset of the hyperextended part of the margin (**Figs. 2.12 and 3.1A**). It is at the shelf/slope break where the frontal thrust of the fold-and-thrust belt goes offshore to form the front of the marine accretionary prism (**Figs. 1.1 and 3.1**; see also, *Lin et al., 2008*). Furthermore, the area encompassed by the Yichu and Hsinhua oblique ramps roughly correlates in location and strike with a significant southeastward increase in thickness of the Miocene through Pleistocene sediments [e.g., *Chou, 1972, 1980*] and with a change in facies toward deeper water deposits [*Chou, 1972; Lin & Watts, 2002; Castelltort et al., 2010; Nagel et al., 2013*]. In addition, the P-wave velocity highs and lows imaged in the 6 km depth map **(**Fig. 3.3) are strongly suggestive that there is topography of the basement, with a roughly northeast striking structural grain; similar to that of extensional fault systems mapped on the margin offshore [e.g., *Yang et al., 1997, 2016; Lin et al., 2003*]. Fault-bounded, regional-scale basement highs and lows are well known just offshore to the west (i.e., the Northern Depression, Central Uplift, and Southern Depression) [*Lin et al., 2003*]. While the resolution of the velocity model (see Section 1.5.4) does not allow us to resolve the detail of the structure mapped at the surface, it is sufficient to be able to see the coincidence between the Yichu and Hsinhua oblique ramps and the northern and southern flanks, respectively, of the Tainan Basement High (**Figs. 2.17 and 3.3**). This coincidence leads us to interpret both these ramps as being linked to topographic highs and lows in the basement (**Figs. 2.17 and 3.3**). This interpretation implies that there is a strong causal relationship between the basement structure and the geometry of the basal thrust. While we draw smooth, continuous contours for the basal thrust, it is likely that the east-northeast striking faults that bound similar basement highs and lows offshore, and which extend

into the Coastal Plain [e.g., *Yang et al., 1991, 2016; Lin et al., 2003; Camanni et al., 2016*], also bound the Tainan Basement High. The widespread occurrence of seismicity with dextral strike-slip focal mechanisms in the area around the Tainan Basement High is, furthermore, suggestive of reactivation of these faults [e.g., *Hsu et al., 2010; Wu et al., 2010*], and they may breach the basal thrust to possibly form structures such as the Hsinhua fault system. Finally, in the very southwestern part of the fold-and-thrust belt, the S_H direction, the strain rate derived directions of ε_H and dextral maximum shear planes (**Fig. 3.2**), and the horizontal displacement field vectors (**Fig. 2.11A**) all take on a roughly east-northeast to west-southwest orientation, parallel to the structures in the margin offshore. A zone of GPS-derived high maximum shear strain rate is also east-northeast striking, into the Coastal Plain at the on-land projection of the failed rift of *Yeh et al., [2012], McIntosh et al., [2014],* and *Lester et al., [2014]* (**Fig. 3.2C**). All of the features given above suggest that the structures of the margin are influencing the deformation style of the southwest fold-and-thrust belt and provide additional evidence that there is a casual relationship between the two.

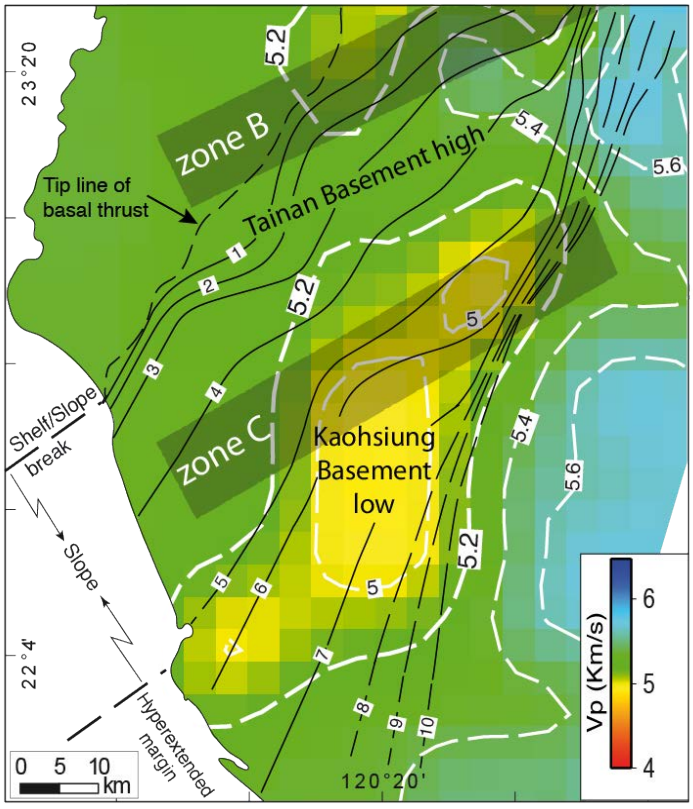

FIGURE 3.3. The 6 km depth slice of the Vp tomography model of *Kuo-Chen et al., [2012]* for the southwest Taiwan area. Several isovelocity lines in km/s are shown in white dashed line, including the 5.2 km/s represented in geological sections. The superposed thin black lines correspond to the depth contours in km of the basal thrust.

Another factor that may be influencing the along-strike structural changes in the southwest Taiwan fold-and-thrust belt could be related to mechanical differences along the basal thrust [e.g., *Albers, 1967; Mugnier et al., 1999; Ruh et al., 2014; Koyi et al., 2016*] that can be caused by changes in sedimentary thickness and facies. Although *Mouthereau et al., [2001]* explore some aspects of the influence of stratigraphic thickness and facies on the structure of the fold-and-thrust belt, we feel that more work, which should include numerical modeling, needs to be carried out before we can begin to draw conclusions about the influence of changes in sedimentary thickness and facies on the fold-and-thrust belt in southwest Taiwan.

CHAPTER 4 Conclusions

In this thesis, we have adopted a multidisciplinary methodological approached to test whether or not the structural (e.g., necking zone, extensional fault system, failed rift) and morphological (e.g., the shelf, shelf/slope break, slope) features of the Eurasian continental margin that are being incorporated in the south central Taiwan fold-and-thrust belt are affecting its structure, as well as transitory features such as seismicity, contemporaneous stress and strain fields, and topography.

We have traced east-northeast striking extensional faults and regional-scale basement highs and lows mapped on the necking zone of Eurasian continental margin in the Taiwan Strait into the Taiwan fold-and-thrust belt. We later suggest that these inherited structures of the margin are being reactivated, causing important along-strike changes in the fold-and-thrust belt, and influencing its structural and architectural development and kinematics.

The most important along-strike changes in the south central Taiwan fold-and-thrust belt takes place across the continental shelf to the necking zone. We suggest that the abrupt north-south change in the structure, increase in the amount of seismicity, and increase in topography, together with, the north-south variation in direction of S_H, ε_H, and the horizontal displacement vectors, have a causal relationship with the reactivation of structures inherited from the upper part of the necking zone of the continental margin. Furthermore, where the upper part of the necking zone is involved in the deformation, east-northeast striking dextral strike-slip active faults estimated from the stress inversion dominate. The orientation of these activated faults is roughly subparallel to known fault systems in the basement, suggesting that the east-northeast striking fault system inherited from the necking zone of the continental margin are optimally oriented relative to S_H for reactivation. These interpretations support the hypothesis that the reactivation of these faults appears to be controlling the structural development and kinematics of the fold-and-thrust belt in this area.

The regional-scale study of southwest Taiwan fold-and-thrust belt show less pronounced along-strike changes across the necking zone. These are marked by en echelon, sigmoidal offsets in the strike of fold axial traces, the surface trace of thrusts, and of topographic ridges. These changes are suggestive of dextral strike-slip fault displacement that is interpreted to be due to the reactivation of east-northeast striking basement faults on the necking zone. The widespread, deep seismicity that is taking place across most of the necking zone provides evidence that the basement is involved in the deformation, but it is difficult to correlate events with individual faults. Nevertheless, the basement appears to be deforming without being incorporated into the thrust sheets. In the far southwest, an east-northeast striking zone of maximum shear strain rate coincides with the on-land projection of a failed rift imaged by reflection seismic data offshore. A paucity of seismicity in this area precludes an estimation of the principal stress axes orientations and determination of fault type, but the calculated strain ellipse is in keeping with it also being a zone of dextral strike-slip faulting (**Fig. 3.2C**).

The detailed structural analysis in southwest Taiwan fold-and-thrust belt reveals along-strike changes in its structure that takes place across the necking zone of the Eurasian continental margin. There, we interpret the structure of the fold-and-thrust belt to be an imbricate thrust system with a pronounced north-south change in structural architecture across a roughly east-west striking zone

that we call the Hsinhua transverse zone, which falls along the on-land projection of the shelf/slope break (**Figs 2.12 and 3.3**). The basal thrust to the imbricate thrust system dips gently south-eastward, but it has two pronounced sigmoidal changes in strike that form what we call the Yichu and Hsinhua oblique ramps. We suggest that the dextral strike-slip faulting, sigmoidal bending of the surface trace of thrusts, folds axes, and bedding (i.e., the Hsinhua transverse zone), together with the along-strike change in structure that occur in the fold-and-thrust belt of southwest Taiwan can be directly linked to these two oblique ramps. We furthermore suggest that both these oblique ramps can be directly correlated with topographic highs and lows that we interpret to occur in the basement (**Fig 3.3**) and that this possibly indicates a causal relationship between the basement structure, the geometry of the basal thrust, and the along-strike changes mapped in the surface geology. We also acknowledge that the along-strike structural changes in the southwest Taiwan fold-and-thrust belt could also, in part, be related to mechanical differences along the basal thrust that can be caused by the changes in sedimentary thickness and facies that take place across the outer part of the shelf and the slope areas of the margin. This hypothesis would need further research, including numerical modeling.

Acknowledgements

Throughout the writing of this thesis I have received a great deal of support and assistance. I would first like to thank the Ministerio de Economia y competititividad, who provide me with the funding without which this thesis will not be here (BES-2014-070122 and PGC2018-094227-B-I00). I would also like to thank this Ministerio for providing funding for me to go in short stays outside my institute, and give me the opportunity to work with different researchers and institutions, which enlarge significantly my experience and knowledge (EEBB-I-16-11039 and EEBBI-17-12702).

I would also like to thank my supervisors, Drs. Joaquina Alvarez Marron and Dennis Brown, first to choose me for this thesis and give me the opportunity for all this "experience in a lifetime", secondly, and more important, for their invaluable expertise, I hope I have learnt a little of it, for their patience especially in teaching me how to writte scientific papers, and of course for their help to push this thesis to be finished in the right time (the waiting for the acceptance of a paper smashed up for some month though…). Many, many thanks!

The two supervisors of my short stays in Taiwan and Sweden are also greatly thanked. Hao Kuo-Chen in the National Central University of Taiwan, provide me with everything needed and help me to learn everything about earthquakes. I don't want to forget Renn Chang, Hoa's assistant during that period, for her invaluable help in finding accommodation, her assistance in how to manage in Taiwan and for showing me around. Björn Lund, from the Uppsala University, is also greatly thanked, he provided all the knowledge in stress which is the body of my last paper, but more importantly for giving me his time although being very very busy! He is of course also thanked for taking me with his colleagues climbing!

Of course I would like to thank my base camp, the Institute of Earth Sciences Jaume Almera, and all its members. Although the building is not the most welcoming one, with its grey and yellow style looks more like a ship than an institute, it has been a pleasure to share this time with all its members, administration staff, maintenance and cleaning staff and principal researchers. A special thanks goes for Marc Español, the solving everything IT guy. He has help in all kind of problems and give unbelievable good advice. Of course, he is also thanked for all the gossipy time we shared, he is the eyes and ears of the institute! I would also like to thank Jordi, the publishing guy, for those coaching conversations in the sofa in front of his office, during a PhD, coaching conversations are above all highly needed and recommendable for survival!!

In the base camp, there is of course special thanks to all my colleagues-friends, with whom I shared conversations, beers, parties, summer and winter activities and a long etcetera. They are very thanked for the support provided, this thesis will not be finished without them! Mar, Encarni, Mari, Juve, Jan, Jonas, Pili, Lavinia, Evelyn, Max, Ajay, Kittipon, Marc, Angel, and all new ones and those who have passed through the institute in those 4 and something years.

Last but not least, are all my friends outside the institute, they have been my coaches, my psychologist and the mates with whom I shared all can of experiences that made me grown as a person, help me in life and of course to survive this PhD. Gemma, Alvaro, Ari, Lluis, Joana, Marti, Muntsa, Elsa, Jaume, Ursula, Berta and Lydia …you are my chosen family, I love you all!!!

A very special and sincere thank goes to my parents, they have been my support and guidance, I do not have words to express all my gratitude, I owe it all to you!! Many thanks! Very special in my life was the too short time learning and knowing Roger, this thesis is dedicated to him, who left too early and gave me the best, and unfortunately, the worst in life, you will be always remembered.

Thanks for all your encouragement!!!

References

Albers, J. P. (1967), Belt of sigmoidal bending and right-lateral faulting in the western Great Basin, Geol. Soc. Am. Bull., 78, 143–156

Allmendinger, R.W., Cardozo, N. & Fisher, D.M. (2012) Structural Geology Algorithms Vectors and Tensors, 1st Editio., Cambridge University Press

Alvarez-Marron, J. (1995). Three-dimensional geometry and interference of fault-bend fold: Examples from the Ponga Unit, Variscan Belt, NW Spain. J. Struct. Geol., 17(4), 549–560. https://doi.org/10.1016/0191-8141(94)00075-B

Alvarez-Marron, J., D. Brown, G. Camanni, Y.-M. Wu, and H. Kuo-Chen (2014), Structural complexities in a foreland thrust belt inherited from the shelf-slope transition: Insights from the Alishan area of Taiwan, Tectonics, 33, 1322–1339, doi:10.1002/2014TC003584.

Arnold, R. & Townend, J., 2007. A Bayesian approach to estimating tectonic stress from seismological data, Geophys. J. Int., 170, 1336–1356, doi: 10.1111/j.1365-246X.2007.03485.x.

Apotria, T.G. (1995) Thrust sheet rotation and out-of-plane strains associated with oblique ramps: An example from the Wyoming salient U.S.A. J. Struct. Geol., 17, 647–662. doi:10.1016/0191-8141(94)00087-G

Arora, B. R., V. K. Gahalaut, and N. Kumar (2012), Structural control on along-strike variation in the seismicity of the northwest Himalaya, J. Asian Earth Sci., 57, 15–24, doi:10.1002/2014TC003584.

Bayona, G., Thomas, W. A., & Van der Voo, R. (2003). Kinematics of thrust sheets within transverse zones: A structural and paleomagnetic investigation in the Appalachian thrust belt of Georgia and Alabama. J. Struct. Geol., 25(8), 1193–1212. https://doi.org/ 10.1016/S0191-8141(02)00162-1

Biete, C., Alvarez-Marron, J., Brown, D. & Kuo-Chen, H. (2018) The Structure of Southwest Taiwan: The Development of a Fold-and-Thrust Belt on a Margins Outer Shelf and Slope. Tectonics, 37, 1973–1993. doi:10.1029/2017TC004910

Biete, C., Brown, D., Lund, B., Alvarez-Marron, J., Wu, Y.-M., Kuo-Chen, H. & Ho, C.-W (in press) The influence of inherited continental margin structures on the stress and strain fields of the south central Taiwan fold-and-thrust belt. Geophys. J. Int. doi: 10.1093/gji/ggz296

Bonilla, M. G. (1975). A review of recently active faults in Taiwan, USGS Open-File Rep. 75-41, 43

Bonini, M., Sani, F. & Antonielli, B. (2012) Basin inversion and contractional reactivation of inherited normal faults: A review based on previous and new experimental models. Tectonophysics, 522–523, 55–88, Elsevier B.V. doi:10.1016/j.tecto.2011.11.014

Bos, A.G., Spakman, W. & Nyst, M.C.J. (2003) Surface deformation and tectonic setting of Taiwan inferred from a GPS velocity field. J. Geophys. Res. Solid Earth, 108, 1–18. doi:10.1029/2002JB002336

Boyer, S. E., & Elliott, D. (1982). Thrust systems. AAPG, 66, 1196–1230.

Briais, A., Patriat, P. & Tapponnier, P. (1993) Updated interpretation of magnetic anomalies and seafloor spreading stages in the south China Sea: Implications for the Tertiary tectonics of Southeast Asia. J. Geophys. Res. Solid Earth, 98, 6299–6328. doi:10.1029/92JB02280

Brown, D., Alvarez-Marron, J., Schimmel, M., Wu, Y.-M., & Camanni, G. (2012). The structure and

kinematics of the central Taiwan mountain belt derived from geological and seismicity data. Tectonics, 31, TC5013. https://doi.org/10.1029/2012TC003156

Brown, D., Alvarez-Marron, J., Biete, C., Kuo-Chen, H., Camanni, G., & Ho, C.-W. (2017). How the structural architecture of the Eurasian conti- nental margin affects the structure, seismicity, and topography of the south central Taiwan fold-and-thrust belt. Tectonics, 36, 1275–1294. https://doi.org/10.1002/2017TC004475

Butler, R.W.H., Tavarnelli, E. & Grasso, M. (2006) Structural inheritance in mountain belts: An Alpine-Apennine perspective. J. Struct. Geol., 28, 1893–1908. doi:10.1016/j.jsg.2006.09.006

Byrne, T., Y.-C. Chan, R.-J. Rau, C.-Y. Lu, Y.-H. Lee, and Y.-J. Wang (2011), The arc–continent collision in Taiwan, in Arc-Continent Collision, Frontiers in Earth Sciences Series, edited by D. Brown and P. D. Ryan, pp., 213–245, Springer, Berlin

Calassou, S., Larroque, C., & Malavieille, J. (1993). Transfer zones of deformation in thrust wedges: An experimental study. Tectonophysics, 221(3-4), 325–344. https://doi.org/10.1016/0040-1951(93)90165-G

Camanni, G (2014). The structure of the south-central Taiwan thrust belt. Ph.D. Thesis. University of Barcelona.

Camanni, G., C.-H. Chen, D. Brown, J. Alvarez-Marron, Y.-M. Wu, H.-A. Chen, H.-H. Huang, H.-T. Chu, M.-M. Chen, and C.-H. Chang (2014a), Basin inversion in central Taiwan and its importance for seismic hazard, Geology, 42, 147–150.

Camanni, G., D. Brown, J. Alvarez-Marron, Y.-M. Wu, and H.-A. Chen (2014b), The Shuilikeng fault in central Taiwan mountain belt, J. Geol. Soc., 171, 117–130.

Camanni, G., J. Alvarez-Marron, D. Brown, C. Ayala, Y.-M. Wu, and H.-H. Hsieh (2016), The deep structure of south-central Taiwan illuminated by seismic tomography and earthquake hypocentre data, Tectonophysics, 679, 235–245.

Castelltort, S., Nagel, S., Moutherreau, F., Lin, A., Wetzel, A., Kaus, B., et al. (2010). Sedimentology of Early Pliocene sandstones in the south- western Taiwan foreland: Implications for basin physiography in the early stages of collision. J. Asian Earth Sci., 40,52–71

Cardozo, N. & Allmendinger, R.W. (2009) SSPX: A program to compute strain from displacement/velocity data. Comput. Geosci., 35, 1343–1357, Elsevier. doi:10.1016/j.cageo.2008.05.008

Carena, S., Suppe, J., Kao, H., 2002. Active detachment of Taiwan illuminated by small earthquakes and its control of first-order topography. Geology 30 (10), 935–938

Célérier, B. (1995) Tectonic regime and slip orientation of reactivated faults. Geophys. J. Int., 121, 143–161. doi:10.1111/j.1365-246X.1995.tb03517.x

Célérier, B. (2008) Seeking Aderson's faulting in seismicity: A centennial celebration. Rev. Geophys., 46, 1–34. doi:10.1029/2007RG000240

Champagnac, J.-D., P. Molnar, C. Sue, and F. Herman (2012), Tectonics, climate, and mountain topography, J. Geophys. Res., 117, B02403, doi:10.1029/2011JB008348

Chang, C.-H., Y.-M. Wu, L. Zhao, and F. T. Wu (2007), Aftershocks of the 1999 Chi-Chi, Taiwan, earthquake: The first hour, Bull. Seismol. Soc. Am., 97, 1245–1258

Chang, C.-P., Chang, T.Y., Angelier, J., Kao, H., Lee, J.C. & Yu, S.B. (2003) Strain and stress field in Taiwan oblique convergent system: Constraints from GPS observation and tectonic data. Earth Planet. Sci. Lett., 214, 115–127. doi:10.1016/S0012-821X(03)00360-1

Chang, S. L. (1963), Regional stratigraphic study of Pliestocene and upper Pliocene formations in Chiayi and Hsinying area, Taiwan, Pet. Geol. Taiwan, 2,65–86.

Chang, S. L. (1964), Regional stratigraphic study of lower Pliocene and upper Miocene formations in Chiayi and Hsinying area, Taiwan, Pet. Geol. Taiwan, 3,1–20.

Chao, W.-A., L. Zhao, and Y.-M. Wu (2011), Centroid fault-plane inversion in three-dimensional velocity structure using strong-motion records, Bull. Seismol. Soc. Am., 101, 1330–1340.

Chen, A. T., and Y.-L. Yang (1996), Lack of compressional overprint on the extensional structure in the offshore Tainan and the tectonic implications, Terr. Atmos. Ocean. Sci., 7, 505–522

Chen, C.-H., et al. (2000), Geological map of Taiwan, scale 1:500,000, Central Geological Survey, Taipei.

Chen, K.-X., H. Kuo-Chen, D. Brown, Q. Li, Z. Ye, W.-T. Liang, C.-Y. Wang, and H. Yao (2016), Three-dimensional ambient noise tomography across the Taiwan Strait: The structure of a magma-poor rifted margin, Tectonics, 35, 1782–1792, doi:10.1002/2015TC004097

Chen, S.K., Wu, Y.-M., Hsu, Y.J. & Chan, Y.C. (2017) Current crustal deformation of the Taiwan orogen reassessed by cGPS strain-rate estimation and focal mechanism stress inversion. Geophys. J. Int., 210, 228–239. doi:10.1093/gji/ggx165

Chen, W. & Molnar, P. (1983) Focal depth of intracontinental and intraplate earthquakes and their implications for thermal and mechanical properties of the lithosphere. J. Geophys. Res., 88, 4183–4214. doi:http://dx.doi.org/10.1029/JB088iB05p04183; doi:10

Chen, W.-S., Ridgway, K. D., Horng, C.-S., Chen, Y.-G., Shea, K.-S., & Yeh, M.-G. (2001). Stratigraphic architecture, magnetostratigraphy, and incised-valley systems of the Pliocene-Pliestocene collisional marine foreland basin of Taiwan. Geol. Soc. Am. Bull., 113(10), 1249–1271. https://doi.org/10.1130/0016-7606(2001)113<1249:SAMAIV>2.0.CO;2

Cheng, W.-B., H.-C. Huang, C. Wang, M.-S. Wu, and T.-H. Hsiuan (2003), Velocity structure, seismicity, and fault structure in the Peikang High are of western Taiwan, Terr. Atmos. Ocean. Sci., 14,63–83. Chiang,

Chiang, S. C. (1971). Seismic study of the Paishatun structure, Miaoli, Taiwan. Pet. Geol. Taiwan, 8(8), 281–294

Chiang, C.-S., H.-S. Yu, and Y.-W. Chou (2004), Characteristics of the wedge-top depozone of the southern Taiwan foreland basin system, Basin Res., 16,65–78

Ching, K.E., Rau, R.J., Lee, J.C. & Hu, J.C. (2007) Contemporary deformation of tectonic escape in SW Taiwan from GPS observations, 1995-2005. Earth Planet. Sci. Lett., 262, 601–619. doi:10.1016/j.epsl.2007.08.017

Ching, K.E., Rau, R.J., Johnson, K.M., Lee, J.C. & Hu, J.C. (2011) Present-day kinematics of active mountain building in Taiwan from GPS observations during 1995-2005. J. Geophys. Res. Solid Earth, 116, 1–22. doi:10.1029/2010JB008058

Chiu, H. T. (1975). Miocene stratigraphy and its relation to the Palaeogene rocks in West - Central Taiwan. Pet. Geol. Taiwan, 12, 51–80

Chou, J.T. (1971) A preliminary study of the stratigraphy and sedimentation of the mudstone formations in the Tainan area, Southern Taiwan. Pet. Geol. Taiwan, 8, 187–220.

Chou, J. T. (1972). A sedimentologic and paleogeographic study of the upper Cenozoic clastic sequences in the Chiayi region, Western Taiwan. Pet. Geol. Taiwan, 10, 141–158

Chou, J. T. (1980). Stratigraphy and sedimentology of the Miocene in western Taiwan. Pet. Geol. Taiwan, 17,33–52.

Chow, J., K.-M. Yang, and H.-M. Chen (1988), Seismic interpretation of the subsurface structures in the Yichu-Chiali area, southern Taiwan, Pet. Geol. Taiwan, 24,60–95

Chuang, R. Y., K. M. Johnson, Y.-M. Wu, K.-E. Ching, and L.-C. Kuo (2013), A midcrustal ramp-fault structure beneath the Taiwan tectonic wedge illuminated by the 2013 Nantou earthquake series, Geophys. Res. Lett., 40, 5080–5084, doi:10.1002/grl.51005

Covey, M. (1986), The evolution of foreland basins to steady state: Evidence from the western Taiwan foreland basin, in Foreland Basins, Spec. Pub. 8. Int. Ass. Sed., edited by P. A. Allen and P. Homewood, pp. 77–90, Blackwell, Oxford, U. K

Christensen, N. I. (1989), Pore pressure, seismic velocities, and crustal structure, in Geophysical Framework of the Continental United States, vol. 172, edited by L. C. Pakiser and W. D. Mooney, pp. 783–798, Geol. Soc. Am. Mem., Boulder, Colo.

Christensen, N. I., and D. Stanley (2003), Seismic velocities and densities of rocks, Inter. Handbook Earthquake Eng. Seis., 81, 1587–1593

Dahlstrom, C. D. A. (1969). Balanced cross sections. Canadian J. Earth Scien., 6(4), 743–757. . https://doi.org/10.1139/e69-069

De Paor, D. G. (1988). Balanced section in thrust belts part 1: Construction. American Association of Pet. Geol, Bull., 72,73–90

Deffontaines, B., O. Lacombe, J. Angelier, H.-T. Chu, F. Mouthereau, C.-T. Lee, J. Deramond, J.-F. Lee, M.-S. Yu, and P.-M. Liew (1997), Quaternary transfer faulting in the Taiwan Foothills: Evidence from a multisource approach, Tectonophysics, 274,61–82

Deng, J.-M., T.-K. Wang, B.-J. Yang, C.-S. Lee, C.-S. Liu, and S.-C. Chen (2012), Crustal velocity structure off SW Taiwan in the northernmost South China Sea imaged from TAIGER OBS and MCS data, Mar. Geophys. Res., 33, 327–349

Ding, Z.Y., Yang, Y.Q., Yao, Z.X., Zhang, G.H., (2001). A thin-skinned collisional model for the Taiwan orogeny. Tectonophysics 332 (3), 321–331

Ding, W.-W., J.-B. Li, M.-B. Li, X.-L. Qiu, Y.-X. Fang, and Y. Tang (2008), A Cenozoic tectonosedimentary model of the Tainan Basin, the South China Sea: Evidence from multi-channel seismic profile, J. Zhejiang Uni. Sci., 9, 702–713

Duncan, C., J. Masek, and E. Fielding (2003), How steep are the Himalaya? Characteristics and implications of along-strike topographic variations, Geology, 31,75–78.

Eakin, D.H., McIntosh, K., Avendonk, H.J.A. Van, Lavier, L., Lester, R., Liu, C.-S., Shine, et al. (2014) Crustal-scale seismic profiles across the Manila subduction zone: The transition from intraoceanic subduction to incipient collision. J. Geophys. Res. Solid Earth, 119, 1–17. doi:10.1002/2013JB010395

Elliott, D., & Johnson, M. R. W. (1980). Structural evolution in the northern part of the Moince thrust belt, NW Scotland. Transactions of the Royal Society of Edinburgh Earth Sciences, 71(02), 69–96. https://doi.org/10.1017/S0263593300013523

Ernst, W. G. (1983). Mineral paragenesis in metamorphic rocks exposed along Tailuko Gorge, Central Mountain Range, Taiwan. Journal of Metamorphic Geology, 1(4), 305–329. https://doi.org/10.1111/j.1525-1314.1983.tb00277.x

Godin, L., and L. B. Harris (2014), Tracking basement cross-strike discontinuities in the Indian

crust beneath the Himalayan orogeny using gravity data—Relationship to upper crustal faults, Geophys. J. Int., 198, 198–215.

Gölke, M. & Coblentz, D. (1996) Origins of the European regional stress field. Tectonophysics, 266, 11–24. doi:10.1016/S0040-1951(96)00180-1

Hardebeck, J.L. & Hauksson, E. (2001) Crustal stress field in southern California and its implications for fault mechanics, J. Geophys. Res., 106, 21,859-21,882

Hardebeck, J.L. & Michael, A.J. (2004) Stress orientations at intermediate angles to the San Andreas Fault, California. J. Geophys. Res. 109, B11303, doi:10.1029/2004JB003239

Hayward, A. B., and R. H. Graham (1989), Some geometrical characteristics of inversion, in Inversion Tectonics, vol. 44, edited by M. A. Cooper and G. D. Willaims, pp. 17–39, Geol. Soc. Spec. Pub.

Hensch, M., Lund, B., Árnadóttir, Th., Brandsdóttir, B. (2016) Temporal stress changes associated with the 2008 May 29 Mw 6 earthquake doublet in the western South Iceland Seismic Zone, Geophys. J. Int., 204, 544-554, doi: 10.1093/gji/ggv465

Koyi, H., Nilfouroushan, F. & Hessami, K. (2016) Modelling role of basement block rotation and strike-slip faulting on structural pattern in cover units of fold-and-thrust belts. Geol. Mag., 153, 1–18. doi:DOI: 10.1017/S0016756816000595

Ho, C. S. (1986). A synthesis of the geologic evolution of Taiwan. Tectonophysics, 125(1-3), 1–16. https://doi.org/10.1016/0040- 1951(86)90004-1

Ho, C.-S. (1988). An Introduction to the Geology of Taiwan: Explanatory text of the Geological Map of Taiwan, Central Geological Survey. Taipei, Taiwan

Hong, E. (1997). Evolution of Pliocene to Pleistocene sedimentary environments in an arc-continent collision zone: Evidence from the analyses of lithofacies and ichnofacies in the southwestern foothills of Taiwan. J. Asian Earth Scien., 15(4–5), 381–392. https://doi. org/10.1016/S0743-9547(97)00022-6

Horng, C.S. & Shea, K.-S. (1994) Study of nannofossil biostratigraphy in the eastern part of the Erhjen-chi section, southwestern Taiwan. Spec. Publ. Cent. Geol. Surv., 8, 181–204.

Horng, C.S. (2014) Age of the Tananwan formation in northern Taiwan: A reexamination of the magnetostratigraphy and calcareous nannofossil biostratigraphy. Terr. Atmos. Ocean. Sci., 25, 137–147. doi:10.3319/TAO.2013.11.05.01(TT)

Hossack, J. R. (1979). The use of balanced cross-sections in the calculation of orogenic contraction: A review. J. Geol. Soc., 136(6), 705–711. https://doi.org/10.1144/gsjgs.136.6.0705

Hossack, J. R. (1983). A cross-section through the Scandinavian Caledonides constructed with the aid of branch-line maps. J. Struct. Geol., 5(2), 103–111. https://doi.org/10.1016/0191-8141(83)90036-6

Hsiao, P.-T. (1970), Seismic study of the area between the Coastal Plain and the Foothills, Chiayi, Taiwan, Pet. Geol. Taiwan, 7,47–52.

Hsu, S.K., Sibuet, J.C. & Shyu, C.T. (2001) Magnetic inversion in the East China Sea and Okinawa Trough: Tectonic implications. Tectonophysics, 333, 111–122. doi:10.1016/S0040-1951(00)00270-5

Hsu, S.-K., Yeh, Y.C., Doo, W. Bin & Tsai, C.H. (2004) New bathymetry and magnetic lineations identifications in the northernmost South China Sea and their tectonic implications. Mar. Geophys. Res., 25, 29–44. doi:10.1007/s11001-005-0731-7

Hsu, Y.J., Yu, S.B., Simons, M., Kuo, L.C. & Chen, H.Y. (2009) Interseismic crustal deformation in the Taiwan plate boundary zone revealed by GPS observations, seismicity, and earthquake focal mechanisms. Tectonophysics, 479, 4–18, Elsevier B.V. doi:10.1016/j.tecto.2008.11.016

Hsu, Y.-J., Rivera, L., Wu, Y.-M., Chang, C.-H., & Kanamori, H. (2010). Spatial heterogeneity of tectonic stress and friction in the crust: New evidence from earthquake focal mechanisms in Taiwan. Geophys. J. Int., 182, 329–342.

Hu, J. & Angelier, J. (1996) Modeling of stress-deformation relationships in a collision belt: Taiwan. Terr. Atmos. Ocean. Sci., 447–465

Hu, J.C., Angelier, J. & Yu, S.B. (1997) An interpretation of the active deformation of southern Taiwan based on numerical simulation and GPS studies. Tectonophysics, 274, 145–169. doi:10.1016/S0040-1951(96)00302-2

Huang, M.-H., Hu, J.-C., Ching, K.-E., Rau, R.-J., Hsieh, C.-S., Pathier, E., et al. (2009). Active deformation of Tainan tableland os southwestern Taiwan based on geodetic measurements and SAR interferometry. Tectonophysics, 466(3-4), 322–334. https://doi.org/10.1016/j. tecto.2007.11.020

Huang, C., Byrne, T.B., (2014). Tectonic evolution ofan active tectonostratigraphic boundary in accretionary wedge: an example from the Tulungwan–Chaochou fault system, southern Taiwan. J. Struct. Geol.. 69, 320–333

Huang, C.-Y., Y. Yen, Q. H. Zhao, and C.-T. Lin (2012), Cenozoic stratigraphy of Taiwan: Window into rifting, stratigraphy and paleoceanography of South China Sea, Chin. Sci. Bull., 57, 3130–3149.

Huang, L.-S. (1984). Iodine contents in formation waters from wildcats, southern Taiwan. Petr. Geol. Taiwan, 20, 215–235

Huang, H.-H., Y.-M. Wu, X. Song, C.-H. Chang, S.-J. Lee, T.-M. Chang, and H.-H. Hsieh (2014), Joint Vp and Vs tomography of Taiwan: Implications for subduction-collision orogeny, Earth Planet. Sci. Lett., 392, 177–191

Huang, M.-M., H. Tung, E.J. Fielding, H.-H. Huang, C. Liang, C. Huang, and J.-C. Hu (2016), Multiple fault slip triggered above the 2016 MW 6.4 Meinong earthquake in Taiwan, Geophys. Res. Lett., 43, 7459–7467, doi:10.1002/2016GL069351

Huang, S. T., Yang, K.-M., Hung, J.-H., Wu, J. C., Ting, H. H., Mei, W. W., et al. (2004). Deformation front development at the northeast margin of the Tainan basin, Tainan-Kaohsiung area, Taiwan. Mar. Geophys. Res., 25(1–2), 139–156. https://doi.org/10.1007/s11001-005- 0739-z

Hung, J.-H., K.-F. Ma, C.-Y. Wang, H. Ito, W. Lin, and E.-C. Yeh (2009), Subsurface structure, physical properties, fault-zone characteristics and stress state in scientific drill holes of Taiwan Chelungpu Fault Drilling Project, Tectonophysics, 466, 307–321

Husen S., Hardebeck J.L. (2010), Earthquake Location Accuracy. Community Online Resour. for Stat. Seism. Anal. (2010), pp. 1-35, 10.5078/corssa 55815573

Jackson, J.A. (1980) Reactivation of basement faults and crustal shortening in orogenic belts. Nature, 283, 343–346. doi:10.1038/283343a0

Jahn, B.-M., Chi, W.-R., & Yui, T.-F. (1992). A Late Permian formation of Taiwan marbles from Chia-Li well No.1: Pb-Pb isochron and Sr isotopic evidence, and its regional geological significance. J. Geol. Soc. China, 35, 193–218

Johnston, J. E., and N. I. Christensen (1992), Shear wave reflectivity, anisotropies, Poissons ratios, and

densities of a southern Appalachian Paleozoic sedimentary sequence, Tectonophysics, 210,1–20.

Johnston, J. E., and N. I. Christensen (1993), Compressional to shear velocity ratios in sedimentary rocks, Int. J. Rock Mech. Min. Sci. Geomech. Abs., 30, 751–754

Kagan, Y.Y. (2005) Double-couple earthquake focal mechanism: random rotation and display, Geophys. J. Int., 163, 1065 – 1072, doi: 10.1111/j.1365-246X.2005.02781.x

Kelly, P.G., Peacock, D.C.P., Sanderson, D.J. & McGurk, A.C. (1999) Selective reverse-reactivation of normal faults, and deformation around reverse-reactivated faults in the Mesozoic of the Somerset coast. J. Struct. Geol., 21, 493–509. doi:10.1016/S0191-8141(99)00041-3

Kim, K.-H., J.-M. Chiu, H. Kao, Q. Liu, and Y.-H. Yeh (2004), A preliminary study of crustal structure in Taiwan region using receiver function analysis, Geophys. J. Int., 159, 146–164

Koyi, H., F. Nilfouroushan, and K. Hessami (2016), Modelling role of basement block rotation and strike-slip faulting on structural pattern in cover units of fold-and-thrust belts, Geol. Mag., 153, 827–844.

Kuo-Chen, H., F. T. Wu, and S. W. Roecker (2012), Three-dimensional P velocity structures of the lithosphere beneath Taiwan from the analysis of TAIGER and related seismic data sets, J. Geophys. Res., 117, B06306, doi:10.1029/2011JB009108.

Kuo-Chen, H., F. T. Wu, W.-L. Chang, C.-Y. Chang, C.-Y. Cheng, and N. Hirata (2015), Is the Lishan fault of Taiwan active?, Tectonophysics, 661, 210–214

Lacombe, O., F. Mouthereau, B. Deffontaines, J. Anglier, H.-T. Chu, and C.-T. Lee (1999) Geometry and Quaternary kinematics of fold-and-thrust units of southwestern Taiwan, Tectonics, 18, 1198–1223

Lacombe, O., Mouthereau, F., Angelier, J., & Deffontaines, B. (2001). Structural, geodetic and seismological evidence for tectonic escape in SW Taiwan. Tectonophysics, 333(1-2), 323–345. https://doi.org/10.1016/S0040-1951(00)00281-X

Lacombe, O. & Mouthereau, F. (2002) Basement-involved shortening and deep detachment tectonics in forelands of orogens: Insights from recent collision belts (Taiwan, Western Alps, Pyrenees). Tectonics, 21. doi:10.1029/2001TC901018

Lacombe, O. & Bellahsen, M. (2016) Thick-skinned tectonics and basement-involved fold–thrust belts: insights from selected Cenozoic orogens. Geol. Mag., Vol. 153. doi:10.1017/S0016756816000078

Lan, C.-Y., C.-S. Lee, T.-F. Yui, H.-T. Chu, and B.-M Jahn (2008), The tectono-thermal events of Taiwan and their relationship with SE China, Terr. Atmos. Ocean. Sci., 19, 257–278

Leclère, H. & Fabbri, O. (2013) A new three-dimensional method of fault reactivation analysis. Journal of Structural Geology., 48, 153–161, Elsevier Ltd. doi:10.1016/j.jsg.2012.11.004

Lee, C.-S. (1979), Paleogene rocks of the Yushan-Shuili area, Nantou, central Taiwan, Mem. Geol. Soc. China, 3, 237–247. Lee,

Lee, T.-Y., C.-H. Tang, J.-S. Ting, and Y.-Y. Hsu (1993), Sequence stratigraphy of the Tainan Basin, offshore southwestern Taiwan, Pet. Geol. Taiwan, 26, 119–158

Lester, R., H. J. A. Van Avendonk, K. McIntosh, L. Lavier, C.-S. Liu, T.-K. Wang, and F. Wu (2014), Rifting and magmatism in the northeastern South China Sea from wide-angle tomography and seismic reflection imaging, J. Geophys. Res. Solid Earth, 119, 2305–2323, doi:10.1002/2013JB010639

Letouzey, J. (1990) Fault reactivation, inversion and fold-thrust belt. Pet. tectonics Mob. belts, pp. 101–128

Li, C.-F., Z. Zhou, J. Li, H. Hao, and J. Geng (2007), Structures of the northeasternmost South China Sea continental margin and ocean basin: Geophysical constraints and tectonic implications, Mar. Geophys. Res., 28,59–79

Lin, A. T., and A. Watts (2002), Origin of the west Taiwan Basin by orogenic loading and flexure of a rifted continental margin, J. Geophys. Res., 107(B9), 2185, doi:10.1029/2001JB000669

Lin, A., A. Watts, and P. Hesselbo (2003), Cenozoic stratigraphy and subsidence history of the South China Sea margin in the Taiwan region, Basin Res., 15, 453–478.

Lin, A. T., C.-S. Liu, C.-C. Lin, P. Schnurle, G.-Y. Chen, W.-Z. Liao, L. S. Teng, H.-J. Chuang, and M.-S. Wu (2008), Tectonic features associated with the overriding of an accretionary wedge on top of a rifted continental margin: An example from Taiwan, Mar. Geol., 255, 186–203

Lin, J.-Y., J.-C. Sibuet, and S.-K. Hsu (2005), Distribution of the East China Sea continental shelf basins and depths of magnetic sources, Earth, Planet. Space, 57, 1063–1072

Lin, C.-W. & Huang, M.-L. (1998) Influence of the Peikang Basement high on the structure development of the western foothills and coastal plain in south central Taiwan: a sandbox approach. Pet. Geol. Taiwan, 32, 105–122

Lu, C.-Y., F.-S. Jeng, K.-J. Chang, and W. T. Jian (1998), Impact of basement high on the structure and kinematics of the western Taiwan thrust wedge: Insights from sandbox models, Terr. Atmos. Ocean. Sci., 9, 533–550

Lund, B. & Slunga, R. (1999) Stress tensor inversion using detailed microearthquake information and stability constraints : Application to Ölfus southwest Iceland. J. Geophys. Res., 104, 14947–14964. doi:10.1029/1999JB900111

Lund, B. & Townend, J. (2007) Calculating horizontal stress orientations with full or partial knowledge of the tectonic stress tensor. Geophys. J. Int., 170, 1328–1335. doi:10.1111/j.1365-246X.2007.03468.x

Macedo, J. & Marshak, S. (1999) Controls on the geometry of fold-thrust belt salients. GSA Bull., 111, 1808–1822. Retrieved from http://dx.doi.org/10.1130/0016-7606(1999)111%3C1808:COTGOF%3E2.3.CO

Malavieille, J., Trullenque, G., 2009. Consequences of continental subduction on forearc basin and accretionary wedge deformation in SE Taiwan: insights from analogue modeling. Tectonophysics 466 (3–4), 377–394

Marshak, S. (2004) Salients, Recesses, Arcs, Oroclines, and Syntaxes — A Review of Ideas Concerning the Formation of Map-view Curves in Fold-thrust Belts. Thrust tectonics Hydrocarb. Syst. AAPG Mem. 82, 82, 131–156.

Mavko, G., T. Mukerji, and J. Dvorkin (1998), The Rock Physics Handbook: Tools for Seismic Analysis in Porous Media, 329 pp., Cambridge Univ. Press, Cambridge, U. K., and New York

McIntosh, K., Nakamura, Y., Wang, T.K., Shih, R.C., Chen, A. & Liu, C.S. (2005) Crustal-scale seismic profiles across Taiwan and the western Philippine Sea. Tectonophysics, 401, 23–54. doi:10.1016/j.tecto.2005.02.015

McIntosh, K., H. Van Avendonk, L. Lavier, W. R. Lester, D. Eakin, F. Wu, C.-S. Liu, and C.-S. Lee (2013), Inversion of a hyper-extended rifted margin in the southern central range of Taiwan, Geology, 41, 871–874

McIntosh, K., Lavier, L., Avendonk, H. van, Lester, R., Eakin, D. & Liu, C.S. (2014) Crustal structure and inferred rifting processes in the northeast South China Sea. Mar. Pet. Geol., 58, 612–626, Elsevier Ltd. doi:10.1016/j.marpetgeo.2014.03.012

Mohn, G., G. Manatschal, M. Beltrando, E. Masini, and N. Kusznir (2012), Necking of the continental crust in magma-poor rifted margins: Evidence from the fossil Alpine Tethys margins, Tectonics, 31, TC1012, doi:10.1029/2011TC002961

Molnar, P. (2009), The state of interactions among tectonics, erosion, and climate: A polemic, GSA Today, 19,44–45

Mouthereau, F., O. Lacombe, B. Deffontaines, J. Angelier, H.-T. Chu, and C.-T. Lee (1999), Quaternary transfer faulting and belt front deformation at Pakuashan (western Taiwan), Tectonics, 18, 215–230.

Mouthereau, F., O. Lacombe, B. Deffontaines, J. Angelier, and S. Brusset (2001), Deformation history of the southwestern Taiwan foreland thrust belt: Insights from tectono-sedimentary analyses and balanced cross-sections, Tectonophysics, 333, 293–322.

Mouthereau, F., B. Deffontaines, O. Lacombe, and J. Angelier (2002), Variations along the strike of the Taiwan thrust belt: Basement control on structural style, wedge geometry, and kinematics, in Geology and Geophysics of an Arc-Continent Collision, Taiwan, vol. 358, edited by T. B. Byrne and C.-S. Liu, pp. 31–54, Geol. Soc. Am. Spec. Paper, Boulder, Colo

Mouthereau, F., O. Lacombe, and B. Meyer (2006), The Zagros folded belt (Fars, Iran): Constraints from topography and critical wedge modeling, Geophys. J. Int., 165, 336–356.

Mouthereau, F., and O. Lacombe (2006), Inversion of the Paleogene Chinese continental margin and thick-skinned deformation in the western foreland of Taiwan, J. Struct. Geol., 28, 1977–1993.

Mugnier, J. L., P. Leturmy, G. Mascle, P. Huyghe, E. Chalaron, G. Vidal, L. Husson, and B. Delcaillau (1999), The Siwaliks of western Nepal I. Geometry and kinematics, J. Asian Earth Sci., 17, 629–642

Nagel, S., Castelltort, S., Wetzel, A., Willett, S. D., Mouthereau, F., & Lin, A. T. (2013). Sedimentology and foreland basin paleogeography during Taiwan arc continent collision. J. Asian Earth Sci., 62, 180–204. https://doi.org/10.1016/j.jseaes.2012.09.001

Nissen, S. S., D. E. Hayes, P. Buhl, and J. Diebold (1995), Deep penetration seismic soundings across the northern margin of the South China Sea, J. Geophys. Res., 100, 22,407–22,433

Oncken, O., von Winterfeld, C., & Dittmar, U. (1999). Accretion of a rifted passive margin: The Late Paleozoic Rhenohercynian fold and thrust belt (Middle European Variscides). Tectonics, 18(1), 75–91. https://doi.org/10.1029/98TC02763

Perez-Estaun, A., J. Alvarez-Marron, D. Brown, V. Puchkov, Y. Gorozhanina, and V. Baryshev (1997), Along-strike structural variations in the foreland thrust and fold belt of the southern Urals, Tectonophysics, 276, 265–280.

Poblet, J. & Lisle, R.J. (2011) Kinematic evolution and structural styles of fold-and-thrust belts. Geol. Soc. London, Spec. Publ., 349, 1–24. doi:10.1144/SP349.1

Richard, P. & Krantz, R.W. (1991) Experiments on fault reactivation in strike slip mode. Tectonophysics, 188, 117–131. Retrieved from file://localhost/Users/jescartin/WORK/Referencias/pdfs/Richard1991.pdf

Richardson, R.M., 1992. Ridge Forces, Absolute Plate Motions, and the Intraplate Stress Field, J. Geophys. Res., 97: 11,739-11,748.

Rodgers, J. (1990) Fold-and-thrust belts in sedimentary rocks; Part 1, Typical examples. Am. J. Sci. April 1, 290:321-359

Rodriguez-Roa, F. A., and D. V. Wiltschko (2010), Thrust belt architecture of the central and southern western foothills of Taiwan, in Hydrocarbons in Contractional Belts, vol. 348, edited by G. P. Goffey et al., pp. 137–168, Geol. Soc. London, Spec. Pub., Boulder, Colo.

Ruh, J. B., T. Gerya, and J.-P. Burg (2014), 3D effects of strain vs. velocity weakening on deformation patterns in accretionary wedges, Tectonophysics, 615-616, 122–141

Shaw, C.-L. (1996), Stratigraphic correlation and isopach maps of the western Taiwan Basin, Terr. Atmos. Ocean. Sci., 7, 333–360.

Shea, K.-S., H.-C. Chang, T.-Y. Huang, H.-C. Ho, W.-H. Lin, C.-W. Lin, and H.-W. Chen (2003), Geological column in Taiwan, Central Geol. Surv. Taiwan, Taiwan

Shi, X., H. Xu, X. Qiu, K. Xia, X. Yang, and Y. Li (2008), Numerical modeling on the relationship between thermal uplift and subsequent rapid subsidence: Discussion on the evolution of the Tainan Basin, Tectonics, 27, TC6003, doi:10.1029/2007TC002163

Shyu, J. B. H., K. Sieh, Y.-G. Chen, and C.-S. Liu (2005), Neotectonic architecture of Taiwan and its implications for future large earthquakes, J. Geophys. Res., 110, B08402, doi:10.1029/2004JB003251.

Shyu, J. B. H., Y.-R. Chuang, Y.-L. Chen, Y.-R. Lee, and C.-T. Cheng (2016), A new on-land seismogenic structure source database from the Taiwan earthquake model (TEM) project for seismic hazard analysis of Taiwan, Terr. Atmos. Ocean. Sci., 27, 311–323

Scott Wilkerson, M., Apotria, T.G. & Farid, T. (2002) Interpreting the geologic map expression of contractional fault-related fold terminations: Lateral/oblique ramps versus displacement gradients. J. Struct. Geol., 24, 593–607. doi:10.1016/S0191-8141(01)00111-0

Sibson, R.H. (1983) Continental fault structure and the shallow earthquake source. J. Geol. Soc. London., 140, 741–767. doi:10.1144/gsjgs.140.5.0741

Sibson, R.H. (1985) A note on fault reactivation. J. Struct. Geol., 7, 3–6

Sibson, R.H. (1990) Conditions for fault-valve behaviour. Geol. Soc. London, Spec. Publ., 54, 15–28. doi:10.1144/GSL.SP.1990.054.01.02

Sibson, R.H. (1994) Crustal stress, faulting and fluid flow. Geol. Soc. London, Spec. Publ., 78, 69 LP-84. doi:https://doi.org/10.1144/GSL.SP.1994.078.01.07

Sibuet, J.-C. & Hsu, S.-K. (1997) Geodynamics of the Taiwan arc-arc collision. Tectonophysics, 274, 221–251. doi:10.1016/S0040-1951(96)00305-8

Srivastava, P., & Mitra, G. (1994). Thrust geometries and deep structure of the outer and lesser Himalaya, Kumaon and Garhwal (India): Implications for the evolution of the Himalayan fold-and-thrust belt. Tectonics, 13(1), 89–109. https://doi.org/10.1029/93TC01130

Stanley, R. S., Hill, L. B., Chang, H. C., & Hu, H. N. (1981). A transect through the metamorphic core of the central mountains, southern Taiwan. Mem. Geol. Soc. China, 4, 443–473

Suppe, J., 1976. Decollement folding in southwestern Taiwan. Pet. Geol. Taiwan 13, 25–35

Suppe, J., 1980. A retrodeformable cross section ofnorthern Taiwan. Proc. Geol. Soc. China 23, 46–55

Suppe, J. (1981). Mechanics of mountain-building and metamorphism in Taiwan. Mem. Geol. Soc. China, 4,67–89

Suppe, J. (1986), Reactivated normal faults in the western Taiwan fold-and-thrust belt, Mem. Geol. Soc. China, 7, 187–200. Tang, Q., and C. Zheng (2010), Seismic velocity structure and improved seismic image of the southern depression of the Tainan Basin from pre-stack depth migration, Terr. Atmos. Ocean. Sci., 21, 807–816

Tang, C.-H. (1977). Late Miocene erosional unconformity on the subsurface Peikang high Chiayi Yulin. Mem. Geol. Soc. China, 2, 155–167

Tang, C.-C., Zhu, L., Chen, C.-H., Teng, T.-L., (2011). Significant crustal structural variation across the Chaochou Fault, southern Taiwan: new tectonic implications for convergent plate boundary. J. Asian Earth Sci. 41 (6), 564–570

Tang, Q., and C. Zheng (2010), Seismic velocity structure and improved seismic image of the southern depression of the Tainan Basin from pre-stack depth migration, Terr. Atmos. Ocean. Sci., 21, 807–816

Tavani, S., Storti, F., Lacombe, O., Corradetti, A., Muñoz, J.A. & Mazzoli, S. (2015) A review of deformation pattern templates in foreland basin systems and fold-and-thrust belts: Implications for the state of stress in the frontal regions of thrust wedges. Earth-Science Rev., 141, 82–104, Elsevier B.V. doi:10.1016/j.earscirev.2014.11.013

Teng, L.-S. (1987), Stratigraphic records of the late Cenozoic Penglai orogeny of Taiwan, Acta Geol. Taiwanica, 25, 205–224.

Teng, L. S., Y. Wang, C.-H. Tang, C.-Y. Huang, T.-C. Huang, M.-S. Yu, and A. Ke (1991), Tectonic aspects of the Paleogene depositional basin of northern Taiwan, Proc. Geol. Soc. China, 34, 313–336

Teng, L.-S. (1992), Geotectonic evolution of Tertiary continental margin basins of Taiwan, Pet. Geol. Taiwan, 27,1–19.

Teng, L.-S., and A.-T. Lin (2004), Cenozoic tectonics of the China continental margin; insights from Taiwan, in Aspects ofthe Tectonic Evolution of China, vol. 226, edited by J. Malpas, C. J. N. Fletcher, J. R. Ali, and J. C. Aitchison, pp. 313–332, Geol. Soc. London Spec. Pub., London.

Tensi, J., Mouthereau, F., & Lacombe, O. (2006). Lithospheric bulge in the West Taiwan Basin. Basin Research, 18(3), 277–299. https://doi.org/ 10.1111/j.1365-2117.2006.00296.x

Thomas, W. A. (1985), The Appalachian-Ouachita connection: Paleozoic orogenic belt at the southern margin of North America, Annu. Rev. Earth Planet. Sci., 13, 175–199.

Thomas, W. A. (1990). Controls on locations of transverse zones in thrust belts. Eclogae Geologicae Helvetiae, 83, 727–744.

Thomas, W. A., & Bayona, G. (2002). Palinspastic restoration of the Anniston transverse zone in the Appalachian thrust belt, Alabama. J. Struct. Geol., 24(4), 797–826. https://doi.org/10.1016/S0191-8141(01)00117-1

Townend, J. & Zoback, M.D., 2006. Stress, strain, and mountain building in central Japan, J. geophys. Res., 111, B03411, doi:10.1029/2005JB003759

Tsai, C.-H., S.-K. Hsu, Y.-C. Yeh, C.-S. Lee, and K. Xia (2004), Crustal thinning of the northern continental margin of the South China Sea, Mar. Geophys. Res., 25,63–78.

Turner, S. A., J. W. Cosgrove, and J. G. Liu (2010), Controls on lateral structural variability along the Keping Shan Thrust Belt, SW Tien Shan foreland, China, in Hydrocarbons in Contractional Belts, vol. 348, edited by G. P. Goffey et al., 71–85, Geol. Soc. London Spec. Pub., London

Turner, J.P. & Williams, G.A. (2004) Sedimentary basin inversion and intra-plate shortening. Earth-Science Rev., 65, 277–304. doi:10.1016/j.earscirev.2003.10.002

Vavrycuk, V. (2014) Iterative joint inversion for stress and fault orientations from focal mechanisms. Geophys. J. Int., 199, 69–77. doi:10.1093/gji/ggu224

Waldhauser, F. (2001) hypoDD - A program to compute double-difference hypocenter locations. U.S. Geol. Surv. Open File Rep., 1–25. doi:https://doi.org/10.3133/ofr01113

Waldhauser, F. & Ellsworth, W.L. (2000) A Double-Difference Earthquake Location Algorithm: Method and Application to the Northern Hayward Fault, California. Bull. Seismol. Soc. Am., 90, 1353–1368. doi:10.1785/0120000006

Willet, S. D. (1999), Orogeny and orography: The effects of erosion on the structure of mountain belts, J. Geophys. Res., 104, 28,957–28,981

Wiltschko, D. & Eastman, D. (1983) Role of basement warps and faults in localizing thrust fault ramps. in Geol. Soc. Am., pp. 177–190. doi:10.1130/MEM158-p177

Wiltschko, D. V., Hassler, L., Hung, J.-H. & Liao, H.-S. (2010) From accretion to collision: Motion and evolution of the Chaochou Fault, southern Taiwan. Tectonics, 29, 1–23. doi:10.1029/2008TC002398

Woodward, N. B. (1986). Thrust fault geometry of the Snake River Range, Idaho and Wyoming. Geol. Soc. Am. Bull., 97(2), 178–193. https://doi.org/10.1130/0016-7606(1986)97<178:TFGOTS>2.0.CO;2

Wu, S.K., Chi, W.C., Hsu, S.M., Ke, C.C. & Wang, Y. (2013) Shallow crustal thermal structures of central Taiwan foothills region. Terr. Atmos. Ocean. Sci., 24, 695–707. doi:10.3319/TAO.2013.03.13.01(T)

Wu, F.T., Rau, R.-J., Salzberg, D., (1997). Taiwan orogeny: thin-skinned or lithospheric collision? Tectonophysics 274 (1–3), 191–220

Wu, F.T., C.-H. Chang, and Y.-M. Wu (2004), Precisely relocated hypocentres, focal mechanisms and active orogeny in central Taiwan, in Aspects of the Tectonic Evolution of China, vol. 226, edited by J. Malpas, et al., pp. 333–354, Geol. Soc. London Spec. Pub., London

Wu, F. T., H. Kuo-Chen, and K. D. McIntosh (2014), Subsurface imaging, TAIGER experiments and tectonic models of Taiwan, J. Asian Earth Sci., 90, 173–208

Wu, Y.-M., C.-H. Chang, L. Zhao, J. B. H. Shyu, Y.-G. Chen, K. Sieh, and J. P. Avouac (2007), Seismic tomography of Taiwan: Improved constraints from a dense network of strong motion stations, J. Geophys. Res., 112, B08312, doi:10.1029/2007JB004983

Wu, Y.-M., Zhao, L., Chang, C.-H. & Hsu, Y.J. (2008) Focal-mechanism determination in Taiwan by genetic algorithm. Bull. Seismol. Soc. Am., 98, 651–661. doi:10.1785/0120070115

Wu, Y.-M., Hsu, Y.-J., Chang, C.-H., Teng, L.S. & Nakamura, M. (2010) Temporal and spatial variation of stress field in Taiwan from 1991 to 2007: Insights from comprehensive first motion focal mechanism catalog. Earth Planet. Sci. Lett., 298, 306–316. doi:10.1016/j.epsl.2010.07.047

Yang, K.-M., H.-H. Ting, and J. Yuan (1991), Structural styles and tectonic modes of Neogene extensional tectonics in southwestern Taiwan: Implications for hydrocarbon exploration, Pet. Geol. Taiwan, 26,1–31.

Yang, K.-M., S.-T. Huang, J.-C. Wu, H.-H. Ting, and W.-W. Mei (2006), Review and new insights on foreland tectonics in western Taiwan, Int. Geol. Rev., 48, 910–941.

Yang, K.-M., S.-T. Huang, J.-C. Wu, H.-H. Ting, and W.-W. Mei, M. Lee, H.-H. Hsu, and C.-J. Lee (2007), 3D geometry of the Chelungpu thrust system in central Taiwan: Its implications for active tectonics, Terr. Atmos. Ocean. Sci., 18, 143–181

Yang, K.-M., Wu, J.-C., Cheng, E.-W., Chen, Y.-R., Huang, W.-C., Tsai, C.-C., et al. (2014). Development of tectonostratigraphy in distal part of foreland basin in southwestern Taiwan. J. Asian Earth Sci., 88,98–115. https://doi.org/10.1016/j.jseaes.2014.03.005

Yang, K.-M., R.-J. Rau, H.-Y. Chang, C.-Y. Hsieh, H.-H. Ting, S.-T. Huang, J.-C. Wu, and Y.-J. Tang (2016), The role of basement-involved normal faults in the recent tectonics of western Taiwan, Geol. Mag., 153, 1166–1191

Yeh, Y.-H., et al. (1998), Onshore/offshore wide-angle deep seismic profiling in Taiwan, Terr. Atmos. Ocean. Sci., 9, 301–316. Yeh, Y.-C., S.-K. Hsu, W.-B. Doo, J.-C. Sibuet, C.-S. Liu, and C.-S. Lee (2012), Crustal features of the northeastern South China Sea: Insights from seismic and magnetic interpretations, Mar. Geophys. Res., 33, 307–326

Yeh, Y.-C., S.-K. Hsu, W.-B. Doo, J.-C. Sibuet, C.-S. Liu, and C.-S. Lee (2012), Crustal features of the northeastern South China Sea: Insights from seismic and magnetic interpretations, Mar. Geophys. Res., 33, 307–326

Yin, A. (2006), Cenozoic tectonic evolution of the Himalayan orogeny as constrained by along-strike variation of structural geometry, exhumation history, and foreland sedimentation, Earth Sci. Rev., 76,1–131

Yu, S., Chen, H. & Kuo, L. (1997), Velocity field of GPS stations in the Taiwan area. Tectonophysics, 274, 41–59. doi:10.1016/S0040-1951(96)00297-1

Yuan, J., & Huang, S. T. (1985). Stratigraphic study on the pre Miocene under the Peikang Area.

Yue, L.-F., Suppe, J., Hung, J.-H., (2005). Structural geology of a classic thrust belt earth- quake: the 1999 Chi-Chi earthquake Taiwan (Mw = 7.6). J. Struct. Geol., 27 (11), 2058–2083.

Zhao, M., X. Qiu, S. Xia, H. Xu, P. Wang, T. K. Wang, C.-S. Lee, and K. Xia (2010), Seismic structure in the northeastern South China Sea: S-wave velocity and Vp/Vs ratios derived from three-component OBS data, Tectonophysics, 480, 183–197

Zoback, M.L., Zoback, M.D., Adams, J., Assumpaçao, M., Bell, S., bergman, E.A., Blümling, P., Brereton, N.R., Denham, D., Ding, J., Fuchs, K., Gay, N., gregersen, S., Gupta, H.K., Gvishiani, A., Jacob, K., Kñein, R., Knoll, P., Magee, M., Mercier, J.L., Müller, B.C.,

APPENDIX 1 Published Scientific Articles

Paper I:

How the structural architecture of the Eurasian continental margin affects the structure, seismicity, and topography of the south central Taiwan fold-and-thrust belt.

Dennis Brown[1], Joaquina Alvarez-Marron[1], **Cristina Biete[1],** Hao Kuo-Chen[2], Giovanni Camanni[3] and Chun-Wei Ho[2,4].

[1] Institute of Earth Sciences Jaume Almera, ICTJA-CSIC, Lluis Sole i Sabaris s/n, 08028 Barcelona, Spain

[2] Department of Earth Sciences, National Central University, Jongli, Taiwan

[3] Fault Analysis Group, School of Earth Sciences, University College Dublin, Dublin, Ireland

[4] Central Weather Bureau, Taipei, Taiwan

Status of the paper: Published in ***Tectonics***, 2017, 36. doi:10.1002/2017TC004475

Contributions of the Ph.D. candidate to the article:

- Carried out structural mapping fieldwork;
- Constructed one of the geological cross-sections in collaboration with Ph.D. supervisors;
- Produced figures of the seismicity, the P-wave velocity slices and vertical sections from the available tomography and the shadow relief map from the topography;
- Reviewed the text.

AGU PUBLICATIONS

Tectonics

RESEARCH ARTICLE
10.1002/2017TC004475

Key Points:
- Taiwan provides insight into how a margin structure contributes to along-strike changes in a fold-and-thrust belt
- Structural inheritance of basement faults is a key component in producing along-strike changes in structure, seismicity, and topography
- These along-strike changes vary depending on which morphological part of the margin is involved in the deformation

Correspondence to:
D. Brown,
dbrown@ictja.csic.es

Citation:
Brown, D., J. Alvarez-Marron, C. Biete, H. Kuo-Chen, G. Camanni, and C.-W. Ho (2017), How the structural architecture of the Eurasian continental margin affects the structure, seismicity, and topography of the south central Taiwan fold-and-thrust belt, *Tectonics*, *36*, doi:10.1002/2017TC004475.

Received 11 JAN 2017
Accepted 14 JUN 2017
Accepted article online 22 JUN 2017

How the structural architecture of the Eurasian continental margin affects the structure, seismicity, and topography of the south central Taiwan fold-and-thrust belt

Dennis Brown[1], Joaquina Alvarez-Marron[1], Cristina Biete[1], Hao Kuo-Chen[2], Giovanni Camanni[3], and Chun-Wei Ho[2,4]

[1]Institute of Earth Sciences "Jaume Almera", ITCJA-CSIC, Barcelona, Spain, [2]Department of Earth Sciences, National Central University, Jongli, Taiwan, [3]Fault Analysis Group, School of Earth Sciences, University College Dublin, Dublin, Ireland, [4]Central Weather Bureau, Taipei, Taiwan

Abstract Studies of mountain belts worldwide show that along-strike changes are common in their foreland fold-and-thrust belts. These are typically caused by processes related to fault reactivation and/or fault focusing along changes in sedimentary sequences. The study of active orogens, like Taiwan, can also provide insights into how these processes influence transient features such as seismicity and topography. In this paper, we trace regional-scale features from the Eurasian continental margin in the Taiwan Strait into the south central Taiwan fold-and-thrust belt. We then present newly mapped surface geology, *P* wave velocity maps and sections, seismicity, and topography data to test the hypothesis of whether or not these regional-scale features of the margin are contributing to along-strike changes in structural style, and the distribution of seismicity and topography in this part of the Taiwan fold-and-thrust belt. These data show that the most important along-strike change takes place at the eastward prolongation of the upper part of the margin necking zone, where there is a causal link between fault reactivation, involvement of basement in the thrusting, concentration of seismicity, and the formation of high topography. On the area correlated with the necking zone, the strike-slip reactivation of east northeast striking extensional faults is causing sigmoidal offset of structures and topography along two main zones. Here basement is not involved in the thrusting; there is weak focusing of seismicity and localized development of topography. We also show that there are important differences in structure, seismicity, and topography between the margin shelf and its necking zone.

Plain Language Summary We present newly mapped surface geology, which is integrated with *P* wave velocity maps and sections, with an accurately relocated seismicity data set, and with high-resolution topography to test the hypothesis of whether or not the regional-scale features of the margin are contributing to along-strike changes in structural style, seismicity, and topography of the south central Taiwan fold-and-thrust belt. As a corollary to this hypothesis, we also investigate whether or not there are differences in structural architecture, seismicity, and topography between the margin shelf and its necking zone.

1. Introduction

Studies of mountain belts worldwide have shown that along-strike changes in many features of their foreland fold-and-thrust belts are common [e.g., *Thomas*, 1985; *Perez-Estaun et al.*, 1997; *Duncan et al.*, 2003; *Mouthereau et al.*, 2006; *Yin*, 2006; *Turner et al.*, 2010; *Arora et al.*, 2012]. In most cases, these along-strike changes can be related to the reactivation of preexisting faults that were inherited from the continental margins that were involved in the deformation or to changes in sedimentary thickness and facies [e.g., *Jackson*, 1980; *Wiltschko and Eastman*, 1983; *Perez-Estaun et al.*, 1997; *Brown et al.*, 1999; *Kelly et al.*, 1999; *Calamita et al.*, 2011; *Turner et al.*, 2010; *Butler et al.*, 2006; *Chatzaras et al.*, 2013; *Boutoux et al.*, 2014; *Godin and Harris*, 2014]. While along-strike changes in structural architecture and in sedimentary depositional systems of fold-and-thrust belts are well documented in fossil orogens, investigating those in active orogens can also yield important information about variations in transient features such as seismicity and topography. For example, *Yin* [2006], *Arora et al.* [2012], and *Godin and Harris* [2014] have shown how preexisting faults on the Indian Plate that are oriented at a high angle to the structural grain of the foreland of the Himalaya and are causing along-strike changes in the structure, seismicity, and topography of its foreland fold-and-thrust belt. Likewise,

AGU Tectonics 10.1002/2017TC004475

Blanc et al. [2003], *Mouthereau et al.* [2006], and *Koyi et al.* [2016] have shown how preexisting structures in the Arabian Plate are similarly affecting various features of the Zagros fold-and-thrust belt. Investigating the role played by margin features in the development of along-strike changes is therefore not only of importance for determining structural processes, sediment pathways, and facies distribution in a fold-and-thrust belt, it is also important for understanding, and possibly mitigating, the focusing of geological hazards that are related to seismicity and topographic relief.

The area on and around the island of Taiwan provides an excellent opportunity to investigate how the structural and the morphological features of a continental margin could possibly contribute to along-strike changes in the structure, seismicity, and topography of a fold-and-thrust belt because the preexisting structural and basin architecture of the margin shelf, shelf-to-slope transition, and slope are well known [e.g., *Teng et al.*, 1991; *Yang et al.*, 1991; *Lin et al.*, 2003; *Teng and Lin*, 2004] and because there is a wealth of on-land geological, geophysical, and geodetic data that can be used to trace them into the fold-and-thrust belt [e.g., *Suppe*, 1986; *Deffontaines et al.*, 1997, *Lacombe et al.*, 1999; *Mouthereau et al.*, 2002; *Yang et al.*, 2006, 2016; *Byrne et al.*, 2011; *Alvarez-Marron et al.*, 2014; *Camanni et al.*, 2016]. In this paper, we combine the top of the Mesozoic basement map from the Taiwan Strait [*Lin et al.*, 2003] with seismic tomography to trace the regional-scale structural and morphological features of the continental margin into the south central Taiwan fold-and-thrust belt. We then present newly mapped surface geology, which is integrated with *P* wave velocity maps and sections, with an accurately relocated seismicity data set and with high-resolution topography to test the hypothesis of whether or not the regional-scale features of the margin are contributing to along-strike changes in structural style, seismicity, and topography of the south central Taiwan fold-and-thrust belt. As a corollary to this hypothesis, we also investigate whether or not there are differences in structural architecture, seismicity, and topography between the margin shelf and its necking zone.

2. Background: The Southeastern Eurasian Margin and the Taiwan Orogen

2.1. Tectonic Evolution and Structure of the Margin

The part of the continental margin of the Eurasian Plate that is currently involved in the Taiwan orogeny is thought to have evolved from a subcontinental subduction system in the Late Cretaceous [*Hall*, 2001; *Li et al.*, 2007; *Lan et al.*, 2008] to a rifting margin by the early Eocene followed, during the late early Oligocene, by seafloor spreading and, from the early Miocene to the present, the subduction of Eurasian Plate beneath the Philippine Sea Plate [*Hall*, 1996; *Lin et al.*, 2003; *Huang et al.*, 2012]. Here we define the margin's prerift Mesozoic rocks as the basement upon which the Eocene and younger sediments of the margin were deposited. The morphology of the Eurasian margin that is now entering into the collision with the Philippine Sea Plate to form the Taiwan orogen consists of a broad shelf with deep, fault-bounded Eocene age basins, a roughly northeast striking shelf slope break (the 200 m bathymetry contour), a steep, narrow slope with Miocene age basins, and a broad distal margin (Figures 1 and 2). Throughout this paper, we use the structural term necking zone [e.g., *Mohn et al.*, 2012] when referring to the area of the margin where the basement thins and slope when referring to the morphological feature where sediments were deposited on the necking zone (Figure 2). We refer to that part of the margin where the basement begins to thin as the upper part of the necking zone (Figure 2). In Taiwan, the upper part of the necking zone roughly coincides with the northern bounding-fault system of the Tainan Basin [e.g., *Lee et al.*, 1993; *Lin et al.*, 2003; *Ding et al.*, 2008]. The crustal thickness of the shelf part of the Eurasian margin has been determined from a variety of geophysical data to be about 30 ± 5 km [*Yeh et al.*, 1998; *Kim et al.*, 2004; *Kuo-Chen et al.*, 2012; *Huang et al.*, 2014; *Wu et al.*, 2014; *Chen et al.*, 2016]. Reflection and wide-angle seismic data show that the continental crust thins across the necking zone, from approximately 30 km of the shelf to approximately 18 km along the more than 300 km wide hyperextended, distal part of the margin (Figure 2) [*Chen and Yang*, 1996; *Li et al.*, 2007; *Lin et al.*, 2008; *Huang et al.*, 2012; *Yeh et al.*, 2012; *Deng et al.*, 2012; *McIntosh et al.*, 2013, 2014; *Lester et al.*, 2014]. *Yeh et al.* [2012], *McIntosh et al.* [2014], and *Lester et al.* [2014] also interpret a failed rift to occur at the base of the slope (FR in Figure 2) that projects on shore in southwestern Taiwan. The transition from continental to oceanic crust occurs to the south of the area shown in Figure 1 [e.g., *Nissen et al.*, 1995; *Zhao et al.*, 2010; *Tsai et al.*, 2004: *Deng et al.*, 2012; *Yeh et al.*, 2012; *McIntosh et al.*, 2013; *Lester et al.*, 2014].

The Eocene age synrift basins that developed on the margin shelf are oriented roughly northeast-southwest [*Lin and Watts*, 2002; *Lin et al.*, 2003; *Teng and Lin*, 2004; *Lin et al.*, 2005; *Cukur et al.*, 2011] and locally

AGU Tectonics 10.1002/2017TC004475

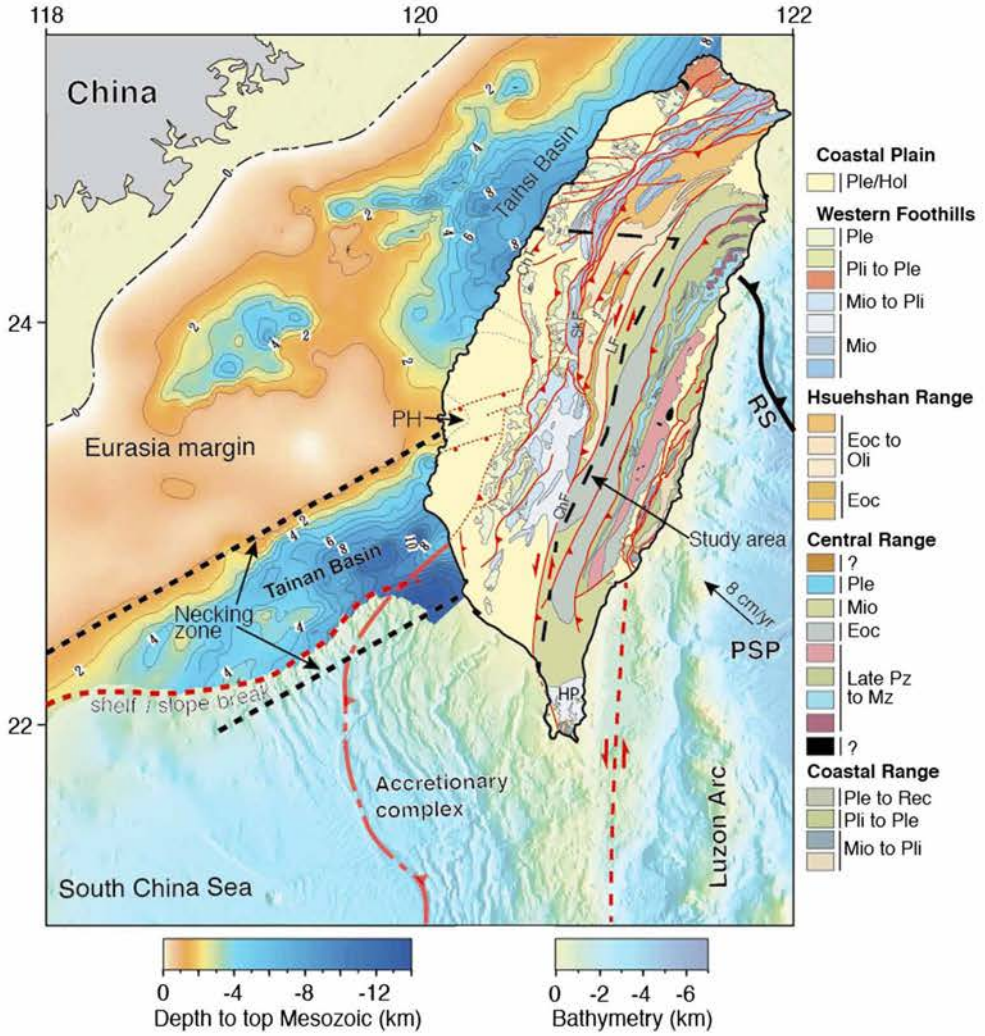

Figure 1. Simplified geological map of the island of Taiwan (redrawn from *Chen et al.* [2000]). In the Taiwan Strait, the depth to the top of the Mesozoic basement [from *Lin et al.*, 2003]. The location of the necking zone offshore is indicated by the thick dashed lines and the shelf slope break by the thick dashed red line. The bathymetry is shown to the south and east of Taiwan. The study area on land in Taiwan is outlined by the dashed box. PH = Peikang Basement High, RS = Ryukyu subduction zone, PSP = Philipinne Sea Plate, ChT = Changhua Thrust, SkF = Shuilikeng Fault, LF = Lishan Fault, ChF = Chaochou Fault, HP = Hengchun Peninsula.

accumulated up to approximately 5 km of sediments [e.g., *Lin et al.*, 2003]. Of these, the Taihsi Basin is now involved in the Taiwan orogeny (Figure 1), with its eastern flank, the Hsuehshan Trough of *Teng et al.* [1991] and *Teng and Lin* [2004], now forming the Hsuehshan Range (Figure 1). During the late Oligocene to late Miocene, several extensional events further affected the outer shelf and necking zone areas to various degrees, resulting in an array of roughly east northeast striking extensional faults and development of the Tainan Basin [*Yang et al.*, 1991; *Lee et al.*, 1993; *Lin et al.*, 2003; *Lin et al.*, 2005; *Ding et al.*, 2008; *Shi et al.*, 2008; *Tang and Zheng*, 2010; *Yang et al.*, 2016]. Reactivation of the east northeast striking faults of the Tainan Basin is having a widespread, variable effect on the fold-and-thrust belt in southwestern Taiwan [e.g., *Suppe*, 1986; *Rodriguez-Roa and Wiltschko*, 2010; *Alvarez-Marron et al.*, 2014; *Yang et al.*, 2007, 2016], and it is here that we focus our investigation to test the hypothesis of along-strike changes caused by inheritance of structures from the margin.

AGU Tectonics 10.1002/2017TC004475

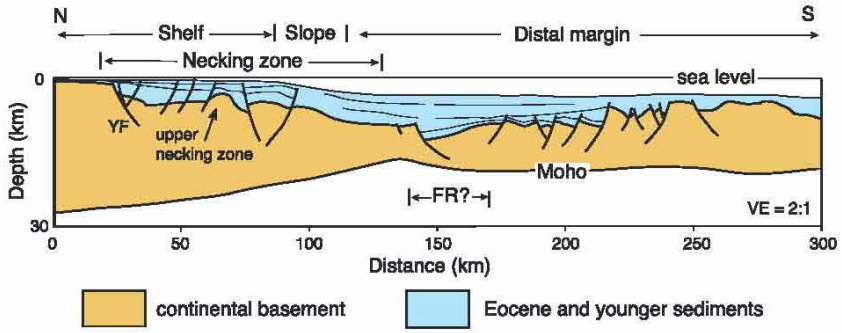

Figure 2. A schematic cross section of the continental margin to the southwest of Taiwan that shows the terminology for the margin used in the text and a simplified structural interpretation. The location of the section is shown in Figure 1. The structure depicted in the upper crust of the shelf area is from *Lin et al.* [2003], whereas that in the slope and distal margin is simplified from *Yeh et al.* [2012] and *Lester et al.* [2014]. The Moho depth in the distal margin is from *Lester et al.* [2014], whereas that beneath the shelf and slope area is from *Tsai et al.* [2004]. The continent to ocean transition lies to the south of this diagram. YF = Yichu fault. FR = failed rift of *Yeh et al.* [2012], *Lester et al.* [2014], and *McIntosh et al.* [2014]. The vertical exaggeration is 2:1.

2.2. Tectonostratigraphy of the Taiwan Orogen

The Taiwan orogen is divided into five roughly N-S oriented tectonostratigraphic zones that are separated by major faults (Figure 1). From west to east these zones are the Coastal Plain (CP), Western Foothills (WF), the Hsuehshan Range (HR), the Central Range (CR), and the Coastal Range. In much of south central Taiwan, the boundary between the Coastal Plain and the Western Foothills is interpreted to coincide with the mostly buried tip line of the Changhua Thrust (ChT in Figure 1). In the north of the study area, the Western Foothills is in turn juxtaposed against the Hsuehshan Range across the Shuilikeng Fault (SkF). In the east, the Hsuehshan Range is juxtaposed against the Central Range across the Lishan Fault (LF). Southward, the Central Range is juxtaposed against the Western Foothills along the Chaochou Fault (ChF). Below, we give an overview of the outcropping stratigraphy and depositional environment of the Coastal Plain, the Western Foothills, the Hsuehshan Range, and the western part of the Central Range, beginning with the Mesozoic rocks that we define as basement.

Although the Central Range is outside of our study area, we give a brief description of it because the Mesozoic rocks that crop out there may make up a part of the basement in western Taiwan and in the Taiwan Strait [*Jahn et al.*, 1992]. The Mesozoic rocks in the Central Range comprise predominantly marbles and schists [*Stanley et al.*, 1981; *Ernst*, 1983; *Ho*, 1988; *Lan et al.*, 2008] whose absolute ages are not well constrained, although a number of Permian to Cretaceous isotopic ages have been determined [*Jahn et al.*, 1986; *Lo and Onstott*, 1995; *Lan et al.*, 2008; *Yui et al.*, 2009, 2012; *Wintsch et al.*, 2011]. In western Taiwan and its offshore, several boreholes intersect weakly metamorphosed continental to shallow marine siliciclastic deposits that have been interpreted to range in age from Late Permian to Cretaceous [e.g., *Jahn et al.*, 1992; *Chiu*, 1975; *Ho*, 1988; *Shaw*, 1996]. There is, however, some disagreement about the interpretations of the age of these rocks [e.g., *Chiu*, 1975; *Ho*, 1988; *Shaw*, 1996].

In the western part of the Central Range, the Mesozoic rocks are either unconformably overlain by, or in fault contact with, Eocene age siliciclastic rocks that are interpreted to have been deposited on the outer part of the margin, in an outer neritic to upper bathyal environment [e.g., *Ho*, 1988; *Teng*, 1992; *Huang et al.*, 1997]. These are unconformably overlain by predominantly middle Miocene age siliciclastic rocks that in northern to central Taiwan are interpreted to have been deposited in the upper to middle bathyal zone of the margin slope [*Chang*, 1976; *Sung and Wang*, 1985; *Huang et al.*, 1997, 2006, 2012]. Farther south, pillow lavas intercalated with middle Miocene siliciclastics are interpreted to have been erupted near the base of the slope [*Smith and Lewis*, 2007]. On the Hengchun Peninsula, in southeastern Taiwan, middle to late Miocene age turbidites are interpreted to have been deposited on the slope [*Huang et al.*, 2012; *Zhang et al.*, 2014].

The ages of the stratigraphic units of the Hsuehshan Range are poorly constrained because of a paucity of fossil assemblages that would allow a detailed stratigraphic succession to be determined [*Ho*, 1988] and because of its complex structure [e.g., *Tillman and Byrne*, 1995; *Brown et al.*, 2012]. Recently, *Chen et al.*

AGU Tectonics 10.1002/2017TC004475

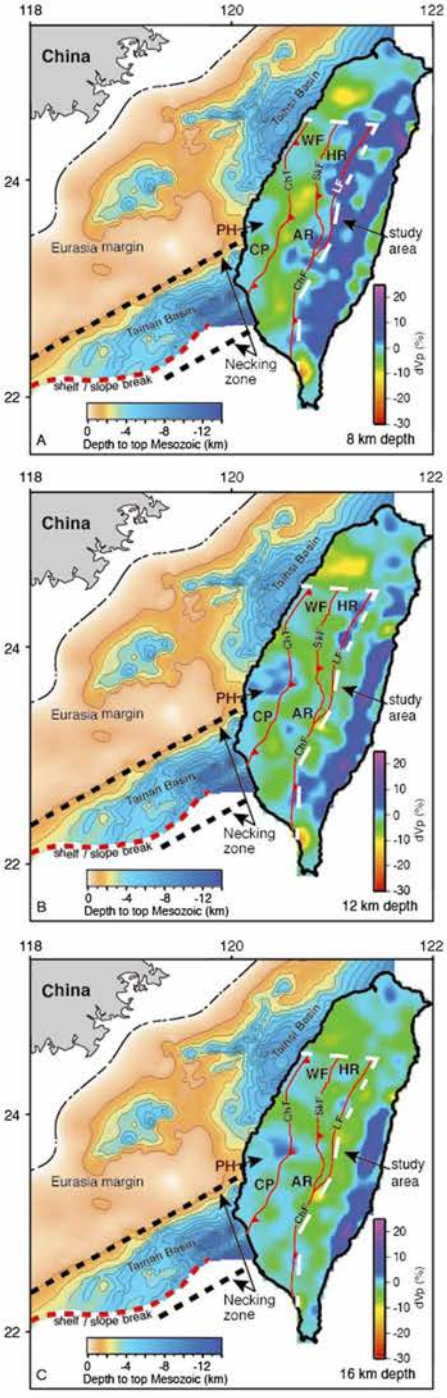

Figure 3. *P* wave velocity perturbation models (dVp (%)) for the island of Taiwan at various depths. The depth to the top of the Mesozoic basement in the Taiwan Strait is as in Figure 1. The location of the necking zone offshore is indicated by the thick dashed lines and the shelf slope break by the thick dashed red line. The study area on land in Taiwan is outlined by the dashed box. CP = Coastal Plain, WF = Western Foothills, HR = Hsuehshan Range, CR = Central Range. Other labels are as in Figure 1.

[2009] and *Huang et al.* [2012] reported the presence of Early to middle Eocene age foraminifera from the Hsuehshan Range. These Eocene rocks are thought to have been deposited in either a shallow marine or fluvial environment [*Huang et al.*, 2012] in what is commonly interpreted to have been the rift-related Hsuehshan Trough (or Basin) [*Ho*, 1988; *Teng et al.*, 1991; *Lin et al.*, 2003; *Teng and Lin*, 2004; *Huang et al.*, 2012]. By extrapolation from other basins of similar age to the west and north of Taiwan (Figure 1) [e.g., *Lin et al.*, 2003; *Cukur et al.*, 2011] the Eocene rocks of the Hsuehshan Trough can also be interpreted to directly overlie the Mesozoic basement. The Eocene rocks of the Hsuehshan Range are themselves unconformably overlain by late Oligocene shallow marine siliciclastic rocks [*Lee*, 1979; *Lin et al.*, 2003; *Huang et al.*, 2012] that are interpreted to have been deposited on the shelf to upper slope and to reflect thermal subsidence of the rifted margin following the opening of the South China Sea [*Lin et al.*, 2003; *Teng and Lin*, 2004].

The outcropping stratigraphy of the Western Foothills and Coastal Plain consists predominantly of Eocene through Holocene age siliciclastic rocks and unconsolidated sediments [*Chiu*, 1975; *Covey*, 1986; *Ho*, 1988; *Teng*, 1992; *Shaw*, 1996; *Chen et al.*, 2001; *Lin et al.*, 2003; *Huang et al.*, 2012, 2013]. The Eocene through to latest Miocene rocks are interpreted to have been deposited in shallow marine to fluvial environments [*Chiu*, 1975; *Ho*, 1988; *Shaw*, 1996; *Huang et al.*, 2012, 2013], whereas the latest Miocene through Holocene rocks and sediments were (and are being) predominately deposited in shallow marine and fluvial environments in the foreland basin [*Covey*, 1986; *Teng*, 1987; *Chen et al.*, 2001; *Lin and Watts*, 2002; *Castelltort et al.*, 2010; *Nagel et al.*, 2013]. A possible exception to this is in southwestern Taiwan where a thick mudstone unit is interpreted to have been deposited in a moderately deep water (upper slope?), open sea,

AGU Tectonics 10.1002/2017TC004475

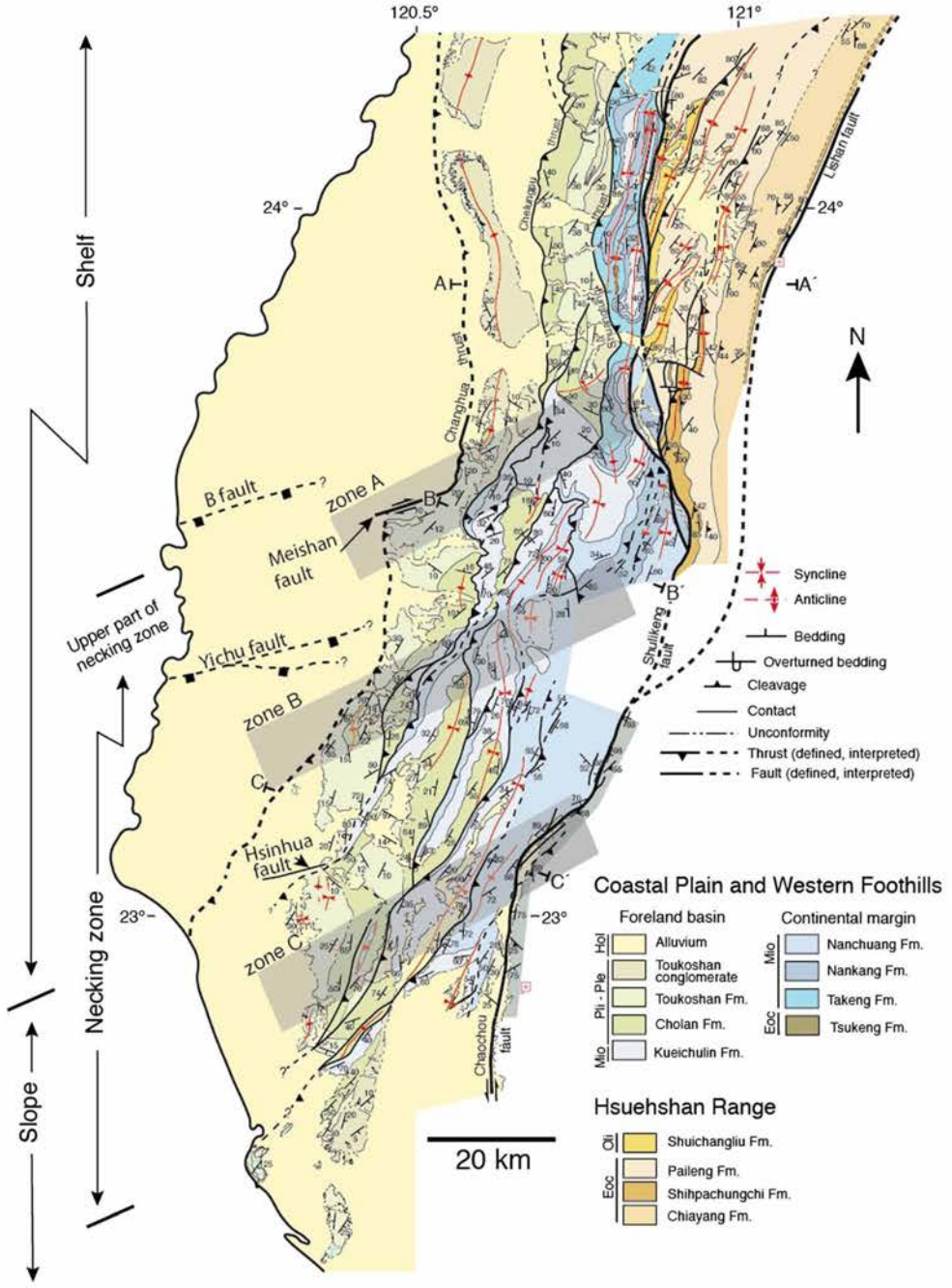

Figure 4. Geological map of the study area, with representative structural data. The locations of the cross sections in Figure 5 are shown. The transparent gray boxes, called zones A, B, and C, highlight areas where there are marked changes in the structural grain of the fold-and-thrust belt that we interpret to be due to reactivation of faults in the basement. The northernmost of these corresponds to the on-land projection of the upper part of the necking zone. The stratigraphic scheme used in the map is given in Table 1.

AGU Tectonics 10.1002/2017TC004475

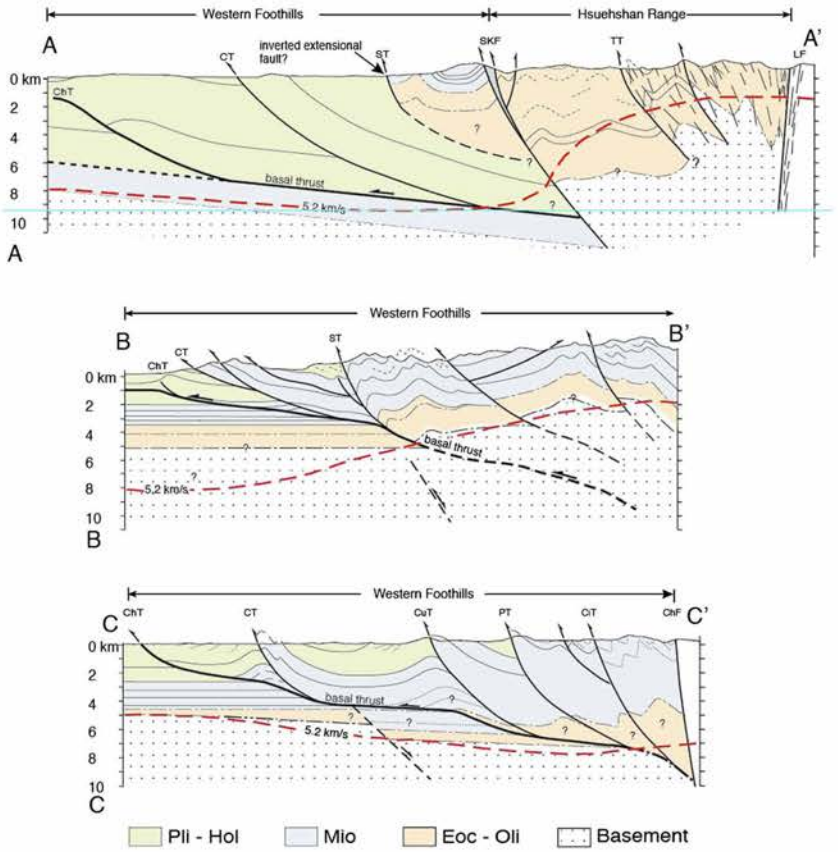

Figure 5. Geological cross sections through south central Taiwan. The locations are given in Figure 4. ChT = Changhua Thrust, CT = Chelungpu Thrust, SkF = Shuilikeng Fault, ST = Shuangtung Thrust, CuT = Chutochi Thrust, PT = Pingshi Thrust, CiT = Chishan Thrust, LF = Lishan Fault, ChF = Chaochou Fault, The dashed red line is the 5.2 km/s isovelocity line.

environment [*Covey*, 1986]. Neither the Eocene nor the Oligocene rocks are present everywhere, so in places, the lower Miocene rocks can either unconformably overlie the basement or conformably overlie the Oligocene [*Chiu*, 1975; *Ho*, 1988; *Shaw*, 1996]. The Miocene sequence thickens significantly southward across the on-land prolongation of the Tainan Basin and may reach as much as 6 km in thickness in southwestern Taiwan [*Ho*, 1988; *Shaw*, 1996; *Lin et al.*, 2003]. These rocks make up a significant part of the stratigraphy involved in the thrust system in this southern part of the Western Foothills (Figure 1).

2.3. Tracing the Margin Structure Into South Central Taiwan

To aid in the correlation of regional-scale structures from the margin in the Taiwan Strait with velocity anomalies on land in Taiwan, we present three depth slices from a 3-D *P* wave perturbation (dVp) model derived from the local tomography of *Kuo-Chen et al.* [2012] (Figure 3). The description below is confined to our study area, which is shown in Figure 3. In the northwest of the study area, at 8 km depth, the dominant negative dVp values to the west of the Shulikeng fault (SkF in Figure 3a) provide good correlation with the sediments of the Taihsi and foreland basins. At this depth there is also a significant increase in the relative dVp in the Hsuehshan Range and a well-developed positive anomaly below the Alishan Range (HR and AR, respectively, in Figure 3). We interpret the increase in the relative velocity in the Hsuehshan and Alishan ranges to be caused by the presence of high-velocity basement rocks at a shallow crustal level [see *Camanni et al.*, 2014a, 2016; *Alvarez-Marron et al.*, 2014]. Beginning at 8 km depth, but becoming especially prominent at 12 km and 16 km depth, there is an embayment of relatively high dVp that is associated with the high-velocity basement rocks that comprise the Peikang Basement High (PH in Figure 3) [e.g., *Wu et al.*, 2007; *Byrne et al.*, 2011; *Kuo-Chen et al.*, 2012; *Huang et al.*, 2014]. The southern flank of this area of relatively

AGU Tectonics 10.1002/2017TC004475

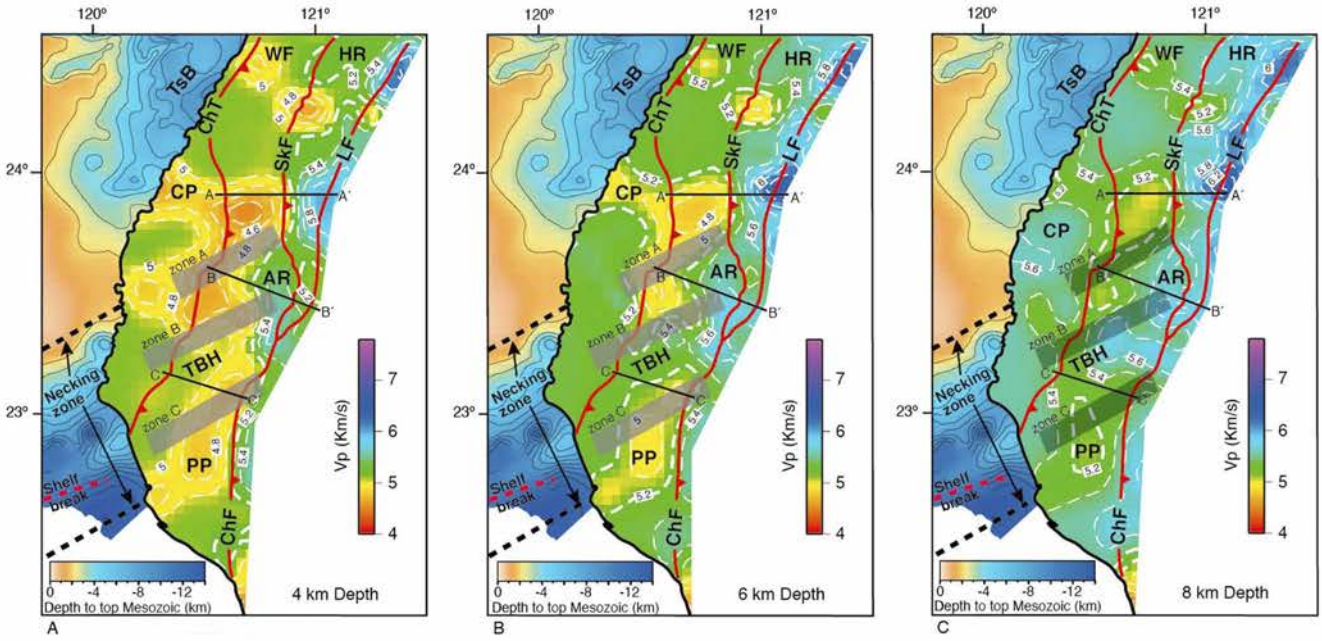

Figure 6. Horizontal Vp maps at (a) 4 km depth, (b) 6 km depth, and (c) 8 km depth. The depth to the top of the Mesozoic basement in the Taiwan Strait is as in Figure 1. The Tainan Basement High (TBH) is interpreted to represent a fault-bounded basement high whose southern flank corresponds to the upper part of the necking zone. Zones A, B, and C are shown as transparent gray boxes marking the areas where there is a change in the structural grain of the fold-and-thrust belt. The location of the necking zone offshore is indicated by the thick dashed lines and the shelf slope break by the thick dashed red line. The locations of the velocity sections in Figure 7 are shown. TsB = Taihsi Basin. Other labels are as in Figure 1.

high dVp coincides with the on-land projection of the upper part of the necking zone, clearly indicating that it can be traced from the margin into the fold-and-thrust belt. South of this, in the Western Foothills and on the Coastal Plain, the negative dVp values reach to about 12 km depth and are interpreted to be due to thicker Miocene and foreland basin sediments that were deposited on the slope of the margin and which are now involved in the fold-and-thrust belt deformation [e.g., *Wu et al.*, 2007; *Kuo-Chen et al.*, 2012; *Huang et al.*, 2014]. By 16 km depth, the Peikang Basement High still produces a significant dVp anomaly. Below the southwestern part of the fold-and-thrust belt, there is a weak dVp high extending northeastward from a basement high on the margin.

3. The South Central Taiwan Fold-and-Thrust Belt

3.1. Data and Methodology

In this section we present the geology of south central Taiwan (Figures 4 and 5), which is integrated with the TAIGER *P* wave velocity model [*Kuo-Chen et al.*, 2012] (Figures 6 and 7), with earthquake hypocenter data from 1994 to 2014 (Figure 8) and with a 40 m pixel digital elevation model (Figure 9a). The geological map (Figure 4) is from our own fieldwork [see *Brown et al.*, 2012; *Alvarez-Marron et al.*, 2014]. In the map, the stratigraphy of the Miocene through Pleistocene rocks is simplified as a chronostratigraphic sequence whose north to south correlation follows that of *Shea et al.* [2003] (Table 1). We also correlate major faults from north to south in the manner of *Ho* [1986]. The cross sections shown in Figure 5 were drawn using the geological map, field structural data, and the standard section construction techniques [e.g., *Dahlstrom*, 1969; *Hossack*, 1979]. We refer the reader to *Kuo-Chen et al.* [2012] and its supplementary data set for the acquisition and processing parameters, the reference velocity function used for the Vp perturbation model, and the resolution testing of the TAIGER local tomography. In the velocity maps and sections presented here, we can expect a resolution of at least 20 × 20 × 10 km (see the checkerboard test of *Kuo-Chen et al.* [2012]). The discretization of the 3-D velocity grid is 4 × 4 km horizontally and 2 km vertically to a depth of 24 km. At a depth of greater than 24 km the spatial resolution is 4 × 4 × 4 km. The earthquake hypocenters have been relocated by the double-difference

AGU Tectonics 10.1002/2017TC004475

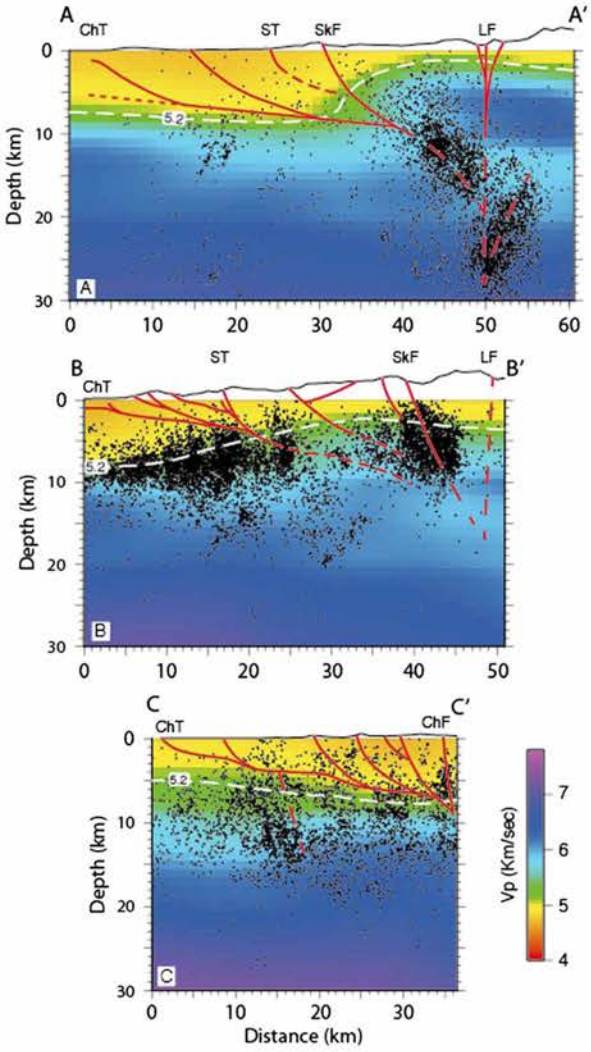

Figure 7. Vp sections with the fault traces taken from the geological cross sections shown in red. Locations are shown in Figure 6. Earthquake hypocenters are projected on to the sections from 3 km either side. Fault labels are as in Figure 1.

technique [*Waldhauser and Ellsworth*, 2000] within the local 3-D Vp model of *Kuo-Chen et al.* [2012] using the HypoDD3D software [*Waldhauser*, 2001]. The relocation was carried out on all events shallower than 60 km depth that had a minimum of six readings with a reading weighting <3 (good quality). Calculations of travel time residuals of earthquakes in the Central Weather Bureau database indicate that the starting uncertainty in their locations was less than 1 km. After the HypoDD relocation the average residual was reduced, indicating that the uncertainty had improved. In the description of the structure that follows, we differentiate between the morphological features of the margin in the footwall (the shelf, the necking zone, and the slope) and those in the hanging wall of the fold-and-thrust belt (Western Foothills, Hsuehshan Range, zones A, B, and C) (Figure 4) whose structures we wish to link to those in the margin.

Finally, an important feature of the subsurface geology for the interpretations that follow is the contact between the Mesozoic basement rocks and the overlying sediments. Understanding where this contact is allows us to interpret the role played by the margin basement in the structure of the fold-and-thrust belt. In the absence of any surface data about this contact in south central Taiwan, and with a limited number of borehole data, we choose to make a seismic velocity description in which a Vp of 5.2 km/s is taken as a proxy for the velocity of the rocks near the top of the basement. We choose this velocity for two reasons: (1) because it is in keeping with laboratory measurements of Vp carried out on clastic rocks [*Christensen*, 1989; *Mavko et al.*, 1998; *Christensen and Stanley*, 2003; *Johnston and Christensen*, 1992, 1993] that are similar in lithology to those described as Mesozoic in boreholes from south central Taiwan [*Chiu*, 1975; *Shaw*, 1996] and (2) because it is in keeping with the measured Vp (<5 km/s) of the late Miocene and younger sediments intersected by the Taiwan Chelungpu Fault Drilling Project borehole A [*Hung et al.*, 2009]. We stress, however, that a Vp of 5.2 km/s serves only as a proxy. It is meant to help with the interpretation of the location of these rocks at depth, but because of the uncertainties in the velocity model and in the petrophysical assumptions it may not coincide exactly with the basement-cover interface.

3.2. Structure, Seismicity, and Topography of South Central Taiwan

In the northern part of the study area (north of zone A in Figure 4), the outcropping geology of the Coastal Plain and Western Foothills comprises Pliocene to Holocene synorogenic sediments of the foreland basin with, eastward, synrift Eocene age sedimentary and minor volcanic rocks that are unconformably overlain

AGU Tectonics 10.1002/2017TC004475

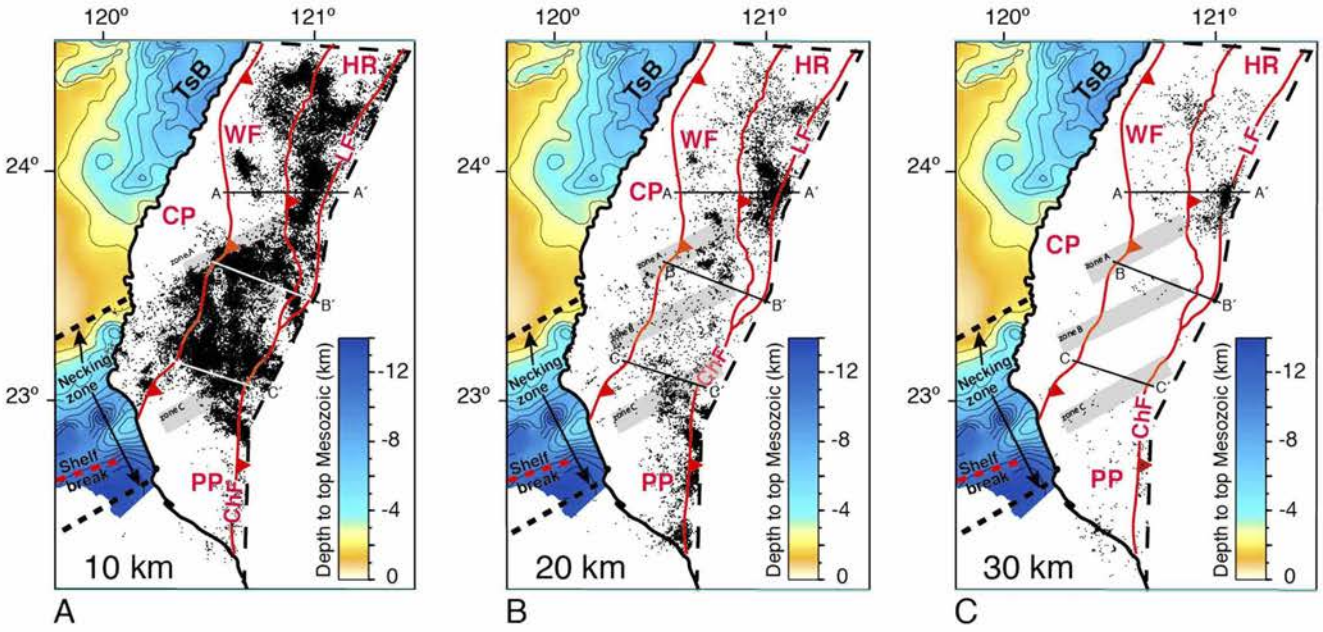

Figure 8. Earthquake epicenter depth slices for the study area. Events are projected 4.99 km each side of the depth slice. The depth to the top of the Mesozoic basement in the Taiwan Strait is as in Figure 1. The locations of the seismicity sections in Figure 7 are shown. The location of the necking zone offshore is indicated by the thick dashed lines and the shelf slope break by the thick dashed red line. Other labels are as in Figures 1, 3, and 6.

by Miocene sedimentary rocks (Figure 4). The Nanchuang Fm (middle to late Miocene) is absent here, and the early Miocene rocks are unconformably overlain by the late Miocene synorogenic Kuechulin Fm. The structure is that of a west verging imbricate thrust system with a roughly N-S striking structural grain (Figures 4 and 5a). Its basal thrust is interpreted to be located near the base of the low velocity (<5 km/s [*Hung et al.*, 2009]) synorogenic sediments in the Western Foothills (Figures 6 and 7a). Along the eastern flank of the Western Foothills, Eocene and Miocene rocks overthrust the Pliocene to Holocene synorogenic sediments along the Shuangtung thrust (ST in Figures 5a and 7a). Seismicity in this imbricate thrust system is scattered (Figure 8), with no clear correlation with any individual fault (Figure 7a). Beneath the imbricate thrust system, seismicity reaches to approximately 30 km depth, but there is no well-defined clustering that would suggest the location of any particular fault in the basement (Figures 7a and 8). The topography of the imbricate thrust system is dominantly subdued, with elongated hills developed in the immediate hanging walls of the frontal thrusts (Figure 9a). Only at the rear of the thrust system, where Miocene sediments crop out, do elevations reach more than 500 m.

The Shuilikeng fault is a major structural boundary across which there is an important change in the outcropping rocks and in the structure of the fold-and-thrust belt [*Camanni et al.*, 2014b] (Figures 4 and 5a). East of it, the Hsuehshan Range comprises Eocene age synrift sediments from the Hsuehshan Trough, which are unconformably overlain by late Oligocene postrift sediments. The structure of the Hsuehshan Range can be divided into two thrust sheets, the westernmost of which comprises open to tight, west verging anticlines and synclines and, from the Tili thrust (TT in Figure 5a) to the east, a set of west verging folds with a penetrative axial planar cleavage and associated thrusts that overall form an anticlinorium with a steep to overturned forelimb. The involvement of older and, at depth, higher Vp (Figures 6 and 7a) rocks in this part of the fold-and-thrust belt provides unequivocal evidence that the basal thrust ramps down to a deeper crustal level beneath the Hsuehshan Range [see *Yue et al.*, 2005; *Brown et al.*, 2012; *Chuang et al.*, 2013]. In the subsurface, the location of the ramp can be inferred from an east dipping cluster of seismicity that reaches to about 20 km depth (Figure 7a) [see *Chuang et al.*, 2013; *Camanni et al.*, 2014a, 2014b]. We interpret both the Shuangtung and Shuilikeng faults to be linked to this ramp, with the Shuangtung thrust having been cut by the Shuilikeng fault [*Brown et al.*, 2012; *Chuang et al.*, 2013]. The uplift of higher Vp rocks (>5.2 km/s) beneath the Hsuehshan Range (Figures 6 and 7a) is interpreted to indicate the involvement of Mesozoic

AGU Tectonics 10.1002/2017TC004475

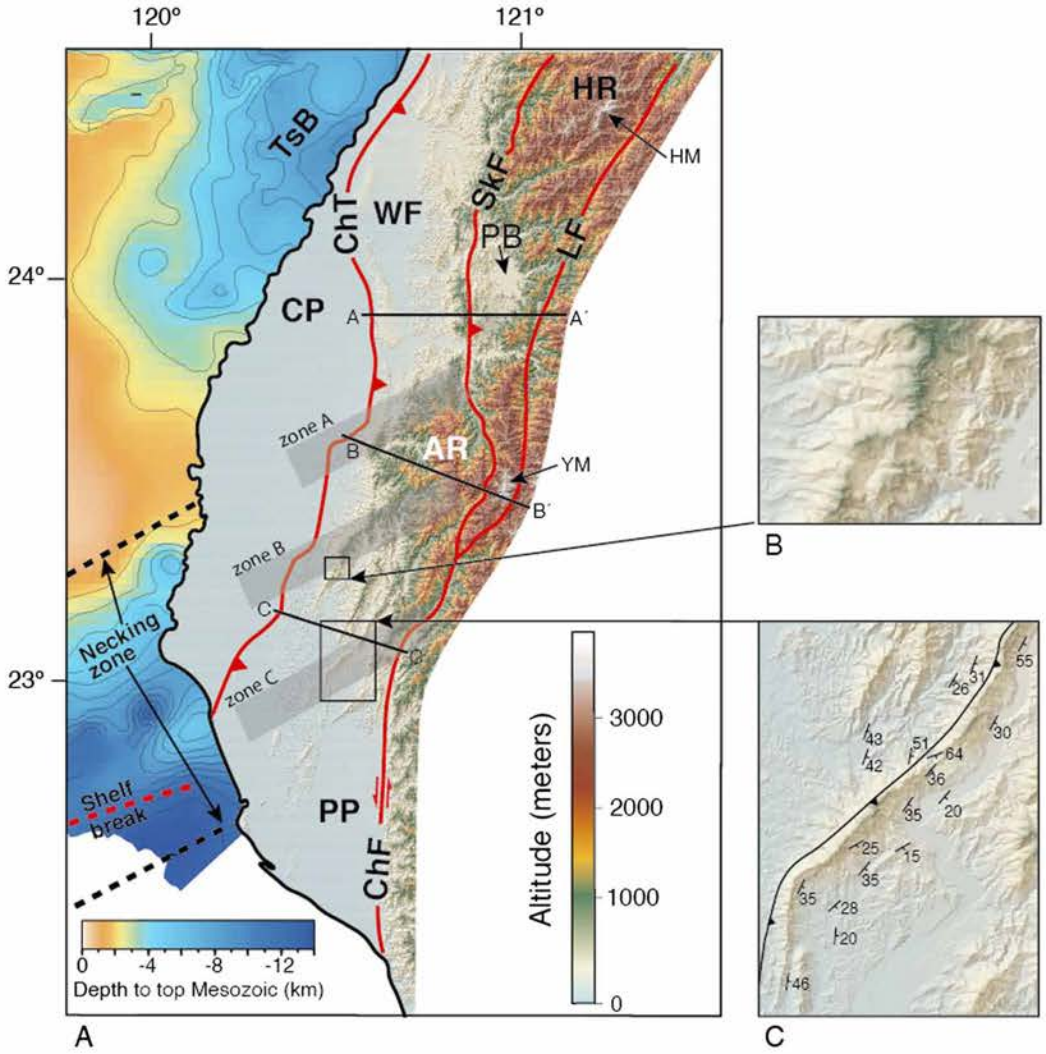

Figure 9. (a) Digital elevation model of the study area and (b and c) details of sigmoidal topographic features in southwestern Taiwan. The location of the necking zone offshore is indicated by the thick dashed lines and the shelf slope break by the thick dashed red line. The locations are shown by black boxes. The depth to the top of the Mesozoic basement in the Taiwan Strait is as in Figure 1. The locations of the topography sections in Figure 7 are shown. YM = Yushan Mountain, HM = Hsuehshan Mountain. Other labels are as in Figures 1, 3, and 6.

basement in the deformation. In this northern part of the study area, the Hsuehshan Range is the most seismically active part of the fold-and-thrust belt, with significant seismicity extending to over 30 km depth (Figure 8). The deepest seismicity in the Hsuehshan Range is seen in the cross section to form a steeply west dipping cluster that is interpreted to be associated with the Lishan fault (LF in Figures 7a and 8) [see *Wu et al.*, 2004; *Brown et al.*, 2012; *Camanni et al.*, 2014a, 2014b; *Kuo-Chen et al.*, 2015]. In the study area, the Hsuehshan Range has the highest elevations in the fold-and-thrust belt. The two highest mountains in Taiwan are found there: Yushan and Hsuehshan mountains, respectively (YM and HM, in Figure 9). The Puli Basin (PB in Figure 9) forms a pronounced topographic low within the Hsuehshan Range, and it is roughly centered on a marked Vp high (Figures 3 and 6).

The upper part of the necking zone marks a major change in the structure of the margin offshore western Taiwan, and across its on-land prolongation (zone A, Figure 4) there are significant along-strike changes in structure, stratigraphy, seismicity, and topography of fold-and-thrust belts (Figures 4, 6, 8, and 9a). With regard to the structure, zone A highlights a roughly north-south to northeast-southwest, en echelon

AGU Tectonics 10.1002/2017TC004475

Table 1. North to South Miocene Through Pleistocene Chronostratigraphic Correlation Used in the Geological Map [From *Shea et al.*, 2003]

		Shelf	Mesozoic Shelf Break		Upper Slope	
	This Map	Nantou / Yunlin	Chiayi / Tainan		Tainan	Kaohsiung
Pli - Ple	Toukoshan CC.[a]		Liushuang Fm. Erchungchi Fm. Kanhsialiao Fm.		Chiting Fm.	Linkou CC. Tashe Fm. (with limestone)
	Toukoshan SS.[a]			Yuching Sh.[a]		
	Cholan Fm.[a]		Liuchungchi Fm. Yunshuichi Fm.	Peiliao Sh. Chutouchi Fm.	Gutingkeng Fm. (with limestone)	
Mio	Kueichulin Fm.	Tawo SS Shihliufeng Sh. Kuantaoshan SS	Niaotsui Fm. Chunglun Fm.	Maopu Sh. Ailiaochiao Fm. Yenshuikeng Sh. Tangenshan SS.	Wushan Fm.	Nanshihlun SS Kaitzuliao Sh. Wushan Fm.
	Nanchuang Fm.			Changchihkeng Fm. Hunghuatze Fm. Sanmin Sh.		
	Nankang Fm.	Fulungyuan Fm. Hourdongkeng Fm. Shihmentsun Fm.	Shenkeng SS Changhukeng Sh. Shihmen Fm.			
	Takeng Fm.		Tanliaoti Sh. Shihszeku Fm.			

[a]CC = conglomerate, SS = sandstone, Sh. = shale, FM. = formation.

change in the strike of thrusts that culminates with approximately 10 km westward shift of the tip line of the Changhua thrust along the dextral strike-slip Meishan fault (Figure 4). The Meishan fault is thought to link westward under the Coastal Plain with an extensional fault system that is also found offshore, along the upper part of the necking zone [e.g., *Lin et al.*, 2003; *Yang et al.*, 2016]. Immediately south of zone A, the Changhua (ChT) and Chelungpu (CT) thrusts in the western part of the fold-and-thrust belt merge into a gently east dipping basal thrust that is much shallower than to the north (compare ChT and CT in Figures 5a and 5b). Concomitant with the shallowing of the basal thrust, there is a decrease in the thickness of the Pliocene to Recent synorogenic sediments of about 5 km, and its base is uplifted by approximately 7 km in the Chelungpu thrust sheet. East of the Shuangtung thrust (ST in Figure 5b), the basal thrust is interpreted to ramp down section, and the hanging wall structure is that of an approximately 20 km wide anticlinorium. This anticlinorium includes a thicker Miocene sequence than is to the north of zone A. The southward appearance of the middle to late Miocene Nanchuang Fm at zone A (Figure 4) occurs along the northern margin of the Tainan Basin. In structural cross sections [e.g., *Suppe*, 1986; *Rodriguez-Roa and Wiltschko*, 2010; *Yang et al.*, 2007, 2016; *Alvarez-Marron et al.*, 2014], its appearance in the fold-and-thrust belt is interpreted to take place along a reactivated middle Miocene age extensional fault that coincides with the Chelungpu thrust (also known as the Tachienshan thrust).

Through zone A, the upper crustal Vp contours have a NE strike (note in particular the trace of 5.2 km/s contour in Figure 6) that parallels the surface structural grain (Figure 4) and which continues with higher Vp values through the Alishan Ranges (AR in Figure 6), at the rear of the fold-and-thrust belt. We interpret the shallowing of the 5.2 km/s isovelocity contour across the Shuangtung thrust in the Alishan Ranges to indicate the presence of basement rocks that are involved in this part of the fold-and-thrust belt (Figures 5b and 7b) [see *Alvarez-Marron et al.*, 2014]. Zone A also marks an abrupt north to south increase in the amount of upper crustal seismicity (Figures 8a and 8b). South of zone A, seismicity is widespread in the upper 10 km across the Western Foothills and extends up to the coastline in the Coastal Plain. Events at 20 km depth are scattered, both to the north and south of zone A, while at 30 km depth seismicity occurs dominantly to the north. Beneath the Alishan Ranges, there is a good correlation between seismicity and the Shuilikeng fault (Figure 7b), although to the west seismicity clusters near the basement-cover interface, well below the interpreted location of the basal thrust. Finally, zone A marks a significant north-south increase in the topography of the fold-and-thrust belt, especially in the Western Foothills but also in the Hsuehshan Range, to the south of the Puli Basin (Figure 9a). Across zone A, the topography of the Western Foothills rises from just above sea level to form the northwest facing slope of the Alishan Ranges, which, at over 2400 m high, has the highest elevation in the Western Foothills of south central Taiwan.

Farther south, on the area that correlates with the necking zone (Figure 4), zones B and C both mark northeast striking, en echelon changes in the orientations of thrusts and curvature of fold axial traces as they take on a northeast-southwest strike. The thrust front is also interpreted to turn northeast-southwest and then continue southwestward into the offshore where it becomes the deformation front of the marine accretionary

AGU Tectonics 10.1002/2017TC004475

prism that is climbing up the slope [e.g., *Shyu et al.*, 2005; *Lin et al.*, 2008]. From zone B southward, the fold-and-thrust belt widens into an imbricate thrust system that comprises wide synclines and narrow anticlines in its western part (Figures 4 and 5c). The synclines in the Chelungpu and Chutochi thrust sheets terminate northward at zone B, from where they plunge gently southward, and Miocene and younger sediments thicken. Eastward, across the Chishan thrust (CiT in Figure 5c), the broad anticlinorium of the Alishan Ranges narrows to less than half its width before terminating southward in a syncline that plunges beneath the alluvial sediments of the Pingtung Plain (Figure 4). South of zone C, which coincides with the on-land prolongation of the present shelf slope break, thrusts are almost entirely buried by the synorogenic sediments, and an active thrust top basin (the Pingtung Basin of *Chiang et al.* [2004]) is forming in the hanging wall of the Chishan thrust. The basal thrust is interpreted to comprise a series of narrow ramps and wide flats as it cuts gently down through the sedimentary section toward the east where it ramps steeply into the basement.

Zones B and C are located on the northern and southern flanks, respectively, of a roughly northeast striking *P* wave velocity high (>5.2 km/s) that extends northeastward from beneath the Coastal Plain through to the velocity high beneath the Alishan Ranges (Figure 6). We interpret this velocity high to be caused by basement rocks, and herein call it the Tainan Basement High (TBH in Figure 6). South of zone C, a pronounced velocity low suggests a deepening of the basement rocks and a concomitant increase in the thickness of the slope and foreland basin sediments. Along section C-C′, the basement-cover interface ($Vp \geq 5.2$ km/s) dips gently eastward below the basal thrust (Figures 5c and 7c). There is widespread but scattered seismicity between zones B and C that roughly coincides with the Tainan Basement High (Figure 8). In the upper 10 km there is a southward decrease in seismicity across zone C in the western part of the fold-and-thrust belt, although at 20 km and 30 km depth there are events scattered throughout the southwest. The absence of any clear clustering of events makes it difficult to interpret the seismicity in terms of the structure of the fold-and-thrust belt in this area (Figure 7c). There is a very marked change in topography across zone B, from the widespread, high elevations of the Alishan Ranges to several roughly southwest-northeast oriented ridges that end southwestward (Figure 9a). At both zones B and C, these ridges undergo sharp, sigmoidal changes in strike that offset them up to several kilometers toward the west (e.g., Figures 9b and 9c). The ridges follow the trace of related thrusts and confine a set of south and southwest draining river basins. South of zone C, the topography is very subdued and only a few hills reach elevations of up to several tens of meters. In a large part of this area, the fold-and-thrust belt is buried by around 5000 m of Pliocene to Holocene sediments [see *Mouthereau et al.*, 2002; *Chiang et al.*, 2004].

4. Discussion

4.1. Along-Strike Changes Related to the Margin Structure

The necking zone of the Eurasian continental margin offshore southwestern Taiwan comprises an east northeast trending extensional fault system [*Lee et al.*, 1993; *Lin et al.*, 2003; *Lin et al.*, 2005; *Ding et al.*, 2008; *Shi et al.*, 2008; *Tang and Zheng*, 2010; *Yang et al.*, 1991, 2016; *Yeh et al.*, 2012; *McIntosh et al.*, 2014] that can be traced from the margin in the Taiwan Strait across the Coastal Plain [*Chang*, 1963, 1964; *Lin et al.*, 2003; *Yang et al.*, 2014] and into the fold-and-thrust belt where some of its faults are being reactivated [*Suppe*, 1986; *Mouthereau et al.*, 2001, 2002; *Mouthereau and Lacombe*, 2006; *Yang et al.*, 2007, 2016; *Rodriguez-Roa and Wiltschko*, 2010; *Alvarez-Marron et al.*, 2014; *Camanni et al.*, 2016]. In particular, the fault system along the upper part of the necking zone, the Yichu (or A), Meishan, and B faults (Figures 1 and 4), which also comprise the northern bounding faults of the Tainan Basin [*Yang et al.*, 1991; *Lee et al.*, 1993; *Lin et al.*, 2003], are of particular importance. The entire necking zone has regional-scale basement highs and lows (i.e., the Northern Depression, Central Uplift, and Southern Depression [*Lin et al.*, 2003] or the failed rift of *Yeh et al.* [2012] and *McIntosh et al.* [2014]) (Figure 2) that can be traced into the Coastal Plain (Figure 1) and, we suggest, into the fold-and-thrust belt where the Tainan Basement High correlates with the Central Uplift of the Tainan Basin [cf. *Lin et al.*, 2003; *Li et al.*, 2007; *Ding et al.*, 2008]. These basement highs and lows result in important changes in thickness of the Miocene and Pleistocene sediments [e.g., *Hsiao*, 1970; *Shaw*, 1996; *Yang et al.*, 2014]. The changes in sediment thickness from one thrust sheet to another has led to the interpretation of extensional fault reactivation in the fold-and-thrust [e.g., *Suppe*, 1986; *Rodriguez-Roa and Wiltschko*, 2010; *Yang et al.*, 2007, 2016; *Alvarez-Marron et al.*, 2014]. Furthermore, several east northeast striking faults have been historically active in the Coastal Plain area, with the 1906 Meishan and the 1946 Hsinhua earthquakes causing dextral oblique-slip surface ruptures [*Bonilla*, 1977; *Shyu et al.*, 2016]. We suggest, therefore, that

AGU Tectonics 10.1002/2017TC004475

there is ample evidence that regional-scale east northeast striking faults that have been mapped on the necking zone of the Eurasian continental margin can be traced into the fold-and-thrust belt in southwest Taiwan where they are being reactivated, supporting our hypothesis that a number of these are causing important along-strike changes in structural architecture, seismicity, and topography of the fold-and-thrust belt in this area.

The most important along-strike change in the south central Taiwan fold-and-thrust belt takes place at zone A, which is the on-land prolongation of the upper part of the necking zone (Figures 4, 6, 8, and 9). Zone A forms the southern flank of Peikang Basement High, which has been widely recognized as an area of significant change in the structure, fault kinematics, and seismicity of the thrust belt [e.g., *Lu et al.*, 1998; *Deffontaines et al.*, 1997; *Lacombe et al.*, 1999; *Mouthereau et al.*, 2002; *Cheng et al.*, 2003; *Mouthereau and Lacombe*, 2006; *Wu et al.*, 2008, 2010; *Byrne et al.*, 2011; *Alvarez-Marron et al.*, 2014]. It has been suggested that these along-strike changes are largely due to buttressing [*Hayward and Graham*, 1989] of the thrust system by the basement high [e.g., *Lu et al.*, 1998; *Lacombe et al.*, 1999]. *Lu et al.* [1998] and *Lacombe et al.* [1999] also suggested that this basement high partially controls the tectonic escape that they interpret to take place in southwestern Taiwan. We concur with the previous authors that buttressing across the upper part of the necking zone appears to be an important deformation process. This is shown by the intensification of internal folding, back thrusting, and basement involvement in the immediate hanging wall of the Shuangtung thrust (Figure 5b). There is a significant increase in seismicity associated with the on-land projection of the upper part of the necking zone (Figure 8). Importantly, in this area, focal mechanism determinations by *Chang et al.* [2007], *Hsu et al.* [2010], *Wu et al.* [2010], *Chao et al.* [2011], and *Yang et al.* [2016] have shown that the dominant fault type to the west of the Chelungpu thrust is dextral strike-slip with lesser oblique thrusting; both of which have one roughly east northeast oriented nodal plane. To the east, these authors show a mixture of dextral strike-slip and oblique thrusting (with one nodal plane striking roughly east northeast) fault types. Likewise, modeling of GPS data [*Ching et al.*, 2011a] indicates that the deformation style in zone A is characterized by east northeast oriented, dextral strike-slip faulting. The dominance of east northeast oriented strike-slip faulting at zone A suggests a causal relationship with faults of this orientation mapped in the subsurface in the upper part of the necking zone [e.g., *Chow et al.*, 1988; *Lin et al.*, 2003; *Yang et al.*, 2014]. We suggest, therefore, that the along-strike change in structural architecture that takes place at zone A, together with the change in seismicity, are indicative of an east northeast striking lateral structure [the Choshui lateral structure of *Alvarez-Marron et al.* [2014]] that has an important component of dextral strike-slip movement. This lateral structure is forming by the reactivation of preexisting Miocene basin-bounding faults along the upper part of the necking zone, thereby accounting for the appearance and rapid increase in thickness of the middle Miocene Nanchuang Fm. In this interpretation, the abrupt southeastward increase in topography across zone A comprises the surface expression of the north dipping culmination wall that is forming above the Choshui lateral structure, with the maximum elevations reached in the basement-involved thrust sheets. While there are a number of factors that can influence topography [e.g., *Willet*, 1999; *Molnar*, 2009; *Champagnac et al.*, 2012], in south central Taiwan we agree with *Mouthereau et al.* [2002] that there appears to be a causal link between high elevations and the involvement of basement in the thrusting.

Southward, zones B and C illuminate two areas of along-strike change that are developing on the necking zone of the margin as it enters into the fold-and-thrust belt. These changes are not as pronounced as those at the upper part of the necking zone, but they are nevertheless significant features. There is an important change in the structural architecture across zone B, from the broad, basement-cored anticlinorium of the Alishan Ranges to the open synclines above a nearly horizontal basal thrust located in the Miocene and younger sediments (compare Figures 5b and 5c). En echelon, sigmoidal changes in the strike of fold axial traces, the surface trace of thrusts (Figure 4), and of topographic ridges (Figures 9b and 9c) at zones B and C all combine to suggest that these are being offset dextrally by east northeast oriented strike-slip faults. Note that in their modeled tectonic blocks *Ching et al.* [2011a] also identify two east northeast striking, dextral strike faults that roughly coincide with the locations of zones A and B. Sigmoidal offsets of structures and topography in fold-and-thrust belts are generally attributed either to reactivation of footwall basement faults or as transfer zones (tear faults) in the hanging wall that are caused by mechanical differences along the basal thrust [e.g., *Albers*, 1967; *Mugnier et al.*, 1999; *Ruh et al.*, 2014; *Koyi et al.*, 2016]. In southwestern Taiwan, the homogeneity of the hanging wall structural architecture from zone B southward seems to militate against strong mechanical differences along the basal thrust. Finally, the numerous earthquakes in the area of the

AGU Tectonics 10.1002/2017TC004475

Tainan Basement High that have dextral strike-slip focal mechanisms with one roughly east northeast to northeast striking nodal plane [e.g., *Hsu et al.*, 2010; *Wu et al.*, 2010], together with the dextral east northeast striking surface rupture of the 1946 Hsinhua earthquake (Figure 4) [*Bonilla*, 1977], provide further support for the interpretation that the en echelon sigmoidal features observed at zones A and B are related to the dextral strike-slip reactivation of east northeast striking basement faults along the flanks of the Tainan Basement High (Figure 6).

Our proposal for east northeast striking along-strike changes in the south central Taiwan fold-and-thrust belt that are caused by the reactivation of margin structure with this orientation differs from that of other authors. For example, using various types of data, including structure, seismicity, and topography, *Deffontaines et al.* [1997], *Lacombe et al.* [1999], *Mouthereau et al.* [1999, 2002], and *Mouthereau and Lacombe* [2006] have suggested that there are a number of west northwest to northwest striking transfer zones in the western Taiwan fold-and-thrust belt. Of these, the Fengshan, Chishan, and Chiayi transfer zones are within our geological map area. Our mapping and analyses of the seismicity and topography data show no concrete evidence for the Fengshan and Chiayi transfer zones. In outcrop, the area of the Chishan transfer zone is a narrow, roughly west northwest striking fault (the Zuojhen fault (Figure 4)) developed predominantly in mudstone [see *Deffontaines et al.*, 1997]. Interpreting the regional structure of this area is complicated by the thick, monotonous mudstone lithology, several important thrusts, and what appears to be very little displacement across the Zuojhen fault. Nevertheless, more fieldwork is required to clarify the nature and importance of this fault. *Deffontaines et al.* [1997] point out that there is very little evidence for basement faults with a WNW strike, and they therefore suggest that the transfer zones are not caused by reactivation of basement faults but are newly formed in the hanging wall of the fold-and-thrust belt. *Lacombe et al.* [1999], *Mouthereau et al.* [1999, 2002], and *Mouthereau and Lacombe* [2006] do, however, suggest that basement fault reactivation is responsible for these transfer zones. In fact, *Ching et al.* [2011b] argue, on the basis of coseismic GPS displacements for sinistral displacement along the Chishan transfer fault during the 2010 Jiashian earthquake. Likewise, *Huang et al.* [2016] suggest that coseismic displacement during the 2016 Meinong earthquake took place, in part, along a NW striking fault surface, but they make no mention of the Chishan structure. Although these faults may exist in the subsurface, we do not see any evidence for them in our data. Finally, north-south oriented extensional transfer faults have been interpreted to occur on the necking zone [*Yang et al.*, 1991], but these are at a significant angle to the Chishan and Chiayi transfer zones and roughly parallel to the Fengshan transfer.

4.2. Changes in Structure, Seismicity, and Topography From the Shelf to the Necking Zone

We furthermore suggest that the data supports the corollary to our proposed hypothesis, since it is possible to observe differences in structure, seismicity, and topography of the fold-and-thrust belt depending on whether it is the shelf or necking zone areas of the margin that are involved in the deformation. There is, for example, a very different style of basement involvement between the shelf and the necking zone. On the shelf, the roughly northeast oriented Hsuehshan Trough is inverting along almost north-south striking basin-bounding faults that penetrate deep into the crust [e.g., *Wu et al.*, 2004; *Camanni et al.*, 2014b; *Kuo-Chen et al.*, 2015], exposing deep levels of the synrift sediments that, along the eastern part of the Hsuehshan Range, have been metamorphosed to lower greenschist facies [e.g., *Clark et al.*, 1993; *Beyssac et al.*, 2007; *Simoes et al.*, 2012] and have a penetrative pressure solution cleavage [e.g., *Clark et al.*, 1993; *Tillman and Byrne*, 1995; *Fisher et al.*, 2002; *Brown et al.*, 2012]. The uplift of relatively high Vp material (Figure 7a) indicates that the Mesozoic basement rocks are involved in the thrusting. On the shelf part of the study area, seismicity is largely concentrated within the inverting Hsuehshan Trough, where it forms well-defined clusters along the basin-bounding faults (Figures 7a and 8) [e.g., *Wu et al.*, 2004; *Camanni et al.*, 2014a, 2014b; *Kuo-Chen et al.*, 2015]. We suggest that the roughly north-south oriented basin faults of the Hsuehshan Trough are ideally oriented for reactivation and the incorporation of basement rocks into the thrusting. Finally, the Hsuehshan Range has the highest elevations in the south central Taiwan fold-and-thrust belt (Figure 9), providing further evidence for the causal link between basement involvement in the thrusting and the development of high topography alluded to in section 3.1.

The upper part of the necking zone comprises a transitional area with complex structure that includes basement involvement in the thrusting, reactivation of east northeast oriented faults, widespread seismicity, and the formation of high topography. In contrast, farther down the necking zone, the basement appears to be

AGU Tectonics 10.1002/2017TC004475

deforming without being incorporated into the thrust sheets. That the basement is deforming is attested to by the widespread, deep seismicity that is taking place across most of the necking zone. Seismicity is, however, dispersed and does not cluster in a way that highlights any particular fault, as it does in the Hsuehshan Range. This could imply that the basement in this area is highly fractured, with fractures optimally oriented for reactivation. It may also indicate that the seismicity data window we present (20 years) is too short to illuminate the major linked fault system that is forming the foreland thrust-and-fold belt. A further indication that basement rocks are not involved in the thrusting is the gentle eastward dip of 5.2 km/s isovelocity surface, which contrasts with what happens in the Hsuehshan Range where there is a marked shallowing of higher velocities. The Zagros [*Koyi et al.*, 2016] and the Keping Shan [*Turner et al.*, 2010] are two well-documented examples in which, as along the necking zone in southwestern Taiwan, basement faults that are at a high angle to the structural grain of a thrust belt are either bending structures into a sigmoidal geometry (Zagros) or even cut completely through the thrust belt (Kepin Shan) but are not involved in the thrusting. We suggest that, in southwest Taiwan, the east northeast striking extensional faults on the necking zone of the margin [i.e., *Yang et al.*, 2014] are, like those in Zagros and Kepin Shan, ideally oriented for reactivation as strike-slip faults and that they are beginning to affect the fold-and-thrust belt, causing the dextral, sigmoidal offset of thrusts, fold axes, and topography (Figures 4 and 9). Without basement involvement in the thrusting, topography on the necking zone is subdued, with no change in elevation associated with the basement faults.

5. Conclusions

Regional-scale east northeast striking faults that have been mapped on the necking zone of the Eurasian continental margin in the Taiwan Strait can be traced into the fold-and-thrust belt in southwest Taiwan where they are being reactivated, supporting our hypothesis that a number of these are causing important along-strike changes in structural architecture, seismicity, and topography of the fold-and-thrust belt in this area. The most important along-strike change takes place in the upper part of the necking zone where there is an abrupt north-south change in structure, an increase in the amount of seismicity, and an increase in topography. These changes are interpreted to be caused by the east northeast striking, dextral strike-slip Choshui lateral structure that is forming by the reactivation of preexisting faults along the upper part of the necking zone. The abrupt southeastward increase in topography across the upper part of the necking zone is the surface expression of the north dipping culmination wall of the Choshui lateral structure. Maximum elevations in this area are reached in the basement-involved thrust sheets, suggesting a causal link between basement involvement in the thrusting and high topography. Farther south, on the necking zone proper, along-strike changes are marked by en echelon, sigmoidal offsets in the strike of fold axial traces, the surface trace of thrusts, and of topographic ridges. The widespread, deep seismicity that is taking place across most of the necking zone provides evidence that the basement is involved in the deformation, but it is difficult to correlate events with individual faults. Nevertheless, basement appears to be deforming without being incorporated into the thrust sheets, and the sigmoidal offset of structures and topography is suggestive of the dextral strike-slip reactivation of east northeast striking basement faults.

It is also possible to observe differences in structure, seismicity, and topography of the fold-and-thrust belt depending on whether it is the shelf or necking zone areas of the margin that are involved in the deformation. On the shelf, the roughly northeast oriented Hsuehshan Trough is inverting along almost north-south striking basin-bounding faults that penetrate into the middle crust and have well-clustered, deep seismicity. The relationship between basement involvement in the thrusting and high topography is particularly apparent in the Hsuehshan Range. On the necking zone, east northeast oriented faults are at a high angle to the thrusting and are being reactivated as dextral strike-slip faults that are causing en echelon, sigmoidal offset of structures and topography. Seismicity is scattered, and there is no basement involvement in the thrusting.

Acknowledgments
D.B., J.A-M., and C.B. acknowledge funding provided by the Spanish Ministerio de Economia y Competividad grant CGL2013-43877-P. H.K-C. acknowledges funding by MOST 104-2628-M-008-005-MY3. We thank two anonymous reviewers for their comments. The geophysical data are available at http://140.115.22.221/download/data.

References

Albers, J. P. (1967), Belt of sigmoidal bending and right-lateral faulting in the western Great Basin, *Geol. Soc. Am. Bull.*, *78*, 143–156.
Alvarez-Marron, J., D. Brown, G. Camanni, Y.-M. Wu, and H. Kuo-Chen (2014), Structural complexities in a foreland thrust belt inherited from the shelf-slope transition: Insights from the Alishan area of Taiwan, *Tectonics*, *33*, 1322–1339, doi:10.1002/2014TC003584.
Arora, B. R., V. K. Gahalaut, and N. Kumar (2012), Structural control on along-strike variation in the seismicity of the northwest Himalaya, *J. Asian Earth Sci.*, *57*, 15–24, doi:10.1002/2014TC003584.

AGU Tectonics 10.1002/2017TC004475

Beyssac, O., M. Simoes, J. P. Avouac, K. A. Farley, Y.-G. Chen, Y.-C Chan, and B. Goffé (2007), Late Cenozoic metamorphic evolution and exhumation of Taiwan, *Tectonics*, *26*, TC6001, doi:10.1029/2006TC002064.

Blanc, E. J.-P., M.B. Allen, S. Inger, and H. Hassani (2003), Structural styles in the Zagros simple folded zone, Iran, *J. Geol. Soc., 160*, 401–412.

Bonilla, M. G. (1977), Summary of Quaternary faulting and elevation changes in Taiwan, *Mem. Geol. Soc. China*, *2*, 43–55.

Boutoux, A., N. Bellahsen, O. Lacombe, A. Verlaguet, and F. Mouthereau (2014), Inversion of pre-orogenic extensional basins in the external western Alps: Structure, microstructures and restoration, *J. Struct. Geol., 60*, 13–29.

Brown, D., J. Alvarez-Marron, A. Perez-Estaun, V. Puchkov, and C. Ayala (1999), Basement influence on foreland thrust and fold belt development: An example from the southern Urals, *Tectonophysics*, *308*, 459–472.

Brown, D., J. Alvarez-Marron, M. Schimmel, Y.-M. Wu, and G. Camanni (2012), The structure and kinematics of the central Taiwan mountain belt derived from geological and seismicity data, *Tectonics*, *31*, TC5013, doi:10.1029/2012TC003156.

Butler, R. W. H., E. Tavarnelli, and M. Grasso (2006), Structural inheritance in mountain belts: An Alpine–Apennine perspective, *J. Struct. Geol., 28*, 1893–1908.

Byrne, T., Y.-C. Chan, R.-J. Rau, C.-Y. Lu, Y.-H. Lee, and Y.-J. Wang (2011), The arc–continent collision in Taiwan, in *Arc-Continent Collision, Frontiers in Earth Sciences Series*, edited by D. Brown and P. D. Ryan, pp., 213–245, Springer, Berlin.

Calamita, F., S. Satolli, V. Scisciani, P. Esestime, and P. Pace (2011), Contrasting styles of fault reactivation in curved orogenic belts: Examples from the central Apennines (Italy), *Geol. Soc. Am. Bull., 123*, 1097–1111.

Camanni, G., C.-H. Chen, D. Brown, J. Alvarez-Marron, Y.-M. Wu, H.-A. Chen, H.-H. Huang, H.-T. Chu, M.-M. Chen, and C.-H. Chang (2014a), Basin inversion in central Taiwan and its importance for seismic hazard, *Geology*, *42*, 147–150.

Camanni, G., D. Brown, J. Alvarez-Marron, Y.-M. Wu, and H.-A. Chen (2014b), The Shuilikeng fault in central Taiwan mountain belt, *J. Geol. Soc., 171*, 117–130.

Camanni, G., J. Alvarez-Marron, D. Brown, C. Ayala, Y.-M. Wu, and H.-H. Hsieh (2016), The deep structure of south-central Taiwan illuminated by seismic tomography and earthquake hypocentre data, *Tectonophysics*, *679*, 235–245.

Castelltort, S., S. Nagel, F. Moutherreau, A. Lin, A. Wetzel, B. Kaus, S. Willet, S.-P. Chiang, and W.-Y. Chiu (2010), Sedimentology of early Pliocene sandstones in the southwestern Taiwan foreland: Implications for basin physiography in the early stages of collision, *J. Asian Earth Sci., 40*, 52–71.

Champagnac, J.-D., P. Molnar, C. Sue, and F. Herman (2012), Tectonics, climate, and mountain topography, *J. Geophys. Res., 117*, B02403, doi:10.1029/2011JB008348.

Chang, C.-H., Y.-M. Wu, L. Zhao, and F. T. Wu (2007), Aftershocks of the 1999 Chi-Chi, Taiwan, earthquake: The first hour, *Bull. Seismol. Soc. Am., 97*, 1245–1258.

Chang, L. S. (1976), The Lushanian stage in the central range of Taiwan and its fauna, in *Progress in Micropaleontology, The Am. Museum of Natural History*, edited by Y. Takayanagi, and T. Saito, pp. 27–35, Micropaleontology Press, New York.

Chang, S. L. (1963), Regional stratigraphic study of Pliestocene and upper Pliocene formations in Chiayi and Hsinying area, Taiwan, *Pet. Geol. Taiwan*, *2*, 65–86.

Chang, S. L. (1964), Regional stratigraphic study of lower Pliocene and upper Miocene formations in Chiayi and Hsinying area, Taiwan, *Pet. Geol. Taiwan*, *3*, 1–20.

Chao, W.-A., L. Zhao, and Y.-M. Wu (2011), Centroid fault-plane inversion in three-dimensional velocity structure using strong-motion records, *Bull. Seismol. Soc. Am., 101*, 1330–1340.

Chatzaras, V., P. Xypolias, S. Kokkalas, and I. Koukouvelas (2013), Tectonic evolution of a crustal-scale oblique ramp, Hellenides thrust belt, Greece, *J. Struct. Geol., 57*, 16–37.

Chen, C.-H., et al. (2000), Geological map of Taiwan, scale 1:500,000, Central Geological Survey, Taipei.

Chen, A. T., and Y.-L. Yang (1996), Lack of compressional overprint on the extensional structure in the offshore Tainan and the tectonic implications, *Terr. Atmos. Ocean. Sci., 7*, 505–522.

Chen, W.-S., K. D. Ridgway, C.-S. Horng, Y.-G. Chen, K.-S. Shea, and M.-G. Yeh (2001), Stratigraphic architecture, magnetostratigraphy, and incised-valley systems of the Pliocene-Pliestocene collisional marine foreland basin of Taiwan, *Geol. Soc. Am. Bull., 113*, 1249–1271.

Chen, M.-M., N.-T. Yu, H.-T. Chu, K.-S. Shea, and Y.-C. Hsieh (2009), Larger foraminifera in the so-called "Meichi sandstone" of Wujie area, southern Hsuehshan range, *Central Geol. Surv. Spec. Pub., 22*, 227–242.

Chen, K.-X., H. Kuo-Chen, D. Brown, Q. Li, Z. Ye, W.-T. Liang, C.-Y. Wang, and H. Yao (2016), Three-dimensional ambient noise tomography across the Taiwan Strait: The structure of a magma-poor rifted margin, *Tectonics*, *35*, 1782–1792, doi:10.1002/2015TC004097.

Cheng, W.-B., H.-C. Huang, C. Wang, M.-S. Wu, and T.-H. Hsiuan (2003), Velocity structure, seismicity, and fault structure in the Peikang High are of western Taiwan, *Terr. Atmos. Ocean. Sci., 14*, 63–83.

Chiang, C.-S., H.-S. Yu, and Y.-W. Chou (2004), Characteristics of the wedge-top depozone of the southern Taiwan foreland basin system, *Basin Res., 16*, 65–78.

Ching, K.-E., R.-J. Rau, K. M. Johnson, J.-C. Lee, and J.-C. Hu (2011a), Present-day kinematics of active mountain building in Taiwan from GPS observations during 1995–2005, *J. Geophys. Res., 116*, B09405, doi:10.1029/2010JB008058.

Ching, K.-E., K. M. Johnson, R.-J. Rau, R. Y. Chuang, L.-C. Kuo, and P.-L. Leu (2011b), Inferred fault geometry and slip distribution of the 2010 Jiashian, Taiwan, earthquake is consistent with a thick-skinned deformation model, *Earth Planet. Sci. Lett., 301*, 78–86.

Chiu, H.-T. (1975), Miocene stratigraphy and its relation to the Palaeogene rocks in west-central Taiwan, *Pet. Geol. Taiwan*, *12*, 51–80.

Chow, J., K.-M. Yang, and H.-M. Chen (1988), Seismic interpretation of the subsurface structures in the Yichu-Chiali area, southern Taiwan, *Pet. Geol. Taiwan*, *24*, 60–95.

Christensen, N. I. (1989), Pore pressure, seismic velocities, and crustal structure, in *Geophysical Framework of the Continental United States*, vol. 172, edited by L. C. Pakiser and W. D. Mooney, pp. 783–798, Geol. Soc. Am. Mem., Boulder, Colo.

Christensen, N. I., and D. Stanley (2003), Seismic velocities and densities of rocks, *Inter. Handbook Earthquake Eng. Seis., 81*, 1587–1593.

Chuang, R. Y., K. M. Johnson, Y.-M. Wu, K.-E. Ching, and L.-C. Kuo (2013), A midcrustal ramp-fault structure beneath the Taiwan tectonic wedge illuminated by the 2013 Nantou earthquake series, *Geophys. Res. Lett., 40*, 5080–5084, doi:10.1002/grl.51005.

Clark, M. B., D. M. Fisher, C.-Y. Lu, and C.-H. Chen (1993), Kinematic analyses of the Hsüehshan range, Taiwan: A large-scale pop-up structure, *Tectonics*, *12*, 205–217.

Covey, M. (1986), The evolution of foreland basins to steady state: Evidence from the western Taiwan foreland basin, in *Foreland Basins, Spec. Pub. 8. Int. Ass. Sed.*, edited by P. A. Allen and P. Homewood, pp. 77–90, Blackwell, Oxford, U. K.

Cukur, D., S. Horozal, D. C. Kim, and H. C. Han (2011), Seismic stratigraphy and structural analysis of the northern East China Sea Shelf Basin interpreted from multi-channel seismic reflection data and cross-section restoration, *Mar. Pet. Geol., 28*, 1003–1022.

Dahlstrom, C. D. A. (1969), Balanced cross sections, *Can. J. Earth Sci., 6*, 743–757.

Deffontaines, B., O. Lacombe, J. Angelier, H.-T. Chu, F. Mouthereau, C.-T. Lee, J. Deramond, J.-F. Lee, M.-S. Yu, and P.-M. Liew (1997), Quaternary transfer faulting in the Taiwan Foothills: Evidence from a multisource approach, *Tectonophysics, 274*, 61–82.
Deng, J.-M., T.-K. Wang, B.-J. Yang, C.-S. Lee, C.-S. Liu, and S.-C. Chen (2012), Crustal velocity structure off SW Taiwan in the northernmost South China Sea imaged from TAIGER OBS and MCS data, *Mar. Geophys. Res., 33*, 327–349.
Ding, W.-W., J.-B. Li, M.-B. Li, X.-L. Qiu, Y.-X. Fang, and Y. Tang (2008), A Cenozoic tectono-sedimentary model of the Tainan Basin, the South China Sea: Evidence from multi-channel seismic profile, *J. Zhejiang Uni. Sci., 9*, 702–713.
Duncan, C., J. Masek, and E. Fielding (2003), How steep are the Himalaya? Characteristics and implications of along-strike topographic variations, *Geology, 31*, 75–78.
Ernst, W. G., (1983), Mineral paragenesis in metamorphic rocks exposed along Tailuko gorge, Central Mountain range, Taiwan, *J. Metamorph. Geol., 1*, 305–329.
Fisher, D. M., C.-Y. Lu, and H.-T. Chu (2002), Taiwan slate belt: Insights into the ductile interior of an arc-continent collision, in *Geology and Geophysics of an Arc-Continent Collision, Taiwan*, vol. 358, edited by T. B. Byrne and C.-S. Liu, pp. 93–106, Geol. Soc. Am. Spec. Paper, Boulder, Colo.
Godin, L., and L. B. Harris (2014), Tracking basement cross-strike discontinuities in the Indian crust beneath the Himalayan orogeny using gravity data—Relationship to upper crustal faults, *Geophys. J. Int., 198*, 198–215.
Hall, R. (1996), Reconstructing Cenozoic SE Asia, in *Tectonic Evolution of Southeast Asia*, vol. 106, edited by R. Hall and D. Blundell, pp. 153–184, Geol. Soc. London Spec. Pub.
Hall, R. (2001), Cenozoic reconstructions of SE Asia and the SW Pacific: Changing patterns of land and sea, in *Faunal and Floral Migrations and Evolution in SE Asia-Australasia*, edited by I. Metcalfe, et al., pp. 35–56, Swets and Zeitlinger, Lisse.
Hayward, A. B., and R. H. Graham (1989), Some geometrical characteristics of inversion, in *Inversion Tectonics*, vol. 44, edited by M. A. Cooper and G. D. Willaims, pp. 17–39, Geol. Soc. Spec. Pub.
Ho, C.-S. (1986), A sysnthesis of the geologic evolution of Taiwan, *Tectonophysics, 125*, 1–16.
Ho, C.-S. (1988), *An Introduction to the Geology of Taiwan: Explanatory Text of the Geological Map of Taiwan*, 192 pp., Central Geol. Sur., Taipei.
Hossack, J. R. (1979), The use of balanced cross-sections in the calculation of orogenic contraction: A review, *J. Geol. Soc., 136*, 705–711.
Hsiao, P.-T. (1970), Seismic study of the area between the Coastal Plain and the Foothills, Chiayi, Taiwan, *Pet. Geol. Taiwan, 7*, 47–52.
Hsu, Y.-J., L. Rivera, Y.-M. Wu, C.-H. Chang, and H. Kanamori (2010), Spatial heterogeneity of tectonic stress and friction in the crust: New evidence from earthquake focal mechanisms in Taiwan, *Geophys. J. Int., 182*, 329–342.
Huang, C.-Y., W.-Y. Wu, C.-P. Chang, S. Tsao, P.-B. Yuan, C.-W. Lin, and K.-Y. Xia (1997), Tectonic evolution of accretionary prism in the arc-continent collision terrane of Taiwan, *Tectonophysics, 281*, 31–51.
Huang, C.-Y., P. B. Yuan, and S. J. Tsao (2006), Temporal and spatial records of active arc-continent collision in Taiwan: A synthesis, *Geol. Soc. Am. Bull., 118*, 274–288.
Huang, C.-Y., Y. Yen, Q. H. Zhao, and C.-T. Lin (2012), Cenozoic stratigraphy of Taiwan: Window into rifting, stratigraphy and paleoceanography of South China Sea, *Chin. Sci. Bull., 57*, 3130–3149.
Huang, C.-Y., W.-R. Chi, Y. Yan, K.-M. Yang, P.-M. Liew, M.-S. Wu, J.-C. Wu, and C. Zhang (2013), The first record of Eocene tuff in a Paleogene rift basin near Nantou, Western Foothills, central Taiwan, *J. Asian Earth Sci., 69*, 3–16.
Huang, H.-H., Y.-M. Wu, X. Song, C.-H. Chang, S.-J. Lee, T.-M. Chang, and H.-H. Hsieh (2014), Joint Vp and Vs tomography of Taiwan: Implications for subduction-collision orogeny, *Earth Planet. Sci. Lett., 392*, 177–191.
Huang, M.-M., H. Tung, E.J. Fielding, H.-H. Huang, C. Liang, C. Huang, and J.-C. Hu (2016), Multiple fault slip triggered above the 2016 M_W 6.4 Meinong earthquake in Taiwan, *Geophys. Res. Lett., 43*, 7459–7467, doi:10.1002/2016GL069351.
Hung, J.-H., K.-F. Ma, C.-Y. Wang, H. Ito, W. Lin, and E.-C. Yeh (2009), Subsurface structure, physical properties, fault-zone characteristics and stress state in scientific drill holes of Taiwan Chelungpu Fault Drilling Project, *Tectonophysics, 466*, 307–321.
Jackson, J. A. (1980), Reactivation of basement faults and crustal shortening in orogenic belts, *Nature, 283*, 343–346.
Jahn, B.-M., F. Martineau, J. J. Peucat, and J. Cornichet (1986), Geochronology of the Tananao schist complex, Taiwan, and its regional tectonic significance, *Tectonophysics, 125*, 103–124.
Jahn, B.-M., W.-R. Chi, and T.-F. Yui (1992), A Late Permian formation of Taiwan marbles from Chia-Li well no.1: Pb-Pb isochron and Sr isotopic evidence, and its regional geological significance, *J. Geol. Soc. China, 35*, 193–218.
Johnston, J. E., and N. I. Christensen (1992), Shear wave reflectivity, anisotropies, Poissons ratios, and densities of a southern Appalachian Paleozoic sedimentary sequence, *Tectonophysics, 210*, 1–20.
Johnston, J. E., and N. I. Christensen (1993), Compressional to shear velocity ratios in sedimentary rocks, *Int. J. Rock Mech. Min. Sci. Geomech. Abs., 30*, 751–754.
Kelly, P. G., D. C. P. Peacock, D. J. Sanderson, and A. C. McGurk (1999), Selective reverse-reactivation of normal faults, and deformation around reverse-reactivated faults in the Mesozoic of the Somerset coast, *J. Struct. Geol., 21*, 493–509.
Kim, K.-H., J.-M. Chiu, H. Kao, Q. Liu, and Y.-H. Yeh (2004), A preliminary study of crustal structure in Taiwan region using receiver function analysis, *Geophys. J. Int., 159*, 146–164.
Koyi, H., F. Nilfouroushan, and K. Hessami (2016), Modelling role of basement block rotation and strike-slip faulting on structural pattern in cover units of fold-and-thrust belts, *Geol. Mag., 153*, 827–844.
Kuo-Chen, H., F. T. Wu, and S. W. Roecker (2012), Three-dimensional *P* velocity structures of the lithosphere beneath Taiwan from the analysis of TAIGER and related seismic data sets, *J. Geophys. Res., 117*, B06306, doi:10.1029/2011JB009108.
Kuo-Chen, H., F. T. Wu, W.-L. Chang, C.-Y. Chang, C.-Y. Cheng, and N. Hirata (2015), Is the Lishan fault of Taiwan active?, *Tectonophysics, 661*, 210–214.
Lacombe, O., F. Mouthereau, B. Deffontaines, J. Anglier, H.-T. Chu, and C.-T. Lee (1999) Geometry and Quaternary kinematics of fold-and-thrust units of southwestern Taiwan, *Tectonics, 18*, 1198–1223.
Lan, C.-Y., C.-S. Lee, T.-F. Yui, H.-T. Chu, and B.-M Jahn (2008), The tectono-thermal events of Taiwan and their relationship with SE China, *Terr. Atmos. Ocean. Sci., 19*, 257–278.
Lee, C.-S. (1979), Paleogene rocks of the Yushan-Shuili area, Nantou, central Taiwan, *Mem. Geol. Soc. China, 3*, 237–247.
Lee, T.-Y., C.-H. Tang, J.-S. Ting, and Y.-Y. Hsu (1993), Sequence stratigraphy of the Tainan Basin, offshore southwestern Taiwan, *Pet. Geol. Taiwan, 26*, 119–158.
Lester, R., H. J. A. Van Avendonk, K. McIntosh, L. Lavier, C.-S. Liu, T.-K. Wang, and F. Wu (2014), Rifting and magmatism in the northeastern South China Sea from wide-angle tomography and seismic reflection imaging, *J. Geophys. Res. Solid Earth, 119*, 2305–2323, doi:10.1002/2013JB010639.
Li, C.-F., Z. Zhou, J. Li, H. Hao, and J. Geng (2007), Structures of the northeasternmost South China Sea continental margin and ocean basin: Geophysical constraints and tectonic implications, *Mar. Geophys. Res., 28*, 59–79.

AGU Tectonics 10.1002/2017TC004475

Lin, A. T., and A. Watts (2002), Origin of the west Taiwan Basin by orogenic loading and flexure of a rifted continental margin, *J. Geophys. Res.*, *107*(B9), 2185, doi:10.1029/2001JB000669.
Lin, A., A. Watts, and P. Hesselbo (2003), Cenozoic stratigraphy and subsidence history of the South China Sea margin in the Taiwan region, *Basin Res.*, *15*, 453–478.
Lin, J.-Y., J.-C. Sibuet, and S.-K. Hsu (2005), Distribution of the East China Sea continental shelf basins and depths of magnetic sources, *Earth, Planet. Space*, *57*, 1063–1072.
Lin, A. T., C.-S. Liu, C.-C. Lin, P. Schnurle, G.-Y. Chen, W.-Z. Liao, L. S. Teng, H.-J. Chuang, and M.-S. Wu (2008), Tectonic features associated with the overriding of an accretionary wedge on top of a rifted continental margin: An example from Taiwan, *Mar. Geol.*, *255*, 186–203.
Lo, C.-H., and T. C. Onstott (1995), Rejuvenation of K–Ar systems for minerals in the Taiwan mountain belt, *Earth Planet Sci Lett*, *131*, 71–98.
Lu, C.-Y., F.-S. Jeng, K.-J. Chang, and W. T. Jian (1998), Impact of basement high on the structure and kinematics of the western Taiwan thrust wedge: Insights from sandbox models, *Terr. Atmos. Ocean. Sci.*, *9*, 533–550.
Mavko, G., T. Mukerji, and J. Dvorkin (1998), *The Rock Physics Handbook: Tools for Seismic Analysis in Porous Media*, 329 pp., Cambridge Univ. Press, Cambridge, U. K., and New York.
McIntosh, K., H. Van Avendonk, L. Lavier, W. R. Lester, D. Eakin, F. Wu, C.-S. Liu, and C.-S. Lee (2013), Inversion of a hyper-extended rifted margin in the southern central range of Taiwan, *Geology*, *41*, 871–874.
McIntosh, K., L. Lavier, H. Van Avendonk, R. Lester, D. Eakin, and C.-S. Liu (2014), Crustal structure and inferred rifting processes in the northeast South China Sea, *Mar. Pet. Geol*, *58*, 612–626.
Mohn, G., G. Manatschal, M. Beltrando, E. Masini, and N. Kusznir (2012), Necking of the continental crust in magma-poor rifted margins: Evidence from the fossil Alpine Tethys margins, *Tectonics*, *31*, TC1012, doi:10.1029/2011TC002961.
Molnar, P. (2009), The state of interactions among tectonics, erosion, and climate: A polemic, *GSA Today*, *19*, 44–45.
Mouthereau, F., and O. Lacombe (2006), Inversion of the Paleogene Chinese continental margin and thick-skinned deformation in the western foreland of Taiwan, *J. Struct. Geol.*, *28*, 1977–1993.
Mouthereau, F., O. Lacombe, B. Deffontaines, J. Angelier, H.-T. Chu, and C.-T. Lee (1999), Quaternary transfer faulting and belt front deformation at Pakuashan (western Taiwan), *Tectonics*, *18*, 215–230.
Mouthereau, F., O. Lacombe, B. Deffontaines, J. Angelier, and S. Brusset (2001), Deformation history of the southwestern Taiwan foreland thrust belt: Insights from tectono-sedimentary analyses and balanced cross-sections, *Tectonophysics*, *333*, 293–322.
Mouthereau, F., B. Deffontaines, O. Lacombe, and J. Angelier (2002), Variations along the strike of the Taiwan thrust belt: Basement control on structural style, wedge geometry, and kinematics, in *Geology and Geophysics of an Arc-Continent Collision, Taiwan*, vol. 358, edited by T. B. Byrne and C.-S. Liu, pp. 31–54, Geol. Soc. Am. Spec. Paper, Boulder, Colo.
Mouthereau, F., O. Lacombe, and B. Meyer (2006), The Zagros folded belt (Fars, Iran): Constraints from topography and critical wedge modeling, *Geophys. J. Int.*, *165*, 336–356.
Mugnier, J. L., P. Leturmy, G. Mascle, P. Huyghe, E. Chalaron, G. Vidal, L. Husson, and B. Delcaillau (1999), The Siwaliks of western Nepal I. Geometry and kinematics, *J. Asian Earth Sci.*, *17*, 629–642.
Nagel, S., S. Castelltort, A. Wetzel, S. D. Willett, F. Mouthereau, and A. T. Lin (2013), Sedimentology and foreland basin paleogeography during Taiwan arc continent collision, *J. Asian Earth Sci.*, *62*, 180–204.
Nissen, S. S., D. E. Hayes, P. Buhl, and J. Diebold (1995), Deep penetration seismic soundings across the northern margin of the South China Sea, *J. Geophys. Res.*, *100*, 22,407–22,433.
Perez-Estaun, A., J. Alvarez-Marron, D. Brown, V. Puchkov, Y. Gorozhanina, and V. Baryshev (1997), Along-strike structural variations in the foreland thrust and fold belt of the southern Urals, *Tectonophysics*, *276*, 265–280.
Rodriguez-Roa, F. A., and D. V. Wiltschko (2010), Thrust belt architecture of the central and southern western foothills of Taiwan, in *Hydrocarbons in Contractional Belts*, vol. 348, edited by G. P. Goffey et al., pp. 137–168, Geol. Soc. London, Spec. Pub., Boulder, Colo.
Ruh, J. B., T. Gerya, and J.-P. Burg (2014), 3D effects of strain vs. velocity weakening on deformation patterns in accretionary wedges, *Tectonophysics*, *615-616*, 122–141.
Shaw, C.-L. (1996), Stratigraphic correlation and isopach maps of the western Taiwan Basin, *Terr. Atmos. Ocean. Sci.*, *7*, 333–360.
Shea, K.-S., H.-C. Chang, T.-Y. Huang, H.-C. Ho, W.-H. Lin, C.-W. Lin, and H.-W. Chen (2003), Geological column in Taiwan, Central Geol. Surv. *Taiwan*, Taiwan.
Shi, X., H. Xu, X. Qiu, K. Xia, X. Yang, and Y. Li (2008), Numerical modeling on the relationship between thermal uplift and subsequent rapid subsidence: Discussion on the evolution of the Tainan Basin, *Tectonics*, *27*, TC6003, doi:10.1029/2007TC002163.
Shyu, J. B. H., K. Sieh, Y.-G. Chen, and C.-S. Liu (2005), Neotectonic architecture of Taiwan and its implications for future large earthquakes, *J. Geophys. Res.*, *110*, B08402, doi:10.1029/2004JB003251.
Shyu, J. B. H., Y.-R. Chuang, Y.-L. Chen, Y.-R. Lee, and C.-T. Cheng (2016), A new on-land seismogenic structure source database from the Taiwan earthquake model (TEM) project for seismic hazard analysis of Taiwan, *Terr. Atmos. Ocean. Sci.*, *27*, 311–323.
Simoes, M., O. Beyssac, and Y.-G. Chen (2012), Late Cenozoic metamorphism and mountain building in Taiwan: A review, *J. Asian Earth Sci.*, *46*, 92–119.
Smith, A. D., and C. Lewis (2007), Geochemistry of metabasalts and associated metasedimentary rocks from the Lushan formation of the upthrust slate belt, south-central Taiwan, *Int. Geol. Rev.*, *49*, 1–13.
Stanley, R. S., L. B. Hill, H. C. Chang, and H. N. Hu (1981), A transect through the metamorphic core of the central mountains, southern Taiwan, *Mem. Geol. Soc. China*, *4*, 443–473.
Sung, Q.-C., and Y. Wang (1985), Petrofacies of late Miocene sediments in the Hengchun Peninsula and its tectonic implication, *Proc. Geol. Soc. China*, *28*, 23–44.
Suppe, J. (1986), Reactivated normal faults in the western Taiwan fold-and-thrust belt, *Mem. Geol. Soc. China*, *7*, 187–200.
Tang, Q., and C. Zheng (2010), Seismic velocity structure and improved seismic image of the southern depression of the Tainan Basin from pre-stack depth migration, *Terr. Atmos. Ocean. Sci.*, *21*, 807–816.
Teng, L.-S. (1987), Stratigraphic records of the late Cenozoic Penglai orogeny of Taiwan, *Acta Geol. Taiwanica*, *25*, 205–224.
Teng, L.-S. (1992), Geotectonic evolution of Tertiary continental margin basins of Taiwan, *Pet. Geol. Taiwan*, *27*, 1–19.
Teng, L.-S., and A.-T. Lin (2004), Cenozoic tectonics of the China continental margin; insights from Taiwan, in *Aspects of the Tectonic Evolution of China*, vol. 226, edited by J. Malpas, C. J. N. Fletcher, J. R. Ali, and J. C. Aitchison, pp. 313–332, Geol. Soc. London Spec. Pub., London.
Teng, L. S., Y. Wang, C.-H. Tang, C.-Y. Huang, T.-C. Huang, M.-S. Yu, and A. Ke (1991), Tectonic aspects of the Paleogene depositional basin of northern Taiwan, *Proc. Geol. Soc. China*, *34*, 313–336.
Thomas, W. A. (1985), The Appalachian-Ouachita connection: Paleozoic orogenic belt at the southern margin of North America, *Annu. Rev. Earth Planet. Sci.*, *13*, 175–199.
Tillman, K. S., and T. B. Byrne (1995), Kinematic analysis of the Taiwan Slate Belt, *Tectonics*, *14*, 322–341.

Tsai, C.-H., S.-K. Hsu, Y.-C. Yeh, C.-S. Lee, and K. Xia (2004), Crustal thinning of the northern continental margin of the South China Sea, *Mar. Geophys. Res., 25*, 63–78.
Turner, S. A., J. W. Cosgrove, and J. G. Liu (2010), Controls on lateral structural variability along the Keping Shan Thrust Belt, SW Tien Shan foreland, China, in *Hydrocarbons in Contractional Belts*, vol. 348, edited by G. P. Goffey et al., 71–85, Geol. Soc. London Spec. Pub., London.
Waldhauser, F. (2001), hypoDD: A computer program to compute double-difference hypocenter locations, *U.S. Geol. Surv. Open File Rep., 01–113*, 25 pp.
Waldhauser, F., and W. L. Ellsworth (2000), A double-difference earthquake location algorithm: Method and application to the northern Hayward fault, California, *Bull. Seismol. Soc. Am., 90*, 1353–1368.
Willet, S. D. (1999), Orogeny and orography: The effects of erosion on the structure of mountain belts, *J. Geophys. Res., 104*, 28,957–28,981.
Wiltschko, D., and D. Eastman (1983), Role of basement warps and faults in localizing thrust fault ramps, in *Contributions to the Tectonics and Geophysics of Mountain Chains*, vol. 158, edited by R. D. Hatcher, H. Williams, and I. Zietz, pp. 177–190, Geol. Soc. Am. Mem, Boulder, Colo.
Wintsch, R. P., H. J. Yang, X.-H. Li, and K.-A. Tung (2011), Geochronologic evidence for a cold arc–continent collision; the Taiwan orogeny, *Lithos, 125*, 236–248.
Wu, F.T., C.-H. Chang, and Y.-M. Wu (2004), Precisely relocated hypocentres, focal mechanisms and active orogeny in central Taiwan, in *Aspects of the Tectonic Evolution of China*, vol. 226, edited by J. Malpas, et al., pp. 333–354, Geol. Soc. London Spec. Pub., London.
Wu, Y.-M., C.-H. Chang, L. Zhao, J. B. H. Shyu, Y.-G. Chen, K. Sieh, and J. P. Avouac (2007), Seismic tomography of Taiwan: Improved constraints from a dense network of strong motion stations, *J. Geophys. Res., 112*, B08312, doi:10.1029/2007JB004983.
Wu, Y.-M., L. Zhao, C.-H. Chang, and Y.-J. Hsu (2008), Focal-mechanism determination in Taiwan by genetic algorithm, *Bull. Seismol. Soc. Am., 98*, 651–661.
Wu, Y.-M., Y.-J. Hsu, C.-H. Chang, L. S.-Y. Teng, and M. Nakamura (2010), Temporal and spatial variation of stress in Taiwan from 1991 to 2007: Insights from compressive first motion focal mechanism catalog, *Earth Planet. Sci. Lett., 298*, 306–316.
Wu, F. T., H. Kuo-Chen, and K. D. McIntosh (2014), Subsurface imaging, TAIGER experiments and tectonic models of Taiwan, *J. Asian Earth Sci., 90*, 173–208.
Yang, K.-M., H.-H. Ting, and J. Yuan (1991), Structural styles and tectonic modes of Neogene extensional tectonics in southwestern Taiwan: Implications for hydrocarbon exploration, *Pet. Geol. Taiwan, 26*, 1–31.
Yang, K.-M., S.-T. Huang, J.-C. Wu, H.-H. Ting, and W.-W. Mei (2006), Review and new insights on foreland tectonics in western Taiwan, *Int. Geol. Rev., 48*, 910–941.
Yang, K.-M., S.-T. Huang, J.-C. Wu, H.-H. Ting, and W.-W. Mei, M. Lee, H.-H. Hsu, and C.-J. Lee (2007), 3D geometry of the Chelungpu thrust system in central Taiwan: Its implications for active tectonics, *Terr. Atmos. Ocean. Sci., 18*, 143–181.
Yang, K.-M., J.-C. Wu, E.-W. Cheng, Y.-R. Chen, W.-C. Huang, C.-C. Tsai, J.-B. Wang, and H.-H. Ting (2014), Development of tectonostratigraphy in distal part of foreland basin in southwestern Taiwan, *J. Asian Earth Sci., 88*, 98–115.
Yang, K.-M., R.-J. Rau, H.-Y. Chang, C.-Y. Hsieh, H.-H. Ting, S.-T. Huang, J.-C. Wu, and Y.-J. Tang (2016), The role of basement-involved normal faults in the recent tectonics of western Taiwan, *Geol. Mag., 153*, 1166–1191.
Yeh, Y.-H., et al. (1998), Onshore/offshore wide-angle deep seismic profiling in Taiwan, *Terr. Atmos. Ocean. Sci., 9*, 301–316.
Yeh, Y.-C., S.-K. Hsu, W.-B. Doo, J.-C. Sibuet, C.-S. Liu, and C.-S. Lee (2012), Crustal features of the northeastern South China Sea: Insights from seismic and magnetic interpretations, *Mar. Geophys. Res., 33*, 307–326.
Yin, A. (2006), Cenozoic tectonic evolution of the Himalayan orogeny as constrained by along-strike variation of structural geometry, exhumation history, and foreland sedimentation, *Earth Sci. Rev., 76*, 1–131.
Yue, L.-F., J. Suppe, and J-H. Hung (2005), Structural geology of a classic thrust belt earthquake: The 1999 Chi-Chi earthquake Taiwan (M_w = 7.6), *J. Struct. Geol., 27*, 2058–2083.
Yui, T.-F., K. Okamoto, T. Usuki, C.-Y. Lan, H.-T. Chu, and J.-G. Liou (2009), Late Triassic–Late Cretaceous accretion/subduction in the Taiwan region along the eastern margin of South China: Evidence from zircon SHRIMP dating, *Int. Geol. Rev., 51*, 304–328.
Yui, T.-F., K. Maki, C.-Y. Lan, T. Hirata, H.-T. Chu, Y. Kon, T. D. Yokoyama, B.-M. Jahn, and W. G. Ernst (2012), Detrital zircons from the Tananao metamorphic complex of Taiwan: Implications for sediment provenance and Mesozoic tectonics, *Tectonophysics, 541–543*, 31–42.
Zhang, X., Y. Yan, C.-Y. Huang, D. Chen, Y. Shan, Q. Lan, W. Chen, and M. Yu (2014), Provenance analysis of the Miocene accretionary prism of the Hengchun Peninsula, southern Taiwan, and regional geological significance, *J. Asian Earth Sci., 85*, 26–39.
Zhao, M., X. Qiu, S. Xia, H. Xu, P. Wang, T. K. Wang, C.-S. Lee, and K. Xia (2010), Seismic structure in the northeastern South China Sea: *S*-wave velocity and Vp/Vs ratios derived from three-component OBS data, *Tectonophysics, 480*, 183–197.

Paper II:

The influence of inherited continental margin structures on the stress and strain fields of the south-central Taiwan fold-and-thrust belt

Cristina Biete[1,2], Dennis Brown[1,3], Björn Lund[4], Joaquina Alvarez-Marron[1], Yih-Min Wu[5,6,7], Hao Kuo-Chen[3], Chun-Wei Ho[3,8]

[1] Institute of Earth Sciences, Jaume Almera, ICTJA, CSIC, Lluis Sole i Sabaris s/n, 08028 Barcelona, Spain. cristina.biete@gmail.com

[2] Departament de Dinàmica de la Terra i de l'Oceà, Universitat de Barcelona, Barcelona, Spain

[3] Department of Earth Science, National Central University, Zhongli District, Taoyuan City, Taiwan

[4] Department of Earth Sciences, Uppsala University, Uppsala, Sweden

[5] Department of Geosciences, National Taiwan University, Taipei 10617, Taiwan

[6] Institute of Earth Sciences, Academia Sinica, Taipei 11529, Taiwan

[7] NTU Research Center for Future Earth, National Taiwan University, Taipei 10617, Taiwan

[8] Central Weather Bureau, Taipei, Taiwan

Status of the paper: in press in ***Geophysical International Journal***. doi: 10.1093/gji/ggz296

Contributions of the Ph.D. candidate to the article:

- Analyzed the earthquake focal mechanism data, set up the binning system and performed the stress inversion during a three month stay under the supervision of Dr. Björn Lund at the Earth Sciences Department of Uppsala University, Sweden;
- Analyzed the GPS data, plot the displacement vectors and the determine the strain field and rates;
- Did the illustrations;
- Wrote the manuscript with the supervision of the Ph.D. supervisors

The influence of inherited continental margin structures on the stress and strain fields of the south-central Taiwan fold-and-thrust belt

Cristina Biete[1,2,] Dennis Brown[1,3], Björn Lund[4], Joaquina Alvarez-Marron[1], Yih-Min Wu[5,6,7,] Hao Kuo-Chen[3], Chun-Wei Ho[3,8]

[1] Institute of Earth Sciences, Jaume Almera, ICTJA, CSIC, Lluis Sole i Sabaris s/n, 08028 Barcelona, Spain. cristina.biete@gmail.com

[2] Departament de Dinàmica de la Terra i de l'Oceà, Universitat de Barcelona, Barcelona, Spain

[3] Department of Earth Science, National Central University, Zhongli District, Taoyuan City, Taiwan

[4] Department of Earth Sciences, Uppsala University, Uppsala, Sweden

[5] Department of Geosciences, National Taiwan University, Taipei 10617, Taiwan

[6] Institute of Earth Sciences, Academia Sinica, Taipei 11529, Taiwan

[7] NTU Research Center for Future Earth, National Taiwan University, Taipei 10617, Taiwan

[8] Central Weather Bureau, Taipei, Taiwan

Abbreviated title: The stress and strain fields of the south-central Taiwan FTB

Corresponding author: Cristina Biete Castells, Telf: (+34)934095410, cristina.biete@gmail.com

Summary

In this paper we test whether or not structural and morphological features inherited from the Eurasian continental margin are affecting the contemporary stress and strain fields in south-central Taiwan. Principal stress directions (σ_1, σ_2, and σ_3) are estimated from the inversion of clustered earthquake focal mechanisms and the direction of maximum compressive horizontal stress (S_H) is calculated throughout the study area. From these data the most likely fault plane orientations and their kinematics are inferred. The results of the stress inversion are then discussed together with the directions of displacement, compressional strain rate, and maximum shear strain rate derived from GPS data. These data show that there is a marked contrast in the direction of S_H from north to south across the study area, with the direction of S_H remaining roughly sub-parallel to the relative plate motion vector in the north, whereas in the south it rotates nearly 45° counterclockwise. The direction of horizontal maximum compression strain rate (ε_H) and associated maximum shear planes, together with the displacement field display an overall similar pattern between them, although undergoing a less marked rotation. We interpret the southward change in the S_H, ε_H, and the dextral maximum shear planes directions, together with that of the horizontal displacement field to be related to the reactivation of east-northeast striking faults inherited from the rifted Eurasian margin and to the shelf/slope break. Inherited faults in the basement are typically reactivated as strike-slip faults, whereas newly formed faults in the fold-and-thrust belt are commonly thrusts or oblique thrusts. Eastward, the stress inversions and strain data show that the western flank of the Central Range is undergoing extension in the upper crust. S_H in the Central Range is roughly parallel to the relative plate convergence vector, but in southwestern Taiwan it undergoes a marked counterclockwise rotation westward across the Chaochou fault. Farther north, however, there is no significant change across the Lishan fault. This north to south difference is likely due to different margin structures, although local topographic effects may also play a role.

Keywords: Principal stress, strain rate, Taiwan, fold-and-thrust belt, reactivation of inherited structures.

Issue Section: Geodynamics and tectonics

1. Introduction

The determination of the stress and strain fields in a fold-and-thrust belt is important because these are necessary parameters for the understanding of its mechanic, geometric, and kinematic evolution (e.g. Angelier et al. 1986, Oncken 1988, Erslev 1993, Becker 2000, Homberg et al. 2002, Saintot & Angelier, 2002, Lacombe et al. 2006, King et al. 2009, Peyret et al. 2011, Tavani et al. 2015). For example, based on studies in both active and fossil fold-and-thrust belts, Tavani et al. (2015) concluded that, although the stress and strain fields can be locally complex, even during syn-thrusting a strike-slip stress field is the most common. While they suggest that this conclusion is perhaps somewhat counterintuitive, they interpret it to result from the reactivation of inherited structures. Célérier (2008) proposed that the reactivation of faults with near optimal orientations (e.g. Sibson 1990, 1994, Kelly et al. 1999, Leclère & Fabbri 2013) controls the state of stress in the crust. Knowledge of the

stress and strain fields can, therefore, play an important part in a data set aimed at deciphering the role of reactivation of inherited structures in the development of a fold-and-thrust belt.

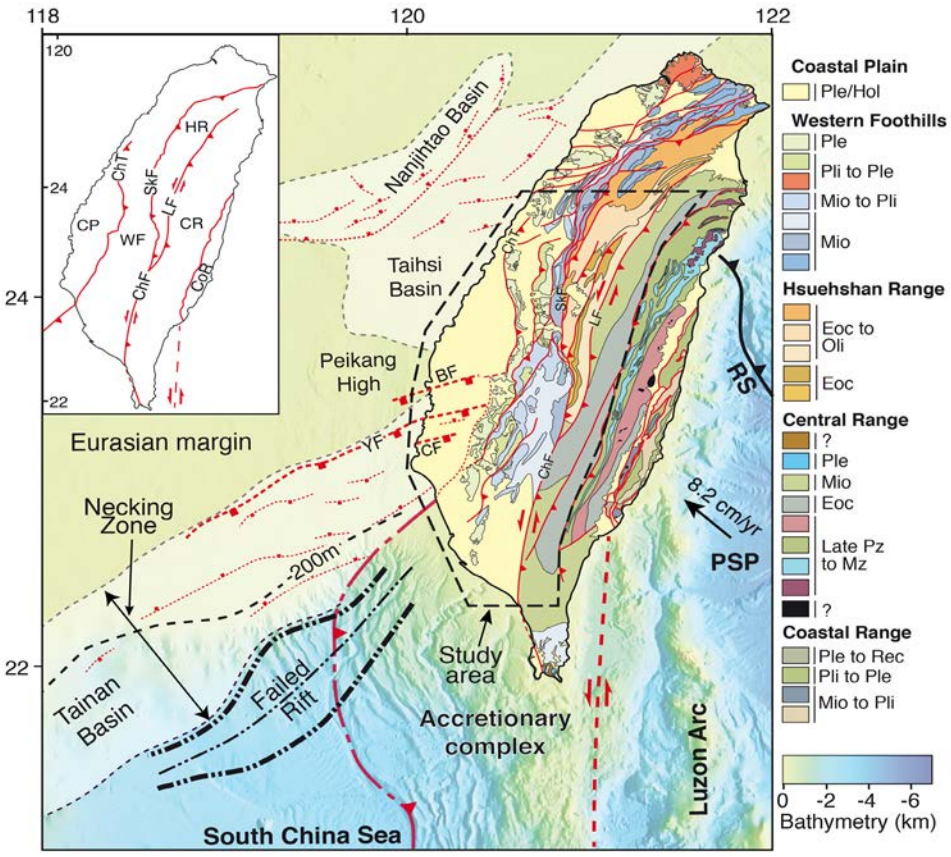

Figure 1: Tectonic setting of the Taiwan orogen. The geology of Taiwan is from C.-H. Chen (2000) with our modifications. The inset shows the main tectono-stratigraphic units discussed in the text. The structural (necking zone, failed rift, extensional basins, major faults) and morphological features (shelf/slope break at 200 m water depth) of the Eurasian continental margin are shown. The study area is highlighted by the black dashed line. The relative plate motion vector of 8.2 cm/yr toward 306° (Yu et al. 1997) between the Eurasian margin and the Philippine Sea Plate is given. RS = Ryukyu subduction zone, PSP = Philippine Sea Plate, ChT = Changhua thrust, LF = Lishan Fault, SkF = Shuilikeng Fault, ChF = Chauchou Fault, BF = B fault, YF = Yichu fault, CF = Chiali fault. The inset shows the tectono-stratigraphic units of the Taiwan orogen. CP = Coastal Plain, WF = Western Foothills, HR = Hsuehshan Range, CR = Central Range, CoR = Coastal Range.

With this in mind, in this paper we continue to explore the possible effects that the morphology and inherited structures of the Eurasian continental margin are having on the fold-and-thrust belt in south-central Taiwan (Fig. 1) which we have investigated in a series of recent publications (Brown et al. 2012, 2017, Camanni et al. 2014, 2016, Alvarez-Marron et al. 2014, Biete et al. 2018). In these studies, we used seismicity data, P-wave velocity models, and geodetic data, together with geometric analyses of surface and subsurface geological structures to propose that there is a causal link between along-strike changes in these features and the reactivation of fault systems inherited from the margin's outer shelf and necking zone. Here, we investigate this proposal further by estimating the principal stress directions (σ_1, σ_2, and σ_3) using inversion of clustered earthquake focal mechanisms and calculating the direction of maximum compressive horizontal stress (S_H) throughout the fold-and-thrust belt in the study area. From these data we then determine the fault planes that are likely to have been activated at depth. We discuss the combined results of the stress inversions with the directions of displacement, and the compressional, rotational, and maximum shear strain rates derived from GPS data. The hypothesis to be tested is whether or not the previously proposed causal link between

the inherited features of the margin and the structure of the fold-and-thrust belt is supported by the contemporary stress and strain fields in south-central Taiwan.

2. Geological setting

2.1. Eurasian continental margin

The continental margin of Eurasia that is involved in the Taiwan fold-and-thrust belt evolved from a sub-continental subduction system in the Late Cretaceous (Li et al. 2007, Lan et al. 2008) to a rifting margin by the Early Eocene, with sea-floor spreading starting in the South China Sea by the late Early Oligocene (e.g. Briais et al. 1993). Beginning in the Early Miocene several extensional events further affected the outer margin (e.g. A. T. Lin et al. 2003). Throughout this paper, we follow the scheme of Alvarez-Marron et al. (2014) and Brown et al. (2017), when describing the geology of the continental margin, defining the pre-Eocene rift-related rocks as its basement, the area of basement thinning towards the South China Sea ocean basin as the necking zone (see Mohn et al. (2012) for a definition of necking zone), and the slope as the morphological feature where the sediments were deposited on the necking zone. Today's shelf/slope break is defined as the 200 m bathymetry contour (Fig. 1).

During the Eocene rifting, several roughly northeast trending basins (e.g. Taishi and the Nanjihtao basins) developed and were filled with up to 5 km of sediment (S. K. Hsu et al. 2001, A. T. Lin & Watts 2002, A. T. Lin et al. 2008, C. Y. Huang et al. 2012, Yeh et al. 2012) (Fig. 1). The Taihsi Basin is thought to extend eastward into the Taiwan mountain belt where it is now exposed in the Hsuehshan Range (Fig. 1) (L. S. Teng, 1992, L. S. Teng & Lin 2004). The Miocene extension resulted in the formation of a number of east-northeast striking extensional faults (B, Yichu, etc. Fig. 1) and the formation of the Tainan Basin on the necking zone of the margin (e.g. Yang et al. 1991, A. T. Lin & Watts 2002, A. T. Lin et al. 2003, Ding et al. 2008). From north to south, the area of transition from the shelf to the necking zone is commonly called the Peikang High (Fig. 1). The Tainan Basin and the faults associated with it extend from the offshore southwestern Taiwan on land through the undeformed foreland and into the fold-and-trust belt (Fig. 1) (e.g. A. T. Lin et al. 2003, Rodriguez-Roa & Wiltschko 2010, Alvarez-Marron et al. 2014, Yang et al. 2016, Brown et al. 2017). Recently, Yeh et al. (2012), McIntosh et al. (2014) and Lester et al. (2014) identified what they interpreted to be a failed rift located at the base of the slope. Reflection seismic data show that it extends northeastward along the base of the slope (McIntosh et al., 2014) and possibly into the southwestern part of the island (Brown et al., 2017; Biete et al., 2018). This failed rift marks the onset of the hyper-extended part of the margin, which extends for more than 200 km to the south (Lester et al., 2014). It is the reactivation of these Eocene and Miocene extensional faults that we have previously proposed to be having an important effect on the geometrical development of the fold-and-thrust belt, its seismicity and its topography (Brown et al. 2012, 2017, Camanni et al. 2014, 2016, Alvarez-Marron et al. 2014, Biete et al. 2018).

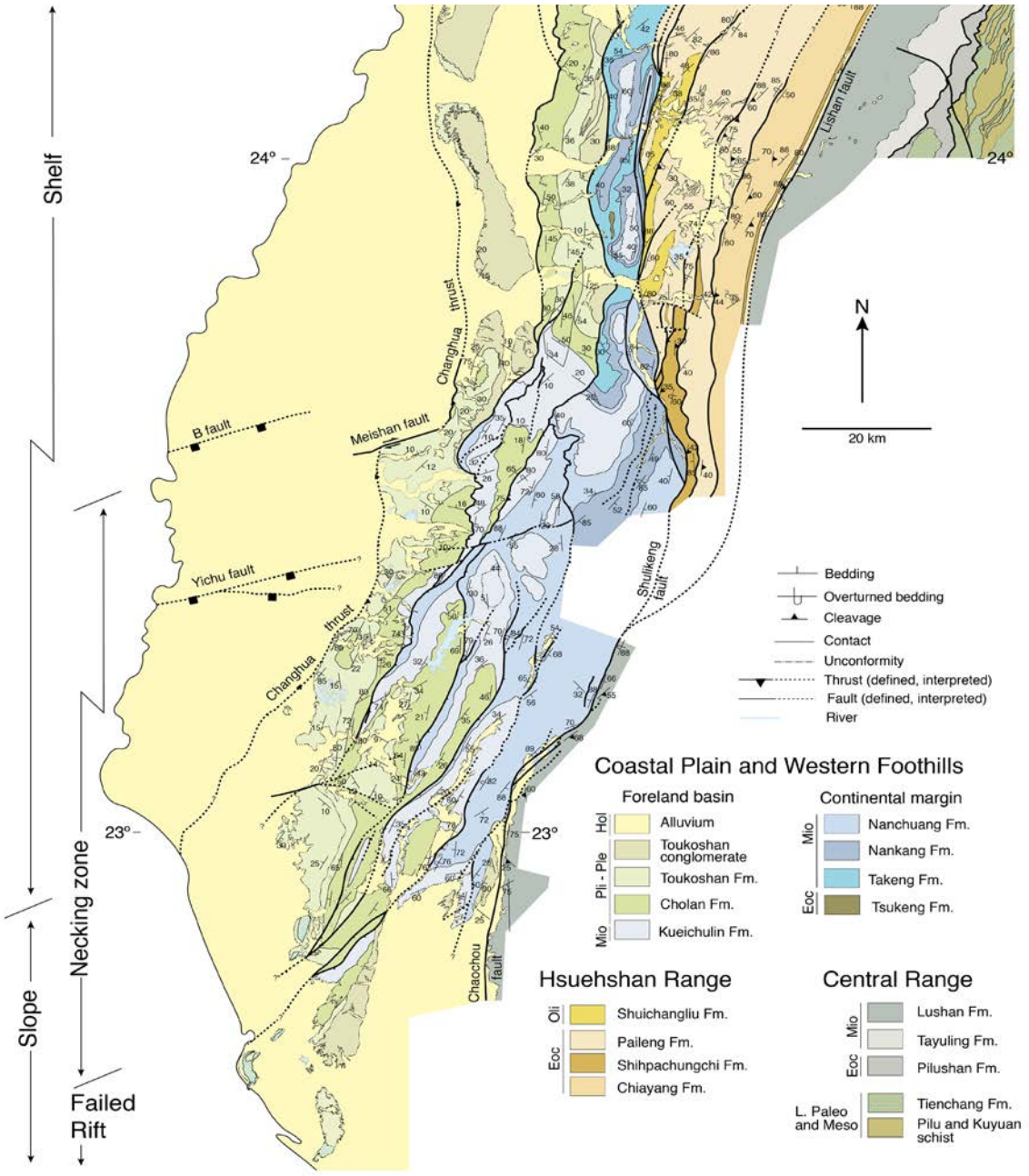

Figure 2

Figure 2: Geological map of the study area with representative structural data. The location of the main structural and morphological features of the Eurasian continental margin are shown.

2.2. South-central Taiwan fold-and-thrust belt

Within the Taiwan mountain belt (Fig. 1), the study area is divided into several roughly N-S striking tectono-stratigraphic units (e.g. Ho, 1988) that, from west to east are: the Coastal Plain (CP), the Western Foothills (WF), the Hsuehshan Range (HR) and the Central Range (CR). The Coastal Range (CoR) is outside the study area and will not be mentioned further. For the sake of simplicity, in this study we group the Coastal Plain, Western Foothills, and Hsuehshan Ranges under the term

fold-and-thrust belt, which is juxtaposed against the Central Range along the Lishan–Chaochou fault system (Fig. 2). While we have only limited structural data for the Central Range, we include its western flank in this study because of the important changes in the stress and strain fields that occur from west to east across the Lishan–Chaochou fault system (see sections 3 and 4 below).

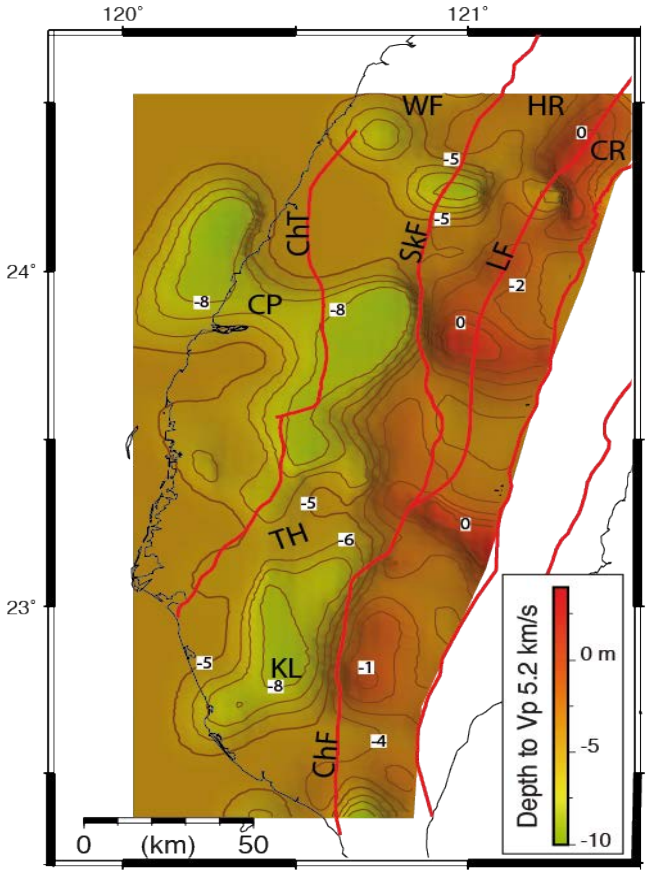

Figure 3

Figure 3: Map of the 5.2km/s proxy for the depth to the top of the basement extracted from the 3D tomographic model of Kuo-Chen et al. (2012). The Tainan basement high (TH) and the Kaoshiang basement low (KL) are highlighted. Labels of faults and tectono-stratigraphic units are as in the inset of Figure 1.

In this paper, we follow the structural interpretations of the fold-and-thrust belt that have been proposed by Brown et al., (2012, 2017), Alvarez-Marron et al., (2014), and Biete et al., (2018). Within the study area, the fold-and-thrust belt has a roughly N-S structural grain that becomes more NE-SW in the southwestern part (Fig. 2). It is a west-verging imbricate thrust system developed above a basal thrust that dips overall eastward from its tip line along the Changhua thrust in the west to a maximum depth of about 7 km before ramping down into the basement (Brown et al., 2012; Alvarez-Marron et al., 2014; Biete et al., 2018). A number of pronounced ENE-striking lateral and oblique ramps have been interpreted to occur along the basal thrust over its north-south extent. This interpretation is based on along-strike changes in structure, seismicity, topography, and P-wave velocity (e.g., Brown et al., 2017). Alvarez-Marron et al. (2014), Brown et al. (2017), and Biete et al. (2018) have proposed that these along-strike changes have a causal relationship with the extensional faults inherited from the continental margin. Along its eastern flank, the fold-and-thrust belt is juxtaposed against the Central Range along the oblique thrust to sinistral strike-slip Chaochou-Lishan fault sys-

tem that extends along the entire length of the mountain belt and has been interpreted to penetrate into the middle and even lower crust (Wiltschko et al. 2010, Tang et al. 2011, C. Huang & Byrne 2014, Kuo-Chen et al. 2015) (Figs. 1 and 2). A geological description of the Central Range is out of the scope of this paper.

In the study area, much of the seismicity is located below the basal thrust of the fold-and-thrust belt, in the basement (e.g. Wang et al., 2000, Carena et al. 2002, Yue et al., 2005, Camanni et al. 2016, Brown et al. 2017), so knowing the depth to the top of the basement is important to our study (see Section 2.1. for our definition of basement). The exact depth to the top of the basement is not well known since it does not crop out in the study area and it has been intersected only in several boreholes in the Coastal Plain (e.g. Chiu 1975, Jahn et al. 1992, Shaw 1996). Therefore, we use a petrophyscial proxy to define its location. The rationale for this has been presented by Camanni et al. (2016) and Brown et al. (2017) and the reader is referred there for extensive discussions of it. We use a P-wave velocity of 5.2 km/s to describe the top of the basement (or, to view it another way, the base of the clastic sediments, whose maximum P-wave velocity is about 5.2 km/s (Brocher, 2005)). Using this velocity description, the basement/cover interface is between 5 km and 8 km depth throughout much of the study area, except beneath the Hsuehshan Range and along the eastern part of the fold-and-thrust belt between 23°N and 24°N (Fig. 3). East of the Chaochou-Lishan fault system the basement rocks approach the surface, and in fact crop out extensively in the Central Range, east of our study area.

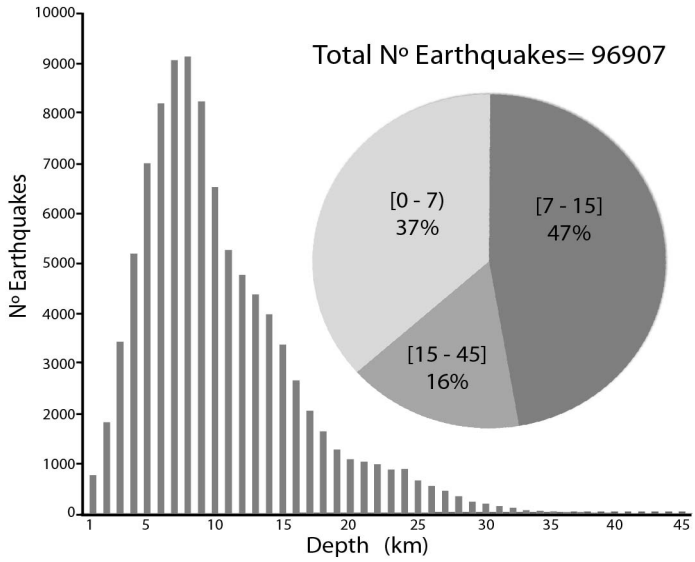

Figure 4

Figure 4: A) Depth distribution histogram for the seismicity in the study area from 1994 through 2014. The pie plot shows the percentage of seismicity for each depth level discussed in the text.

3. Contemporaneous stress field in south-central Taiwan

3.1 Methodology

In this study we use earthquake focal mechanisms to estimate the contemporaneous stress field in south-central Taiwan. The earthquakes were recorded between 1994 through 2014 and all hypocen-

ters have been relocated by the double-difference technique (Waldhauser & Ellsworth 2000) using the HypoDD3D software (Waldhauser 2001) within the 3D P-wave velocity model of Kuo-Chen et al. (2012). The average horizontal uncertainties in earthquake locations are estimated to be ±1 km, while the vertical is ±2 km (Brown et al. 2017). In this study we have used all events over the time period given, regardless of transitory stress changes caused by large events like the 1999 Chi-Chi earthquake. It is well known that large earthquakes can cause transitory changes in the stress field (e.g. Michael 1987, Hardebeck & Hauksson 2001, Y.-M. Wu et al. 2010, Hensch et al. 2016, Hardebeck & Okada 2018), but it is not well understood how long such a stress change can last (Hardebeck & Okada 2018). For example, while there was a marked change in the stress field in parts of Taiwan following the 1999 M_W 7.6 Chi-Chi, this change was spatially heterogeneous and took several months to more than a year to return to what it was prior to the earthquake (Y.-M. Wu et al. 2010, Y. J. Hsu et al. 2011). Removing earthquake data during a period of time after the Chi-Chi event in order to take into account its effect on the contemporaneous stress field would, therefore, not be necessarily correct since the changes recorded and the time it took to return to what it was before are spatially heterogeneous. Furthermore, there have been a number of other large earthquakes in the study area, such as the 1998 M_L 6.2 Rueyli, the 1999 ML 6.4 Chiayi, and the 2010 M_L 6.4 Jiashian events, whose spatial and temporal effect on the contemporaneous stress field in western Taiwan have not been studied. Therefore, selectively removing a time period of data related to the large earthquakes would bias the data set in areas unaffected by them.

In this study we use a hypothesis driven approach (e.g., Hardebeck & Michael, 2004) to do the binning of the focal mechanism data for the stress inversion. It is designed to test whether or not the pre-existing structure of the margin is influencing the contemporaneous stress field. Since much of the seismicity of the study area occurs within the basement (Fig. 4) we have divided the crust into three depth levels. From 0 to 6.9 km comprises the fold-and-thrust belt and/or the sedimentary carapace overlying the basement. Some 37% of earthquakes occur within this depth level (Fig. 4). From 7 to 45 km comprises basement, which is divided into two depth levels. From 7 to 14.9 km contains 47% of earthquakes and its base is chosen to coincide with the depth to the expected thermal cut-off for seismicity (about 350 + 100 °C; Sibson (1983), W. Chen & Molnar (1983)) given a geothermal gradient of around 30°C/km in western Taiwan (S. K. Wu et al. 2013). Finally, we include a layer from 15 to 45 km depth that includes the deepest earthquakes, which accounts for 16% of the total seismicity.

The focal mechanism data set comprises 2465 events with magnitudes ranging from 1.4 to 6.8, with a mean M_L of 3.(Fig. 5a) and where the 90% of the events magnitudes range between 2.5 and 4.8 (see supplementary data set table SD1). Focal mechanisms were calculated using first motion polarities of P waves (Y.-M. Wu et al. 2008). Each focal mechanism was assigned a quality index factor (Qfp) to assess the uncertainty and solution quality depending on the number of polarity readings (Npor), the azimuthal gap (Gap), a relative number of up versus down polarity readings (Rup), and the data fit from the genetic focal mechanisms estimation algorithm (for details on Qfp calculations see Y.-M. Wu et al., (2008)). Values for Qfp, Npor, Gap and Rup can be found in supplementary Table SD1. The data set is composed of focal mechanisms solutions with Npor > 10 and Gap < 180° and, generally, a solution is considered to be unconstrained if Qfp = 0, and good with Qfp > 1 (Y.-M. Wu et al., 2008). All event locations and focal mechanism solutions, which include strike, dip, rake with

standard deviations (1s), and the corresponding P, T, and B axes are also presented in supplementary Table SD1.

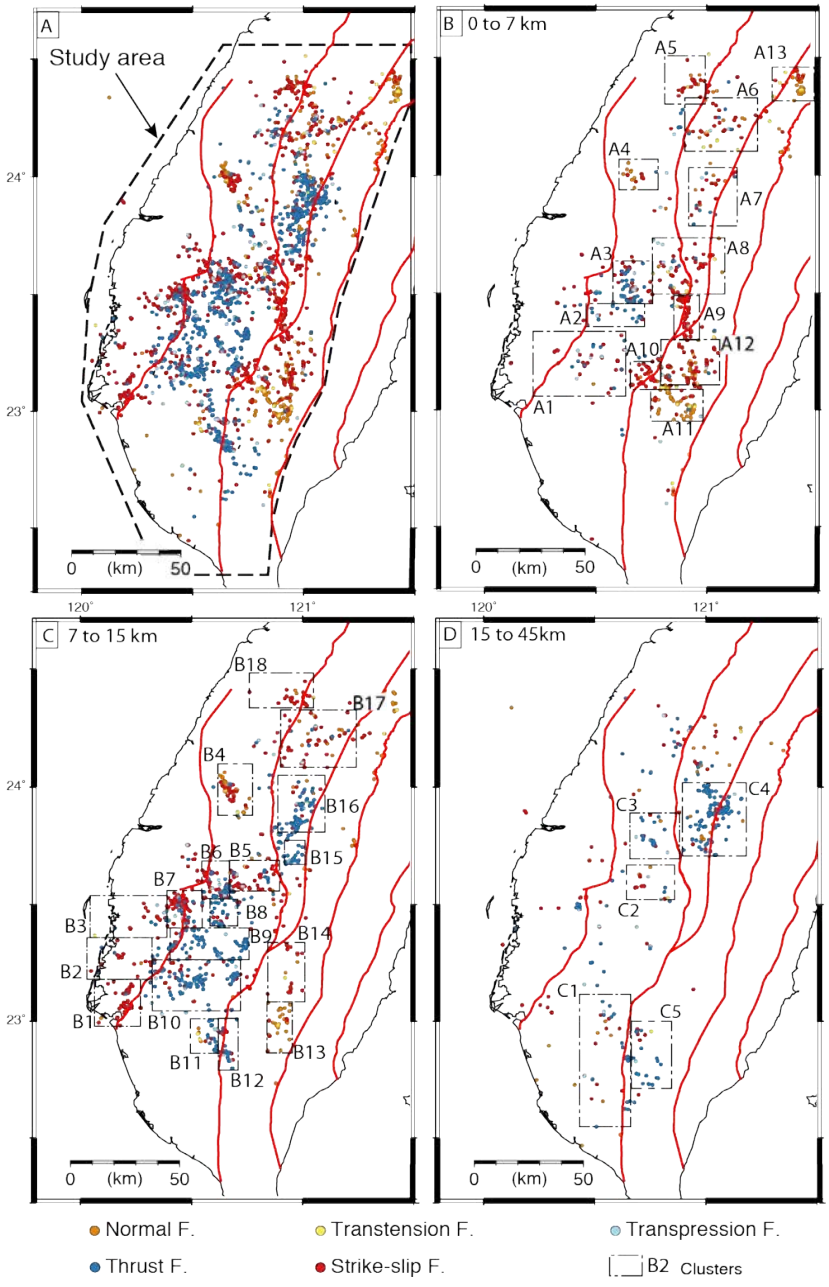

Figure 5

Figure 5: A) Distribution and faulting type for all focal mechanism used in this study. The location of the study area is shown with a black dashed line. The faulting types follow the classification scheme of Zoback (1992). B) The 0 to 7 km depth level with 13 clusters labelled A1 to A13. C) The 7 to 15 km depth level with 18 clusters labelled B1 to B18. D) The 15 to 45 km depth level with 5 clusters labelled C1 to A5. Clusters correspond to the results shown in Figure 6 and SD1.

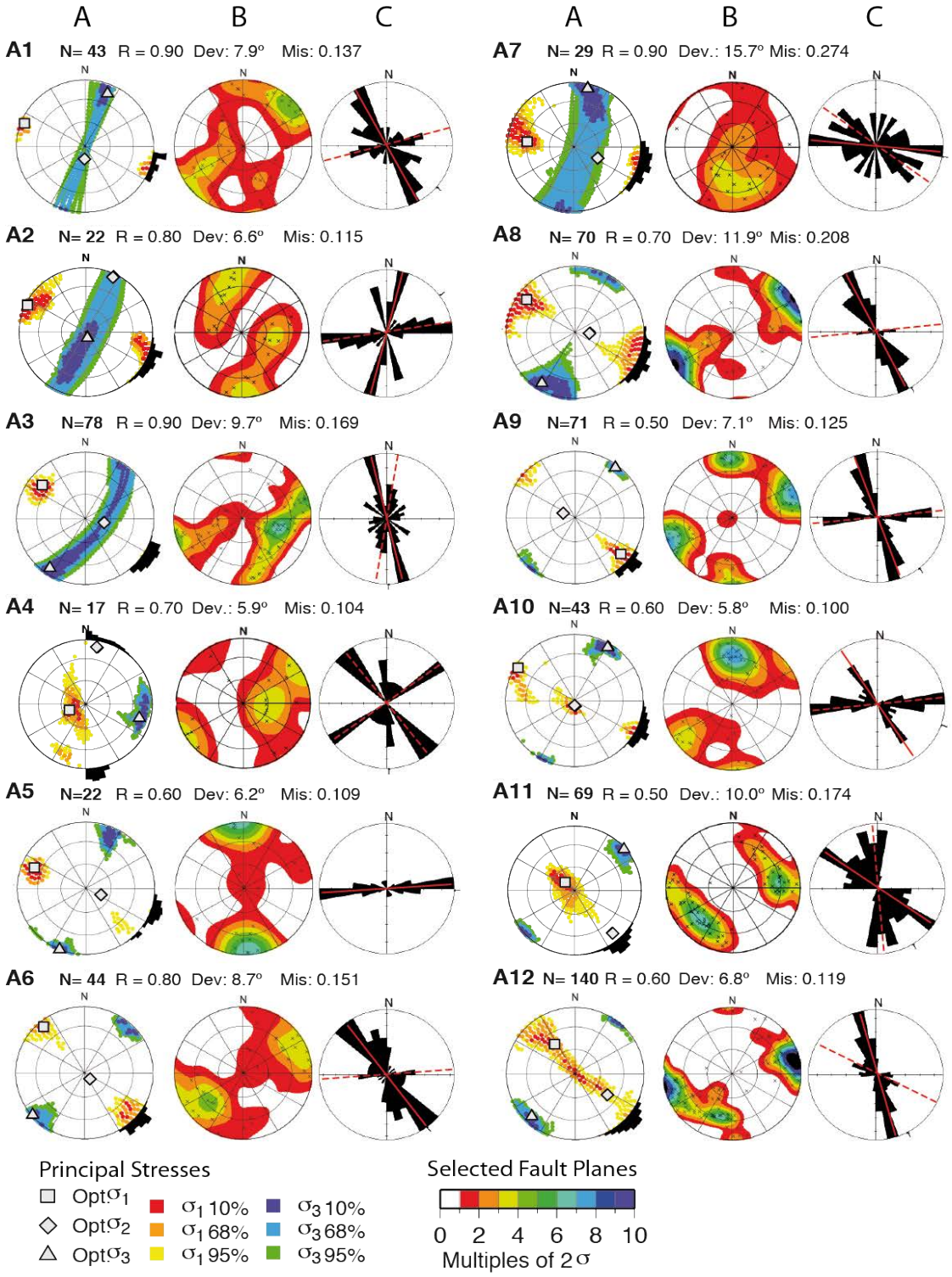
A
B
C
A1 N= 43 R = 0.90 Dev: 7.9° Mis: 0.137
A2 N= 22 R = 0.80 Dev: 6.6° Mis: 0.115
A3 N=78 R = 0.90 Dev: 9.7° Mis: 0.169
A4 N= 17 R = 0.70 Dev.: 5.9° Mis: 0.104
A5 N=22 R = 0.60 Dev: 6.2° Mis: 0.109
A6 N= 44 R = 0.80 Dev: 8.7° Mis: 0.151
A7 N= 29 R = 0.90 Dev.: 15.7° Mis: 0.274
A8 N= 70 R = 0.70 Dev: 11.9° Mis: 0.208
A9 N=71 R = 0.50 Dev: 7.1° Mis: 0.125
A10 N=43 R = 0.60 Dev: 5.8° Mis: 0.100
A11 N= 69 R = 0.50 Dev.: 10.0° Mis: 0.174
A12 N= 140 R = 0.60 Dev: 6.8° Mis: 0.119
Principal Stresses
Opt σ1
Opt σ2
Opt σ3
σ1 10%
σ1 68%
σ1 95%
σ3 10%
σ3 68%
σ3 95%
Selected Fault Planes
0 2 4 6 8 10
Multiples of 2 σ

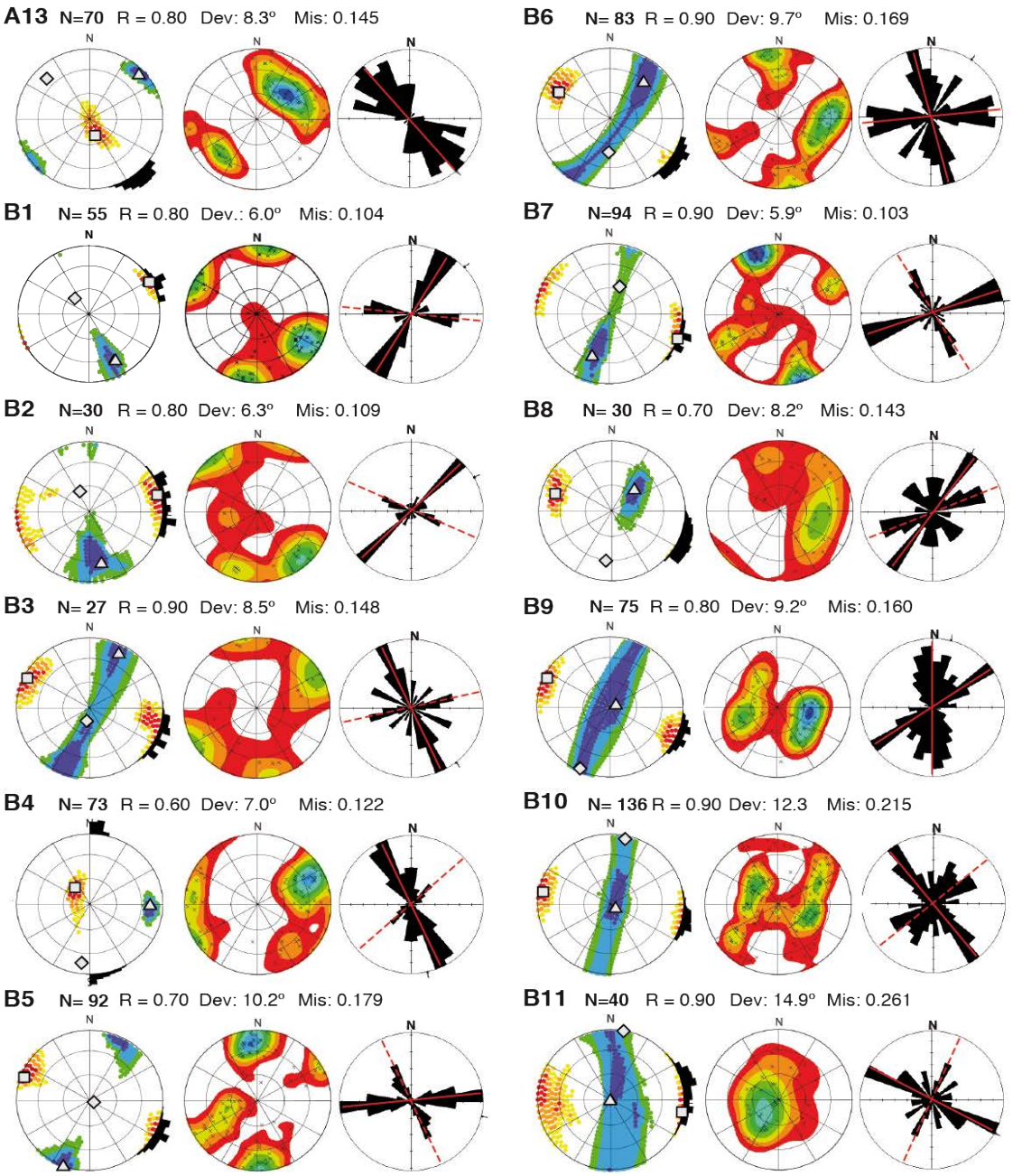
A13 N=70 R = 0.80 Dev: 8.3º Mis: 0.145
B1 N= 55 R = 0.80 Dev.: 6.0º Mis: 0.104
B2 N=30 R = 0.80 Dev: 6.3º Mis: 0.109
B3 N= 27 R = 0.90 Dev: 8.5º Mis: 0.148
B4 N= 73 R = 0.60 Dev: 7.0º Mis: 0.122
B5 N= 92 R = 0.70 Dev: 10.2º Mis: 0.179
B6 N= 83 R = 0.90 Dev: 9.7º Mis: 0.169
B7 N=94 R = 0.90 Dev: 5.9º Mis: 0.103
B8 N= 30 R = 0.70 Dev: 8.2º Mis: 0.143
B9 N= 75 R = 0.80 Dev: 9.2º Mis: 0.160
B10 N= 136 R = 0.90 Dev: 12.3 Mis: 0.215
B11 N=40 R = 0.90 Dev: 14.9º Mis: 0.261

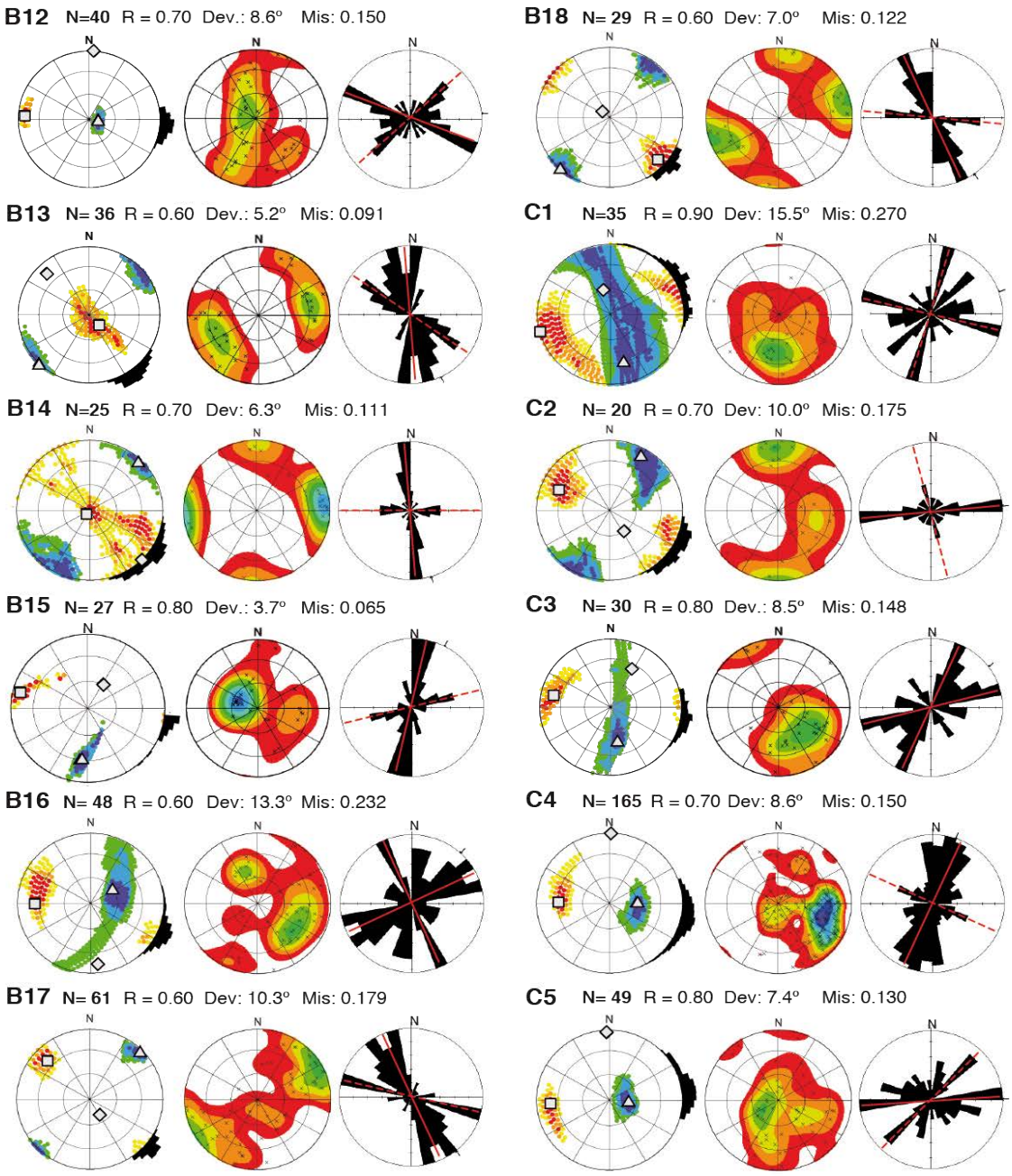

Figure 6: Results from the inversion of earthquake focal mechanisms for each cluster shown in Figure 5. Column A is the best fitting Principal stress directions on lower hemisphere equal area plots, with confidence regions of σ1 (red colors) and σ3 (blue colors), and the optimal solution (symbols). Histograms of S_H direction are shown on the periphery of the stereonet. Column B shows the Kamb contours of the poles to the selected fault planes that best fit the stress tensor. Column C shows rose diagrams of the strikes of the selected fault planes from column B, highlighting the mean strike of the primary (solid) and secondary (dashed) fault families in red. N = number of events, R = relative size of the intermediate principal stress, Dev = Deviation and Mis = Misfit. The locations of the clusters are shown in Figure 4. A complete output from the inversion is given in Figure SD1.

The data set has been divided into clusters (Fig. 5) where the proximity of events and their distribution in swarms (i.e., main shock and aftershocks) were taken into account. Each cluster has a minimum of 20 events (except cluster A4 with 17 events), which has been shown to be a sufficient number to give a stable inversion result (e.g. Hardebeck & Hauksson, 2001; Townend & Zoback, 2006; Arnold & Townend, 2007; Vavrycuk, 2014) and 29 of the clusters have more than 30 events. In keeping with Y.-M. Wu et al. (2008, 2010) and S.K. Chen et al. (2017), we use only events with a Qfp > 0.1. Overall, the clusters have an average of Qfp 1.15 ± 0.46 (average of the median cluster Qfp), with only an 11% ± 6 in average of percentage of events with Qfp < 0.2 in each cluster (supplementary Table SD2). Nineteen clusters have a median Qfp > 1, which we consider being high quality clusters. Eleven clusters have a median Qfp between 0.7 and 1, which is fair, and 6 have median Qfp below 0.7, which is acceptable (Y.-M. Wu et al. 2008) (supplementary Table SD2 contains more information on cluster Qfp statistics). In the stress inversion all events are treated equally, with no weighting being applied.

The focal mechanism data in the various clusters are displayed in supplementary Figure SD1. We show nodal plane normals, P- and T-axes and the faulting states, and see that most clusters have rather well-defined directions of P-, T- axes and nodal plane normals, while some (A7, B11, B17 or C3) show more scattered directions. The P- and T- axes distributions suggest that events in some clusters are produced by a thrust state of stress (T-axes roughly vertical, 90° away from P) (B8, B9, B10, B16 and C4), some by a strike-slip environment (90° along the horizontal between P and T axes) (A8, A9, B1 and B5), and a few by a normal state of stress (P-axes roughly vertical, 90° away from T) (A11, A13 and B13). Other clusters seem to be located in more oblique stress states of either transtenstion or transpression, where some P- and T- axes show thrust or normal and others strike-slip (A3, A11, A12, B4 and B6) (column A of supplementary Figure SD1). However, as individual focal mechanisms can vary significantly even when events are produced by the same stress state (e.g. McKenzie, 1969) we need a formalized inversion methodology to assess the causative stresses in the clusters.

To estimate the principal stress directions ($\sigma1$, $\sigma2$, and $\sigma3$) we use the stress tensor inversion scheme of Lund & Slunga (1999). The methodology accounts for uncertainties in the focal mechanisms by perturbations to the P-, T- and B-axes up to some angle during the inversion (Lund & Slunga, 1999; Hensch et al., 2016). Here we allowed 10 – 15 degrees maximum perturbation in keeping with the 18 degree average focal mechanism uncertainty estimated by Wu et al. (2008). In order to select which of the two nodal planes is the most likely fault plane, the Lund & Slunga (1999) methodology applies a Mohr-Coulomb stability criterion to assess which nodal plane is more unstable over a range of coefficient of friction (m) values. Here we use a m-range of 0.4 – 1.2 and if one nodal plane is consistently more unstable over this range, that nodal plane is chosen as the fault plane and used in the inversion. If, on the other hand, the most unstable nodal plane changes over this range then the nodal planes are similarly stable and choosing one over the other would mean an implicit choice of m. The fault plane is then instead chosen based on the goodness of fit. Using the focal mechanisms of the considered cluster, the inversion performs a grid search of the principal stress directions and the stress ratio $R=(\sigma1 - \sigma2)/(\sigma1 - \sigma3)$. For each point on the grid it searches through all perturbations of the focal mechanisms and for each calculates the angular misfit between the shear stress direction on the chosen fault plane and the observed slip direction. This process determines the directions of

the three principal stress axes and an estimate of the relative size of the intermediate principal stress, the stress ratio R (Lund & Slunga 1999). When the entire set of focal mechanisms of the cluster has been searched at all stress directions, the optimal stress tensors and its confidence limits are calculated using statistics for one-norm misfit (Fig. 6 column A). The direction of the maximum compressive horizontal stress (S_H) and its confidence limits are then determined using the methodology of Lund & Townend (2007). The S_H results are plotted as a histogram around the stereonet (Fig. 6 column A). In map view, S_H is plotted as wedges that represent the 95% confidence limit (Fig. 7) and the stress regime of each (i.e., reverse, normal, strike-slip) is determined from the stress tensor. Then, the poles to the estimated fault planes, determined from the two nodal planes of each focal mechanism (e.g. Lund & Slunga 1999) are plotted and contoured using the Kamb method (Fig. 6 column B). We also plot the strikes of the estimated fault planes in a rose diagram (Fig. 6 column C) using the Stereonet3D software of Allmendinger et al. (2012). The length of the petals corresponds to the percentage of the total number of strikes that falls within a 10° bin, and the two most frequent strikes are chosen as the primary (most frequent) and secondary fault planes (Fig. 7). Finally, to assess how the instability fault selection criterion performed we note that on average 70% ± 12% of the fault planes were chosen based on stability and that in only three clusters (A4, B14 and B16) were less than 50% of the planes chosen by stability (supplementary Table SD2). In supplementary Figure SD1 we illustrate the chosen fault planes in Mohr-Coulomb diagrams, with the relative stress magnitudes calculated in the inversion using an average coefficient of friction (m) of 0.6 (supplementary Figure SD1 column G). A complete set of inputs and outputs for each cluster is given in Supplementary data set Figure SD1.

3.2 Stress tensors and maximum horizontal compressive stress

An analysis of faulting types (calculated using the method of Zoback (1992)) shows that strike-slip and thrust faulting dominate in the fold-and-thrust belt (Fig. 5A). Strike-slip faulting occurs mostly in the Coastal Plain and in the Western Foothills at about 23.5°N to a depth of 15 km, whereas thrusting and transpressional faulting dominate in the Western Foothills and the Hsuehshan Range from the surface to the base of the seismicity (Fig. 5B, C and D). Extensional faulting in the northwest (clusters A4 and B4) and strike-slip faulting in the southeast (cluster A9) are related to the Chi-Chi earthquake sequence. Extensional and strike-slip faulting dominate at all depths along the western flank of the Central Range, with thrusting being common at the deepest level in the south (Figs. 5B, C and D).

Throughout the fold-and-thrust belt, σ1 at all depth levels generally plunges gently toward the west-northwest to west (Fig. 6 column A). There are local exceptions to this, such as clusters B1, B2 and C1 in which s1 plunges gently east-northeast. From 0 to 7 km depth, the state of stress in the Coastal Plain, Western Foothills, and the Hsuehshan Range is predominantly in the strike-slip regime. In the southern part of the Western Foothills, from 7 to 15 km depth, there is a dominantly compressional stress regime that is important. Although there are few data in the 15 to 45 km depth level, these show a compressional stress regime in the north and a strike-slip regime in the central and southern parts of the study area. An extensional stress regime is rare in the fold-and-thrust belt, being found only in clusters A4 and B4, where σ3 plunges gently toward the east-southeast. An extensional

stress regime is common, however, in the upper 15 kms of the Central Range, where σ3 is gently northeast and southwest plunging (clusters A11, A12, A13, B13, and B14). At the deepest level, in the southern part of the Central Range, a compressional stress regime dominates, with σ1 plunging gently toward the west (cluster C5).

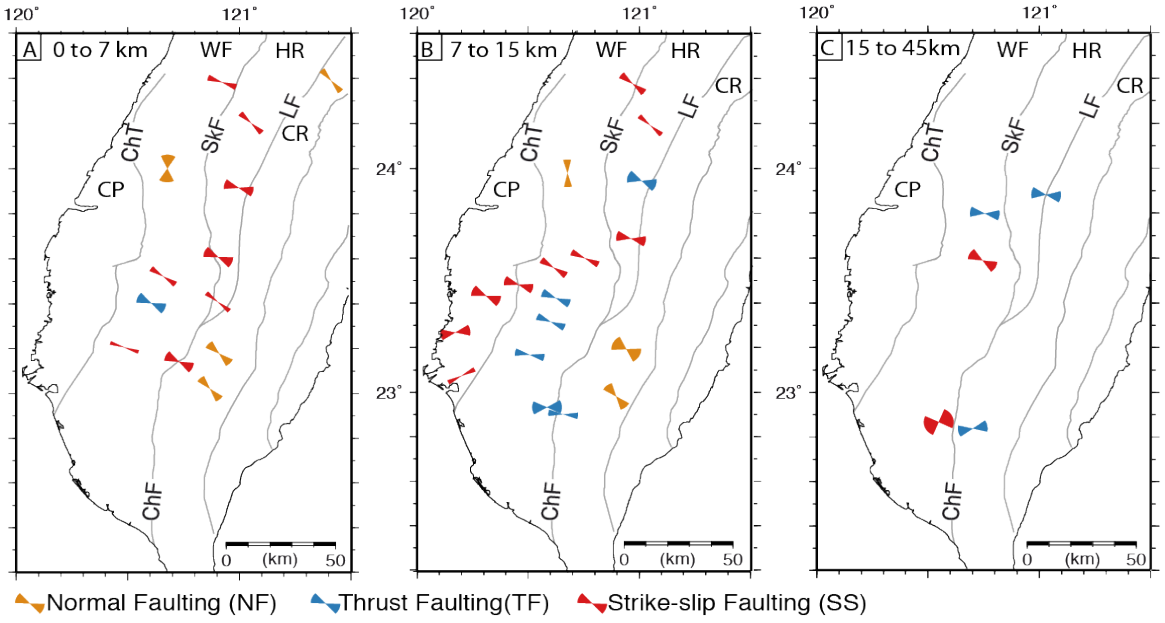

Figure 7

Figure 7: Direction of the maximum horizontal compressive stress (S_H) for each cluster at their respective depth level. Each wedge corresponds to the 95% confidence interval. The result from each cluster is colored depending on fault type. A) The 0 to 7 km depth level, B) The 7 to 15 km depth level, and C) The 15 to 45 km depth level. All the relevant data of the resultant inversion for each cluster are in Figure 6 and the location of the clusters in Figure 5. Labels of faults and tectono-stratigraphic units are as in the inset of Figure 1.

Throughout the fold-and-thrust belt, the direction of the maximum compressive horizontal stress (S_H) varies appreciably from north to south, although it shows only minor, local variation with depth (Fig. 7). In general, the direction of S_H fans from roughly northwest in the north (clusters A4 and B4 are exceptions), through to west-southwest in the southwest part of the study area. The direction of S_H in the Central Range is constantly northwest oriented, except at the deepest depth level in the south, where it is west-southwest oriented.

3.3. Most likely active fault planes

A derivative of the process of determining the stress tensor is the possibility to estimate the most likely fault plane orientations and kinematics for the region of each earthquake cluster (Figs. 8). We have done this using the fault selection during inversion methodology outlined above and orientations are given following the right hand rule. The quality of the fault plane determinations can be observed from the deviation angles (Dev in Fig. 6) (defined as the mean of the angular differences in the fault planes between the observed slip directions and the directions of calculated maximum shear stress) given for each cluster. As an estimate of quality, we divide the results into 3 classes based on

the estimated average uncertainties in the focal mechanisms (Y.-M. Wu et al., 2008): <10° is good (26 clusters), 10° to 15° is fair (8 clusters), and > 15° is poor (2 clusters) (Lund and Slunga, 1999). From 0 to 7 km depth (Fig. 8A), northwest to north-northeast striking sinistral transpressional faulting to thrust faulting dominate in the southern part of the Western Foothills, whereas nearly east striking dextral strike-slip faulting and northwest striking dextral transtensional faulting occurs in the north. Roughly northwest striking sinistral transpressional faulting dominates in the Hsuehshan Range, whereas northwest striking extensional to sinistral transtensional faulting are typical in the Central Range. From 7 to 15 km depth (Fig. 8B), north-northwest and north-northeast striking dextral and sinistral stike-slip faulting are common in the south of the Coastal Plain. Faulting in the southern part of the Western Foothills is characterized by north-northwest and north-northeast striking dextral and sinistral transpressional faulting together with north-northeast and north striking thrust faulting, whereas in the north only northwest striking transtensional faulting takes place. The central part of the Western Foothills is dominated by a zone of east-northeast striking, dextral strike-slip faulting (Fig. 8B). At this depth level, the Hsuehshan Range is characterized by northwest through northeast striking sinistral and dextral transpressional and thrust faulting. The southern part of the Central Range has roughly north striking extensional faulting with predominantly roughly east-west sinistral transpressional faulting in the immediate hangingwall of the Chaochou fault. From 15 to 45 km depth (Fig. 8C), southwest and nearly east striking dextral transpressional faulting is taking place in the Western Foothills, whereas in the far southeast north striking dextral faulting is taking place in the immediate footwall to the Chaochou fault. At this depth level, in the Central Range north-northeast striking thrust faulting is taking place along the hangingwall of the Lishan fault, and roughly east-west sinistral strike-slip faulting in the immediate hangingwall of the Chaochou fault.

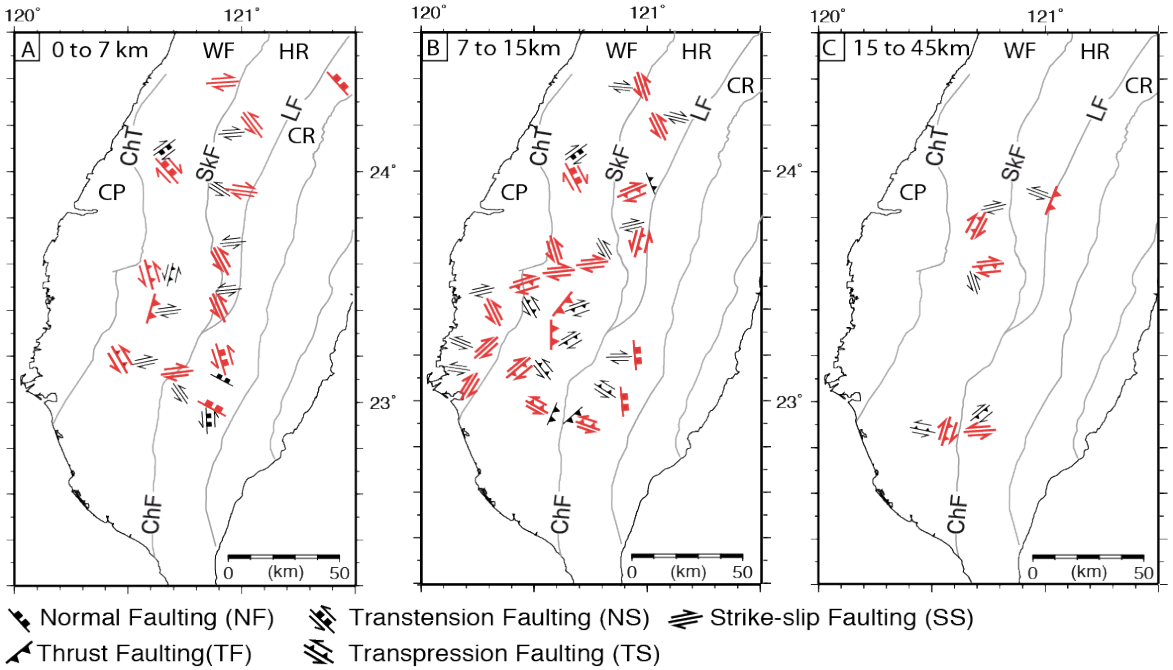

Figure 8: Selected fault planes orientations with their interpreted kinematics depending on σ_1, σ_2, and σ_3 and S_H from the inversion results shown in figures 6B and C (primary orientations/kinematics in red, secondary in black). A) The 0 to 7 km depth level, B) The 7 to 15 km depth level, and C) The 15 to 45 km depth level. All the relevant data of the resultant inversion for each cluster are in Figure 6 and the location of the clusters in Figure 5. Labels of main faults and tectono-stratigraphic units are as in the inset of Figure 1.

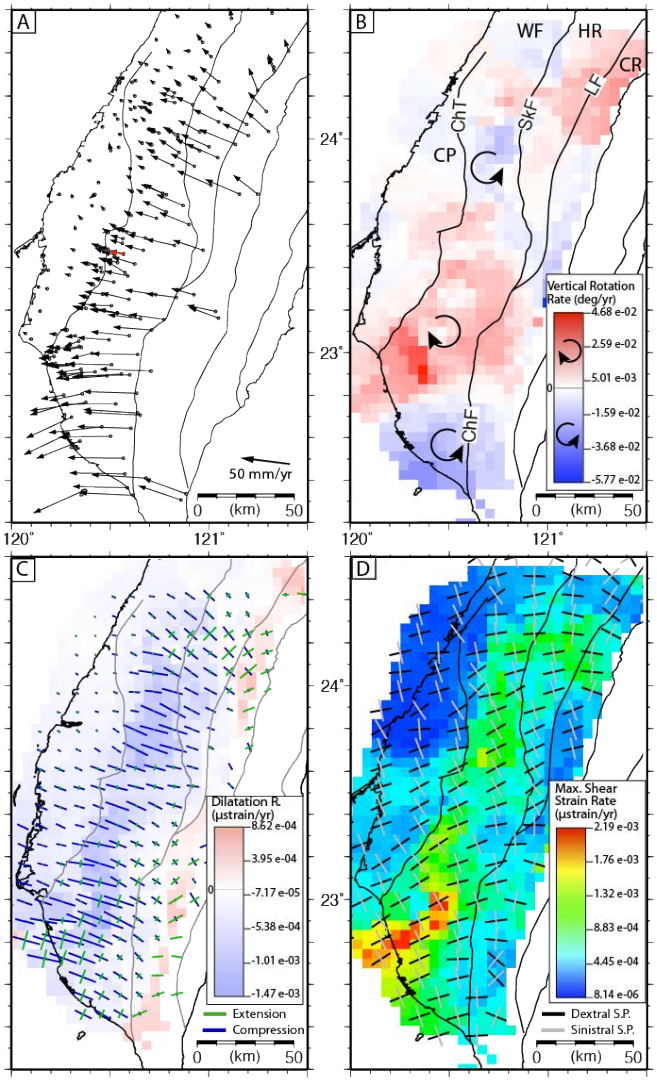

Figure 9: Geodetic velocities and strain rates. A) GPS horizontal velocity vectors. B) Vertical rotation strain rate. Blue colors represent counterclockwise and red colors clockwise rotation, respectively. C) Dilatation strain rates. Blue colors representing compression and red extension. The horizontal maximum compression (ε_H) and extension strain rate axes are shown by the blue and green lines, respectively. D) Maximum shear strain rates. Dextral and sinistral shear planes (black and gray lines, respectively) are given. Labels of main faults, tectono-stratigraphic units are shown in Figure 9b and are as in the inset of Figure 1.

4. Displacement and strain rate analysis from GPS data

4.1 Data and methodology

In this section we investigate the deformation and strain rates of the south-central Taiwan fold-and-thrust belt and the western flank of the Central Range using data from the Taiwan GPS network. The station coverage of the network is dense in most of the study area (Fig. 9A), with the exception of the high mountainous areas of the Central Range, the east-central part of the Western Foothills, and the southern part of the Hsuehshan Range. The data set used here is from the period 2005 through 2009 and was processed according to the method of Yu et al., (1997), and the reader is referred there for details. Horizontal velocities are calculated relative to station S01R located on the island of Penghu,

in the Taiwan Strait on stable Eurasia. Strain rates are calculated from the GPS data using the SSPX software of Cardozo & Allmendinger (2009), and the reader is referred there for the background theory. We used a 5 km by 5 km grid and a grid-nearest neighbour interpolation method using the 10 nearest stations within a maximum radius of 35 km. SSPX determines the best fitting strain tensors for each 2D surface of the grid and its corresponding strain ellipse. In Figure 9, we show the displacement vectors, the rotation rate about a vertical axis, the dilatation strain rate, and the maximum shear strain rate, as well as the horizontal maximum compressive and extension strain axes (ε_H) and the maximum shear strain planes. For the sake of clarity in Figure 9, only every second set of horizontal maximum compressive and extension axes are plotted. Below we describe the data set using the kinematic analysis of a body of rock that undergoes translation, rotation, dilation and shear.

5. Displacement vectors and strain rates of south-central Taiwan

The horizontal velocity vectors display an overall northwest to west-northwest sense of displacement in the northern part of the study area, changing to dominantly west directed in the central and much of the southern areas (Fig. 9A). In the southwest, along the coast, the velocity vectors are more southwest directed. Horizontal displacement along the northwestern part of the Western Foothills and throughout the Coastal Plain is very small, whereas in the rest of the study area the horizontal velocities increase overall toward the south and east.

The sense of vertical rotation undergoes several changes from north to south (Fig. 9B), with a clockwise rotation dominating in the Hsuehshan Range and the northern part of the Central Range, whereas counter clockwise rotation is more common in the northern part of the Western Foothills and the Coastal Plain. From about 23.5° N to 22.8° N there is a pronounced zone of clockwise rotation that ends abruptly southward, where a counter clockwise rotation dominates in the extreme southwest. The dilatation strain rate pattern shows a clear change from west to east across the Chaochou- Lishan fault system, with negative values (compression) everywhere in the fold-and-thrust belt and positive values (extension) in the Central Range (Fig. 9C). Note, however, that the small number of stations in the Central Range means that there is a large uncertainty associated with this area. There is a marked decrease in the dilation strain rate in the northwestern part of the Western Foothills and the northern part of the Coastal Plain. The direction of ε_H is oriented roughly northwestward in the northern and northeastern part of the fold-and-thrust belt, rotating to west-northwest in the central and southern part. In the Central Range, the orientation of the extension axes is roughly northeast in the northern part, becoming more westward to west-southwest in the south. The maximum shear strain rate is fairly uniform throughout much of the study area (Fig. 9D). The Western Foothills show slightly higher shear strain rate than the surrounding areas, and there is a slight southward increase. There is a local, east-northeast striking, zone of high shear strain rate in the southwest of the study area. There is a marked, although moderate, decrease in the maximum shear strain rate in the northwestern part of the Western Foothills and the northern part of the Coastal Plain and a moderate, roughly east-northeast striking southward increase at about 23.5° N. The orientations of the dextral maximum shear planes (black in Fig. 9D) change from nearly east-west striking in the northern part of the study area to more southwest striking from c. 24° N southward. In the south, the orientations of the dextral maximum shear planes change eastward from southwest striking to more west striking.

6. Discussion

The importance of reactivation of pre-existing faults in the deformation of an area is thought to be such that this process can control the stress distribution in the crust (Célérier 1995, 2008, Tavani et al. 2015). In the case of pre-existing faults, why reactivation happens is a complex and selective process that depends on several factors, the most important of which are; the orientation and steepness of the pre-existing faults with respect to the principal stress axes, the friction along the fault plane, and the geothermal gradient (Sibson 1985, 1990, 1994, Letouzey 1990, Kelly et al. 1999, Leclère & Fabbri 2013). Fold-and-thrust belts commonly develop in areas where the basement rocks have undergone a previous deformation history and the sediments that overlie them can also have fault systems, facies changes, and possibly a weak contact with the basement [e.g., Rodgers, 1990]. All of these form heterogeneities that can be (re)activated in the compressional stress field of a developing thrust system (Jackson 1980, Wiltschko & Eastman 1983, Sibson 1985, Richard & Krantz 1991, Célérier 1995, 2008, Turner & Williams 2004, Butler et al. 2006, Poblet & Lisle 2011, Bonini et al. 2012, Lacombe & Bellahsen 2016). Below, we first compare and contrast our results with previous stress and strain studies in the area and then go on to investigate whether or not the reactivation of faults inherited from the Eurasian continental margin is a contributing factor to the contemporary stress and strain fields of the south-central Taiwan fold-and-thrust belt.

The result of the contemporary stress analysis of the south-central Taiwan fold-and-thrust belt obtained in this study, which includes the data related to large earthquakes such as Chi-Chi, is in good agreement with that obtained from both paleostress and contemporaneous stress studies carried out in the same area (e.g. Angelier et al. 1986, Suppe, 1995; Lacombe et al. 1999, Chang et al. 2003, Mouthereau & Lacombe 2006, Y.-M. Wu et al. 2008, Y. J. Hsu et al. 2009, S. K. Chen et al. 2017). For example, our analyses of the direction of the contemporary S_H (Fig. 10) shows that it undergoes an important east-west change across the Chaochou fault (but not the Lishan fault) and a north-south change that takes place at about 23.5° N, in agreement with that determined by Chang et al. (2003), Mouthereau & Lacombe (2006), Y.-M. Wu et al. (2008; 2010), Y. J. Hsu et al. (2009) and S. K. Chen et al. (2017). Likewise, there is coincidence in that there is a change in the plunge of $\sigma 1$, from near vertical in the Central Range to subhorizontal in the Western Foothills and the Hsuehshan Range. Our results also coincide with those of S. K. Chen et al. (2017) in that the direction of SH and the plunge of s1 display only minor, if any, change with depth. However, Y.-M. Wu et al. (2010) indicate that there is a 10° to 20° counterclockwise rotation with depth in southern Taiwan that we do not see this in our results. Furthermore, paleostress studies carried out by Angelier et al. (1986), Lacombe et al. (1999) and Chang et al. (2003) are also in general agreement with our calculations of contemporaneous s1. All regional GPS studies indicate a change in the horizontal displacement vector in the fold-and-thrust belt from roughly west-northwest in the north to west and southwest in south. This change takes place at about 23.5° N. Our strain rate results are also in excellent agreement with previous studies carried out in the study area using GPS data (e.g. Bos et al. 2003, Chang et al. 2003, Ching et al. 2007, 2011, J. C. Hu et al. 2007, S. K. Chen et al. 2017). The close agreement between all studies of the contemporaneous stress and strain fields in the fold-and-thrust belt of south-central Taiwan indicate that the features they delineate are robust on a regional scale and can therefore be used to address the hypothesis put forth in Section 1.

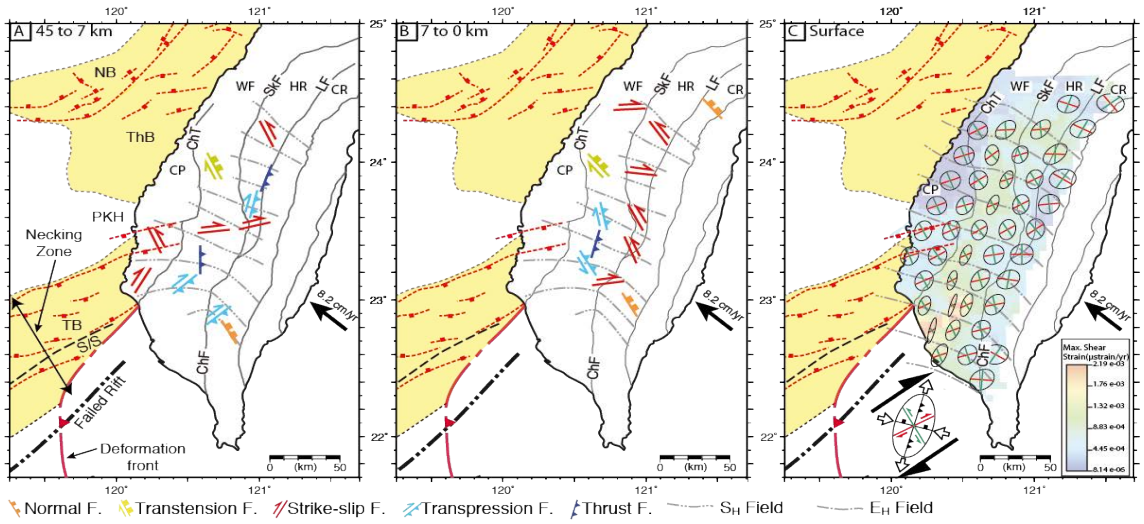

Figure 10

Figure 10: Summary of the stress and strain results for the study area set within the structural and morphological features of the Eurasian continental margin. The relative plate motion vector between the Philippine Sea Plate and Eurasia is shown. A) The most probable fault planes and their kinematics calculated for the basement (the orientations of the secondary planes are shown in Figure 8). An interpolated S_H trajectories are shown by dashed gray lines. B) The most probable fault planes and their kinematics calculated in the fold-and-thrust belt and sedimentary carapace (the orientations of the secondary planes are shown in Figure 8). S_H as in A. C) Maximum shear strain with deformation ellipses determined for groups of four grid units. Dextral and sinistral maximum shear planes are shown in red and green. The interpolated horizontal maximum compression strain rate (ε_H) trajectories are shown by the dashed gray lines. The inset shows the expected fault orientations and kinematics in a dextral strike-slip fault system. The maximum compressive strain field (ε_H) directions from Figure C are shown by dashed gray contour lines. Labels of faults and tectono-stratigraphic units are as in the inset of Figure 1. The failed rift axis shown in Figure 1 is shown in thick black dashed line. S/S = shelf/slope break, TB = Tainan Basin, ThB = Tahishi Basin, NB = Nanjihtao Basin and PkH = Peikang High.

The maximum horizontal stress (S_H) of an area is typically oriented sub-parallel to the relative plate motion (Zoback et al., 1989; Zoback 1992, Gölke & Coblentz 1996; Townend et al., 2012), which, in the case of Taiwan, is roughly toward about 306° (Figs. 1 and 10) (Yu et al., 1997, J. Wu et al. 2016). Large intraplate forces, such as isostatic compensation or lithosphere flexure can also have an important effect on the regional stress field, while at a more local scale S_H can also be affected by features such as weak faults, structural highs, recent sedimentation or topography (e.g. Tingay et al., 2005). In the study area, there is a marked contrast in the direction of S_H from north to south (Fig. 10). In the north, the direction of S_H remains roughly sub-parallel to the relative plate motion vector from the Central Range westward into the Coastal Plain. In the south, however, there is a nearly 45° counterclockwise rotation in the direction of S_H from the Central Range westward across the Chaochou fault and into the Coastal Plain (Fig. 10) (see also Chang et al. (2003), Y.-M. Wu et al. (2010), S. K. Chen et al. (2017)). The direction of ε_H and the orientations of the dextral maximum shear planes both display an overall rotation southward (Fig. 9).

The north-south change in the directions of the contemporaneous S_H, ε_H, the dextral maximum shear planes, and the horizontal velocity vectors at about 23.5° N has been interpreted to be related to the so-called Peikang High (Fig. 1) (J. C. Hu et al. 1997, Bos et al. 2003, Chang et al. 2003, Mouthereau & Lacombe 2006, Ching et al. 2007, 2011, Y.-M. Wu et al. 2008, 2010, Y. J. Hsu et al. 2009, S. K.

Chen et al. 2017). Many of these authors interpret the Peikang High to be a symmetrical structural high, or horst (see Twiss & Moores (1992) for a definition of horst), in the extensional fault system developed on the margin shelf that acts as a symmetrical indenter around which rocks in the fold-and-thrust belt are moving. Nevertheless, as was pointed out by Mouthereau & Lacombe (2006), neither the paleostress nor the contemporaneous s1 trajectories around the Peikang High fit with those estimated by analogue (C.-W. Lin & Huang 1998) and numerical models of it (e.g. J. Hu & Angelier 1996, J. C. Hu et al. 1997, C.-W. Lin & Huang 1998). Nor do the contemporaneous stress trajectories, the horizontal displacement field, or the strain field (Fig. 10) fit with those predicted to occur around an indentor into a fold-and-thrust belt (e.g. Macedo & Marshak 1999, Marshak 2004).

Reflection seismic and wide-angle velocity profiling show that from about 23.5° N (the southern flank of the Peikang High) (Figs. 1 and 2) the basement thins from c. 30 km on the shelf area to less than 10 km in the area of the failed rift at the base of the slope (e.g. Yeh et al. 2012, Lester et al. 2014, McIntosh et al. 2014, Brown et al. 2017). This is the structural feature that we call the necking zone. Southward, is the morphological feature that is the continental slope. It is across this highly structured area, with its east-northeast strike for both the onset of the necking zone and the shelf/slope break (Figs. 1 and 2), its thinning basement and thickening sedimentary cover, and its extensional fault system where the major changes in the stress, strain, and displacement fields of the southern part of the Taiwan fold-and-thrust belt take place (Figs. 7, 9, and 10). We therefore suggest, in agreement with Mouthereau & Lacombe (2006), that the southward change in the SH direction, in the strain rate derived directions of eH and dextral maximum shear planes, and in the horizontal displacement field vectors that begin at about 23.5° N are not due to a symmetrical indentor, but rather to the reactivation of faults related to the complex rifted margin geometry in this area.

The change across the Chaochou fault, but not the Lishan fault is more difficult to interpret. It is possible that it reflects a local stress perturbation related to differences in the topography from east to west (large difference across the Chaochou fault, but almost no difference across the Lishan fault). It can also, in part, be the effect of differently oriented pre-existing faults in the basement between southern Taiwan and the Hsuehshan Range in the north. Nevertheless, there is close agreement between the inferred extensional faulting stress regime and the strain rate derived extension in the Central Range.

7. Conclusions

In this study, we have shown that there are important changes, particularly in the contemporaneous stress and GPS velocity fields, but also in the strain field, from the continental shelf to the margins necking zone. In the north of the study area, and along the entire western flank of the Central Range, the S_H and the ε_H directions are sub-parallel to the direction of relative plate motion (306°) between the Philippine Sea and the Eurasian plates. In the southwest, where the necking zone of the margin is entering into the deformation of the fold-and-thrust belt, S_H, and both the directions of ε_H and dextral maximum shear planes undergo important rotations. In the case of S_H, these rotations go up to 45°. Where the upper part of the necking zone is involved in the deformation, the estimated most likely activated fault orientations determined from the stress inversion is east-northeast, roughly

parallel to known fault systems in the basement. The fault type is dominantly dextral strike-slip and transpressive. In the far southwest, an east-northeast striking zone of high shear strain rate coincides with the onshore projection of a failed rift imaged by reflection seismic data offshore. A paucity of seismicity in this area precludes an estimation of the principal stress axes orientations and determination of fault type, but the calculated strain ellipse is in keeping with it also being a zone of dextral strike-slip faulting (Fig. 10C).

These observations further corroborate our previous interpretations (Brown et al. 2012, 2017, Camanni et al. 2014, 2016, Alvarez-Marron et al. 2014, Biete et al. 2018) that there is a causal link between the reactivation of the inherited morphology and structure of the Eurasian continental margin. In particular, the east-northeast striking fault systems inherited from the necking zone of the continental margin are optimally oriented relative to SH for reactivation (Sibson 1990, 1994, Kelly et al. 1999, Leclère & Fabbri 2013). In the southwest of the study area, therefore, it appears that it is the reactivation of these inherited structures that is controlling the contemporaneous stress field (e.g., Célérier 2008, Tavani et al. 2015) since this stress field is calculated from earthquakes that occur along them. Farther north, however, the close coincidence between directions of S_H and ε_H with the relative plate motion vector suggest that it is the plate boundary forces that control the stress and strain fields (e.g., Richardson 1992, Zoback 1992, Gölke & Coblentz 1996).

Finally, there are important north to south changes in both the stress and strain fields from the western flank of the Central Range across the Chaochou-Lishan fault system into the fold-and-thrust belt. The results of both the stress inversion and the GPS derived strain rates show that the upper crust of western flank of the Central Range (we do not investigate the east part in this study) is under extension while that of the fold-and-thrust belt to the west is under compression. Few data exist in the Central Range for depths greater than 15 km, but these appear to indicate that the deeper crust is under compression (see also, S.K. Chen et al. 2017). Nevertheless, there is a clear rotation of the directions of SH and the directions of eH and dextral maximum shear planes across the Chaochou fault in the south, but no noticeable change across the Lishan fault in the north. A possible explanation for this difference may be that the north-south differences in topography across this fault system are locally influencing the stress and strain fields (e.g., Richardson 1992, Gölke & Coblentz 1996).

Acknowledgments

D. B., J. A-M., and C. B. acknowledge funding provided by the Spanish Ministerio de Ciencia, Innovación y Universidades grants CGL2013-43877-P. H. and PGC2018-094227-B-I00, with additional support from the Generalitat de Catalunya grant 2017SGR1022. The editor A. Ferreira, and the reviewers O. Lacombe and V. Vavrycuk are acknowledged. The authors gratefully acknowledge Wessel et al. (1998) for the Generic Mapping Tool (GMT) software that was used in plotting some of the figures.

References

Allmendinger, R.W., Cardozo, N. & Fisher, D.M. (2012). Structural Geology Algorithms Vectors and Tensors, 1st Editio., Cambridge University Press.

Alvarez-Marron, J., Brown, D., Camanni, G., Wu, Y.-M. & Kuo-Chen, H. (2014). Structural complexities in a foreland thrust belt inherited from the shelf-slope transition: Insights from the Alishan area of Taiwan. Tectonics, 33, 1322–1339, American Geophysical Union. doi:10.1002/2014TC003584

Angelier, J., Barrier, E. & Hao Tsu Chu. (1986) Plate collision and paleostress trajectories in a fold-thrust belt: The foothills of Taiwan. Tectonophysics, 125, 161–178. doi:10.1016/0040-1951(86)90012-0

Arnold, R. & Townend, J., 2007. A Bayesian approach to estimating tectonic stress from seismological data, Geophys. J. Int., 170, 1336–1356, doi: 10.1111/j.1365-246X.2007.03485.x.

Becker, A. (2000) The Jura Mountains -- an active foreland fold-and-thrust belt? Tectonophysics, 321, 381. doi:10.1016/s0040-1951(00)00089-5

Biete, C., Alvarez-Marron, J., Brown, D. & Kuo-Chen, H. (2018) The Structure of Southwest Taiwan: The Development of a Fold-and-Thrust Belt on a Margins Outer Shelf and Slope. Tectonics, 37, 1973–1993. doi:10.1029/2017TC004910

Bonini, M., Sani, F. & Antonielli, B. (2012) Basin inversion and contractional reactivation of inherited normal faults: A review based on previous and new experimental models. Tectonophysics, 522–523, 55–88, Elsevier B.V. doi:10.1016/j.tecto.2011.11.014

Bos, A.G., Spakman, W. & Nyst, M.C.J. (2003) Surface deformation and tectonic setting of Taiwan inferred from a GPS velocity field. J. Geophys. Res. Solid Earth, 108, 1–18. doi:10.1029/2002JB002336

Briais, A., Patriat, P. & Tapponnier, P. (1993) Updated interpretation of magnetic anomalies and seafloor spreading stages in the south China Sea: Implications for the Tertiary tectonics of Southeast Asia. J. Geophys. Res. Solid Earth, 98, 6299–6328. doi:10.1029/92JB02280

Brocher, T.M. (2005) Empirical Relations between Elastic Wavespeeds and Density in the Earth's Crust. Am. J. Heal. Pharm., 62, 889–890. doi:10.1785/0120050077

Brown, D., Alvarez-Marron, J., Biete, C., Kuo-Chen, H., Camanni, G. & Ho, C.-W. (2017) How the structural architecture of the Eurasian continental margin affects the structure, seismicity, and topography of the south central Taiwan fold-and-thrust belt. Tectonics, 36. doi:10.1002/2017TC004475

Brown, D., Alvarez-Marron, J., Schimmel, M., Wu, Y.-M. & Camanni, G. (2012) The structure and kinematics of the central Taiwan mountain belt derived from geological and seismicity data. Tectonics, 31, 1–25. doi:10.1029/2012TC003156

Butler, R.W.H., Tavarnelli, E. & Grasso, M. (2006) Structural inheritance in mountain belts: An Alpine-Apennine perspective. J. Struct. Geol., 28, 1893–1908. doi:10.1016/j.jsg.2006.09.006

Camanni, G., Alvarez-Marron, J., Brown, D., Ayala, C., Wu, Y.-M. & Hsieh, H.-H. (2016) The deep

structure of south-central Taiwan illuminated by seismic tomography and earthquake hypocenter data. Tectonophysics. doi:10.1016/j.tecto.2015.09.016

Camanni, G., Brown, D., Alvarez-Marron, J., Wu, Y.-M. & Chen, H. -a. (2014) The Shuilikeng fault in the central Taiwan mountain belt. J. Geol. Soc. London., 171, 117–130. //doi.org/10.1144/jgs2013-014

Cardozo, N. & Allmendinger, R.W. (2009) SSPX: A program to compute strain from displacement/velocity data. Comput. Geosci., 35, 1343–1357, Elsevier. doi:10.1016/j.cageo.2008.05.008

Carena, S., Suppe, J. & Kao, H. (2002) Active detachment of Taiwan illuminated by small earthquakes and its control of first-order topography. Geology, 30, 935–938. doi:10.1130/0091-7613(2002)030<0935:ADOTIB>2.0.CO;2

Célérier, B. (1995) Tectonic regime and slip orientation of reactivated faults. Geophys. J. Int., 121, 143–161. doi:10.1111/j.1365-246X.1995.tb03517.x

Célérier, B. (2008) Seeking Aderson's faulting in seismicity: A centennial celebration. Rev. Geophys., 46, 1–34. doi:10.1029/2007RG000240

Chang, C.-P., Chang, T.Y., Angelier, J., Kao, H., Lee, J.C. & Yu, S.B. (2003) Strain and stress field in Taiwan oblique convergent system: Constraints from GPS observation and tectonic data. Earth Planet. Sci. Lett., 214, 115–127. doi:10.1016/S0012-821X(03)00360-1

Chen, C.-H. (2000), Geological map of Taiwan, scale 1:500,000, Central Geological Survey, Taipei.

Chen, S.K., Wu, Y.-M., Hsu, Y.J. & Chan, Y.C. (2017) Current crustal deformation of the Taiwan orogen reassessed by cGPS strain-rate estimation and focal mechanism stress inversion. Geophys. J. Int., 210, 228–239. doi:10.1093/gji/ggx165

Chen, W. & Molnar, P. (1983) Focal depth of intracontinental and intraplate earthquakes and their implications for thermal and mechanical properties of the lithosphere. J. Geophys. Res., 88, 4183–4214. doi:http://dx.doi.org/10.1029/JB088iB05p04183; doi:10.

Ching, K.E., Rau, R.J., Johnson, K.M., Lee, J.C. & Hu, J.C. (2011) Present-day kinematics of active mountain building in Taiwan from GPS observations during 1995-2005. J. Geophys. Res. Solid Earth, 116, 1–22. doi:10.1029/2010JB008058

Ching, K.E., Rau, R.J., Lee, J.C. & Hu, J.C. (2007) Contemporary deformation of tectonic escape in SW Taiwan from GPS observations, 1995-2005. Earth Planet. Sci. Lett., 262, 601–619. doi:10.1016/j.epsl.2007.08.017

Chiu, H.T. (1975) Miocene stratigraphy and its relation to the Palaeogene rocks in West - Central Taiwan. Pet. Geol. Taiwan, 12, 51–80.

Ding, W., Li, J., Li, M., Qiu, X., Fang, Y. & Tang, Y. (2008) A Cenozoic tectono-sedimentary model of the Tainan Basin, the South China Sea: evidence from a multi-channel seismic profile. J. Zhejiang Univ. A, 9, 702–713. doi:10.1631/jzus.A071572

Erslev, E.A. (1993) Thrusts, back-thrusts, and detachment of Rocky Mountain foreland arches. in Laramide basement deformation in the rocky mountains foreland of the western United States: Boulder, Colorado, pp. 339–358. doi:10.1130/SPE280-p339

Gölke, M. & Coblentz, D. (1996) Origins of the European regional stress field. Tectonophysics, 266, 11–24. doi:10.1016/S0040-1951(96)00180-1

Hardebeck, J.L. & Hauksson, E. (2001) Crustal stress field in southern California and its implications for fault mechanics, , J. Geophys. Res., 106, 21,859-21,882

Hardebeck, J.L. & Michael, A.J. (2004) Stress orientations at intermediate angles to the San Andreas Fault, California. J. Geophys. Res. 109, B11303, doi:10.1029/2004JB003239

Hardebeck, J.L. & Okada, T. (2018) Temporal Stress Changes Caused by Earthquakes: A Review. J. Geophys. Res. Solid Earth, 123, 1350–1365. doi:10.1002/2017JB014617

Hensch, M., Lund, B., Árnadóttir, Th., Brandsdóttir, B. (2016) Temporal stress changes associated with the 2008 May 29 Mw 6 earthquake doublet in the western South Iceland Seismic Zone, Geophys. J. Int., 204, 544-554, doi: 10.1093/gji/ggv465

Ho, C.S. (1988) An Introduction to the Geology of Taiwan: Explanatory text of the Geological Map of Taiwan, Central Geol. Sur., Taipei, Taiwan.

Homberg, C., Bergerat, F., Philippe, Y., Lacombe, O. & Angelier, J. (2002) Structural inheritance and cenozoic stress fields in the Jura fold-and-thrust belt (France). Tectonophysics, 357, 137–158. doi:10.1016/S0040-1951(02)00366-9

Hsu, S.K., Sibuet, J.C. & Shyu, C.T. (2001) Magnetic inversion in the East China Sea and Okinawa Trough: Tectonic implications. Tectonophysics, 333, 111–122. doi:10.1016/S0040-1951(00)00270-5

Hsu, Y.J., Yu, S.B., Kuo, L.C., Tsai, Y.C. & Chen, H.Y. (2011) Coseismic deformation of the 2010 Jiashian, Taiwan earthquake and implications for fault activities in southwestern Taiwan. Tectonophysics, 502, 328–335, Elsevier B.V. doi:10.1016/j.tecto.2011.02.005

Hsu, Y.J., Yu, S.B., Simons, M., Kuo, L.C. & Chen, H.Y. (2009) Interseismic crustal deformation in the Taiwan plate boundary zone revealed by GPS observations, seismicity, and earthquake focal mechanisms. Tectonophysics, 479, 4–18, Elsevier B.V. doi:10.1016/j.tecto.2008.11.016

Hu, J. & Angelier, J. (1996) Modeling of stress-deformation relationships in a collision belt: Taiwan. Terr. Atmos. Ocean. Sci., 447–465.

Hu, J.C., Angelier, J. & Yu, S.B. (1997) An interpretation of the active deformation of southern Taiwan based on numerical simulation and GPS studies. Tectonophysics, 274, 145–169. doi:10.1016/S0040-1951(96)00302-2

Hu, J.C., Hou, C.S., Shen, L.C., Chan, Y.C., Chen, R.F., Huang, C., Rau, R.J., et al. (2007) Fault activity and lateral extrusion inferred from velocity field revealed by GPS measurements in the Pingtung area of southwestern Taiwan. J. Asian Earth Sci., 31, 287–302. doi:10.1016/j.jseaes.2006.07.020

Huang, C. & Byrne, T.B. (2014) Tectonic evolution of an active tectonostratigraphic boundary in accretionary wedge: An example from the Tulungwan-Chaochou Fault system, southern Taiwan. J. Struct. Geol., 69, 320–333, Elsevier Ltd. doi:10.1016/j.jsg.2014.06.007

Huang, C.Y., Yen, Y., Zhao, Q.H. & Lin, C.T. (2012) Cenozoic stratigraphy of Taiwan: Window into rifting, stratigraphy and paleoceanography of South China Sea. Chinese Sci. Bull., 57, 3130–3149. doi:10.1007/s11434-012-5349-y

Husen S., Hardebeck J.L. (2010), Earthquake Location Accuracy. Community Online Resour. for Stat. Seism. Anal. (2010), pp. 1-35, 10.5078/corssa 55815573

Jackson, J.A. (1980) Reactivation of basement faults and crustal shortening in orogenic belts. Nature, 283, 343–346. doi:10.1038/283343a0

Jahn, B.-M., Chi, W.R. & Yui, T.F. (1992) A late permian formation of Taiwan (marbles from Chia-Li well no.1) Pb-Pb isochron and Sr isotopic evidence, and its regional geological significance. J. Geol. Soc. China.

Kagan, Y.Y. (2005) Double-couple earthquake focal mechanism: random rotation and display, Geophys. J. Int., 163, 1065 – 1072, doi: 10.1111/j.1365-246X.2005.02781.x

Kelly, P.G., Peacock, D.C.P., Sanderson, D.J. & McGurk, A.C. (1999) Selective reverse-reactivation of normal faults, and deformation around reverse-reactivated faults in the Mesozoic of the Somerset coast. J. Struct. Geol., 21, 493–509. doi:10.1016/S0191-8141(99)00041-3

King, R.C., Hillis, R.R., Tingay, M.R.P. & Morley, C.K. (2009) Present-day stress and neotectonic provinces of the Baram Delta and deep-water fold-thrust belt. J. Geol. Soc. London., 166, 197–200. doi:10.1144/0016-76492008-062R

Kuo-Chen, H., Wu, F., Chang, W.L., Chang, C.Y., Cheng, C.Y. & Hirata, N. (2015) Is the Lishan fault of Taiwan active? Tectonophysics, 661, 210–214, Elsevier B.V. doi:10.1016/j.tecto.2015.09.002

Kuo-Chen, H., Wu, F.T. & Roecker, S.W. (2012) Three-dimensional P velocity structures of the lithosphere beneath Taiwan from the analysis of TAIGER and related seismic data sets. J. Geophys. Res. Solid Earth, 117, 1–19. doi:10.1029/2011JB009108

Lacombe, O. & Bellahsen, M. (2016) Thick-skinned tectonics and basement-involved fold–thrust belts: insights from selected Cenozoic orogens. Geol. Mag., Vol. 153. doi:10.1017/S0016756816000078

Lacombe, O., Mouthereau, F., Deffontaines, B., Angelier, J., Chu, H.T. & Lee, C.T. (1999) Geometry and Quaternary kinematics of fold-and-thrust units of southwestern Taiwan. Tectonics, 18, 1198–1223. doi:10.1029/1999TC900036

Lacombe, O., Mouthereau, F., Kargar, S. & Meyer, B. (2006) Late Cenozoic and modern stress fields in the western Fars (Iran): Implications for the tectonic and kinematic evolution of central Zagros. Tectonics, 25, 1–27. doi:10.1029/2005TC001831

Lan, C.Y., Lee, C.S., Yui, T.F., Chu, H.T. & Jahn, B.M. (2008) The tectono-thermal events of Taiwan and their relationship with SE China. Terr. Atmos. Ocean. Sci., 19, 257–278. doi:10.3319/

TAO.2008.19.3.257(TT)

Leclère, H. & Fabbri, O. (2013) A new three-dimensional method of fault reactivation analysis. J. Struct. Geol., 48, 153–161, Elsevier Ltd. doi:10.1016/j.jsg.2012.11.004

Lester, R., Avendonk, H.J. a. Van, Mcintosh, K., Lavier, L., Liu, C.-S., Wang, T.K. & Wu, F. (2014) Rifting and magmatism in the northeastern South China Sea from wide-angle tomography and seismic reflection imaging. J. Geophys. Res. Solid Earth, 119, 2305–2323. doi:10.1002/2013JB010639

Letouzey, J. (1990) Fault reactivation, inversion and fold-thrust belt. Pet. tectonics Mob. belts, pp. 101–128.

Li, C.F., Zhou, Z., Li, J., Hao, H. & Geng, J. (2007) Structures of the northeastern most South China Sea continental margin and ocean basin: Geophysical constraints and tectonic implications. Mar. Geophys. Res., 28, 59–79. doi:10.1007/s11001-007-9014-9

Lin, A.T., Liu, C.-S., Lin, C.C., Schnurle, P., Chen, G.Y., Liao, W.Z., Teng, L.S., et al. (2008) Tectonic features associated with the overriding of an accretionary wedge on top of a rifted continental margin: An example from Taiwan. Mar. Geol., 255, 186–203, Elsevier B.V. doi:10.1016/j.margeo.2008.10.002

Lin, A.T. & Watts, A.B. (2002) Origin of the West Taiwan basin by orogenic loading and flexure of a rifted continental margin. J. Geophys. Res., 107, 2185. doi:10.1029/2001JB000669

Lin, A.T., Watts, A.B. & Hesselbo, S.P. (2003) Cenozoic stratigraphy and subsidence history of the South China Sea margin in the Taiwan region. Basin Res., 15, 453–478. doi:10.1046/j.1365-2117.2003.00215.x

Lin, C.-W. & Huang, M.-L. (1998) Influence of the Peikang Basement high on the structure development of the western foothills and coastal plain in south central Taiwan: a sandbox approach. Pet. Geol. Taiwan, 32, 105–122

Lund, B. & Slunga, R. (1999) Stress tensor inversion using detailed microearthquake information and stability constraints : Application to to Ölfus southwest Iceland. J. Geophys. Res., 104, 14947–14964. doi:10.1029/1999JB900111

Lund, B. & Townend, J. (2007) Calculating horizontal stress orientations with full or partial knowledge of the tectonic stress tensor. Geophys. J. Int., 170, 1328–1335. doi:10.1111/j.1365-246X.2007.03468.x

Macedo, J. & Marshak, S. (1999) Controls on the geometry of fold-thrust belt salients. GSA Bull., 111, 1808–1822. Retrieved from http://dx.doi.org/10.1130/0016-7606(1999)111%3C1808:COTGOF%3E2.3.CO

Marshak, S. (2004) Salients, Recesses, Arcs, Oroclines, and Syntaxes — A Review of Ideas Concerning the Formation of Map-view Curves in Fold-thrust Belts. Thrust tectonics Hydrocarb. Syst. AAPG Mem. 82, 82, 131–156.

McIntosh, K., Lavier, L., Avendonk, H. van, Lester, R., Eakin, D. & Liu, C.S. (2014) Crustal structure and inferred rifting processes in the northeast South China Sea. Mar. Pet. Geol., 58, 612–626,

Elsevier Ltd. doi:10.1016/j.marpetgeo.2014.03.012

McKenzie, D. P., (1969). The relation between fault plane solutions for earthquakes and the directions of the principal stresses, Bull. Seismol. So . Am. , 59 , 591-601.

Michael, A. (1987) Use of Focal Mechanims to Determine Stress: A Control Study, 92, 357–368.

Mohn, G., Manatschal, G., Beltrando, M., Masini, E. & Kusznir, N. (2012) Necking of continental crust in magma-poor rifted margins: Evidence from the fossil Alpine Tethys margins. Tectonics, 31, 1–28. doi:10.1029/2011TC002961

Mouthereau, F. & Lacombe, O. (2006) Inversion of the Paleogene Chinese continental margin and thick-skinned deformation in the Western Foreland of Taiwan. J. Struct. Geol., 28, 1977–1993. doi:10.1016/j.jsg.2006.08.007

Oncken, O. (1988) Aspects of the Reconstruction of the Stress History of a Fold and Thrust Belt (Rhenish-Massif, Federal-Republic-of-Germany). Tectonophysics, 152, 19–40.

Peyret, M., Dominguez, S., Cattin, R., Champenois, J., Leroy, M. & Zajac, A. (2011) Present-day interseismic surface deformation along the Longitudinal Valley, eastern Taiwan, from a PS-InSAR analysis of the ERS satellite archives. J. Geophys. Res. Solid Earth, 116, 1–21. doi:10.1029/2010JB007898

Poblet, J. & Lisle, R.J. (2011) Kinematic evolution and structural styles of fold-and-thrust belts. Geol. Soc. London, Spec. Publ., 349, 1–24. doi:10.1144/SP349.1

Richard, P. & Krantz, R.W. (1991) Experiments on fault reactivation in strike slip mode. Tectonophysics, 188, 117–131. Retrieved from file://localhost/Users/jescartin/WORK/Referencias/pdfs/Richard1991.pdf

Richardson, R.M., 1992. Ridge Forces, Absolute Plate Motions, and the Intraplate Stress Field, Journal of Geophysical Research, 97: 11,739-11,748.

Rodgers, J. (1990) Fold-and-thrust belts in sedimentary rocks; Part 1, Typical examples. Am. J. Sci. April 1, 290:321-359

Rodriguez-Roa, F. a. & Wiltschko, D. V. (2010) Thrust belt architecture of the central and southern Western Foothills of Taiwan. Geol. Soc. London, Spec. Publ., 348, 137–168. doi:10.1144/SP348.8

Saintot, A. & Angelier, J. (2002) Tectonic paleostress fields and structural evolution of the NW-Caucasus fold-and-thrust belt from Late Cretaceous to Quaternary. Tectonophysics, 357, 1–31. doi:10.1016/S0040-1951(02)00360-8

Shaw, C.-L. (1996) Stratigraphic correlation and isopach maps of the western Taiwan Basin. Terr. Atmos. Ocean. Sci., 7, 333–360.

Sibson, R.H. (1983) Continental fault structure and the shallow earthquake source. J. Geol. Soc. London., 140, 741–767. doi:10.1144/gsjgs.140.5.0741

Sibson, R.H. (1985) A note on fault reactivation. J. Struct. Geol., 7, 3–6.

Sibson, R.H. (1990) Conditions for fault-valve behaviour. Geol. Soc. London, Spec. Publ., 54, 15–28. doi:10.1144/GSL.SP.1990.054.01.02

Sibson, R.H. (1994) Crustal stress, faulting and fluid flow. Geol. Soc. London, Spec. Publ., 78, 69 LP-84. doi:https://doi.org/10.1144/GSL.SP.1994.078.01.07

Suppe, J. (1995) Present-day stress directions in Western Taiwan inferred from borehole elongation. Petrol. Geol. Taiwan, 21, 1-12.

Tang, C.C., Zhu, L., Chen, C.H. & Teng, T.L. (2011) Significant crustal structural variation across the Chaochou Fault, southern Taiwan: New tectonic implications for convergent plate boundary. J. Asian Earth Sci., 41, 564–570, Elsevier Ltd. doi:10.1016/j.jseaes.2010.12.003

Tavani, S., Storti, F., Lacombe, O., Corradetti, A., Muñoz, J.A. & Mazzoli, S. (2015) A review of deformation pattern templates in foreland basin systems and fold-and-thrust belts: Implications for the state of stress in the frontal regions of thrust wedges. Earth-Science Rev., 141, 82–104, Elsevier B.V. doi:10.1016/j.earscirev.2014.11.013

Teng, L.S. (1992) Geotectonic evolution of the Tertiary continental margin basins of Taiwan. Petroleum. Geol. Taiwan, 27, 1-19.

Teng, L.S. & Lin, A.T. (2004) Cenozoic tectonics of the China continental margin: insights from Taiwan. Geol. Soc. London, Spec. Publ., 226, 313–332. doi:10.1144/GSL.SP.2004.226.01.17

Tingay, M., Müller, B., Reinecker, J., Heidbach, O., Wenzel, F. & Fleckenstein, P. (2005) Understanding tectonic stress in the oil patch: The World Stress Map Project. Lead. Edge, 24, 1276–1282. doi:10.1190/1.2149653

Townend, J., Sherburn, S., Arnold, R., Boese, C. & Woods, L. (2012) Three-dimensional variations in present-day tectonic stress along the Australia-Pacific plate boundary in New Zealand. Earth Planet. Sci. Lett., 353-354, 47-59.

Townend, J. & Zoback, M.D., 2006. Stress, strain, and mountain building in central Japan, J. geophys. Res., 111, B03411, doi:10.1029/2005JB003759.

Twiss, R.J. & Moores, E.M. (1992) Structural Geology. W.H. Freeman and Company, New York, p. 532

Turner, J.P. & Williams, G.A. (2004) Sedimentary basin inversion and intra-plate shortening. Earth-Science Rev., 65, 277–304. doi:10.1016/j.earscirev.2003.10.002

Vavrycuk, V. (2014) Iterative joint inversion for stress and fault orientations from focal mechanisms. Geophys. J. Int., 199, 69–77. doi:10.1093/gji/ggu224

Waldhauser, F. (2001) hypoDD - A program to compute double-difference hypocenter locations. U.S. Geol. Surv. Open File Rep., 1–25. doi:https://doi.org/10.3133/ofr01113

Waldhauser, F. & Ellsworth, W.L. (2000) A Double-Difference Earthquake Location Algorithm: Method and Application to the Northern Hayward Fault, California. Bull. Seismol. Soc. Am., 90,

1353–1368. doi:10.1785/0120000006

Wang, C.-Y., Chang, C.-H., & Yen, H.-Y. (2000) An interpretation of the 1999 Chi-Chi earthquake on the thin-skinned thrust model. Terr. Atmos. Ocean. 11, 609-630.

Wessel, P., & Smith, W. (1998). New, improved version of generic mapping tools released. Eos., 79(47), 579.

Wiltschko, D. & Eastman, D. (1983) Role of basement warps and faults in localizing thrust fault ramps. in Geological Society of America, pp. 177–190. doi:10.1130/MEM158-p177

Wiltschko, D. V., Hassler, L., Hung, J.-H. & Liao, H.-S. (2010) From accretion to collision: Motion and evolution of the Chaochou Fault, southern Taiwan. Tectonics, 29, 1–23. doi:10.1029/2008TC002398

Wu, J., Suppe, J., Lu, R., & Kanda, R. (2016) Philippine Sea and East Asian plate tectonics since 52 Ma constrained by new subducted slab reconstruction methods. J. Geophys. Res. Solid Earth, 121, 4670–4741, doi:10.1002/ 2016JB012923.

Wu, S.K., Chi, W.C., Hsu, S.M., Ke, C.C. & Wang, Y. (2013) Shallow crustal thermal structures of central Taiwan foothills region. Terr. Atmos. Ocean. Sci., 24, 695–707. doi:10.3319/TAO.2013.03.13.01(T)

Wu, Y.-M., Hsu, Y.-J., Chang, C.-H., Teng, L.S. & Nakamura, M. (2010) Temporal and spatial variation of stress field in Taiwan from 1991 to 2007: Insights from comprehensive first motion focal mechanism catalog. Earth Planet. Sci. Lett., 298, 306–316. doi:10.1016/j.epsl.2010.07.047

Wu, Y.-M., Zhao, L., Chang, C.-H. & Hsu, Y.J. (2008) Focal-mechanism determination in Taiwan by genetic algorithm. Bull. Seismol. Soc. Am., 98, 651–661. doi:10.1785/0120070115

Yang, K.-M., Rau, R.-J., Chang, H.-Y., Hsieh, C.-Y., Ting, H.-H., Huang, S.-T., Wu, J.-C., et al. (2016) The role of basement-involved normal faults in the recent tectonics of western Taiwan. Geol. Mag., 1–26. doi:10.1017/S0016756816000637

Yang, K.-M., Ting, H.-H. & Yuan, J. (1991) Structural Styles and tectonic Modes of Neogene Extensional Tectonics in Southwestern Taiwan: Implications for Hydrocarbon Exploration. Pet. Geol. Taiwan, 26, 31

Yeh, Y.C., Hsu, S.K., Doo, W. Bin, Sibuet, J.C., Liu, C.S. & Lee, C.S. (2012) Crustal features of the northeastern South China Sea: Insights from seismic and magnetic interpretations. Mar. Geophys. Res., 33, 307–326. doi:10.1007/s11001-012-9154-4

Yu, S., Chen, H. & Kuo, L. (1997) Velocity field of GPS stations in the Taiwan area. Tectonophysics, 274, 41–59. doi:10.1016/S0040-1951(96)00297-1

Yue, L.-F., Suppe, J., Hung, J.-H., (2005). Structural geology of a classic thrust belt earth- quake: the 1999 Chi-Chi earthquake Taiwan (Mw = 7.6). J. Struct. Geol. 27 (11), 2058–2083.

Zoback, M.L. (1992) First- and second-order patterns of stress in the lithosphere: the World stress map project. J. Geophys. Res. Earth, 97, 11703–11728.

Zoback, M.L., Zoback, M.D., Adams, J., Assumpaçao, M., Bell, S., bergman, E.A., Blümling, P., Brereton, N.R., Denham, D., Ding, J., Fuchs, K., Gay, N., gregersen, S., Gupta, H.K., Gvishiani, A., Jacob, K., Kñein, R., Knoll, P., Magee, M., Mercier, J.L., Müller, B.C., Paquin, C., Rajendran, K., Stephansson, O., Suarez, G., Suter, M., udias, A., Xu, Z.H. & Zhizhin, M. (1989) Global patterns of tectonic stress. Nature, 341, 291-298.

Paper III:

The Structure of Southwest Taiwan: The Development of a Fold-and-Thrust Belt on a Margins Outer Shelf and Slope

Cristina Biete[1], Joaquina Alvarez-Marron[1], Dennis Brown[1], and Hao Kuo-Chen[2]

[1] Institute of Earth Sciences Jaume Almera, ICTJA-CSIC, Lluis Sole i Sabaris s/n, 08028 Barcelona, Spain

[2] Department of Earth Sciences, National Central University, Jongli, Taiwan

Status of the paper: Published in Tectonics, 2018, 37, 1973–1993. https://doi.org/10.1029/2017TC004910

Contributions of the Ph.D. candidate to the article:

- Carried out structural mapping fieldwork;
- Constructed the balanced and restored cross-sections, the along-strike sections, the 3D basal thrust and cut-off maps in collaboration with Ph.D. supervisors;
- Did the illustrations;
- Wrote the manuscript with the supervision of the Ph.D. supervisors.

AGU100 ADVANCING EARTH AND SPACE SCIENCE

Tectonics

RESEARCH ARTICLE
10.1029/2017TC004910

Key Points:
- Structure of the fold-and-trust belt in southwest Taiwan
- Development of a fold-and-thrust belt on the outer continental margin and slope
- Along-strike changes in structure that have a causal relationship with variations in the basal thrust that, in turn, is related to basement

Supporting Information:
- Supporting Information S1
- Table S1
- Figure S1

Correspondence to:
D. Brown,
dbrown@ictja.csic.es

Citation:
Biete, C., Alvarez-Marron, J., Brown, D., & Kuo-Chen, H. (2018). The structure of southwest Taiwan: The development of a fold-and-thrust belt on a margins outer shelf and slope. *Tectonics, 37*, 1973–1993. https://doi.org/10.1029/2017TC004910

Received 29 NOV 2017
Accepted 18 JUN 2018
Accepted article online 26 JUN 2018
Published online 16 JUL 2018

The Structure of Southwest Taiwan: The Development of a Fold-and-Thrust Belt on a Margins Outer Shelf and Slope

Cristina Biete[1], Joaquina Alvarez-Marron[1], Dennis Brown[1], and Hao Kuo-Chen[2]

[1]Institute of Earth Sciences, Barcelona, Spain, [2]Department of Earth Science, National Central University, Zhongli, Taiwan

Abstract The southwest Taiwan fold-and-thrust belt is forming on the outer shelf and slope of the Eurasian continental margin. It comprises a roughly N-S striking, west verging imbricate thrust system that has been developing since the Late Miocene. Here we present the results of new surface geological mapping from which we construct balanced and restored cross sections and along-strike sections. From these we compile maps of the basal thrust, thrust branch lines and, where possible, stratigraphic cutoffs. To interpret the structure in the subsurface and beneath the basal thrust, we use a *P* wave velocity of 5.2 km/s as a proxy for the top of the Mesozoic basement. We divide the southwest Taiwan fold-and-thrust belt into a number of thrust sheets that form the basis of our description and interpretations. From these data we interpret the 3-D structure of the fold-and-thrust belt and the influence that the structure and morphology of the continental margin is having on its development. We show that there is a significant along-strike change in the structure. This change takes place across a transverse zone that is composed of a suite of structures at the surface. We suggest that this transverse zone has a causal relationship with variations in the geometry of the basal thrust which in turn is related to (possibly fault bounded) basement highs and lows that are inherited from the continental margin.

Plain Language Summary The southwest Taiwan fold-and-thrust belt comprises a roughly N-S striking, west verging imbricate thrust system that has been developing since the Late Miocene. We present the results of new surface geological mapping from which we construct balanced and restored cross sections and along-strike sections. We compile maps of the basal thrust, thrust branch lines, and stratigraphic cutoffs. We divide the southwest Taiwan fold-and-thrust belt into a number of thrust sheets that form the basis of our description and interpretations. From these data we interpret the 3-D structure of the fold-and-thrust belt and the influence that the structure and morphology of the continental margin is having on its development. We show that there is a significant along-strike change in the structure. This change takes place across a transverse zone that is composed of a suite of structures at the surface. We suggest that this transverse zone has a causal relationship with variations in the geometry of the basal thrust which in turn is related to (possibly fault bounded) basement highs and lows inherited from the continental margin.

1. Introduction

In many fossil orogens, the involvement of the shelf or slope of the incoming continental margin, and the reactivation of faults on these parts of the margin, can often be shown to have played an important role in the structural evolution of their fold-and-thrust belts (e.g., Butler et al., 2006; Faulds & Varga, 1998; Flöttmann & James, 1997; Smith, 1999; Zanchi et al., 2006). Nevertheless, from these preserved rock records it is not always straightforward what the initial configuration of the margins morphological and structural architecture were with respect to the developing fold-and-thrust belt, since they may be masked by large translation along thrusts and/or because of dismemberment by subsequent tectonic activity. Despite the difficulties, along-strike changes in the structural architecture of a fold-and-thrust belt are often interpreted to be caused by the reactivation of preexisting faults or changes in sedimentary thickness and facies that were inherited from the continental margin involved, although generally without specifics of where on the margin these came from or what their original architecture was (e.g., Arora et al., 2012; Duncan et al., 2003; Mouthereau et al., 2006; Pérez-Estaún et al., 1997; Thomas, 1985; Turner et al., 2010; Yin, 2006). Therefore, investigating an active orogen in which a continental margin is being deformed can yield important information about how a margins morphology and structure affect not only the structural architecture of a fold-and-thrust belt but also transient features such as seismicity and topography (e.g., Brown et al., 2017).

Tectonics 10.1029/2017TC004910

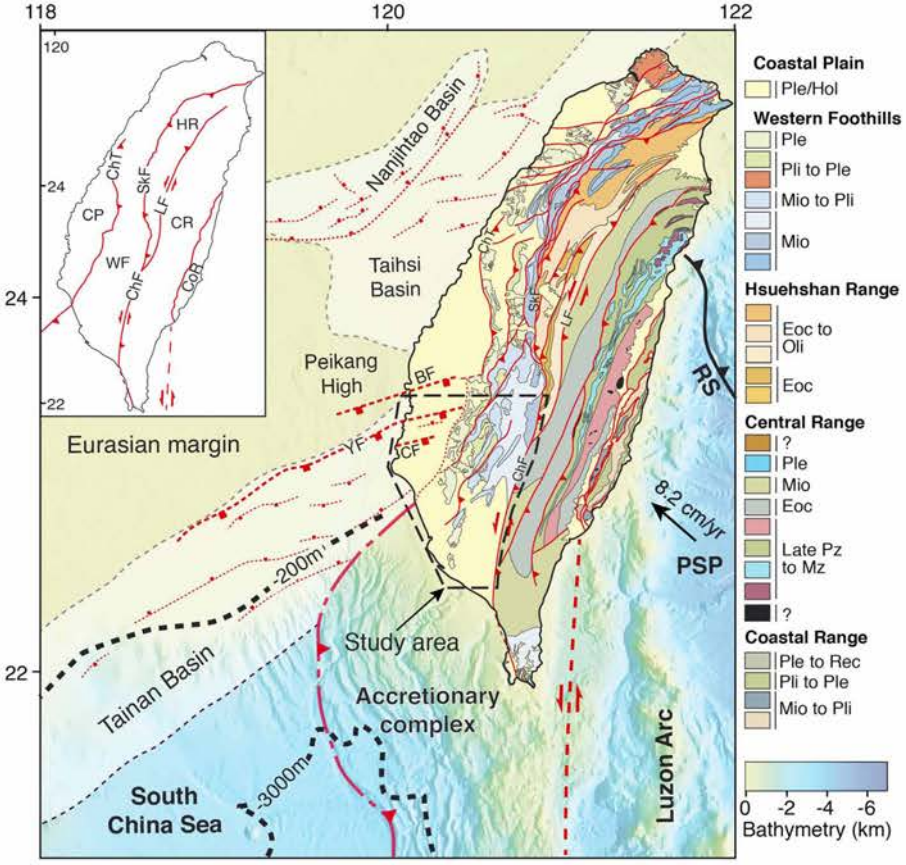

Figure 1. Tectonic setting of the Taiwan arc-continent collision orogen with location of the Taiwan island in relation with the Luzon arc and its accretionary complex, the Ryukyu trench (RS) and major basins of the Eurasian margin. A simplified geological map of the island of Taiwan is shown (after C.-H. Chen et al., 2000), and the main tectonic units are in the inset. The Tainan, Taihsi, and Nanjihtao basins offshore Taiwan include significant extensional structures oriented at a high angle to the structural grain of the orogen. The location of bathymetric contours 200- and 3,000-m depth is shown. The location of the study area is also shown. The convergence vector of 8.3 cm/year between the Philippine Sea Plate and the southern part of the Eurasian Plate is also given. PPS = Philippine Sea Plate; ChT = Changhua thrust; LF = Lishan Fault, SkF = Shuilikeng Fault; ChF = Chauchou Fault; BF = B fault; YF = Yichu fault; CF = Chiali fault. The inset shows the tecto-nostratigraphic units of the Taiwan orogen. CP = coastal plain; WF = western Foothills; HR = Hsuehshan Range; CR = Central Range; CoR = Coastal Range.

Taiwan is a particularly propitious place for carrying out this type of study because the main morphological parts of the margin, including the shelf, the shelf-slope break (defined as the 200-m bathymetry contour), and the hyperextended part of the margin (starting at about the 3,000-m bathymetry contour [e.g., McIntosh et al., 2014]), as well as the extensional fault systems (A. T. Lin et al., 2003; Yang et al., 1991) that make up the structural necking zone (Brown et al., 2017), are all at a high angle to the developing structural grain of the fold-and-thrust belt (Figure 1). Therefore, it is possible to trace these margin features into the fold-and-thrust belt and to readily determine how (or if) they are affecting its structural evolution (e.g., Alvarez-Marron et al., 2014; Brown et al., 2017; Mouthereau et al., 1999, 2002; Suppe, 1986; Yang et al., 2007, 2016). In a number of recent publications (e.g., Alvarez-Marron et al., 2014; Brown et al., 2012, 2017; Camanni et al., 2016), we have explored the effect that the morphology and structure of the Eurasian continental margin is having on the structural evolution of the fold-and-thrust belt of south-central Taiwan. In these publications we proposed that effects of both the morphological (the shelf, the shelf-slope break, the slope) and the structural (the necking zone) parts of the margin can be seen in the Taiwan fold-and-thrust belt as along-strike changes in structure, seismicity, and topography (Brown et al., 2017). In this paper we build on this theme,

Tectonics 10.1029/2017TC004910

Figure 2. Chronostratigraphic correlation chart used in the mapping. It is based on Shea et al. (2003).

presenting the results of new geological mapping of the fold-and-thrust belt in southwest Taiwan (Figure 1), providing a detailed analysis of its structural architecture, how this changes from north to south, and what the suite of structures are that occur along the area of change. We go on to propose how these areas of along-strike structural change can be related to the preexisting structure of the Eurasian continental margin.

2. Geological Background

The Taiwan orogen is evolving as a result of the latest Miocene to present collision between the Luzon Arc, located on the Philippine Sea Plate, and the Eurasian continental margin (Figure 1; Ho, 1986; Suppe, 1981). The Philippine Sea plate is colliding with the Eurasian continental margin with a c. NW46° trend at a rate of about 8.2 cm/year (Yu et al., 1997). The Taiwan orogen is divided into five roughly N-S oriented tectonostratigraphic zones that are separated by major faults (see inset; Figure 1). From west to east these zones are the following: the Coastal Plain, Western Foothills, the Hsuehshan Range, the Central Range, and the Coastal Range. In much of south-central Taiwan, the boundary between the Coastal Plain and the Western Foothills is interpreted to coincide with the mostly buried tip line of the Changhua Thrust (ChT in Figure 1). East of the Changhua Thrust, the low relief areas covered by Holocene sediments in the south and in the Pingtung Plain form thrust-top basins (C. Chiang et al., 2004) on the fold-and-thrust belt. In the study area, the Western Foothills is juxtaposed against the Central Range along the Chaochou Fault. The study area comprises the southwestern part of the Taiwan fold-and-thrust belt and foreland basin to the mountain belt (Figure 1).

The part of the Eurasian continental margin that is involved in the collision has evolved since the Eocene through several extensional episodes that predate the arc-continent collision (C. Y. Huang et al., 2012; A. T. Lin et al., 2003). With the onset of rifting in the Eocene, a number of roughly northeast southwest oriented basins (e.g., Nanjihtao and Taihsi basins) developed on the margins shelf (A. T. Lin & Watts, 2002; A. T. Lin et al., 2003; Teng & Lin, 2004) and locally accumulated up to approximately 5 km of sediments (e.g., A. T. Lin et al., 2003; Figure 1). During the Late Oligocene to Late Miocene, several extensional events further affected the outer shelf and necking zone areas of the margin (A. T. Lin et al., 2003). This resulted in an array of roughly east-northeast striking extensional faults and development of the Tainan Basin (Ding et al., 2008; Lee et al., 1993; A. T. Lin et al., 2003; Y.-J. Lin et al., 2005; Shi et al., 2008; Q. Tang & Zheng, 2010; Yang et al., 1991, 2016; Figure 1). A number of extensional faults that developed along the outer part of the margin and its slope can be traced on land (e.g., the Yichu [YF] and B [BF] faults in Figure 1), into the Coastal plain area of southwestern Taiwan (A. T. Lin et al., 2008; Yang et al., 2006, 2016), where they have been shown to affect the structure of the foreland thrust-and-fold belt (Alvarez-Marron et al., 2014; Brown et al., 2017; Camanni et al., 2016; Rodriguez-Roa & Wiltschko, 2010; Suppe, 1986; Yang et al., 2007, 2016).

3. Stratigraphy

To maintain consistency with our previous publications, we use the same chronostratigraphic nomenclature as in Brown et al. (2012, 2017) and Alvarez-Marron et al. (2014; Figure 2). For the Miocene through Holocene

Tectonics 10.1029/2017TC004910

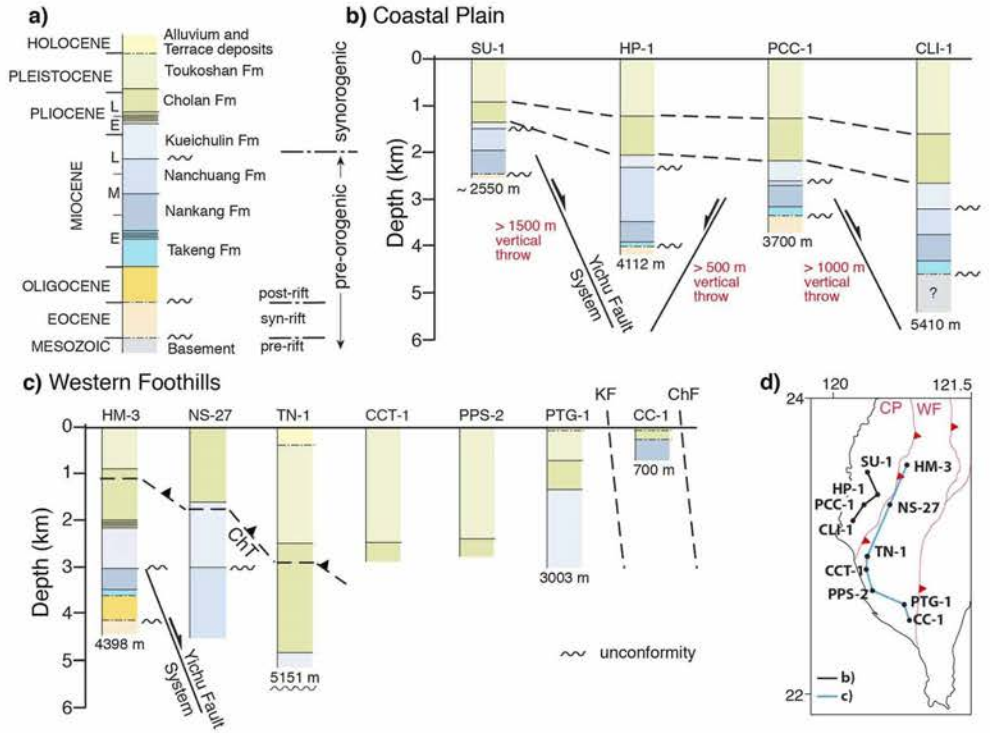

Figure 3. (a) General stratigraphy and tectonostratigraphic units showing the names of formations used in this study. (b) Stratigraphic correlation of boreholes SU-1, HP-1, PCC-1, and CLI-1 along the Coastal Plain (taken from Tensi et al., 2006; Shaw, 1996; C.-H. Tang, 1977). The interpreted approximate vertical throw accumulated by structures between boreholes is shown. (c) Stratigraphic correlation of boreholes HM-3, NS-27, TN-1, CCT-1, PPS-2, PTG-1, and CC-1 from the frontal and southern parts of the fold-and-thrust belt (taken from S. C. Chiang, 1971; Chou, 1972; Huang, 1984; S. T. Huang et al., 2004; C.-H. Tang, 1977). The location of the basal thrust in HM-3, NS-27, and TN-1 is marked as ChT (Changua thrust). (d) Inset indicates location of the boreholes. Boreholes are also shown in map of Figure 4. CP = Coastal Plain; WF = Western Foothills.

rocks, this scheme follows the stratigraphic correlation of Shea et al. (2003; Figure 2). We have subdivided a thick, latest Miocene through to Late Pleistocene-age, unit of mudstone with ribbons of sandstone that crops out in the southwestern part of the study area (the Gutingkeng Fm: Figure 2) using the chronological divisions for it that are provided by Horng and Shea (1994) and Horng (2014). The stratigraphic thickness for each formation is, where possible, taken from published borehole data (Figure 3; Chang, 1963; S. C. Chiang, 1971; Chou, 1971; S. T. Huang et al., 2004; Shaw, 1996; C.-H. Tang, 1977; Tensi et al., 2006; Yuan & Huang, 1985) and isopach maps (Chou, 1980; A. T. Lin et al., 2003; Shaw, 1996; C.-H. Tang, 1977) within the study area, and from the geological map (Figure 4).

Throughout this paper we define the basement as all pre-Eocene rifting rocks upon which the Cenozoic Eurasian continental margin was built. Basement rocks do not crop out in the study area. Although, weakly metamorphosed siliciclastic rocks and marble that have been interpreted to be Mesozoic in age have been intersected in one borehole (CLI-1) on land (Figure 3) and several boreholes offshore southwestern Taiwan (Chiu, 1975; Ho, 1988; Jahn et al., 1992; Shaw, 1996). Mesozoic rocks do, however, crop out extensively in the Central Range where they comprise predominantly marbles and schists (Ernst, 1983; Ho, 1988; Lan et al., 2008; Stanley et al., 1981). We therefore interpret these types of lithologies, capped locally by weakly metamorphosed clastic rocks, to comprise the basement beneath the study area. Within the study area, this basement can be unconformably overlain by Eocene through to Early Miocene rocks, since boreholes indicate that neither the Eocene nor the Oligocene rocks are present everywhere (Chiu, 1975; Ho, 1988; Shaw, 1996; Figure 3).

The Eocene through Early Miocene rocks do not crop out in the study area. They have, however, been intersected in several boreholes (Figure 3). In these boreholes, the Eocene and Oligocene each comprise

Tectonics 10.1029/2017TC004910

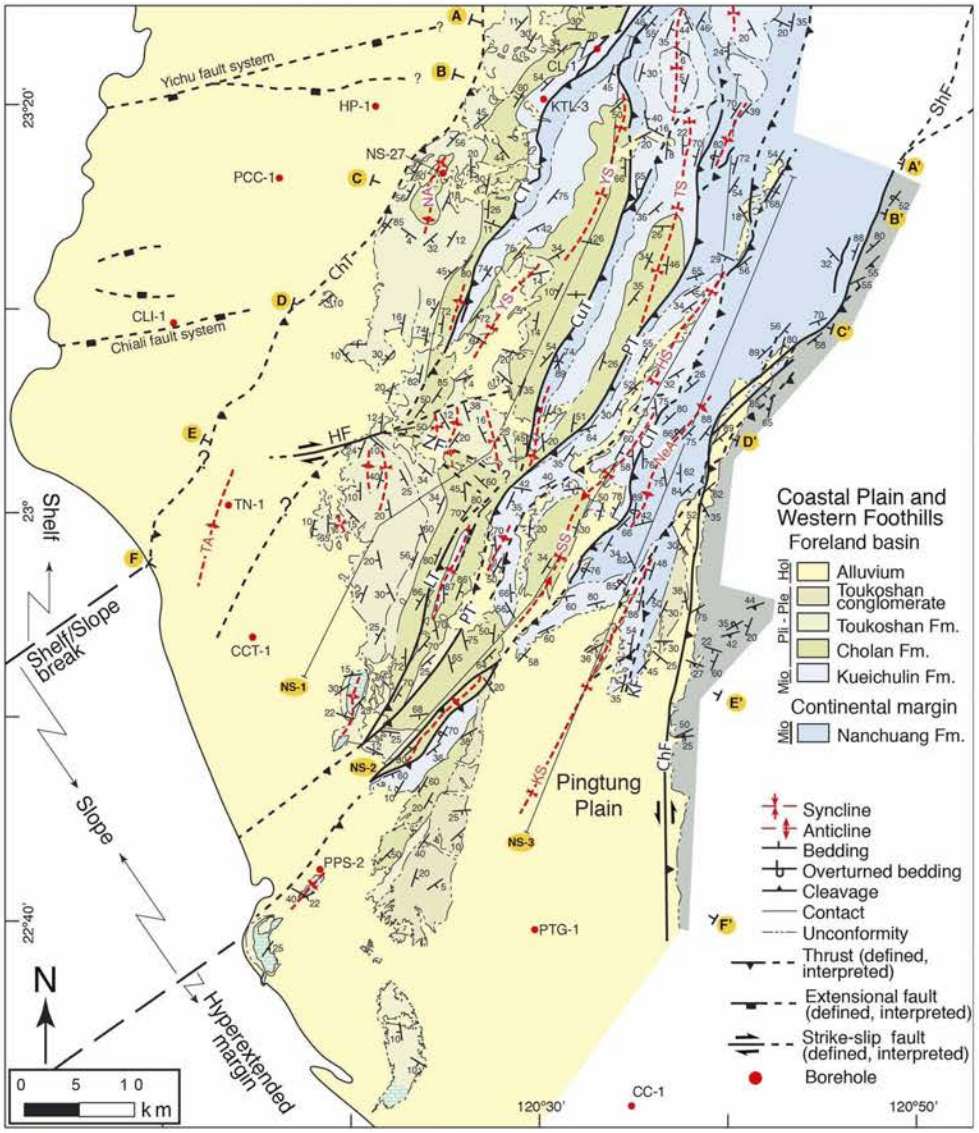

Figure 4. Geological map of southwest Taiwan. It includes the location of the geological cross sections A to F shown in Figure 6, the longitudinal cross-sections NS-1 to NS-3 shown in Figure 8, and the boreholes shown in Figure 2. Structures discussed in the text are labeled. Thrusts: ChT = Changhua thrust; CiT = Chishan thrust; CT = Chelungpu thrust; CuT = Chutochi thrust; LT = Lungchuan thrust; PT = Pingshi thrust. Faults: ChF = Chauchou fault; HF = Hsinshua fault; ZF = Zuojhen fault. Folds: NA = Niushan anticline; NeA = Neiyingshan anticlinorium; SS = Shihchangli syncline; TA = Tainan anticline; TS = Tingpinglin syncline; YS = Yuching syncline; HS = Hsiaolin syncline; KS = Kuanglin synform.

up to several hundred meters of predominantly sandstone and shale, although they may be thicker in certain areas. The Early Miocene Takeng and Nankang formations comprise several hundred meters to nearly 1,000 m of sandstone and shale (Shaw, 1996; Yang et al., 2014; Figure 3).

The outcropping stratigraphy of the study area (Figure 4) comprises Middle Miocene through Holocene clastic rocks with, in the extreme southwest, small, isolated, and laterally discontinuous outcrops of limestone. In the north and east, the Middle to Late Miocene Nanchuang and the Late Miocene to Early Pliocene Kueichulin formations dominate (Figure 4). The Nanchuang Formation is made up of thin- to thick-bedded sandstone intercalated with shale. Its thickness varies widely across the study area, ranging

Tectonics 10.1029/2017TC004910

from several hundred meters to more than 2,000 m. These changes in thickness have been interpreted to be related to deposition of the Nanchuang Fm in marine extensional basins during the Middle Miocene development of the Tainan Basin (A. T. Lin et al., 2003; Yang et al., 2006). The Nanchuang Fm is unconformably overlain by the Kueichulin Fm (A. T. Lin et al., 2003).

The Kueichilin Fm comprises shallow marine facies, thin to very thick-bedded muddy sandstone and sandy mudstone. In agreement with A. T. Lin et al. (2003), we take the Kueichulin Fm to mark the onset of synorogenic sedimentation in the foreland basin because of the regionally developed unconformity at its base that has been interpreted to be related to plate flexure caused by orogenic loading (A. T. Lin & Watts, 2002; Tensi et al., 2006). This is in contrast to Teng (1987), Covey (1986), and Hong (1997), who suggest that the onset of foreland basin sedimentation occurred during the Early Pliocene, and is recorded by the appearance of slate clasts in the Chinshui shale at the base of the Cholan Fm. The Kueichilin Fm crops out extensively in the north and central part of the study area (Figure 4). It thickens significantly from east to west and from north to south, with thickness ranging from ~150 m to more than 3,000 m (Figures 3 and 4; S. C. Chiang, 1971). The Kueichilin Fm is conformably overlain by the Early Pliocene to Early Pleistocene marine facies Cholan Fm. The Cholan Fm may reach more than 4,000 m in thickness and is made up of interbedded mudstone, shale, and muddy sandstone. The Cholan Fm is overlain by the Early Pleistocene marine facies Toukoshan Fm, a coarsening upward sequence made up of thick-bedded muddy sandstone and shale that, upward, becomes interfingered with, and locally unconformably overlain by conglomerate. The Toukoshan Fm contains a number of regional-scale internal unconformities and can reach more than 3,000 m in thickness (Figure 4). The Toukoshan Fm is overlain by Holocene-age fluvial gravels that, in places, are several hundred meters thick.

4. Methodology

The structural analyses and interpretations that follow are based on our new geological mapping (Figure 4). This mapping is the southern continuation of previous work by our group in south-central Taiwan (Alvarez-Marron et al., 2014; Brown et al., 2012). Field mapping was carried out at 1:50,000 scale using the geological maps of the Central Geological Survey of Taiwan as a base. The final map was drawn at 1:50,000 scale using the chronostratigraphic scheme shown in Figure 2. For clarity, in Figure 4 only representative structural data are shown; a 1:100,000 scale map with all of our bedding dip data can be found in supporting information Figure S1 and the bedding database in Table S2. Major thrusts and their names have been correlated from north to south (see Ho, 1986, for a similar correlation). In the description of the structure that follows, the study area has been divided into a number of structural units (Figure 5).

Six balanced and restored cross sections, oriented perpendicular to the regional strike of structures (bedding, thrusts, and major fold traces), have been constructed using the geological map, field structural data, and the standard section construction techniques (Dahlstrom, 1969; De Paor, 1988; Hossack, 1979; Figures 6 and 7). Where possible, additional constraints were placed on the structure and the stratigraphic thicknesses from published borehole data (Figure 3). Boreholes were projected along the bedding strike onto the cross sections (Figure 6). In an iterative process, together with the construction of cross sections, three roughly north-south, strike-parallel sections (NS-1, NS-2, and NS-3 in Figure 4) were also constructed (Figure 8), and maps of the basal thrust, branch line maps, and stratigraphic cutoff maps were drawn (Figures 9a and 9b). This iterative approach insured a 3-D consistency of the structural interpretation and assured the viability of the cross sections. The cross sections have been line balanced (while conserving area) and restored (Figures 6 and 7), with the exception of section A-A′, which was not restored because it crosses the oblique Yichu ramp (see below; Figure 9a). In all the restored sections the western pin line was placed in the undeformed rocks to the west of the Changhua thrust tip line. The sections have been restored to a horizontal top of the Kueichulin Fm, a regional-scale marker that can be mapped throughout much of the study area (Figure 4). Minimum shortening estimations in the cross sections, which is a by-product of their balancing and restoration, is briefly presented but is not the focus of this study.

Finally, to place some constraint on the depth to, and the geometry of, the top of the basement, we interpret it to approximately coincide with a *P* wave (*Vp*) velocity of 5.2 km/s (Figures 6 and 8), which is taken from the 3-D tomography model of Kuo-Chen et al. (2012). See Brown et al. (2017) for a more extensive argumentation for using this velocity as a proxy for the top of the basement. We stress, though, that this isovelocity surface is only meant to help with the interpretation of the location of the top of the basement rocks at depth and that

Tectonics 10.1029/2017TC004910

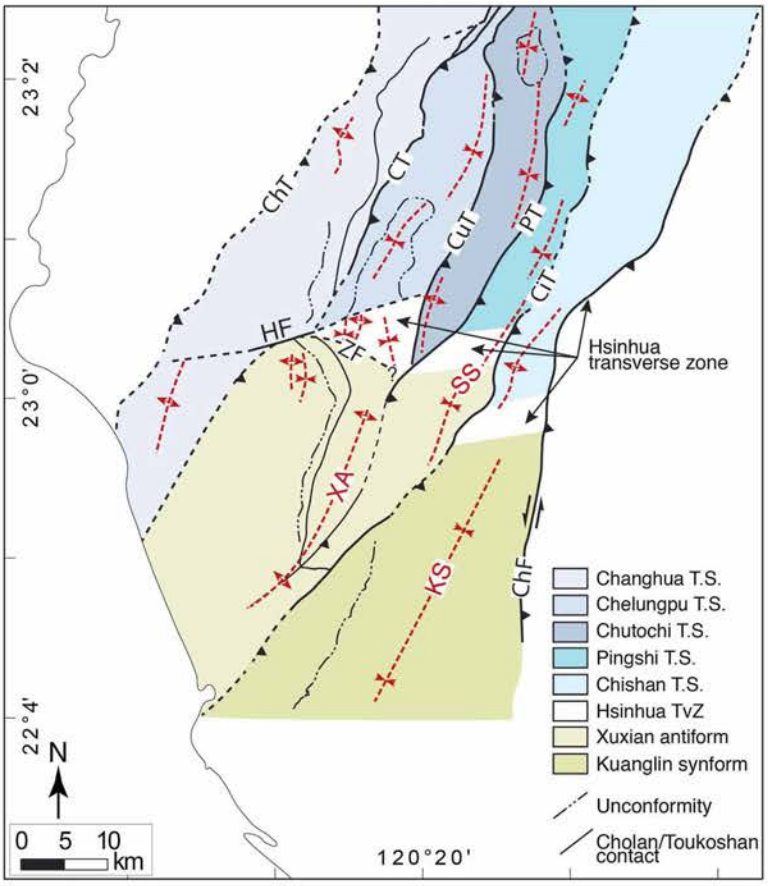

Figure 5. Structural units of the southern Taiwan fold-and-thrust belt described in the text. The Hsinhua transverse zone marks the transition from a mostly emergent thrust system in the north to a southern area dominated by the Xuxian antiform and the Kuanglin synform where large areas of the thrust sheets are buried.

it may not coincide with the depth to basement determined using the section construction methods (see the dashed red lines in Figures 6 and 8).

Before continuing with the presentation and discussion of the structure of the fold-and-thrust belt in the following sections, we feel that some remarks about the uncertainties involved in the interpretations are appropriate. The primary data set for all the interpretations that follow is the geological map (Figure 4). During our mapping we have made a number of assumptions that could have led to errors in the map. These include (1) making a chronostratigraphic correlation that link different rock units and facies together on the basis of age and (2) correlating thrusts and stratigraphic contacts along strike through difficult terrain with, locally, sparse outcrop information. Any errors generated in this way were then introduced into the cross sections and these, together with the general assumptions involved in the cross-section construction, such as plane strain, no layer parallel slip, the fold mechanism, a horizontal top for the Kueichulin, or the depth to the basal thrust calculations, also lead to errors in the cross sections. A weakly constrained stratigraphic template precluded doing rigorous area balancing. See also Judge and Allmendinger (2011) and Groshong et al. (2012) for a general discussion of cross-section balancing and its uncertainties. Furthermore, we did not have access to either the original borehole descriptions or their locations. The borehole information presented here has been taken from various publications and may therefore contain significant errors. A further, and important uncertainty is the use of a *Vp* of 5.2 km/s as a proxy for the top of the basement. The uncertainties inherent in the velocity model, its low resolution (20 km by 20 km by 10 thick) compared to that of the surface geology, and the petrophysical assumptions made for conversion of *Vp* to rock type (e.g., Brown et al., 2017) all mean that

Tectonics 10.1029/2017TC004910

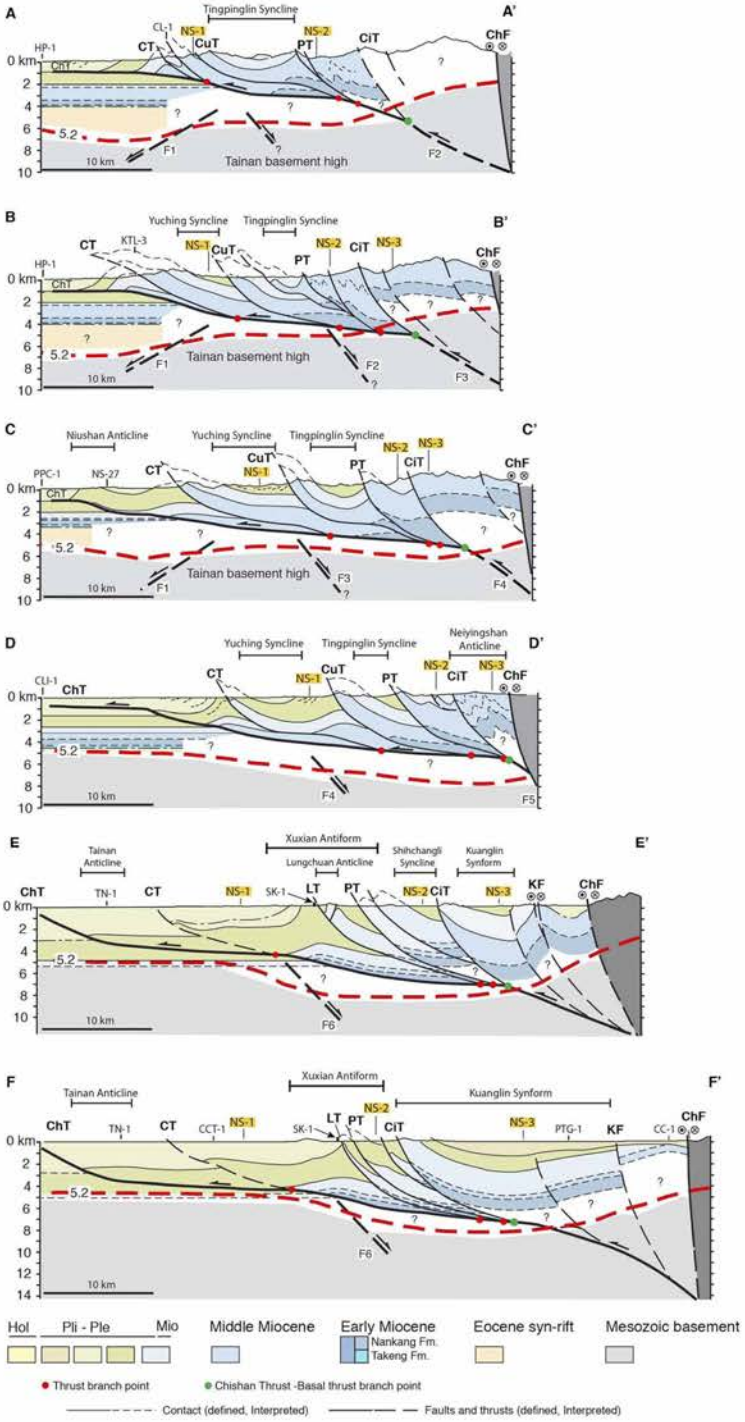

Figure 6. Geological cross sections through the southwestern Taiwan fold-and-thrust belt. Their locations are shown in Figure 4. They include the projected location of the boreholes used for their construction and the branch points (red dots) of individual thrusts. The branch point of the CiT (green dots) is interpreted to mark the ramp down into the basement of the basal thrust. Branch points were used to construct the branch line map in Figure 9. Red dashed line is the 5.2 km/s *Vp* contour from the TAIGER local tomography. Faults interpreted in the basement are labeled F1 to F6 for correlation in Figures 7 and 8. Abbreviations are as in Figure 4.

Tectonics 10.1029/2017TC004910

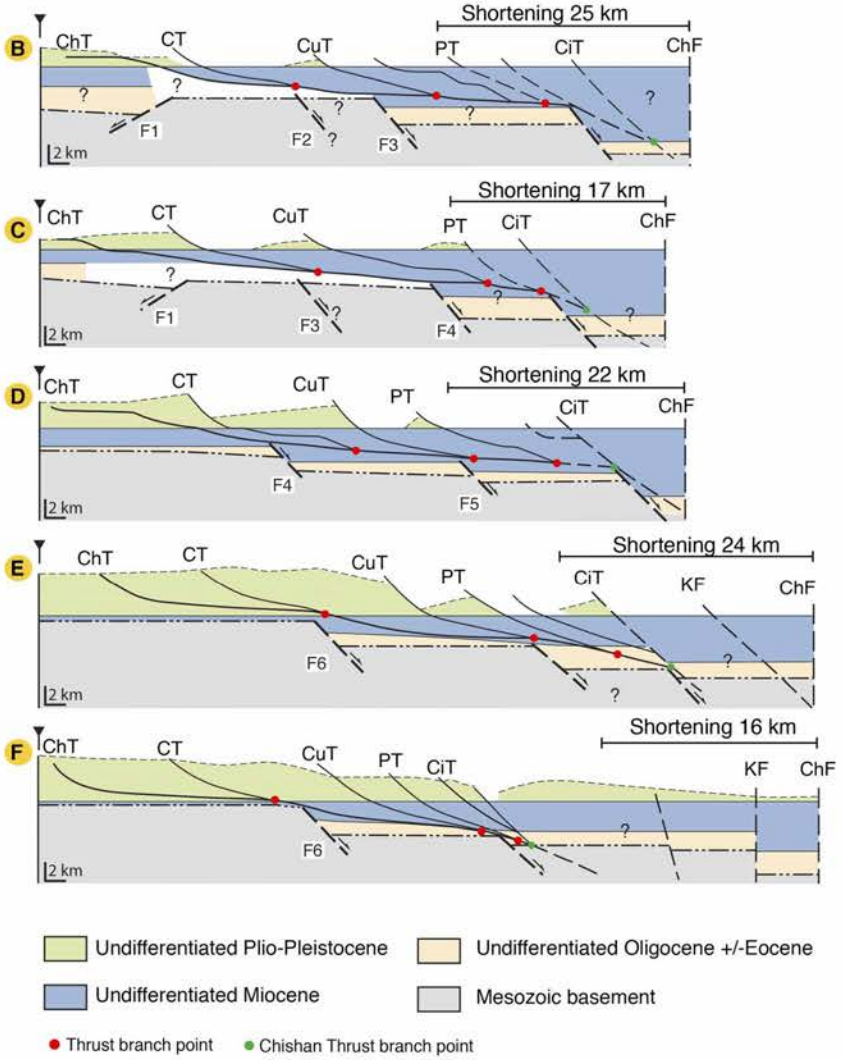

Figure 7. Restored sections B to F. The sections have been restored using bed-length balancing of top and base of Kueichulin Fm and are area balanced for the rest of the Miocene units above the basal thrust. Faults interpreted in the basement are labeled F1 to F6 and correspond to those in Figures 6 and 8. Abbreviations are as in Figure 4.

this assumption for the basement-cover interface may not be valid everywhere. While we have taken care to keep all of these uncertainties to a minimum, we nevertheless present both the map and the cross sections as interpretations, the restorations as approximations, and the displacement and shortening calculations as minimums.

5. Structure of Southwestern Taiwan

5.1. Surface Geology

The study area covers the Coastal Plain and the Western Foothills (including the area covered by Holocene sediments in the south and on the Pingtung Plain) of southwestern Taiwan (Figures 1 and 4). In this area, the fold-and-thust belt is bounded to the east by the Chaochou fault and in the west by the buried tip line of the Changhua thrust (CT; Figure 4; see also, Ching et al., 2011; Rodriguez-Roa & Wiltschko, 2010; Shyu et al., 2005; Yang et al., 2007; Yu et al., 1997). Seismicity to the west of the Changhua thrust indicates, however, that deformation is also taking place beneath this westernmost part of the Coastal Plain (e.g., Brown et al., 2017;

Tectonics 10.1029/2017TC004910

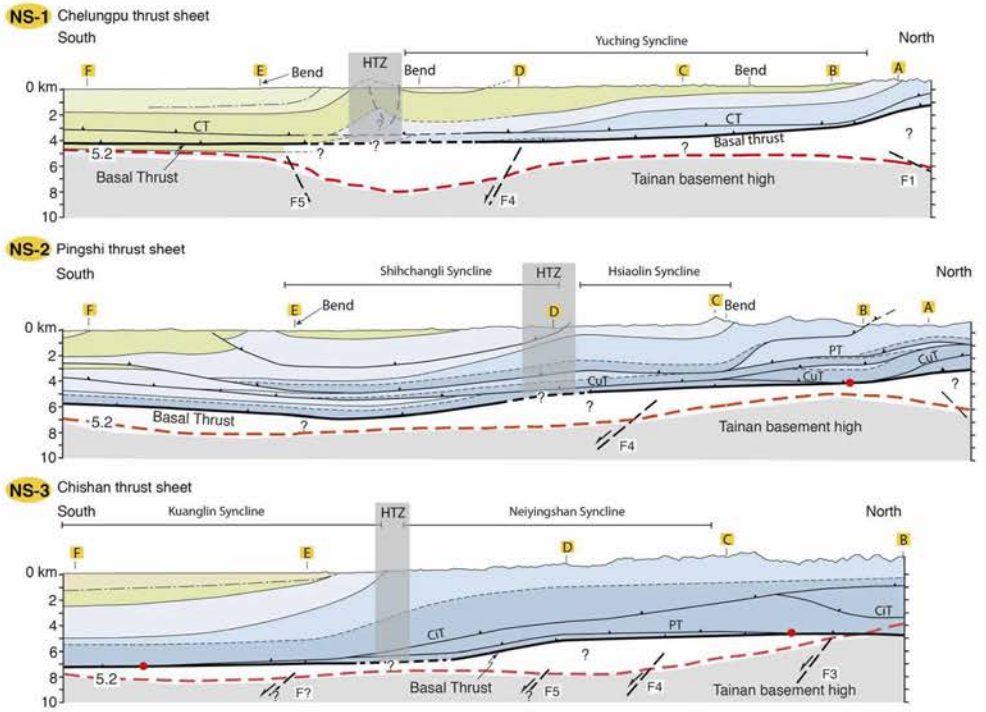

Figure 8. North-south geological cross sections. NS-1 along the Chelungpu thrust sheet, NS-2 along the Pingshi thrust sheet, and NS-3 along the Chishan thrust sheet. The area corresponding to the Hsinhua transverse zone (HTZ) of Figure 5 is shown by the gray shaded box. The dashed part of the basal thrust below the HTZ that is marked by a question mark indicates uncertainty about what the interaction between the two is. Faults labeled F1 to F6 correspond to those in Figures 6 and 7. Legend is as in Figure 6. Red dashed line is the 5.2 km/s *Vp* contour from the TAIGER local tomography. Abbreviations are as in Figure 4.

Camanni et al., 2016; Shyu et al., 2005). In terms of the morphological parts of the continental margin that are entering into the deformation, the study area (Figures 1 and 4) comprises the outer part of the shelf, as well as the on land projections of the shelf-slope break, and part of the slope area. In structural terms it comprises part of the necking zone and the beginning of the hyperextended part of the margin (e.g., Brown et al., 2017; Lester et al., 2014; McIntosh et al., 2014). The boundaries between all of the morphological parts of the margin, as well as the extensional fault system on the necking zone, are oriented at a high angle to the structural grain of the developing fold-and-thrust belt (Figures 1 and 4; Lee et al., 1993; A.T. Lin et al., 2003; Yang et al., 1991, 2016). On the basis of borehole and reflection seismic data, a number of the roughly east-northeast striking extensional faults mapped in the offshore have been traced on land, into the Coastal Plain (the B, Yichu, and Chiali fault systems; e.g., A. T. Lin et al., 2003; Yang et al., 2014, 2016; Figures 1 and 4).

The structural grain of the fold-and-thrust belt in southwestern Taiwan is roughly north-northeast striking, with several pronounced, sigmoidal, en echelon changes toward a more northeast strike (Brown et al., 2017; Figure 4). It has a buried thrust front and all major thrusts are interpreted to extend southwestward into the offshore where they form a marine accretionary complex (C. Chiang et al., 2004; A. T. Lin et al., 2008; Shyu et al., 2005). The surface structure of the study area is that of an imbricate thrust system, but with a pronounced north-south change in structural architecture that is presented and discussed in detail below. In the north, the study area comprises five thrust sheets: the Changhua, Chelungpu, Chutochi, Pingshi, and Chishan thrust sheets, whereas in the south it consists of the Changhua thrust sheet, the Xuxian antiform, and the Kuanglin synform (Figure 5). Below, we will present evidence of, and arguments for, the north-south change in structural architecture taking place across a roughly east-west striking zone that we call the Hsinhua transverse zone (Figure 5). In the southern part of the study area, large areas of the thrust sheets

Tectonics 10.1029/2017TC004910

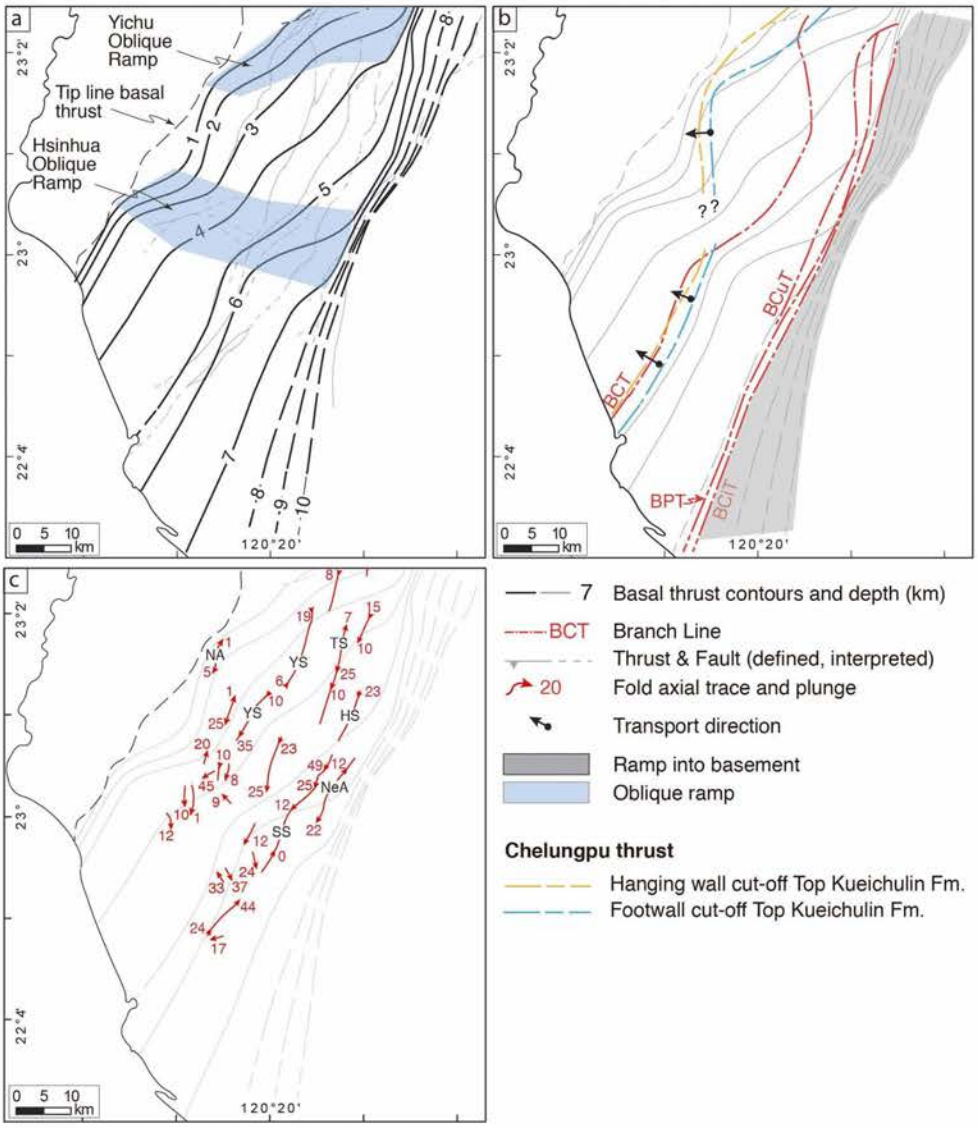

Figure 9. (a) Structural contour line (in km) map of the basal thrust. Thrusts and faults are shown in light gray. (b) Hanging wall and footwall cutoff lines of the top of Kueichulin Fm in the norhtern and southern areas, and branch lines (red) of the Chelungpu, Pingshi, Chutochi, and Chishan thrusts are shown superposed on the basal thrust contour lines. The arrows show the assumed displacement direction, which is interpreted to be perpendicular to the frontal stratigraphic cutoffs. The area where the basal thrust is interpreted to ramp down into the basement is labeled in gray. This ramp starts from the BCiT that is at about 5 km in the north and deepens southward till more than 7 km. (c) Fold axial traces and plunge of the main folds superimposed on the basal thrust contour map. Abbreviations are as in Figure 4.

(all of the proposed continuation of the Changhua thrust sheet, as well as the Kuanglin synform) are buried by Holocene sediments. Below we give a description of the surface geology of each of these, followed by an interpretation of the subsurface structure in section 5.2.

The Changhua thrust sheet (Figure 5) is bounded in the west by the buried Changhua thrust and in the east by the Chelungpu thrust (ChT and CT, respectively, in Figures 4 and 5). It crops out only in the northern half of the study area where it is composed of predominately Cholan and Toukoshan formations, with a minor amount of Kueichulin Fm in the northeast (Figure 4). The southern half is covered by Holocene sediments,

Tectonics 10.1029/2017TC004910

and the trace of the buried Changhua thrust in Figure 4 is interpreted from small topographic highs and published reflection seismic data (see also, S. T. Huang et al., 2004; Shyu et al., 2005). In the north, from east to west, the structure of the Changhua thrust sheet is that of a steep to gently west dipping monocline that is interrupted only by the doubly plunging Niushan anticline (NA in Figure 4), whose western limb is locally steep to overturned. In the southeastern part of the outcropping Toukoshan Fm there is a regional-scale unconformity of Late Pleistocene age that juxtaposes shallow marine sandstone and shale against fluvial sandstone and conglomerate. There are a number of smaller, local, unconformities developed throughout the Pliocene and Pleistocene sequences in the Changhua thrust sheet (W.-S. Chen et al., 2001). In the area covered by Holocene sediments, the roughly east-northeast striking Hsinhua fault (Figure 4) represents the dextral oblique-slip surface rupture of the 1946 Hsinhua earthquake (Bonilla, 1975; Shyu et al., 2016). In the very southwest, the Tainan anticline does not crop out but is marked at the surface by a small area of low topography. It has been imaged in reflection seismic data (S. T. Huang et al., 2004). We interpret the Tainan anticline to be forming in the immediate hanging wall of the Changhua thrust (see also M.-H. Huang et al., 2009; Lacombe et al., 1999).

The Chelungpu thrust sheet (Figure 5) is bounded by the Chelungpu thrust (CT) in the west and by the Chutochi thrust (CuT) in the east (Figure 4). It contains Middle Miocene through Pleistocene rocks that are overlain by Holocene sediments. The Chelungpu thrust sheet is comprised predominately of the gently to moderately south-southwest plunging Yuching syncline (YS in Figure 4). In the immediate hanging wall of the Chelungpu thrust, along the western limb of the Yuching syncline, the Nanchuang and Kueichulin Fms dip steeply to the southeast before the dips shallow in the Cholan Fm where there are numerous local southeast dipping unconformities. Along the eastern limb of the Yuching syncline, bedding dips change direction and amount from north to south, and unconformities are not common. In the core of the Yuching syncline, moderately to steeply dipping Cholan Fm rocks are overlain by gently south dipping Toukoshan Fm along an Early Pleistocene-age unconformity (Figure 4). Southward, the Chelungpu thrust sheet, ends against the Hsinhua fault (HF in Figure 4).

The Chutochi thrust sheet (Figure 5) is bounded in the west by the Chutochi thrust (CuT) and in the east by the Pingshi thrust (PT; Figure 4). The Chutochi thrust sheet is composed of Middle Miocene through Early Pleistocene rocks. The structure of the Chutochi thrust sheet is dominated by the Tingpinglin syncline (TS in Figure 4), a gently south plunging syncline cored in the south by Cholan Fm. In the northernmost part of the thrust sheet, the Tingpinglin syncline is weakly developed within the Kueichulin Fm, which also contains a marked internal unconformity. Unconformities are not found in the Cholan Fm. The northern part of the Chutochi thrust sheet is cut by a connecting splay between the Chutochi and Pingshi thrusts. Southward, the Chutochi thrust ends against the Pingshi thrust, which cuts across both limbs of the Tingpinglin syncline.

The Pingshi thrust sheet (Figure 5) is bounded in the west by the Pingshi thrust (PT) and in the east by the Chishan thrust (CiT; Figure 4). In the north, its internal structure and the traces of both the Pingshi and Chishan thrusts are not well resolved because of difficult access. Despite this, a number of small splays and their related folds have been identified along the margins of the thrust sheet in this area. The structure of the Pingshi thrust sheet is dominated by the moderately southwest plunging Hsiaolin syncline and the doubly plunging Shihchangli syncline (HS and SS, respectively in Figure 4). On the basis of an increased thickness of the Kueichulin Fm along the western limb of the Hsiaolin syncline, we interpret the presence of a minor thrust that thickens the Kueichulin Fm and causes minor folding in its hanging wall. We interpret the Pingshi thrust to continue southward into the eastern limb of the Xuxian antiform (PT in Figure 4).

The Chishan thrust sheet (Figure 5) is bounded by the Chishan thrust (CiT) in the west and by the Chaochou Fault (ChF) in the east (Figure 4). Because of difficult access, only the margins of the northernmost part of the Chishan thrust sheet have been looked at in this study. In this area, the Nanchuang Fm rocks are intensely folded and faulted. The southern part of the Chishan thrust sheet comprises tightly folded and faulted rocks of the Nanchuang Fm, forming the west verging, south-southwest plunging Neiyingshan anticlinorium (NeA in Figure 4). We interpret the Chishan thrust sheet to continue southward beneath the Pingtung Plain, although with a prominent along-strike change from the Neiyingshan anticlinorium to the Kuanglin synform (Figure 4).

Southward, increasing amounts of the fold-and-thrust belt become buried beneath the Holocene synorogenic sediments (Figure 4). This means that we have less outcrop control on the structure. But with the help of published borehole data (S. C. Chiang, 1971; C. Chiang et al., 2004; Chou, 1972; S. T. Huang et al., 2004; C.-H.

Tectonics 10.1029/2017TC004910

Tang, 1977) and reflection seismic profiles (S. T. Huang et al., 2004) we have interpreted a generalized structure in the areas without outcrop, such as the Changhua thrust sheet and the Kuanglin synform. These interpretations are, however, highly speculative. Nevertheless, it is apparent that the Chelungpu thrust sheet ends southward against the Hsinhua fault. South of the Hsinhua and Zoujhen (ZF) faults, bedding dips are steep to gentle toward the west to southwest before taking on a southward dip as the contact between the Cholan and Toukoshan Fms turns to strike east-west, forming a south plunging fold closure (Figure 4). We name this fold the Xuxian antiform. The core and the eastern limb of the Xuxian antiform is cut by the Lungchuan, Pingshi, and Chishan thrusts (LT, PT, and CiT, respectively, in Figure 4). Since it does not appear to continue northward or to merge with the Chutochi thrust, we interpret the Lungchan thrust sheet to form a horse in the footwall of the Pingshi thrust. The Xuxian antiform is composed of Late Miocene through Pleistocene rocks and is bounded to the west by the buried Chelungpu thrust and to the east by the Chishan thrust. Along the western limb of the antiform, there is a pronounced west to southwest dipping Late Pleistocene-age unconformity within the Toukoshan Fm that marks a change from shallow marine to predominately fluvial facies sediments. Smaller, local unconformities are widespread within the shallow marine facies rocks of the lower Toukoshan and Cholan formations.

The Kuanglin synform is bounded by the Chishan thrust in the west and the Chaochou fault in the east (Figure 4). It crops out only along its western side and its hinge area in the north. In the west, the Chishan thrust juxtaposes moderately to steeply southeast dipping Late Miocene through Pleistocene rocks against the eastern flank of the Xuxian antiform. Along the western limb of the synform, there is a marked Late Pleistocene erosional unconformity along which fluvial facies Toukoshan Fm conglomerate overlies shallow marine sandstone of the same formation. In the north, the hinge zone of the Kuanglin synform is composed of steeply southeast dipping and west dipping Kueichuin Fm thick-bedded sandstone, with and isolated outcrop of Late Pleistocene-age, slate-bearing conglomerate.

From the surface geology, it is clear that there is an important change in structural architecture from the thrust sheets in the north to the Xuxian antiform in the south, and from the Neiyingshan antiform in the north to the Kuanglin synform in the south. The zone across which this change takes place is not a single, discrete structure, but is composed of a suite of structures whose northern and southern boundaries are sometimes transitional into the regional-scale structures on either side. In the west, it comprises the roughly east-northeast striking, dextral strike-slip Hsinhua fault (HF in Figures 4 and 5), which extends at least from the surface rupture of the 1946 Hsinhua earthquake (solid line in Figure 4) eastward to the Chutochi thrust. The Zuojhen fault (ZF in Figures 4 and 5) is a zone that consists of several roughly east-southeast striking faults that join the Hsinhua fault in the west to form a conjugate strike-slip fault system. The Zuojhen fault can be traced eastward to the Pingshi thrust. In between the Hsinhua and Zuojhen faults, the structure comprises a series of north-northwest trending, upright folds. Eastward, the Pingshi and the Chishan thrusts display marked sigmoidal bending of their surface traces and of the bedding in their hanging walls. The Pingshi thrust cuts across both limbs of the Tingpinglin syncline, and the Chutochi thrust is cut by it. Between the area of sigmoidal bending of the Pingshi and Chishan thrusts, the Shihchangli syncline (SS in Figure 4) plunges moderately southward (approximately 50°) and gently northward (<5°) in its northern and southern parts, respectively (Figure 4). Eastward, in the hanging wall of the Chishan thrust, where it goes through a change in strike, the Neiyingshan antiform terminates abruptly southward and the Kuanglin synform replaces it (NeA and KS, respectively, in Figure 4). We call this zone of structural changes the Hsinhua transverse zone (Figure 5). We use the term transverse zone, as defined by Thomas (1990), to be *a systematic alignment of lateral connectors between two sets of differing structures*. According to this definition, a transverse zone can be manifested as a suite of possible structures (these are described for the Hsinhua zone below) with a range of probable causes (which we will discuss later, in section 6).

5.2. Subsurface Structure

Because of the north-south differences in structure across the study area, we divide the description that follows into that to the north of the Hsinhua transverse and that to the south. Nevertheless, throughout the study area, we interpret the tip line of the Changhua thrust (ChT) to also be that of the basal thrust (Figure 6). North of the Hsinhua transverse zone, the basal thrust in the west forms a shallow (~1-km depth) flat within the Pliocene or Pleistocene rocks before it ramps down eastward into the Middle Miocene (sections A through D in Figure 6). In this part of the study area, we interpret the juxtaposition of the

Tectonics 10.1029/2017TC004910

Chelungpu, Chutochi, and Pingshi thrust sheets, with their leading thrusts located predominately in the Nanchuang Fm, together with the similar (although slightly increasing toward the east) erosion level in the cores of their respective synclines, to indicate that the basal thrust dips about 4° toward the east within the Middle Miocene rocks beneath these thrust sheets. Eastward, on the basis of the increased thickness of strongly folded Miocene rocks in its hanging wall, and on the uplift of higher velocity rocks (>5.2 km/s), we interpret a ramp into the basement to occur along the Chishan thrust (Figure 6). Displacement (measured as the distance that the top of Kueichulin moved along a thrust surface) along individual thrusts in section A through D generally decreases southward and increases eastward. Note, however, that we have poor control on section A and limited information for the Chishan thrust where this cutoff is not found (Figure 6). From the balanced and restored cross sections, we estimate the minimum shortening in this part of the fold-and-thrust belt to be between 17 and 25 km (Figure 7).

South of the Hsinhua transverse zone, especially along much of section F and the western part of section E, the fold-and-thrust belt is poorly exposed, being buried by Holocene sediments in thrust-top basins. We therefore have variable control on the surface structure south of section E with which to place constraints on the subsurface geometry of the thrust system. Nevertheless, borehole TN-1 (Figure 3) shows that the Cholan and Toukoshan formations thicken significantly compared to north of the Hsinhua transverse zone, whereas along the western limb of the Xuxian anticline the Miocene thins or even disappears. In agreement with the interpretation of M.-H. Huang et al. (2009) and Mouthereau et al. (2001), we interpret the basal (Changhua) thrust to be listric along its westernmost part before forming a flat within the Cholan Fm at ~4-km depth (Figures 6e and 6f). Eastward, we interpret it to ramp down into the Middle Miocene rocks beneath the Xuxian antiform, since these rocks are exposed in its core and in thrust sheets along its eastern flank. Based on the shallowing of the 5.2 km/s isovelocity line, we interpret the basal thrust to ramp down into the basement east of the Chishan thrust (Figure 6).

The Kuanglin synform is only exposed along part of its western flank and in the core of the synform in the north (Figure 4). On the basis of our surface structural data, boreholes PTG-1 and CC-1 (Figure 4), and following Mouthereau et al. (2001) and Chiang et al. (2004), we interpret the Kuanglin synform to widen southward into a broad, open syncline with only minor internal deformation. Despite limited control on stratigraphic cutoffs we nevertheless interpret displacement to increase eastward in Section E and calculate a minimum shortening of around 24 km. Estimates of displacement and shortening for Section F are highly speculative.

In the strike-parallel sections (Figure 8), we interpret the transition in structure across the Hsinhua transverse zone, with the exception of NS-1, to be smooth, continuous, and marked by a general southward dip of all contacts. Although, the details of this area of transition may be more complex, and it cannot be fully resolved with the current data set. Because of this uncertainty, in Figure 8 we show the Hsinhua transverse zone as a gray area and the basal thrust as a dashed line. In Section NS-1, the area of the Hsinhua-Zoujhen fault system displays a pronounced, asymmetrical, and faulted anticline that we interpret to be forming in a dextral, positive flower structure that possibly cuts the basal thrust. In Sections NS-2 and NS-3, however, it is not clear how the transverse zone is reflected in the subsurface structure. Nevertheless, on the basis of the balanced cross sections (Figure 6), we interpret the basal thrust to deepen by up to 2 km from north to south, across the Hsinhua transverse zone (Figure 8), and the borehole data (Figure 2) show a thinning of the Middle Miocene rocks, in particular the Nanchuang Fm, and the concomitant thickening of the Kueichulin, Cholan, and Toukoshan formations.

By contouring the basal thrust from the cross- and strike-parallel sections, we see that it dips gently toward the southeast, with two pronounced sigmoidal changes in strike of the depth contours that form what we call the Yichu and Hsinhua oblique ramps (Figure 9a). From north to south, the branch line of the Chelungpu thrust undergoes a marked change in strike, from nearly downdip along the Yichu ramp to roughly parallel to the basal thrust contours across the Hsinhua ramp (Figure 9b). The branch lines of the Chutochi and Pingshi thrusts are oblique to the basal thrust contours across both the Hsinhua and Yichu ramps. Both ramps end at the Chishan thrust as, on the basis of the shallowing of the 5.2 km/s isovelocity surface, this thrust is interpreted to ramp down into the basement (gray are in Figure 9b). From our data we can only determine the hanging wall and footwall cutoffs with respect to the basal thrust for the Kueichulin Fm along the Chelungpu thrust (Figure 9b). In the north, these cutoffs undergo significant changes in strike and location with respect to the Chelungpu branch line compared to farther south. In the north, the cutoffs parallel the

Tectonics 10.1029/2017TC004910

basal thrust contours along the Yichu ramp, reaching up to nearly 15 km west of the branch line at a depth of 1 to 2 km. They then take on a nearly north-south strike, cutting obliquely across the basal thrust contours along the Hsinhua ramp to become parallel to them along the frontal ramp where they are east of the Chelungpu branch line at a depth of 5 to 6 km. The transport direction, which is calculated to be perpendicular to the footwall and hanging wall cutoffs, is approximately westward in the north, becoming more west-northwest in the south (Figure 9b). These changes in orientation and location of the cutoffs relative to the thrust branch line provide further evidence that the Yichu and, in particular, the Hsinhua oblique ramps have an important effect on the structure of the thrust system. Although these determinations of transport direction provide important kinematic information for our structural model, the information is limited since we were not able to resolve the location of the cutoffs across the Hsinhua oblique ramp, nor the cutoffs for other thrusts. Nevertheless, the transport directions obtained in this way are in good agreement with long-term displacements fields determined by Lacombe et al. (1999, 2001) and modeled with GPS data by Ching et al. (2011). There are also significant changes in fold style, plunge direction, and plunge amount associated with both the Yichu and the Hsinhua oblique ramps (Figure 9c). For example, in the northern part of the study area, the fold structure is dominated by long, shallowly plunging synclines with mildly sinuous axial traces (YS and TS in Figure 9c) as they cross the Yichu oblique ramp, but they terminate abruptly at the Hsinhua oblique ramp. Here axial traces are short and, where there are sharp bends in the oblique ramp, folds have overall moderately to gently northwest or southeast plunges. A notable exception to this is the periclinal Shihchangli syncline (SS in Figure 9c) whose axial trace undergoes marked changes in plunge amount and direction as it crosses the Hsinhua oblique ramp, giving it a geometry common to folds draping over lateral footwall ramps (e.g., Alvarez-Marron, 1995).

The structure beneath the basal thrust is highly interpretative throughout the study area, and to show this, we have left parts of the sections blank (Figures 6 and 8). Nevertheless, we feel that it is essential for understanding the potential role played by the basement in the deformation to attempt some constraints on the structure beneath the basal thrust. From the borehole data and the surface geology (Figures 3 and 4), it is clear that there are changes in thickness of the Miocene rocks from one thrust sheet to another. These changes in thickness have been interpreted here, and in a number of other studies in southwest Taiwan (Alvarez-Marron et al., 2014; Rodriguez-Roa & Wiltschko, 2010; Suppe, 1986; Yang et al., 2007, 2016), to indicate the presence of roughly east-northeast striking, Miocene-age, extensional faults that had developed on the outer shelf, and slope areas of the continental margin (e.g., A. T. Lin et al., 2003; Yang et al., 1991). In our sections (Figures 6 and 8) we have also interpreted changes in depth of the 5.2 km/s isovelocity line to coincide with several of these extensional faults allowing us, in a number of cases, to trace them from one section to another (e.g., F1 and F3 in Figures 6–8) where they affect the geometry of the basement-cover interface proxy. We stress, however, that the details of the basement structure remain speculative.

6. Discussion

An important step for understanding the 3-D structure of a fold-and-thrust belt is to be able to link its mapped surface structure with a well-constrained interpretation of its structure at depth. In general, this is accomplished by the iterative construction of serial cross- and along-strike sections (as described in section 4). Further insights into the subsurface structure can then be obtained by making maps of stratigraphic cutoffs and thrust branch lines off the basal thrust (e.g., Boyer & Elliott, 1982; Elliott & Johnson, 1980; Hossack, 1983; Oncken et al., 1999; Srivastava & Mitra, 1994; Woodward, 1986). This workflow results in an integrated structural model of a fold-and-thrust belt that, while nonunique, reduces the uncertainties inherent in a 2-D model composed of serial cross sections alone. From such a structural model we can make reasonably well-constrained interpretations of the structure and make inferences about the geological processes that went into the development of the structural architecture of the fold-and-thrust belt in southwest Taiwan. Of these processes, the reactivation of faults derived from a continental margin has been shown to be particularly important in many fold-and-thrust belts from around the world, including Taiwan (see the references in the section 1). In the discussion that follows, we focus on the along-strike change in structure that takes place from the Chelungpu, Chutochi, Pingshi, and Chishan thrust sheets in the north to the Xuxian antiform and the Kuanglin synform in the south, arguing, as we did in section 5.1, that this change takes place along a transverse zone. We then go on to argue that this transverse zone is reflecting the response of the deformation in the fold-and-thrust belt to structural and morphological features inherited

Tectonics 10.1029/2017TC004910

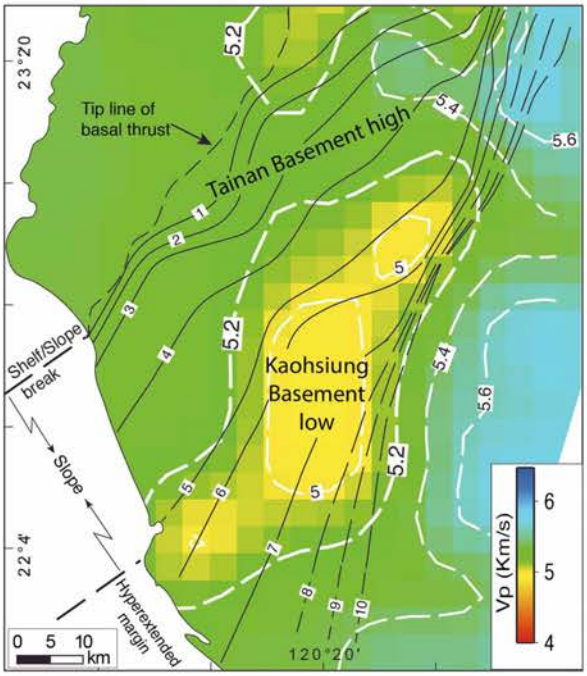

Figure 10. The 6-km depth slice of the *Vp* tomography model of Kuo-Chen et al. (2012) for the south western Taiwan area. Several isovelocity lines in km/s are shown in white dashed line, including the 5.2 km/s represented in sections shown in Figures 6 and 8. The superposed thin black lines correspond to the depth contours in km of the basal thrust.

from the deforming Eurasian continental margin. Other workers have also interpreted transfer zones in this part of the fold-and-thrust belt and interpreted them to be the result of the reactivation of preexisting faults on the margin (e.g., Deffontaines et al., 1997; Lacombe et al., 1999). While our field data do not support the model of transfer zones as proposed by Deffontaines et al. (1997), Lacombe et al. (1999, 2001), Mouthereau et al. (1999, 2002), and Mouthereau and Lacombe (2006), it is noteworthy that the dip directions of the Yichu and Hsinhua oblique ramps (Figure 9) roughly coincide with the interpreted strikes of their Chiayi and Chishan transfer zones. Furthermore, S. T. Huang et al. (2004) interpreted sigmoidal bends in the basal thrust near our Hsinhua oblique ramp to be related to basement highs, going on to suggest that these bends might be the cause of the changes in the GPS displacement field in this area.

If we accept that the suite of structures mapped at the surface (east-northeast striking faults, sigmoidal bends of thrusts, periclinal folds, etc.) and in the subsurface (an oblique ramp in the basal thrust, the change in location and depth of stratigraphic cutoffs, and so on) form a transverse zone (Hsinhua) across which the important north to south change in the structure of the southwest Taiwan fold-and-thrust belt occurs, then we can begin to investigate whether or not there is a causal relationship between this transverse zone and some aspects of the morphology and/or structure of the Eurasian margin. The *P* wave velocity model provides a key data set for investigating whether or not such a causal link exists, since it allows us to interpret features at depth below the fold-and-thrust belt that may be related to structures in the basement that are being inherited from the margin (Brown et al., 2017). For example, a 6-km depth slice through the *P* wave velocity model (Figure 10) shows a north-northeast trending velocity high through the study area that is bounded to the south by a north-northeast trending velocity low. These may be constituted by more than one velocity high and low, but, as stated in section 4, our tomography can only resolve minimum volumes of 20 km by 20 km by 10 km thick (Kuo-Chen et al., 2012). Nevertheless, this is well within the range to resolve basement highs and lows such as those imaged on the necking zone of the margin by reflection seismic and wide-angle tomography profiles (e.g., Brown et al., 2017; Lester et al., 2014; Li et al., 2007; McIntosh et al., 2014). We therefore interpret the velocity high and low in Figure 10 to be related to a basement high (Tainan Basement High) and low (Kaoshiung Basement Low).

By mapping the contours of the basal thrust derived from our 3-D structural model on the 6 km Vp depth slice (Figure 10), it is evident that, even given the resolution of the velocity model, there is good correlation between the location of the Yichu and Hsinhua oblique ramps and the Tainan Basement High. Furthermore, this correlation suggests that the topography of the basement has a roughly northeast to east-northeast striking structural grain, similar to that of extensional fault systems mapped on the margin offshore (e.g., A. T. Lin et al., 2003; Yang et al., 1991, 2016). On the basis of this correlation we suggest that it is possible to interpret a causative link between structures in the fold-and-thrust belt (i.e., oblique ramps and transverse zones) and features that are inherited from the continental margin (basement highs and lows). While we draw smooth, continuous contours for the basal thrust, it is likely that the east-northeast striking faults that bound similar basement highs and lows offshore, and which extend into the Coastal Plain (e.g., S. T. Huang et al., 2004; A. T. Lin et al., 2003; Yang et al., 1991, 2016), also bound the Tainan Basement High. The widespread occurrence of seismicity below the basal thrust and with dextral strike-slip focal mechanisms in the area around the Tainan Basement High (e.g., Hsu et al., 2010; Wu et al., 2010) is, furthermore, suggestive of reactivation of these faults. Since these reactivating faults are active over the same geological time frame as the basal thrust, this will cause the basal thrust to accommodate to the reactivating fault via a lateral ramp and/or a breaching of the basal thrust, implying a complex kinematic and geometrical relationship between them (e.g., Bayona et al., 2003; Calassou et al., 1993; Thomas, 1990; Thomas & Bayona, 2002; Turner et al., 2010) that, we think, will result in the formation of structures such as those described for

Tectonics 10.1029/2017TC004910

Hsinhua transverse zone. Numerous authors (e.g., Alvarez-Marron et al., 2014; Brown et al., 2017; Mouthereau et al., 2001; Mouthereau & Lacombe, 2006; Rodriguez-Roa & Wiltschko, 2010; Suppe, 1986; Yang et al., 2007, 2016) interpret structural complexities in the geology of southwest Taiwan to be related to the reactivation of such faults, although it is not always clear from these interpretations how the interaction between the reactivated faults and the basal thrust is coupled (or not). An exception is Mouthereau and Lacombe (2006) who interpret an imbricate thrust system in which thrusts sole into a ductile shear zone at about 15-km depth. Regardless, widespread seismic activity throughout nearly the entire crust in southwest Taiwan (Chang et al., 2007; Chao et al., 2011; Hsu et al., 2010; Wu et al., 2010; Yang et al., 2016) suggests that both the preexisting faults of the margin and those of the fold-and-thrust belt are all currently active.

Following the interpretation of Brown et al. (2017), the study area corresponds structurally to the intensely faulted necking zone and the beginning of the hyperextended part of the margin and, morphologically, to the outer shelf, the shelf-to-slope transition, and the slope (Figures 1 and 4). In the above discussion, we have dealt with the possible causal relationships between structures inherited from the margin and those in the fold-and-thrust belt. In what follows, we briefly look at possible linkages between the morphological parts of the margin and the structure of the fold-and-thrust belt. In southwestern Taiwan, both the mapped surface trace of thrusts and the subsurface contours of the basal thrust undergo a series of sigmoidal bends to take on an orientation that approximates that of the shelf-slope break and the onset of the hyperextended part of the margin (Brown et al., 2017; Figures 4 and 10). It is at the shelf-slope break where the frontal thrust of the fold-and-thrust belt goes offshore to form the front of the marine accretionary prism (Figure 1; see also A. T. Lin et al., 2008). Furthermore, the area encompassed by the Yichu and Hsinhua oblique ramps roughly correlates in location and strike with a significant southeastward increase in thickness of the Miocene through Pleistocene sediments (e.g., Chou, 1972, 1980) and with a change in facies toward deeper water deposits (Castelltort et al., 2010; Chou, 1972; Lin & Watts, 2002; Nagel et al., 2013). Therefore, another factor that may be influencing the along-strike structural changes in the southwest Taiwan fold-and-thrust belt could be related to mechanical differences along the basal thrust (e.g., Albers, 1967; Koyi et al., 2016; Mugnier et al., 1999; Ruh et al., 2014) that can be caused by changes in sedimentary thickness and facies. Although Mouthereau et al. (2001) explore some aspects of the influence of stratigraphic thickness and facies on the structure of the fold-and-thrust belt, we feel that more work, which should include numerical modeling, needs to be carried out before we can begin to draw conclusions about the influence of changes in sedimentary thickness and facies on the fold-and-thrust belt in southwest Taiwan.

7. Conclusions

On the basis of our new surface geological mapping, we interpret the structure of the fold-and-thrust belt in southwest Taiwan to be an imbricate thrust system with a pronounced north-south change in structural architecture across a roughly east-west striking zone that we call the Hsinhua transverse zone. The Hsinhua transverse zone falls along the on land projection of the shelf-slope break (Figures 4 and 10), and it coincides with Zone C of Brown et al. (2017). In this interpretation, the northern part of the study area comprises five thrust sheets: the Changhua, Chelungpu, Chutochi, Pingshi, and Chishan thrust sheets, whereas to the south of the Hsinhua transverse zone we divide the structure broadly into Changhua thrust sheet, the Xuxian antiform, and the Kuanglin synform (Figure 5). In our balanced and restored cross sections, we interpret the tip line of the basal thrust to be the buried Changhua thrust and, in the west, to lie within the Pliocene or Pleistocene synorogenic sediments before ramping down stratigraphic section eastward into the Early and Middle Miocene rocks and finally into the basement along the Chishan thrust. We estimate the minimum shortening across the fold-and-thrust belt in southwest Taiwan to be on the order of 17 and 25 km.

Overall, the basal thrust to the imbricate thrust system dips gently southeastward, but it has two pronounced sigmoidal changes in strike that form what we call the Yichu and Hsinhua oblique ramps. We suggest that the dextral strike-slip faulting, sigmoidal bending of the surface trace of thrusts, folds axes, and bedding (i.e., the Hsinhua transverse zone), together with the along-strike change in structure that occur in the fold-and-thrust belt of southwest Taiwan can be directly linked to these two oblique ramps. We furthermore suggest that both these oblique ramps can be directly correlated with topographic highs and lows that we interpret to occur in the basement (Figure 10) and that this possibly indicates a causative relationship between the

Tectonics 10.1029/2017TC004910

basement structure, the geometry of the basal thrust, and the along-strike changes mapped in the surface geology. We also acknowledge that the along-strike structural changes in the southwest Taiwan fold-and-thrust belt could also, in part, be related to mechanical differences along the basal thrust that can be caused by the changes in sedimentary thickness and facies that take place across the outer part of the shelf and the slope areas of the margin.

Acknowledgments
D. B., J. A-M., and C. B. acknowledge funding provided by the Spanish Ministerio de Economia y Competividad grant CGL2013-43877-P. H. K-C. acknowledges funding by MOST 104-2628-M-008-005-MY3. Constructive reviews by C. von Hagke and an anonymous reviewer are also acknowledged. The geological data presented in this paper can be found in the supporting information in the form of a 1:100,000 scale map and a.txt file for the structural data. The seismic tomography data from which Figure 10 was plotted can be found at http://140.115.22.221/download/data.

References

Albers, J. P. (1967). Belt of sigmoidal bending and right-lateral faulting in the Western great Basin. *Geological Society of America Bulletin*, *78*(2), 143–156. https://doi.org/10.1130/0016-7606(1967)78[143:BOSBAR]2.0.CO;2

Alvarez-Marron, J. (1995). Three-dimensional geometry and interference of fault-bend fold: Examples from the Ponga Unit, Variscan Belt, NW Spain. *Journal of Structural Geology*, *17*(4), 549–560. https://doi.org/10.1016/0191-8141(94)00075-B

Alvarez-Marron, J., Brown, D., Camanni, G., Wu, Y.-M., & Kuo-Chen, H. (2014). Structural complexities in a foreland thrust belt inherited from the shelf-slope transition: Insights from the Alishan area of Taiwan. *Tectonics*, *33*, 1322–1339. https://doi.org/10.1002/2014TC003584.

Arora, B. R., Gahalaut, V. K., & Kumar, N. (2012). Structural control on along-strike variation in the seismicity of the northwest Himalaya. *Journal of Asian Earth Sciences*, *57*, 15–24. https://doi.org/10.1016/j.jseaes.2012.06.001

Bayona, G., Thomas, W. A., & Van der Voo, R. (2003). Kinematics of thrust sheets within transverse zones: A structural and paleomagnetic investigation in the Appalachian thrust belt of Georgia and Alabama. *Journal of Structural Geology*, *25*(8), 1193–1212. https://doi.org/10.1016/S0191-8141(02)00162-1

Bonilla, M. G. (1975). A review of recently active faults in Taiwan, USGS Open-File Rep. 75-41, 43.

Boyer, S. E., & Elliott, D. (1982). Thrust systems. *American Association of Petroleum Geologists*, *66*, 1196–1230.

Brown, D., Alvarez-Marron, J., Biete, C., Kuo-Chen, H., Camanni, G., & Ho, C.-W. (2017). How the structural architecture of the Eurasian continental margin affects the structure, seismicity, and topography of the south central Taiwan fold-and-thrust belt. *Tectonics*, *36*, 1275–1294. https://doi.org/10.1002/2017TC004475

Brown, D., Alvarez-Marron, J., Schimmel, M., Wu, Y.-M., & Camanni, G. (2012). The structure and kinematics of the central Taiwan mountain belt derived from geological and seismicity data. *Tectonics*, *31*, TC5013. https://doi.org/10.1029/2012TC003156

Butler, R. W. H., Tavarnelli, E., & Grasso, M. (2006). Structural inheritance in mountain belts: An Alpine–Apennine perspective. *Journal of Structural Geology*, *28*(11), 1893–1908. https://doi.org/10.1016/j.jsg.2006.09.006

Calassou, S., Larroque, C., & Malavieille, J. (1993). Transfer zones of deformation in thrust wedges: An experimental study. *Tectonophysics*, *221*(3-4), 325–344. https://doi.org/10.1016/0040-1951(93)90165-G

Camanni, G., Alvarez-Marron, J., Brown, D., Ayala, C., Wu, Y.-M., & Hsieh, H.-H. (2016). The deep structure of south-central Taiwan illuminated by seismic tomography and earthquake hypocentre data. *Tectonophysics*, *679*, 235–245. https://doi.org/10.1016/j.tecto.2015.09.016

Castelltort, S., Nagel, S., Moutherreau, F., Lin, A., Wetzel, A., Kaus, B., et al. (2010). Sedimentology of Early Pliocene sandstones in the southwestern Taiwan foreland: Implications for basin physiography in the early stages of collision. *Journal of Asian Earth Sciences*, *40*, 52–71.

Chang, S. (1963). Regional stratigraphic study of Pleistocene and upper Pliocene formations in Chiayi and Hsinying area. *Petroleum Geology of Taiwan*, *2*, 65–85.

Chang, C.-H., Wu, Y.-M., Zhao, L., & Wu, F. T. (2007). Aftershocks of the 1999 Chi-Chi, Taiwan, Earthquake: The first hour. *Bulletin of the Seismological Society of America*, *97*(4), 1245–1258. https://doi.org/10.1785/0120060184

Chao, W.-A., Zhao, L., & Wu, Y.-M. (2011). Centroid fault-plane inversion in three-dimensional velocity structure using strong-motion records. *Bulletin of the Seismological Society of America*, *101*(3), 1330–1340. https://doi.org/10.1785/0120100245

Chen, C.-H., Ho, H.-C., Shea, K.-S., Lo, W., Lin, W.-H., Chang, H.-C., et al. (2000). Geological map of Taiwan. 1:500,000 scale, Central Geol. Sur., Taiwan.

Chen, W.-S., Ridgway, K. D., Horng, C.-S., Chen, Y.-G., Shea, K.-S., & Yeh, M.-G. (2001). Stratigraphic architecture, magnetostratigraphy, and incised-valley systems of the Pliocene-Pliestocene collisional marine foreland basin of Taiwan. *Geological Society of America Bulletin*, *113*(10), 1249–1271. https://doi.org/10.1130/0016-7606(2001)113<1249:SAMAIV>2.0.CO;2

Chiang, S. C. (1971). Seismic study of the Paishatun structure, Miaoli, Taiwan. *Petroleum Geology of Taiwan*, *8*(8), 281–294.

Chiang, C., Yuw, H., & Chouz, Y. (2004). Characteristics of the wedge-top depozone of the southern Taiwan foreland basin system. *Basin Research*, *16*(1), 65–78. https://doi.org/10.1111/j.1365-2117.2003.00222.x

Ching, K.-E., Rau, R.-J., Johnson, K. M., Lee, J.-C., & Hu, J.-C. (2011). Present-day kinematics of active mountain building in Taiwan from GPS observations during 1995-2005. *Journal of Geophysical Research*, *116*, B09405. https://doi.org/10.1029/2010JB008058

Chiu, H. T. (1975). Miocene stratigraphy and its relation to the Palaeogene rocks in West - Central Taiwan. *Petroleum Geology of Taiwan*, *12*, 51–80.

Chou, J. T. (1971). A preliminary study of the stratigraphy and sedimentation of the mudstone formations in the Tainan area, southern Taiwan. *Petroleum Geology of Taiwan*, *8*, 187–220.

Chou, J. T. (1972). A sedimentologic and paleogeographic study of the upper Cenozoic clastic sequences in the Chiayi region, Western Taiwan. *Petroleum Geology of Taiwan*, *10*, 141–158.

Chou, J. T. (1980). Stratigraphy and sedimentology of the Miocene in western Taiwan. *Petroleum Geology of Taiwan*, *17*, 33–52.

Covey, M. (1986). The evolution of foreland basins to steady state: Evidence from the western Taiwan Foreland Basin. In *Foreland Basins* (pp. 77–90). Oxford, UK: Blackwell Publishing Ltd. https://doi.org/10.1002/9781444303810.ch4

Dahlstrom, C. D. A. (1969). Balanced cross sections. *Canadian Journal of Earth Sciences*, *6*(4), 743–757. https://doi.org/10.1139/e69-069

De Paor, D. G. (1988). Balanced section in thrust belts part 1: Construction. *American Association of Petroleum Geologists Bulletin*, *72*, 73–90.

Deffontaines, B., Lacombe, O., Angelier, J., Chu, H.-T., Mouthereau, F., Lee, C.-T., et al. (1997). Quaternary transfer faulting in the Taiwan Foorhills: Evidence from a multisource approach. *Tectonophysics*, *274*(1-3), 61–82. https://doi.org/10.1016/S0040-1951(96)00298-3

Ding, W.-W., Li, J.-B., Li, M.-B., Qiu, X.-L., Fang, Y.-X., & Tang, Y. (2008). A Cenozoic tectono-sedimentary model of the Tainan Basin, the South China Sea: Evidence from multi-channel seismic profile. *Journal of Zhejiang University. Science*, *9*(5), 702–713. https://doi.org/10.1631/jzus.A071572

Duncan, C., Masek, J., & Fielding, E. (2003). How steep are the Himalaya? Characteristics and implications of along-strike topographic variations. *Geology*, *31*(1), 75–78. https://doi.org/10.1130/0091-7613(2003)031<0075:HSATHC>2.0.CO;2

Elliott, D., & Johnson, M. R. W. (1980). Structural evolution in the northern part of the Moince thrust belt, NW Scotland. *Transactions of the Royal Society of Edinburgh Earth Sciences*, *71*(02), 69–96. https://doi.org/10.1017/S0263593300013523

Ernst, W. G. (1983). Mineral paragenesis in metamorphic rocks exposed along Tailuko Gorge, Central Mountain Range, Taiwan. *Journal of Metamorphic Geology*, *1*(4), 305–329. https://doi.org/10.1111/j.1525-1314.1983.tb00277.x

Faulds, J. E., & Varga, R. J. (1998). The role of accommodation zones and transfer zones in the regional segmentation of extended terranes. In J. E. Faulds & J. H. Stewart (Eds.), *Accommodation zones and transfer zones: The regional segmentation of the basin and range province*, *Geol. Soc. Am. Spec. Paper* (Vol. 323, pp. 1–45). Boulder, CO.

Flöttmann, T., & James, P. (1997). Influence of basin architecture on the style of inversion and fold-thrust belt tectonics—The southern Adelaide fold-thrust belt, South Australia. *Journal of Structural Geology*, *19*(8), 1093–1110. https://doi.org/10.1016/S0191-8141(97)00033-3

Groshong, R. H., Bond, C. E., Gibbs, A., Ratliff, R., & Wiltschko, D. V. (2012). Preface: Structural balancing at the start of the 21st century: 100 years since Chamberlin. *Journal of Structural Geology*, *41*, 1–5. https://doi.org/10.1016/j.jsg.2012.03.010

Ho, C. S. (1986). A synthesis of the geologic evolution of Taiwan. *Tectonophysics*, *125*(1-3), 1–16. https://doi.org/10.1016/0040-1951(86)90004-1

Ho, C.-S. (1988). An Introduction to the Geology of Taiwan: Explanatory text of the Geological Map of Taiwan, Central Geological Survey. Taipei, Taiwan.

Hong, E. (1997). Evolution of Pliocene to Pleistocene sedimentary environments in an arc-continent collision zone: Evidence from the analyses of lithofacies and ichnofacies in the southwestern foothills of Taiwan. *Journal of Asian Earth Sciences*, *15*(4–5), 381–392. https://doi.org/10.1016/S0743-9547(97)00022-6

Horng, C. S., & Shea, K.-S. (1994). Study of nannofossil biostratigraphy in the eastern part of the Erhjen-chi section, southwestern Taiwan. *Special Publication of Centre Geological Survey*, *8*, 181–204.

Horng, C.-S. (2014). Age odd the Tananwan Formation in northern Taiwan: A reexamination of the magnetostratigraphy and calcareous nannofossil biostratigraphy. *Terrestrial, Atmospheric and Oceanic Sciences*, *25*, 137–147.

Hossack, J. R. (1979). The use of balanced cross-sections in the calculation of orogenic contraction: A review. *Journal of the Geological Society*, *136*(6), 705–711. https://doi.org/10.1144/gsjgs.136.6.0705

Hossack, J. R. (1983). A cross-section through the Scandinavian Caledonides constructed with the aid of branch-line maps. *Journal of Structural Geology*, *5*(2), 103–111. https://doi.org/10.1016/0191-8141(83)90036-6

Hsu, Y.-J., Rivera, L., Wu, Y.-M., Chang, C.-H., & Kanamori, H. (2010). Spatial heterogeneity of tectonic stress and friction in the crust: New evidence from earthquake focal mechanisms in Taiwan. *Geophysical Journal International*, *182*, 329–342.

Huang, M.-H., Hu, J.-C., Ching, K.-E., Rau, R.-J., Hsieh, C.-S., Pathier, E., et al. (2009). Active deformation of Tainan tableland os southwestern Taiwan based on geodetic measurements and SAR interferometry. *Tectonophysics*, *466*(3-4), 322–334. https://doi.org/10.1016/j.tecto.2007.11.020

Huang, C. Y., Yen, Y., Zhao, Q. H., & Lin, C. T. (2012). Cenozoic stratigraphy of Taiwan: Window into rifting, stratigraphy and paleoceanography of South China Sea. *Chinese Science Bulletin*, *57*(24), 3130–3149. https://doi.org/10.1007/s11434-012-5349-y

Huang, L.-S. (1984). Iodine contents in formation waters from wildcats, southern Taiwan. *Petroleum Geology of Taiwan*, *20*, 215–235.

Huang, S. T., Yang, K.-M., Hung, J.-H., Wu, J. C., Ting, H. H., Mei, W. W., et al. (2004). Deformation front development at the northeast margin of the Tainan basin, Tainan-Kaohsiung area, Taiwan. *Marine Geophysical Researches*, *25*(1–2), 139–156. https://doi.org/10.1007/s11001-005-0739-z

Jahn, B.-M., Chi, W.-R., & Yui, T.-F. (1992). A Late Permian formation of Taiwan marbles from Chia-Li well No.1: Pb-Pb isochron and Sr isotopic evidence, and its regional geological significance. *Journal of the Geological Society of China*, *35*, 193–218.

Judge, P. A., & Allmendinger, R. W. (2011). Assessing uncertainties in balanced cross sections. *Journal of Structural Geology*, *33*, 458–467.

Koyi, H., Nilfouroushan, F., & Hessami, K. (2016). Modelling role of basement block rotation and strike-slip faulting on structural pattern in cover units of fold-and-thrust belts. *Geological Magazine*, *153*(5-6), 827–844. https://doi.org/10.1017/S0016756816000595

Kuo-Chen, H., Wu, F. T., & Roecker, S. W. (2012). Three-dimensional P velocity structures of the lithosphere beneath Taiwan from the analysis of TAIGER and related seismic data sets. *Journal of Geophysical Research*, *117*, B06306. https://doi.org/10.1029/2011JB009108

Lacombe, O., Mouthereau, F., Angelier, J., & Deffontaines, B. (2001). Structural, geodetic and seismological evidence for tectonic escape in SW Taiwan. *Tectonophysics*, *333*(1-2), 323–345. https://doi.org/10.1016/S0040-1951(00)00281-X

Lacombe, O., Mouthereau, F., Deffontaines, B., Angelier, J., Chu, H. T., & Lee, C. T. (1999). Geometry and Quaternary kinematics of fold-and-thrust units of southwestern Taiwan. *Tectonics*, *18*(6), 1198–1223. https://doi.org/10.1029/1999TC900036

Lan, C.-Y., Lee, C.-S., Yui, T.-F., Chu, H.-T., & Jahn, B.-M. (2008). The tectono-thermal events of Taiwan and their relationship with SE China. *Terrestrial, Atmospheric and Oceanic Sciences*, *19*(3), 257–278. https://doi.org/10.3319/TAO.2008.19.3.257(TT)

Lee, T.-Y., Tang, C.-H., Ting, J.-S., & Hsu, Y.-Y. (1993). Sequence stratigraphy of the Tainan Basin, offshore Southwestern Taiwan. *Petroleum Geology of Taiwan*, *28*, 119–158.

Lester, R., Van Avendonk, H. J. A., McIntosh, K., Lavier, L., Liu, C.-S., Wang, T.-K., & Wu, F. (2014). Rifting and magmatism in the northeastern South China Sea from wide-angle tomography and seismic reflection imaging. *Journal of Geophysical Research: Solid Earth*, *119*, 2305–2323. https://doi.org/10.1002/2013JB010639

Li, C.-F., Zhou, Z., Li, J., Hao, H., & Geng, J. (2007). Structures of the northeasternmost South China Sea continental margin and ocean basin: Geophysical constraints and tectonic implications. *Marine Geophysical Researches*, *28*(1), 59–79. https://doi.org/10.1007/s11001-007-9014-9

Lin, A. T., Liu, C.-S., Lin, C. C., Schnurle, P., Chen, G. Y., Liao, W. Z., et al. (2008). Tectonic features associated with the overriding of an accretionary wedge on top of a rifted continental margin: An example from Taiwan. *Marine Geology*, *255*(3–4), 186–203. https://doi.org/10.1016/j.margeo.2008.10.002

Lin, A. T., & Watts, A. B. (2002). Origin of the West Taiwan basin by orogenic loading and flexure of a rifted continental margin. *Journal of Geophysical Research*, *107*(B9), 2185. https://doi.org/10.1029/2001JB000669

Lin, A. T., Watts, A. B., & Hesselbo, S. P. (2003). Cenozoic stratigraphy and subsidence history of the South China Sea margin in the Taiwan region. *Basin Research*, *15*(4), 453–478. https://doi.org/10.1046/j.1365-2117.2003.00215.x

Lin, J.-Y., Sibuet, J.-C., & Hsu, S.-K. (2005). Distribution of the East China Sea continental shelf basins and depths of magnetic sources. *Earth, Planets and Space*, *57*(11), 1063–1072. https://doi.org/10.1186/BF03351885

McIntosh, K., Lavier, L., Van Avendonk, H., Lester, R., Eakin, D., & Liu, C.-S. (2014). Crustal structure and inferred rifting processes in the northeast South China Sea. *Marine and Petroleum Geology*, *58*, 612–626. https://doi.org/10.1016/j.marpetgeo.2014.03.012

Mouthereau, F., Deffontaines, B., Lacombe, O., & Angelier, J. (2002). Variations along the strike of the Taiwan thrust belt: Basement control on structural style, wedge geometry, and kinematics. In T. B. Byrne & C.-S. Liu (Eds.), *Geology and geophysics of an arc-continent collision, Taiwan*, *Geol. Soc. am. Spec. Paper* (Vol. 358, pp. 31–54).

Mouthereau, F., & Lacombe, O. (2006). Inversion of the Paleogene Chinese continental margin and thick-skinned deformation in the Western Foreland of Taiwan. *Journal of Structural Geology*, *28*(11), 1977–1993. https://doi.org/10.1016/j.jsg.2006.08.007

Mouthereau, F., Lacombe, O., Deffontaines, B., Angelier, J., & Brusset, S. (2001). Deformation history of the southwestern Taiwan foreland thrust belt: Insights from tectono-sedimentary analyses and balanced cross-sections. *Tectonophysics, 333*(1–2), 293–322. https://doi.org/10.1016/S0040-1951(00)00280-8

Mouthereau, F., Lacombe, O., Deffontaines, B., Angelier, J., Chu, H.-T., & Lee, C.-T. (1999). Quaternary transfer faulting and belt front deformation at Pakuashan (western Taiwan). *Tectonics, 18*(2), 215–230. https://doi.org/10.1029/1998TC900025

Mouthereau, F., Lacombe, O., & Meyer, B. (2006). The Zagros folded belt (Fars, Iran): Constraints from topography and critical wedge modeling. *Geophysical Journal International, 165*, 336–356.

Mugnier, J. L., Leturmy, P., Mascle, G., Huyghe, P., Chalaron, E., Vidal, G., et al. (1999). The Siwaliks of western Nepal I. Geometry and kinematics. *Journal of Asian Earth Sciences, 17*(5-6), 629–642. https://doi.org/10.1016/S1367-9120(99)00038-3

Nagel, S., Castelltort, S., Wetzel, A., Willett, S. D., Mouthereau, F., & Lin, A. T. (2013). Sedimentology and foreland basin paleogeography during Taiwan arc continent collision. *Journal of Asian Earth Sciences, 62*, 180–204. https://doi.org/10.1016/j.jseaes.2012.09.001

Oncken, O., von Winterfeld, C., & Dittmar, U. (1999). Accretion of a rifted passive margin: The Late Paleozoic Rhenohercynian fold and thrust belt (Middle European Variscides). *Tectonics, 18*(1), 75–91. https://doi.org/10.1029/98TC02763

Pérez-Estaún, A., Alvarez-Marrón, J., Brown, D., Puchkov, V., Gorozhanina, Y., & Baryshev, V. (1997). Along-strike structural variations in the foreland thrust and fold belt of the southern Urals. *Tectonophysics, 276*(1-4), 265–280. https://doi.org/10.1016/S0040-1951(97)00060-7

Rodriguez-Roa, F. a., & Wiltschko, D. V. (2010). Thrust belt architecture of the central and southern Western Foothills of Taiwan. *Geological Society of London, Special Publication, 348*(1), 137–168. https://doi.org/10.1144/SP348.8

Ruh, J. B., Gerya, T., & Burg, J.-P. (2014). 3D effects of strain vs. velocity weakening on deformation patterns in accretionary wedges. *Tectonophysics, 615-616*, 122–141. https://doi.org/10.1016/j.tecto.2014.01.003

Shaw, C.-L. (1996). Stratigraphic correlation and isopach maps of the western Taiwan Basin. *Terrestrial, Atmospheric and Oceanic Sciences, 7*(3), 333–360. https://doi.org/10.3319/TAO.1996.7.3.333(T)

Shea, K.-S., Chang, H.-C., Huang, T.-Y., Ho, H.-C., Lin, W.-H., Lin, C.-W., & Chen, H.-W. (2003). Geological Column in Taiwan, *Central Geol. Surv. Taiwan*, Taiwan.

Shi, X., Xu, H., Qiu, X., Xia, K., Yang, X., & Li, Y. (2008). Numerical modeling on the relationship between thermal uplift and subsequent rapid subsidence: Discussion on the evolution of the Tainan Basin. *Tectonics, 27*, TC6003. https://doi.org/10.1029/2007TC002163

Shyu, J. B. H., Chuang, Y., Chen, Y., Lee, Y., & Cheng, C. (2016). A new on-land seismogenic structure source database from the Taiwan earthquake model (TEM) project for seismic hazard analysis of Taiwan. *Terrestrial, Atmospheric and Oceanic Sciences, 27*(3), 311–323. https://doi.org/10.3319/TAO.2015.11.27.02(TEM)A

Shyu, J. B. H., Sieh, K., Chen, Y.-G., & Liu, C.-S. (2005). Neotectonic architecture of Taiwan and its implications for future large earthquakes. *Journal of Geophysical Research, 110*, B08402. https://doi.org/10.1029/2004JB003251

Smith, N. T. (1999). Variscan inversion within the Cheshire Basin, England: Carboniferous evolution north of the Variscan Front. *Tectonophysics, 308*, 211–225.

Srivastava, P., & Mitra, G. (1994). Thrust geometries and deep structure of the outer and lesser Himalaya, Kumaon and Garhwal (India): Implications for the evolution of the Himalayan fold-and-thrust belt. *Tectonics, 13*(1), 89–109. https://doi.org/10.1029/93TC01130

Stanley, R. S., Hill, L. B., Chang, H. C., & Hu, H. N. (1981). A transect through the metamorphic core of the central mountains, southern Taiwan. *Memoir of Geological Society of China, 4*, 443–473.

Suppe, J. (1981). Mechanics of mountain-building and metamorphism in Taiwan. *Memoir of Geological Society of China, 4*, 67–89.

Suppe, J. (1986). Reactivated normal faults in the western Taiwan fold-and-thrust belt. *Memoir of Geological Society of China, 7*, 187–200.

Tang, C.-H. (1977). Late Miocene erosional unconformity on the subsurface Peikang high Chiayi Yulin. *Memoir of Geological Society of China, 2*, 155–167.

Tang, Q., & Zheng, C. (2010). Seismic velocity structure and improved seismic image of the Southern Depression of the Tainan Basin from pre-stack depth migration. *Terrestrial, Atmospheric and Oceanic Sciences, 21*(5), 807–816. https://doi.org/10.3319/TAO.2010.01.03.01(TT)

Teng, L.-S. (1987). Stratigraphic records of the Late Cenozoic Penglai Orogeny of Taiwan. *Acta Geologica Taiwanica, 25*, 205–224.

Teng, L.-S., & Lin, A.-T. (2004). Cenozoic tectonics of the China continental margin: Insights from Taiwan. In J. Malpas, C. J. N. Fletcher, J. R. Ali, & J. C. Aitchison (Eds.), *Aspects of the tectonic evolution of China, Geol. Soc. London, Spec. Pub.* (Vol. 226, pp. 313–332). Geological Society, London.

Tensi, J., Mouthereau, F., & Lacombe, O. (2006). Lithospheric bulge in the West Taiwan Basin. *Basin Research, 18*(3), 277–299. https://doi.org/10.1111/j.1365-2117.2006.00296.x

Thomas, W. A. (1985). The Appalachian-Ouachita connection: Paleozoic orogenic belt at the southern margin of North America. *Annual Review of Earth and Planetary Sciences, 13*(1), 175–199. https://doi.org/10.1146/annurev.ea.13.050185.001135

Thomas, W. A. (1990). Controls on locations of transverse zones in thrust belts. *Eclogae Geologicae Helvetiae, 83*, 727–744.

Thomas, W. A., & Bayona, G. (2002). Palinspastic restoration of the Anniston transverse zone in the Appalachian thrust belt, Alabama. *Journal of Structural Geology, 24*(4), 797–826. https://doi.org/10.1016/S0191-8141(01)00117-1

Turner, S. A., Cosgrove, J. W., & Liu, J. G. (2010). Controls on lateral structural variability along the Keping Shan Thrust Belt, SW Tien Shan foreland, China. In G. P. Goffey, J. Craig, T. Needham, & R. Scott (Eds.), *Hydrocarbons in contractional belts, Geological Society of London, Special Publications* (Vol. 348, pp. 71–85). Geological Society, London. https://doi.org/10.1144/SP348.5

Woodward, N. B. (1986). Thrust fault geometry of the Snake River Range, Idaho and Wyoming. *Geological Society of America Bulletin, 97*(2), 178–193. https://doi.org/10.1130/0016-7606(1986)97<178:TFGOTS>2.0.CO;2

Wu, Y.-M., Hsu, Y.-J., Chang, C.-H., Teng, L. S.-Y., & Nakamura, M. (2010). Temporal and spatial variation of stress in Taiwan from 1991 to 2007: Insights from compressive first motion focal mechanism catalog. *Earth and Planetary Science Letters, 298*(3-4), 306–316. https://doi.org/10.1016/j.epsl.2010.07.047

Yang, K.-M., Huang, S. T., Wu, J.-C., Ting, H.-H., & Mei, W.-W. (2006). Review and new insights on foreland tectonics in western Taiwan. *International Geology Review, 48*(10), 910–941. https://doi.org/10.2747/0020-6814.48.10.910

Yang, K.-M., Huang, S.-T., Wu, J.-C., Ting, H.-H., Mei, W.-W., Lee, M., et al. (2007). 3D geometry of the Chelungpu thrust system in Central Taiwan: Its implications for active tectonics. *Terrestrial, Atmospheric and Oceanic Sciences, 18*, 143–181.

Yang, K.-M., Rau, R.-J., Chang, H.-Y., Hseih, C.-Y., Ting, H.-H., Huang, S.-T., et al. (2016). The role of basement-involved normal faults in the recent tectonics of western Taiwan. *Geological Magazine, 153*(5-6), 1166–1191. https://doi.org/10.1017/S0016756816000637

Yang, K.-M., Ting, H.-H., & Yuan, J. (1991). Structural styles and tectonic modes of Neogene extensional tectonics in southwestern Taiwan: Implications for hydrocarbon exploration. *Petroleum Geology of Taiwan, 26*, 31.

Yang, K.-M., Wu, J.-C., Cheng, E.-W., Chen, Y.-R., Huang, W.-C., Tsai, C.-C., et al. (2014). Development of tectonostratigraphy in distal part of foreland basin in southwestern Taiwan. *Journal of Asian Earth Sciences, 88*, 98–115. https://doi.org/10.1016/j.jseaes.2014.03.005

Tectonics 10.1029/2017TC004910

Yin, A. (2006). Cenozoic tectonic evolution of the Himalayan orogeny as constrained by along-strike variation of structural geometry, exhumation history, and foreland sedimentation. *Earth Science Reviews*, *76*(1-2), 1–131. https://doi.org/10.1016/j.earscirev.2005.05.004

Yu, S., Chen, H., & Kuo, L. (1997). Velocity field of GPS stations in the Taiwan area. *Tectonophysics*, *274*(1-3), 41–59. https://doi.org/10.1016/S0040-1951(96)00297-1

Yuan, J., & Huang, S. T. (1985). Stratigraphic study on the pre Miocene under the Peikang Area.

Zanchi, A., Berra, F., Mattei, M., Ghassemi, M. R., & Sabouri, J. (2006). Inversion tectonics in the central Alboraz, Iran. *Journal of Structural Geology*, *28*(11), 2023–2037. https://doi.org/10.1016/j.jsg.2006.06.020

APPENDIX 2 Conference Abstracts

Abstract 1:

How the structure of a continental margin affects the development of a fold and thrust belt. 1: A case study in south-central Taiwan

Dennis Brown[1], Joaquina Alvarez-Marron[1], **Cristina Biete**[1], Giovanni Camanni[2], Hao, Kuo-Chen[3], Chun-Wei Ho[3,4]

- [1]Institute of Earth Sciences Jaume Almera, ICTJA-CSIC, 08028 Barcelona, Spain
- [2]University College, Dublin
- [3]Department of Geosciences, National Central University, Jongli, Taiwan.
- [4]Central Weather Bureau, Taipei 100, Taiwan

Presented at: 2016 EGU General Assembly. Vienna (Austria)

Type of presentation: poster

Abstract:

Studies of mountain belts worldwide have shown that the structural, mechanical, and kinematic evolution of their foreland fold and thrust belts are strongly influenced by the structure of the continental margins that are involved in the deformation. The area on and around the island of Taiwan provides an unparalleled opportunity to investigate this because the entire profile of the Eurasian margin, from the shelf in the north to the slope and continent-ocean transition in the south and the offshore, is currently involved in the collision. Taiwan, then, can provide key insights into how such features as rift basins on the shelf, the extensional faults that form the shelf-slope break in the basement, or the structure of the extended crust and morphology of the sedimentary carapace of the slope can be directly reflected in the location and pattern of its seismicity, in its topography, and in its structural architecture, among other things. The continental margin of the Eurasian Plate that is currently involved in the Taiwan orogeny is thought to have evolved from a sub-continental subduction system in the Late Cretaceous to a rifting margin by the Early Eocene and, during the late Early Oligocene, to sea-floor spreading and the formation of the South China Sea, followed by localized extension in the Middle Miocene and, finally, collision with the Luzon Arc by the Early Miocene. Imaging features of the margin's structure in the Taiwan orogen is possible with seismic tomography, which shows, for example, that there are notable changes in velocity that can be directly attributed to structures in the basement. For example, there is a marked increase in Vp beneath the Hsuehshan Range which can be interpreted to be related to the uplift of higher velocity basement rocks by basin inversion. This is accompanied by significant seismicity that reaches a depth of more than 30 km's, and by surface uplift to form the highest topography in Taiwan. Furthermore, beginning at 8 km depth, but becoming especially prominent at 12 km and 16 km depth, there is an embayment of relatively high Vp that can be interpreted as the onshore projection of a basement high that occurs between the Mesozoic basement shelf break and the Taihsi Basin. Southward, there is a notable

northeast-southwest-oriented increase in seismicity across the on land projection of the Mesozoic basement shelf break, with seismicity predominantly located beneath the Alishan Ranges, the highest topography in this part of the mountain belt. The topography also shows a pronounced re-entrant that coincides with the orientation and onshore projection of the Mesozoic basement shelf break that extends northeastward across the Western Foothills and into the Hsuehshan Range. The shallow structure of south-central Taiwan contains a number of features, such as changes in structural grain, or basement involvement in the deformation, that can be attributed to the presence of pre-existing structures in the Eurasian continental margin as it enters into the deformation of the Taiwan fold and thrust belt.

Abstract 2:

How the structure of a continental margin affects the development of a fold and thrust belt. 2: Imaging basement structures with seismic velocities and seismicity in south-central Taiwan

Cristina Biete[1], Dennis Brown[1], Joaquina Alvarez-Marron[1], Giovanni Camanni[2], Hao Kuo-Chen[3], Chun-Wei Ho[3,4]

[1]Institute of Earth Sciences Jaume Almera, ICTJA-CSIC, 08028 Barcelona, Spain

[2]University College, Dublin

[3]Department of Geosciences, National Central University, Jongli, Taiwan.

[4]Central Weather Bureau, Taipei 100, Taiwan

Presented at: 2016 EGU General Assembly. Vienna (Austria)

Type of presentation: poster

Abstract:

We investigate the geophysical signature within the south-central Taiwan fold and thrust belt of the reactivation of pre-existing structures developed on the Eurasian margin. Seismic tomography (P-wave) and earthquake hypocenters are combined to trace structures mapped on the margin offshore western Taiwan into the fold and thrust belt. The extensional tectonic history of the margin began in the Early Eocene and culminated in the Late Eocene to Early Oligocene with sea-floor spreading and the opening of the South China Sea. Several NE trending basins developed during the rifting of a pre-Cenozoic basement and these were filled with Eocene sediments. Further extension on the outer margin took place during the Middle to Late Miocene, forming basins that are now involved in the Taiwan deformation. Finally, the margin's transition from the platform to the slope takes place across south-central Taiwan and is oriented at a high angle to the active deformation front. We define the basement as pre-Eocene rocks and use a P-wave velocity (Vp) of 5.2 km/s as a proxy for the interface between them and their younger cover. This Vp interface is characterized by highs and lows that can be interpreted to image basement topography whose possible causes we investigate here. In the Hsuehshan Range there is a pronounced shallowing of the 5.2 km/s surface across the Shuilikeng fault. It is accompanied by an east-dipping cluster of seismicity down to more than 25 km depth, and forming what appears to be a crustal ramp across which the Eocene-age Hsuehshan Basin is being inverted. Westward, the 5.2 km/s interface forms a high called Paikang basement high, the southern flank of which is the on land projection of the Mesozoic basement shelf break. Southward, there is an increase in seismicity and topography that is associated to a NE-SW oriented lateral structure in the fold and thrust belt. South of this lateral structure, beneath the Alishan Range, a shallowing of the 5.2 km/s interface marks a change in the structural grain of the fold and thrust belt. This, together with the increase in predominatedly scattered seismicity that reaches greater than 20 km depth, can be interpreted to indicate basement involvement in the deformation.

To the south of the Alishan Range a zone of higher velocity whose orientation is roughly parallel to that of the Mesozoic basement shelf break is interpreted as a basement high. Here, there appears to be SW-dipping clusters of hypocenters associated with the shallowing of the 5.2 km/s surface. We interpret this shallowing of the 5.2 km/s surface to be related to an extensional fault block (or blocks) on the upper slope area of the basement. The seismicity clusters are possibly imaging the reactivation of the extensional faults that bound it.

Abstract 3:

How the structure of a continental margin affects the development of a fold and thrust belt. 3: evidences from field mapping and geological cross-sections in south-central Taiwan

Joaquina Alvarez-Marron[1], **Cristina Biete[1]**, Dennis Brown[1], Giovanni Camanni[2], Hao Kuo-Chen[3], Chun-Wei Ho[3,4]

[1]Institute of Earth Sciences Jaume Almera, ICTJA-CSIC, 08028 Barcelona, Spain

[2]University College, Dublin

[3]Department of Geosciences, National Central University, Jongli, Taiwan.

[4]Central Weather Bureau, Taipei 100, Taiwan

Presented at: 2016 EGU General Assembly. Vienna (Austria)

Type of presentation: poster

Abstract:

The Eurasian Margin is obliquely colliding with the Luzon Arc to form the Taiwan orogen. This configuration is particularly apparent in south-central part of the island providing a case example to investigate the effects of structural inheritance in the development of the thrust and fold belt. The Eurasian Margin evolved from a pre-Cenozoic continental basement that underwent rifting in the Early Eocene and subsequent sea-floor spreading to form the South China Sea during the late Early Oligocene. The margin underwent localized extension in the Middle Miocene, before the initiation of collision with the Luzon Arc by the Early Miocene.

The important along-strike changes in structure and topography of south-central Taiwan thrust and fold belt are evidenced in the detailed geological map and 3 balanced geological cross sections. A 3D tomography model is integrated in this study to help constrain the structure at depth.

Major along-strike changes seem to be related to structures oriented at a high angle to the thrust system. These include changes in strike of thrusts and fold traces, the changing elevation of thrusts and stratigraphic contacts, and the growing importance of Middle Miocene sediments within the thrust system that take place from north to south. Horizontal slices of the tomography model illustrate that N-S changes in velocity have the orientation of the inherited structural grain of the Eurasian margin. In particular, the inherited location of the Mesozoic margin's shelf-slope transition affects the distribution of seismicity and the location of lateral stratigraphic and structural changes. Also, it appears to be associated with the inversion of Eocene- and Miocene-age extensional faults, deeply rooted in the pre-Cenozoic basement that trend oblique to the thrust belt. The inversion of inherited structures affects the uplift of Miocene syn-extensional and syn-tectonic Plio-Pleistocene foreland basin sediments, and of the pre-Cenozoic basement.

Section A shows imbricated thrusts merging into a flat, gently west-dipping detachment at the

base of Plio-Pleistocene syn-tectonic sediments in the foothills. While in the area of the Hsuehshan Range, the involvement and uplift of pre-Cenozoic basement is associated to higher topography and to the occurrence of Eocene-Oligocene sediments at the surface. Section B shows thick Miocene stratigraphy and pre-Cenozoic basement rocks involved in the imbricated thrusts. Basement involvement is here also associated with the increased topography observed in the Alishan Range. The Choshui lateral structure that separates sections A and B is associated with a hangingwall culmination wall. It is evidenced in the map by changes in orientation of contacts and fold axis. This lateral structure is also constrained by larger Vp values in the tomography, corresponding to the Alishan basement involvement area. In section C to the south, the imbricated thrusts involve thick Miocene and Plio-Pleistocene sedimentary strata and the westward dipping sole thrust is above the pre-Cenozoic basement. These sedimentary sequences are interpreted to be offscraped above inherited extensional faults that seem to be associated to significant seismic activity at depths of 5-10 km below the sole thrust.

Abstract 4:

Effects of inherited continental margin structure in the south-central Taiwan fold and thrust belt

Cristina Biete[1], Joaquina Alvarez-Marron[1], Dennis Brown[1], Hao Kuo-Chen[2], Chun-Wei Ho[2,3]

[1]Institute of Earth Sciences Jaume Almera, ICTJA-CSIC, 08028 Barcelona, Spain

[2]Department of Geosciences, National Central University, Jongli, Taiwan.

[3]Central Weather Bureau, Taipei 100, Taiwan

Presented at: 2016, 9th Geological Congress of Spain. Huelva (Spain)

Type of presentation: oral

Abstract (extended):

Abstract 5:

Reactivation of inherited oblique continental margin structures during the development of the south-central Taiwan fold and thrust belt

Cristina Biete[1], Joaquina Alvarez-Marron[1], Dennis Brown[1], Hao Kuo-Chen[2], Chun-Wei Ho[2,3] , Yih-Min Wu[4]

[1]Institute of Earth Sciences Jaume Almera, ICTJA-CSIC, 08028 Barcelona, Spain

[2]Department of Geosciences, National Central University, Jongli, Taiwan.

[3]Central Weather Bureau, Taipei 100, Taiwan

[4] Department of Geoscience, National Taiwan University, Taipei, Taiwan

Presented at: 2016 AGU Fall Meeting, Abstract T43J-03. San Francisco (USA)

Type of presentation: oral

Abstract:

The Taiwan orogen is forming due to the oblique collision between the Eurasian continental margin and the Luzon Arc. This configuration provides an opportunity to study the effect of inherited structures on the development of a fold and thrust belt (FTB). During the extensional tectonic history of the margin several NE trending basins filled with Eocene to Early Oligocene sediments developed on a pre-Cenozoic basement, and further extension took place on the outer margin during the Middle to Late Miocene. The margin transition from the platform to the slope, and the large-scale extensional features of the margin project obliquely onland across south-central Taiwan. These basins are now involved in the Taiwan FTB.

In this study we combine surface geology and balanced cross sections with Vp tomography, seismicity and focal mechanisms from the south-central FTB. We use a Vp of 5.2 km/s as a proxy for the basement-cover interface. We found that the FTB includes significant along strike changes in structure and stratigraphy that may be correlated with reactivating basement structures that are at a high angle to the structural grain. Seismic tomography and seismicity are used to trace structures from the continental margin offshore western Taiwan into the FTB. Major N to S changes in seismic velocities are interpreted as basement highs and lows and these correlate with areas were changes in the structural grain of the FTB take place, including some localized variation in the strike of thrusts and folds that are evident on the map. Several seismicity clusters align along the borders of these basement blocks. Focal mechanisms show mostly strike-slip kinematics in the foreland and thrusting in the FTB. In the FTB weak clustering of strike-slip are also present. The foreland seismicity is interpreted as the result of strike-slip reactivation of inherited extensional basement faults.

Abstract 6:

The structure of the south Taiwan fold-and-thrust belt

Cristina Biete[1], Joaquina Alvarez-Marron[1], Dennis Brown[1], Hao Kuo-Chen[2], Chun-Wei Ho[2,3]

[1] Institute of Earth Sciences Jaume Almera, ICTJA-CSIC, 08028 Barcelona, Spain

[2] Department of Geosciences, National Central University, Jongli, Taiwan.

[3] Central Weather Bureau, Taipei 100, Taiwan

Presented at: 2017 EGU General Assembly. Vienna (Austria)

Type of presentation: poster

Abstract:

The structure of the south Taiwan fold-and-thrust belt (FTB) comprises a roughly N-S striking, west-verging imbricate thrust system that has been developing since the Late Miocene. Here, we present the results of new surface geological mapping, serial balanced cross sections, long sections, and a map of the basal thrust that are combined with published borehole data and a 3D P-wave tomography model to constrain the structure at depth. The stratigraphy of the area comprises Eocene syn-rift sediments that are unconformably overlain by Oligocene through Middle Miocene shallow water post-rift sediments. These are unconformably overlain by Late Miocene through Holocene-age syn-orogenic sediments. We define the basement to these as the Mesozoic pre-rift rocks of the Eurasian margin, and assign it a P-wave velocity of > 5.2 km/s in the velocity model. The syn-orogenic sediments thicken and get progressively involved in the thrust sheets toward the south.

The south Taiwan FTB can be divided into several thrust sheets. In the northern part of the map area, the structural grain is roughly N-S striking, changing southward to become NE-SW oriented. The westernmost thrust sheets form broad, open synclines cored by Pliocene to Holocene sediments, and tight hanging wall anticlines formed by Miocene rocks. Along its eastern flank, a narrow, complexly folded anticlinorium is developed in Miocene rocks. Restoration of the cross-sections indicates about 15 to 17 km of shortening. The basal thrust deepens from the surface towards the E and SE in a staircase trajectory, with narrow ramps and wide flats, reaching up to 8 km depth in the east before ramping down into the basement. The basal thrust has two pronounced, NE-striking oblique ramps that coincide with sigmoidal changes in shape of structures in the hanging wall. These correlate with a SW-NE trending increase in the P-wave velocity that is interpreted to image a basement high. We interpret this basement high to be an inherited extensional structure of the margin, and that faults associated with it are being reactivated, causing the changes in strike of the basal thrust, as well as in the surface trace of thrust and fold axes.

Effects of inherited continental margin structure in the south-central Taiwan fold and thrust belt

Efectos de la estructura heredada del margen continental en el cinturón de pliegues y cabalgamiento del centro-sur de Taiwán

C. Biete[1], J. Alvarez-Marrón[1], D. Brown[1], H. Kuo-Chen[2] y H. Chun Wei[2, 3]

1 Institute of Earth Sciences Jaume Almera, ICTJA-CSIC, 08028 Barcelona, Spain. cristina.biete@gmail.com
2 Dpt. Geoscience, National Central University, Jhongli, Taiwan
3 Central Weather Bureau, Taipei 100, Taiwan

Abstract: Taiwan provides an unparalleled opportunity to investigate the influence of inherited structures of the continental margin in the development of a fold and thrust belt (FTB). There, the Luzon Arc is obliquely colliding with the Eurasian continental margin forming the Taiwan Orogen. For this study we combine surface geological mapping and balanced cross sections with Vp tomography modelling and earthquake hypocenters. The margin's and FTB's basement is defined as pre-Eocene rocks. We use a Vp of 5.2 km/s as a proxy for the interface between basement and sedimentary cover. The south-central FTB includes significant along-strike changes in structure and stratigraphy that may be correlated with active structures in the basement. N to S changes in seismic velocities are interpreted as basement highs and lows and these correlate with areas where changes in the structural grain of the FTB take place. Several seismicity clusters align along the borders of these basement blocks. We interpret these features to indicate that basement is involved in the deformation and that the seismicity is imaging the reactivation of basement faults that influence the structure of the FTB.

Key words: Taiwan fold and thrust belt, earthquakes, tomography, basement reactivation, structural inheritance.

Resumen: *Taiwan nos ofrece una oportunidad inestimable para investigar la influencia de las estructuras heredadas del margen continental en el desarrollo de un cinturón de pliegues y cabalgamientos (CPC). En esta zona, el arco de Luzón colisiona oblicuamente con el margen continental euroasiático formando el Orógeno de Taiwan. Para este estudio combinamos la cartografía geológica y los cortes balanceados con la tomografía sísmica (Vp) y los hipocentros de los terremotos. Se definen las rocas pre-Eocenas como el basamento del margen y del CPC, y se utiliza la Vp de 5.2 km/s como representativa de la interfaz entre el basamento y la cobertera sedimentaria. En la zona centro-sur del CPC se producen cambios a lo largo de la orientación de las estructuras y de la estratigrafía, que pueden ser correlacionados con estructuras activas del basamento. Los cambios de las velocidades sísmicas de N a S se interpretan como altos y bajos de basamento y se correlacionan con las áreas donde se producen cambios de la dirección estructural del CPC. Algunos grupos de sismicidad se alinean a lo largo de los bordes de estos bloques de basamento. Interpretamos estas características como indicativos de que el basamento está involucrado en la deformación y que la sismicidad representa la reactivación de fallas de basamento que influencian la estructura del CPC.*

Palabras clave: *Cinturón de pliegues y cabalgamientos de Taiwan, terremotos, tomografía, reactivación basamento, herencia estructural*

INTRODUCTION & GEOLOGICAL SETTING:

The Eurasian margin is obliquely colliding with the Luzon Arc to form the Taiwan Orogen (Fig. 1). This configuration is particularly apparent in the south-central part of the island providing a case example to investigate the effects of structural inheritance in the development of the FTB.

The extensional tectonic history of the Eurasian margin began in the Early Eocene and culminated in the Late Eocene to Early Oligocene with sea-floor spreading and the opening of the South China Sea (Lin et al, 2003). Several NE trending basins developed during the rifting of the pre-Cenozoic basement. Further extension on the outer margin took place during the Middle to Late Miocene, forming basins whose sediments are now involved in the Taiwan FTB.

The margin's transition from the platform to the slope projects across south-central Taiwan and is oriented at a high angle to the active deformation front. This study is focussed in the south-central region in order to investigate the effects of inherited margin structures on the development of the FTB.

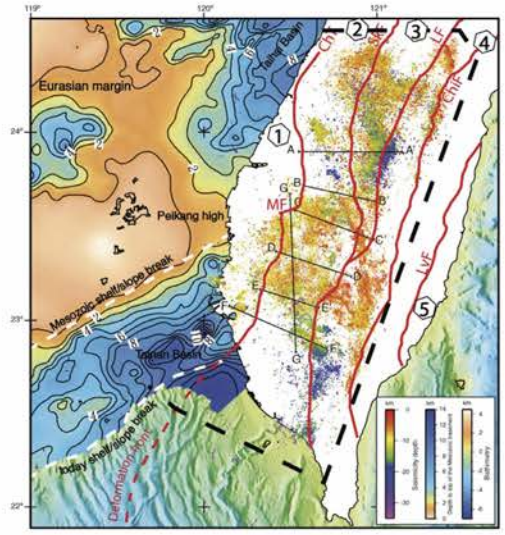

FIGURE 1. *Taiwan Island with depth to the top of Mesozoic basement in the Taiwan Strait (Lin et al, 2003). Location of earthquake epicenters with depth scale color coded, in black lines are showed all the tomography cross sections developed highlited one is shown in Fig.2., main faults in red line (ChT: Changua Thrust; MF: Meishan Fault; SkF: Shuilikeng Fault; LF: Lishan Fault; ChiF:Chinma Fault and LvF: Longitudinal Valley Fault), which divide Taiwan in four major tectonostratigra_c units, 1: Coastal Plain; 2: Western Foothills; 3: Hsuehshan Range; 4: Central Range and 5: Coastal Range. Black dashed line indicates the study area.*

DATA AND METHODS:

The 3D local Vp tomography model (Kuo-Chen et al, 2012) and earthquake hypocenter data from 1994 to 2014 are used. Earthquake hypocenters were relocated using the same 3D velocity model and a double difference technic (Fig. 2).

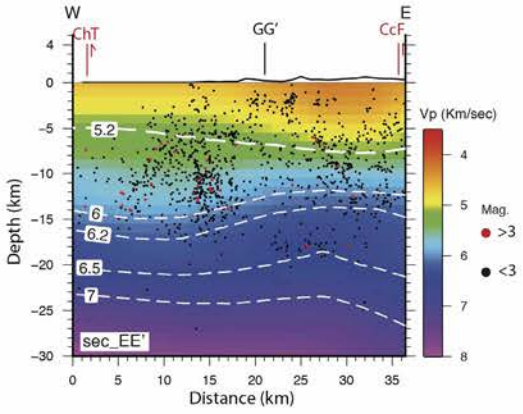

FIGURE 2. *Vertical tomography section EE' with hypocenters projected from 2 km each side. Magnitudes above 3 are in red and below in black. Key to abbreviations and location are in Fig. 1.*

The tomography and earthquake data are integrated with our new geological mapping from which several balanced geological cross sections are constructed (Fig. 3). The tomography and earthquake data help constrain the structure at depth.

RESULTS AND DISCUSION:

We define the basement as pre-Eocene rocks, and use a P-wave velocity (Vp) of 5.2 km/s as a proxy for the basement-cover interface (Camanni et al, in press). This interface is characterized by highs and lows that are interpreted to reflect basement topography.

In all the tomography cross sections we find that the seismicity is located above and below Vp 5.2 km/s contour, meaning that deformation is taking place not only in the FTB but also in the basement.

In the north, under the Hsuehshan Range (3) (Brown et al, 2012 and Camanni et al, 2014) there is a pronounced shallowing of high Vp across the Shuilikeng fault (SkF) (Fig. 4). It is accompanied by an east-dipping cluster of seismicity down to more than 25 km depth (Fig.1), and forming what appears to be a crustal ramp across which the Eocene-age Hsuehshan Basin is being inverted. In the Hsuehshan Range, the involvement and uplift of pre-Cenozoic basement is associated to higher topography and to the occurrence of Eocene-Oligocene sediments at the surface.

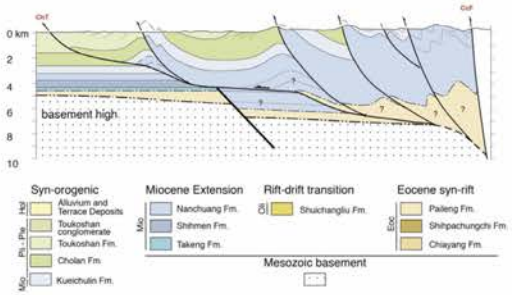

FIGURE 3. *Balanced geological cross section along EE'. Key to abbreviations and location are in Fig. 1.*

The 5.2 km/s Vp boundary defines the Peikang High in the west (Fig. 1 and Fig. 4), the southern flank of which is the onland projection of the Mesozoic shelf/slope break. Southward, there is an increase in seismicity that is associated with a NE-SW oriented Choshui lateral structure in the FTB, expressed at the surface as the Meishan Fault (MF), and continues westward beneath the Alishan Range (AR). In the Alishan Range, the shallowing of the 5.2 km/s Vp interface in the FTB is interpreted as a basement high (Alvarez-Marron et al, 2014). The alignment of MF and the Choshui lateral structure in the northern Alishan basement high is roughly parallel to the Mesozoic shelf/slope break. The increase of predominantly scattered seismicity that reaches greater than 20 km depth, suggest basement involvement in the deformation. In accordance with this, geological cross

sections show thick Miocene stratigraphy in the imbricated thrusts of the Alishan Area.

To the south, another zone of higher velocity is interpreted as a basement high crossing the FTB (Tainan High, Fig. 4). Associated with this basement high, there appears to be a SW-dipping cluster of hypocenters (Fig. 1). We interpret this as an extensional fault block (or blocks) that project from the upper slope area. The seismicity clusters are possibly imaging the reactivation of its bounding extensional faults.

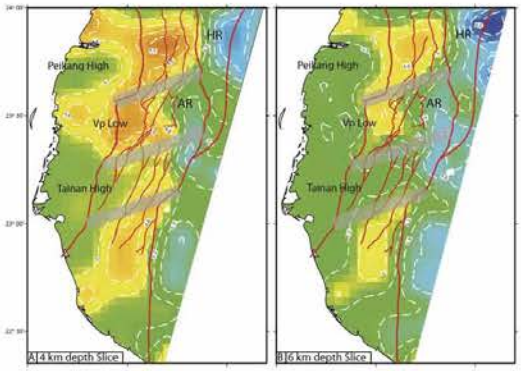

FIGURE 4. *Horizontal tomography slices at 4 and 6 km depth respectively. Major faults in red lines. Major basement structures are highlighted in the Coastal Plain. Transparent grey squares represent basement related structures in the FTB. Contours every 0.2 km/s. The same colour scale as in Fig.2. AR, Alishan Range*

The southern geological cross section shows thicker Miocene and Plio-Pleistocene sediments involved in the imbricated thrusts and the west verging dipping sole thrust is above the pre-Cenozoic basement (Fig.2)

Major along-strike changes in the geological map, such as in thrust strike, in fold traces, in the elevation of the thrusts and stratigraphic contacts and in the thickness of Middle Miocene sediments within the thrust system from N to S, are interpreted to be related to lateral structures in the thrust system. These changes present a good correlation with basement fault blocks that are interpreted from the Vp velocity model and earthquake location.

CONCLUSIONS:

- The geology of south-central Taiwan fold and thrust belt includes important along-strike changes in structure and stratigraphy, as well as in seismic velocities.

- Seismicity appears to be above and below the top of the Mesozoic basement and locally, reaches down to more than 25 km depth. We interpret this as deformation taking place not just in the cover but also in the basement, resulting in fault reactivation and, locally, basin inversion.

- Several major changes in strike and elevation in the orientation of structures, stratigraphic contacts and velocity distribution that take place from north to south are associated to lateral structures. We interpret them to be related to reactivation of inherited northeast-striking basement faults.

- The basement involvement in the deformation and the depth distribution of seismicity are associated to the reactivation of basement fault blocks that influence the building of the mountain belt.

- Our geological mapping, together with the geological cross sections provide an estimate of a minimum amount of horizontal shortening in the FTB of about 15 km. Displacement directions along the main thrusts are, overall, roughly northwest-directed.

AKNOWLEDGEMENTS

This research is supported by BES-2014-070122 grant from MINECO within the project with reference number CGL2013-4377-P.

REFERENCES

- Alvarez-Marron, J., Brown D., Camanni, G., Wu, Y.-M. and Kuo-Chen, H. (2014): Structural complexities in a foreland thrust belt inherited from the shelf-slope transition: Insights from the Alishan area of Taiwan, *Tectonics*, 33.
- Brown, D., Alvarez-Marron, J., Schimmel, M., Wu, Y.-M., and Camanni, G., 2012, The structure and kinematics of the central Taiwan mountain belt derived from geological and seismicity data: *Tectonics*, v. 31, no. 5.
- Camanni, G., Chen, C.-H., Brown, D., Alvarez-Marron, J., Wu, Y.-M., Chen, H.-A., Huang, H.-H., Chu, H.-T., Chen, M.-M., and Chang, C.-H., 2014b, Basin inversion in central Taiwan and its importance for seismic hazard: *Geology*, v.42, no. 2, p. 147-150.
- Camanni, G., et al., (in press): The deep structure of south-central Taiwan illuminated by seismic tomography and earthquake hypocenter data, *Tectonophysics*. http://dx.doi.org/10.1016/j.tecto.2015.09.016.
- Lin, A. T., Watts, A. B. and Hesselbo, S. P. (2003): Cenozoic stratigraphy and subsidence history of the South China Sea margin in the Taiwan region. *Basin Research*, 15 (4), 453-478.
- Kuo-Chen, H., Wu, F.T., Roecker, S.W. (2012): Three-dimensional P velocity structures of the lithosphere beneath Taiwan from the analysis of TAIGER and related seismic data sets. J. *Geophys. Res.*, 117.

Abstract 7:

Along–strike changes in the structure, seismicity, and topography of the south-central Taiwan fold-and-thrust belt inherited from the Eurasian margin

Dennis Brown[1], Joaquina Alvarez-Marron[1], **Cristina Biete**[1], Hao, Kuo-Chen[2], Giovanni Camanni[3], Chun-Wei Ho[2]

- [1]Institute of Earth Sciences Jaume Almera, ICTJA-CSIC, 08028 Barcelona, Spain
- [2]Department of Geosciences, National Central University, Jongli, Taiwan.
- [3] University College, Dublin

Presented at: 2018 EGU General Assembly. Vienna (Austria)

Type of presentation: poster

Abstract:

Studies of mountain belts worldwide show that along-strike changes are common in their foreland fold-and-thrust belts. These are typically caused by processes related to fault reactivation and/or fault focusing along changes in sedimentary sequences. The study of active orogens, like Taiwan, can also provide insights into how these processes influence transient features such as seismicity and topography. In this paper, we trace regional-scale features from the Eurasian continental margin in the Taiwan Strait into the south-central Taiwan fold-and-thrust belt. We then present newly mapped surface geology, P-wave velocity maps and sections, seismicity, and topography to test the hypothesis of whether or not these regional-scale features of the margin are contributing to along-strike changes in structural style, seismicity, and topography in this part of the Taiwan fold-and-thrust belt. These data show that the most important along-strike change takes place at the eastward prolongation of the upper part of the margins necking zone, where there is a causal link between fault reactivation, involvement of basement in the thrusting, concentration of seismicity, and the formation of high topography. On the area correlated with the necking zone, the strike-slip reactivation of east-northeast striking extensional faults is causing sigmoidal offset of structures and topography along two main zones. Here, basement is not involvement in the thrusting, there is weak focusing of seismicity, and localized development of topography.We also show that there are important differences in structure, seismicity, and topography between the margins shelf and its necking zone.

Abstract 8:

Spatial distribution of the horizontal stress in the fold-and-thrust belt of south-central Taiwan from earthquake focal mechanisms

Cristina Biete [1], Björn Lund [2], Dennis Brown [1], Joaquina Alvarez-Marron [1], Yih-Min Wu [3], Hao Kuo-Chen [4], Chun-Wei Ho[4,5]

[1] Institute of Earth Sciences, Jaume Almera, ICTJA-CSIC, 08028 Barcelona, Spain. cbiete@ictja.csic.es

[2] Department of Earth Science Geophysics, University of Uppsala, Uppsala, Sweden

[3] Department of Earth Science, National Taiwan University, Taipei, Taiwan

[4] Department of Earth Science, National Central University, Zhongli District, Taoyuan City, Taiwan

[5] Central Weather Bureau, Taipei, Taiwan

Presented at: 2018 EGU General Assembly. Vienna (Austria)

Type of presentation: poster

Abstract:

The dominant structure of western Taiwan comprises two fault systems: one that consists of the thrusts of the fold-and-thrust belt (FTB) (NNE striking), which are being cut at a high angle by a second system that is inherited from the continental margin (ENE striking). To investigate the complexities that the interaction of these two fault systems introduce into the deformation style and kinematics of the south-central Taiwan FTB we integrate the surface geology with the inversion of more than 2400 earthquake focal mechanisms to calculate the stress tensor, horizontal stress and their more probable failure planes. Earthquakes in the study area occur throughout the crust, but they are predominantly located below the basal thrust of the FTB between 5 to 20km depth. To investigate above the basal thrust, we then compare the horizontal stress azimuths with the strain rate vectors calculated from GPS data. The focal mechanism data set has been manually discretized depending on their distribution in tectono-stratigraphic units, structures and mechanisms. In depth, we take into account the location of the basement, then: from 0-7km depth is above the basement, 7-15km lies within the basement, and 15–45km represents the deeper crust. Using these criteria, we identified 42 clusters with more than the minimum of 20 events needed to obtain a reliable stress tensor and its failure planes, these is used to calculate the maximum horizontal stress azimuth (S_h). The S_h azimuths smoothly turn along the study area from NW in the east to SW in the west, with the exception of the Chi-chi earthquake area, where S_h azimuth strikes N-S. While S_h does not present significant depth variations and is coherent with the surface strain directions, depth changes are found in the stress regime and principal failure planes through the study area. Above the basement, which is predominantly strike-slip, both fault systems are represented but, NE-striking ones (those similar to the margin), are located below surface geology along-strike changes. The upper basement presents a clear

strike-slip band ENE-striking in the center of the FTB with principal failure planes NE-striking, as the ones representing the margin structure also found in the foreland basin basement. Moreover, this band location is just below a cut by an ENE-striking fault of the deformation front surface expression. South of this band, the basement presents contractional tensors and N-S principal failure planes as in the FTB. Finally, the deep basement slice presents clusters with contractional behavior and N-S principal failure planes as are that characteristic from the mountain belt.

This study shows that the tectonic stress of the just above and upper basement of the study area has a clear influence from the continental margin structures and, considering the casual relationship between above and upper basement tectonic stress and failure planes striking distribution and the surface geology along-strike changes it suggests that the structures and configuration of the margin may be also affecting the deformation style and kinematics of the south-central Taiwan FTB.

Abstract 9:

How the structure of a continental margin affects the development of a fold and thrust belt. 3: evidences from field mapping and geological cross-sections in south-central Taiwan

Joaquina Alvarez-Marron[1], **Cristina Biete[1]**, Dennis Brown[1], Hao Kuo-Chen[2]

[1]Institute of Earth Sciences Jaume Almera, ICTJA-CSIC, 08028 Barcelona, Spain

[2]Department of Geosciences, National Central University, Jongli, Taiwan.

Presented at: 2018 EGU General Assembly. Vienna (Austria)

Type of presentation: poster

Abstract:

The southwest Taiwan fold-and-thrust belt is forming on the outer shelf and slope of the Eurasian continental margin. It comprises a roughly N-S striking, west-verging imbricate thrust system that has been developing since the Late Miocene. Here, we present the results of new surface geological mapping from which we construct balanced and restored cross sections and along-strike sections. From these we compile maps of the basal thrust, thrust branch lines and, where possible, stratigraphic cut-offs. To interpret the structure in the subsurface and beneath the basal thrust, we use a P-wave velocity of 5.2 km/s as a proxy for the top of the Mesozoic basement. From these data we interpret the 3D structure of the fold-and-thrust belt and the influence that the structure and morphology of the continental margin is having on its development. We divide the southwest Taiwan fold-and-thrust belt into a number of thrust sheets that form the basis of our description and interpretations. Shortening is variable, ranging from 16 km to 25 km. We show that there are significant along-strike changes in the structure that we suggest have a causal relationship with variations in the geometry of the basal thrust and that these, in turn, are related to basement highs and lows interpreted from the P-wave velocity model. Finally, a number of local- and regional-scale unconformities provide information on the Pliocene through Holocene growth of the fold-and-thrust belt and the change from marine to sub-aerial deformation.

APPENDIX 3 Supplementary Data - Geological Map

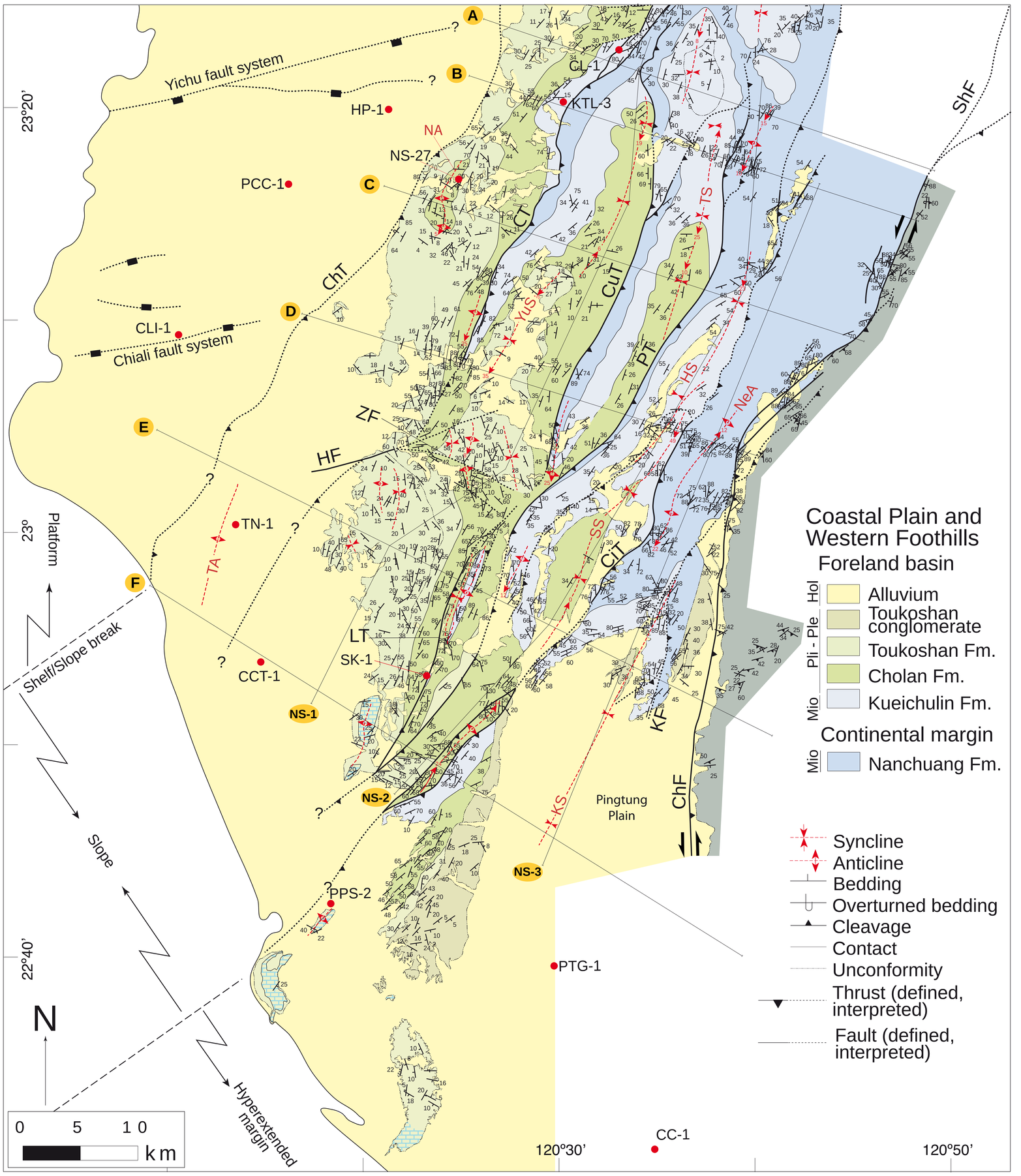
A
B
C
D
E
F
Yichu fault system
Chiali fault system
HP-1
NA
NS-27
PCC-1
CLI-1
TN-1
CCT-1
SK-1
NS-1
NS-2
PPS-2
NS-3
PTG-1
CC-1
CL-1
KTL-3
ShF
CT
TS
ChT
CuT
YuS
PT
HS
NeA
ZF
HF
TA
SS
CiT
LT
KF
ChF
KS
Pingtung Plain
23°20'
23°
22°40'
120°30'
120°50'
Platform
Shelf/Slope break
Slope
Hyperextended margin
N
0 5 10 km
Coastal Plain and Western Foothills
Foreland basin
Hol
Alluvium
Toukoshan conglomerate
Pli - Ple
Toukoshan Fm.
Cholan Fm.
Mio
Kueichulin Fm.
Continental margin
Mio
Nanchuang Fm.
Syncline
Anticline
Bedding
Overturned bedding
Cleavage
Contact
Unconformity
Thrust (defined, interpreted)
Fault (defined, interpreted)

APPENDIX 4 Supplementary Data - Stress Inversion Results

TABLE ST1_A4. Table with clusters statistics values (median, average, one standard deviation) for the focal mechanism solution quality index (Qfp) given by *Y.-M. Wu et al. [2008]*. The number of events in each cluster with Qfp below 0.2 (N_Qfp<0.2), and its percentage (%_Qfp<0.2) are also shown. The number of nodal planes chosen with the instability criterion in each cluster (InstaPlane), along with its percentage (%_InstaPlane), is also shown. The median, average and standard deviation of each column is given at the bottom of the table.

Cluster	N_Events	Median_Qfp	Avg_Qfp	Stdev_Qfp	N_Qfp<0.2	%_Qfp<0.2	InstaPlane	%InstaPlane
A1	43	0.98	1.85	1.82	4	9	39	91
A2	22	1.96	2.64	2.35	1	5	17	77
A3	78	0.91	1.6	1.81	10	13	69	88
A4	17	1.03	1.9	1.63	0	0	8	47
A5	22	1.82	2.99	3.27	4	18	17	77
A6	44	0.79	1.13	1.19	6	14	28	64
A7	29	0.83	1.53	1.76	3	10	17	59
A8	70	1.14	2.09	2.6	8	11	42	60
A9	71	0.85	1.74	2.35	7	10	48	68
A10	43	0.8	1.08	1	10	23	27	63
A11	69	0.61	0.89	0.87	12	17	42	61
A12	140	0.94	1.39	1.55	14	10	74	53
A13	70	0.63	0.87	0.79	7	10	49	70
B1	55	0.65	1.85	2.41	5	9	45	82
B2	30	1.05	1.54	1.43	6	20	23	77
B3	27	2.1	2.69	2.72	2	7	22	81
B4	73	0.95	2.24	2.55	9	12	41	56
B5	92	1.46	2.4	2.72	2	2	68	74
B6	83	1.34	2.52	2.86	5	6	65	78
B7	94	1.36	2.96	3.33	6	6	79	84
B8	30	2.15	4.14	4.11	0	0	21	70
B9	75	1.16	1.92	2	8	11	64	85
B10	136	1.08	1.96	2.21	14	10	107	79
B11	40	1.29	1.58	1.48	7	18	35	88
B12	40	1.24	1.5	1.56	5	13	22	55
B13	36	0.68	1.04	1.19	7	19	21	58
B14	25	0.67	1.39	1.64	3	12	12	48
B15	27	1.49	1.63	1.42	2	7	19	70
B16	95	0.75	1.61	1.79	9	9	22	46
B17	61	0.94	1.28	1.28	4	7	39	64
B18	29	0.58	1.64	2.3	5	17	22	76
C1	35	1.1	1.86	2	2	6	26	74
C2	20	1.76	3.17	3.88	3	15	12	60
C3	30	2.25	2.73	2.61	1	3	24	80
C4	165	1.06	1.67	1.67	15	9	118	72
C5	49	0.95	1.61	1.74	6	12	36	73
Median	43.5	1.04	1.71	1.82	6	10	32	71
Average	57.4	1.15	1.91	2.05	6	11	39	70
St_dev	36	0.46	0.71	0.8	4	6	26	12

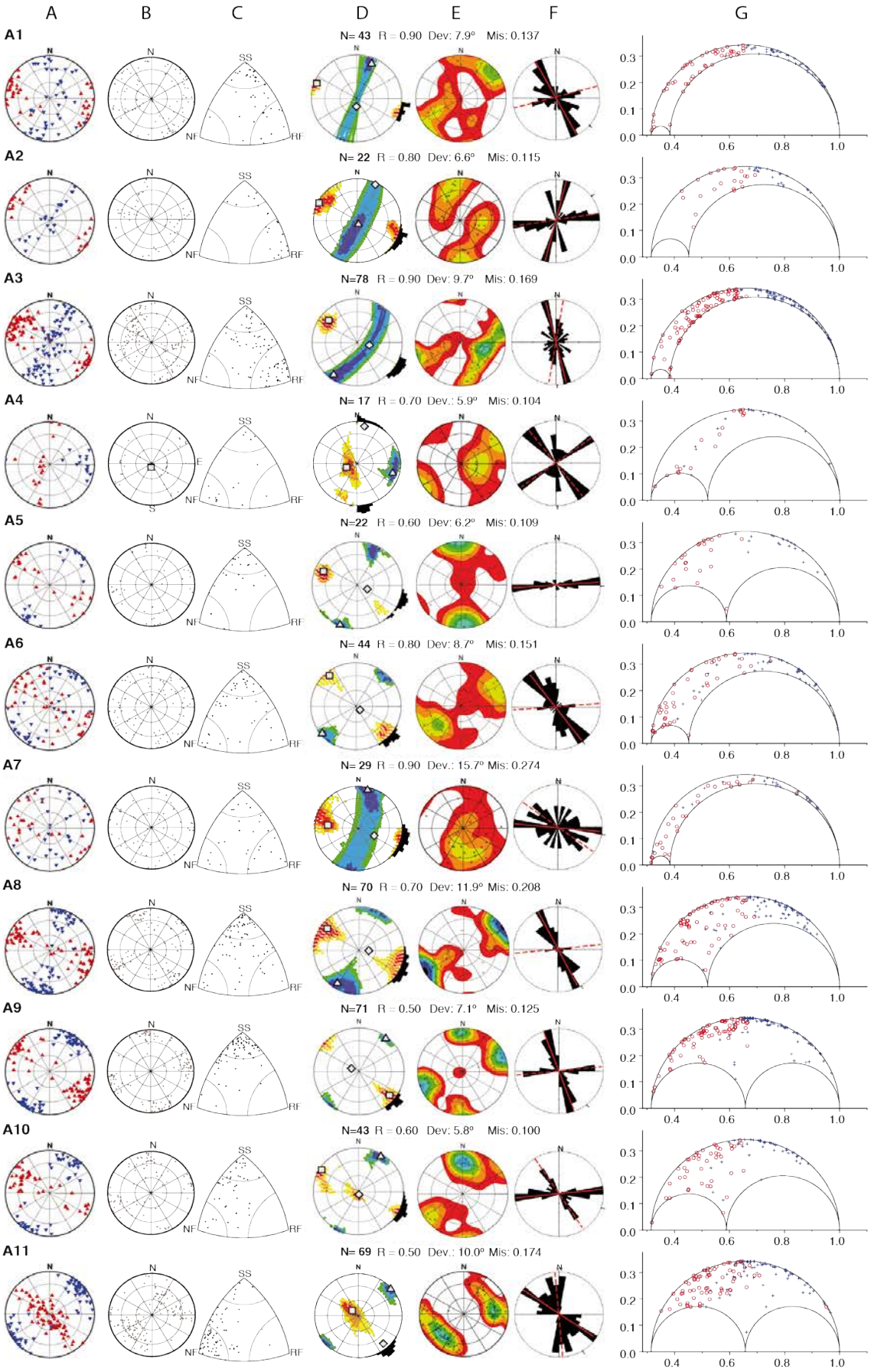
A
B
C
D
E
F
G
A1
N= 43 R = 0.90 Dev: 7.9° Mis: 0.137
A2
N= 22 R = 0.80 Dev: 6.6° Mis: 0.115
A3
N=78 R = 0.90 Dev: 9.7° Mis: 0.169
A4
N= 17 R = 0.70 Dev.: 5.9° Mis: 0.104
A5
N=22 R = 0.60 Dev: 6.2° Mis: 0.109
A6
N= 44 R = 0.80 Dev: 8.7° Mis: 0.151
A7
N= 29 R = 0.90 Dev.: 15.7° Mis: 0.274
A8
N= 70 R = 0.70 Dev: 11.9° Mis: 0.208
A9
N=71 R = 0.50 Dev: 7.1° Mis: 0.125
A10
N=43 R = 0.60 Dev: 5.8° Mis: 0.100
A11
N= 69 R = 0.50 Dev.: 10.0° Mis: 0.174
N
NF
RF
SS
E
S
0.0
0.1
0.2
0.3
0.4
0.6
0.8
1.0

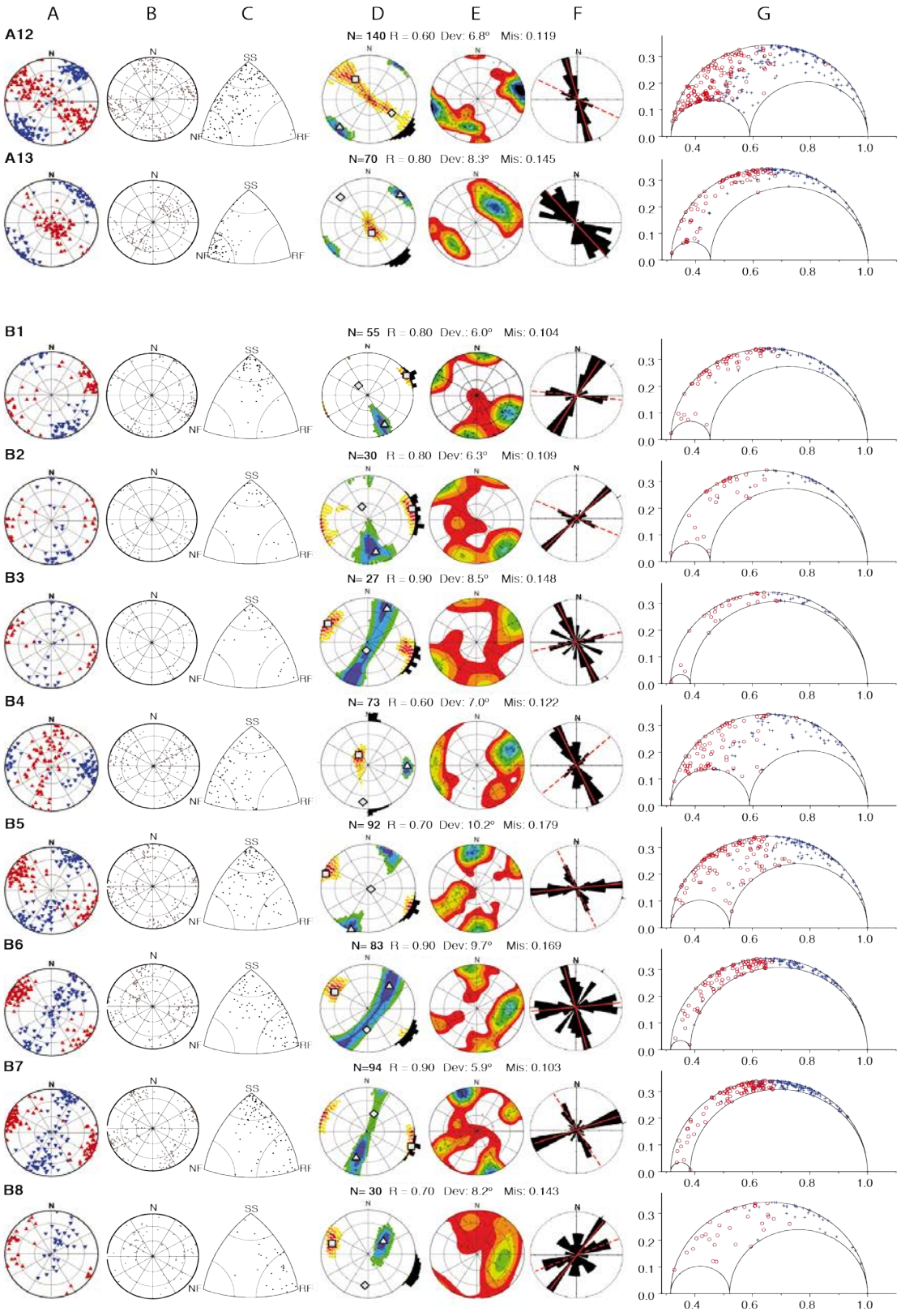
A
B
C
D
E
F
G
A12
N= 140 R = 0.60 Dev: 6.8° Mis: 0.119
A13
N=70 R = 0.80 Dev: 8.3° Mis: 0.145
B1
N= 55 R = 0.80 Dev.: 6.0° Mis: 0.104
B2
N=30 R = 0.80 Dev: 6.3° Mis: 0.109
B3
N= 27 R = 0.90 Dev: 8.5° Mis: 0.148
B4
N= 73 R = 0.60 Dev: 7.0° Mis: 0.122
B5
N= 92 R = 0.70 Dev: 10.2° Mis: 0.179
B6
N= 83 R = 0.90 Dev: 9.7° Mis: 0.169
B7
N=94 R = 0.90 Dev: 5.9° Mis: 0.103
B8
N= 30 R = 0.70 Dev: 8.2° Mis: 0.143
N
SS
NF
RF
0.0
0.1
0.2
0.3
0.4
0.6
0.8
1.0

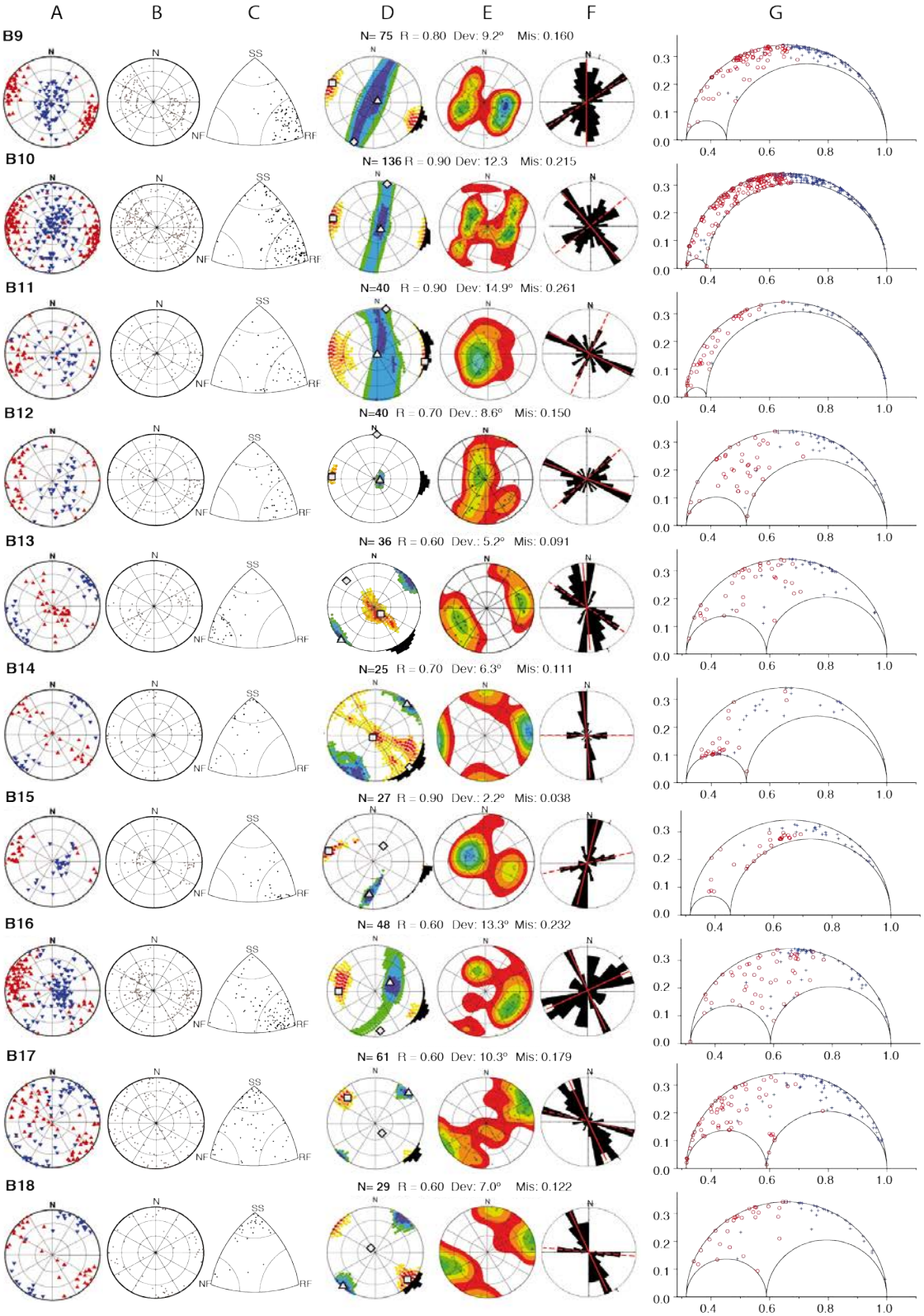
A
B
C
D
E
F
G
B9
N= 75 R = 0.80 Dev: 9.2° Mis: 0.160
B10
N= 136 R = 0.90 Dev: 12.3 Mis: 0.215
B11
N=40 R = 0.90 Dev: 14.9° Mis: 0.261
B12
N=40 R = 0.70 Dev.: 8.6° Mis: 0.150
B13
N= 36 R = 0.60 Dev.: 5.2° Mis: 0.091
B14
N=25 R = 0.70 Dev: 6.3° Mis: 0.111
B15
N= 27 R = 0.90 Dev.: 2.2° Mis: 0.038
B16
N= 48 R = 0.60 Dev: 13.3° Mis: 0.232
B17
N= 61 R = 0.60 Dev: 10.3° Mis: 0.179
B18
N= 29 R = 0.60 Dev: 7.0° Mis: 0.122
N
NF
SS
RF
0.0
0.1
0.2
0.3
0.4
0.6
0.8
1.0

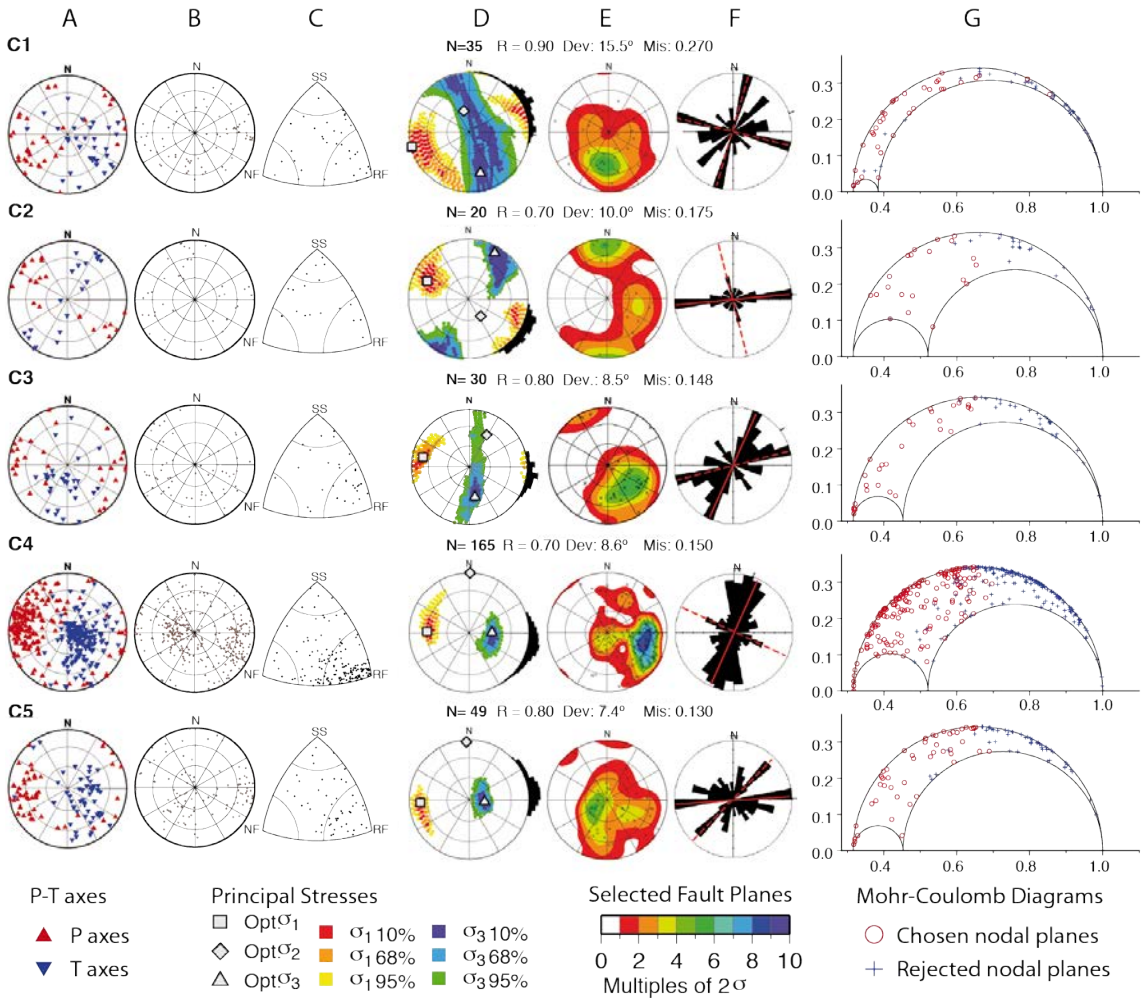

FIGURE SD2_A4. Focal mechanism cluster information and results from the inversion for each depth level cluster of Figure 1.7. For each cluster there are seven plots which in order from left to right show (all steronets are equal area lower hemisphere plots): Column A) stereonets with P- and T-axes. Column B) stereonet with poles to the nodal planes. Column C) Triangular distribution plot depending on the faulting type after *Kagan [2005]*. Column D) Best fitting stress tensor, with σ_1, σ_2, and σ_3 directions (symbols: square, diamond, triangle, respectively) and the 10%, 68% and 95% confidence limits of σ_1, and σ_3 coloured, in warm and cold colours respectively. At the edge of the plot is the S_H direction with its confidence limit as a histogram. Column E) stereonets showing the Kamb contours of the poles to the selected fault planes that best fit the stress tensor. Column F) Rose diagram with the strikes of the selected fault planes from Column D), highlighting the mean strike of the primary and secondary fault families in red solid and dashed lines, respectively. Column G) Mohr-Coulomb diagrams with all nodal planes in the clusters, showing with red circles the selected nodal planes and with blue crosses the nodal planes that were not selected. A coefficient of friction of 0.6 was used to construct the Mohr-Coulomb diagrams. Parameters of the inversion results: N = number of events, R = relative size of the intermediate principal stress, Dev = Deviation and Mis = Misfit. The locations of the clusters are shown in Figure 5.